The Dissertation Committee for Kevin Tung Certifies that this is the approved version of the following dissertation:

Oxygen Scavenging Styrene-Butadiene-Styrene Block Copolymer Films for Barrier Applications

Committee:

Donald R. Paul, Co-Supervisor

Benny D. Freeman, Co-Supervisor

Roger T. Bonnecaze

Isaac C. Sanchez

Wei Li

Oxygen Scavenging Styrene-Butadiene-Styrene Block Copolymer Films for Barrier Applications

by

Kevin Tung, B.S.Ch.; B.Ch.E.; M.S.E.

Dissertation

Presented to the Faculty of the Graduate School of

The University of Texas at Austin

in Partial Fulfillment

of the Requirements

for the Degree of

Doctor of Philosophy

The University of Texas at Austin

August 2013

Dedication

To my father and mother, my sister, and my family, both current and future

Therefore, since we have been justified through faith, we have peace with God through our Lord Jesus Christ, through whom we have gained access by faith into this grace in which we now stand. And we boast in the hope of the glory of God. Not only so, but we also glory in our sufferings, because we know that suffering produces perseverance; perseverance, character; and character, hope. And hope does not put us to shame, because God's love has been poured out into our hearts through the Holy Spirit, who has been given to us.

– Romans 5:1-5 NIV

Acknowledgements

Entering graduate school in the Fall 2006, I was one of those students who had a vision of how Ph.D. studies should be approached. And like most of them, I soon encountered a much different reality that made me re-evaluate my methods and motivation. Graduate school has taught me to think and work independently, build a hypothesis based on physical observations, design experiments around reasonable assumptions, and evaluate data and theoretical predictions, all at a professional level of diligence, perseverance, and concentration.

I want to extend my greatest appreciation to my research advisors Professors Donald Paul and Benny Freeman. Professor Donald Paul has become the most significant figure in my personal and professional life. I am forever inspired by the angle at which he approaches problems and the discipline he has in life-related issues. From the very beginning, Professor Benny Freeman has always made me feel comfortable in sharing with him issues that are either academic or personal. These two giants introduced me to the field of polymer science, broadened the limited range of my mind, and, with their otherworldly patience, allowed me to grow into a different person that I now embrace. Professors Paul and Freeman, who have immense passion and interest and are incredibly skilled and experienced, let me witness first-hand the level of excellence that can be achieved by the power of combined effort and intuition. I am deeply indebted to Professors Paul and Freeman, and I have a tremendous amount of personal and professional respect for both of them.

I will never be able to come to the end of journey had it not been because of the generous help I have received in my doctoral studies. I have to thank Dr. Hua “Richard”

Li and Keith Ashcraft who served as my lab mentors when I was beginning in the lab. Richard, in particularly, has become a great friend of mine. His patience and experimental ideas, as well as his thoughtfulness and caring were invaluable, and will continue to resonate in my professional life that follows. I have to thank Dr. Chiara Ferrari and Dr. Susana Carranza for the constant communication on the simulation work. I have to thank Dr. Wei Xie, Dr. Hugo Celio, and Dr. Domingo Ferrer for their help on the SEM/EDS and TEM analytical work. I have to thank Zach Smith and Dr. Kristofer Gleason for helps on the MSB, low-pressure permeation tests, and error analysis on flux. I have to thank Katrina Czenkusch for valuable discussion on the reaction order and its quantitative determination. I have to thank Dr. Rajkiran Tiwari who seems to have all the answers for all of my equipment-related needs. I have to thank Professors Roger Bonnecaze, Isaac Sanchez, and Wei Li for agreeing to be my dissertation committee members. Also many, many thanks go to Pam Cook, who kindly took her own time to care for my editing needs on all the chapters that are included in this dissertation.

I am fortunate to have befriended some of the nicest people I know. My CLiPS colleagues, Dr. Dan Miller, Dr. Tom Murphy, and Dr. Grant Offord, with whom I entered the University and shared many, many memorable life events have always unselfishly encouraged and lifted me up when I was down in both academic and personal needs. I have to thank Dr. Hao Ju who has brought me along on the basketball court at both the Pickle Research Center Gym and the Gregory Gym in my early years of scavenging. Then it became Dr. David Sanders who let me rain three-pointers in transition at the end of the game. I have had the privilege to share my CPE office 3.464 for the last two years with Hee Jeung Oh, who is always spirited and interested in motivating me with conversations on research, careers, and life. Other past and current lab mates, including Dr. Norman Horn, Dr. Lili Cui, Dr. Brandon Rowe, Dr. Claudio Ribeiro, Dr. Victor

Kusuma, Dr. Alyson Sagle, Dr. Yuan-Hsuan Wu, Dr. Roy Raharjo, Dr. Scott Kelman, Dr. Scott Matteucci, Dr. Liz Van Wagner, Dr. Bryan McCloskey, Dr. Ho Bum Park, Dr. Geoff Geise, James Kyzar, Joe Cook, Sirirat "Peach" Kasemset, Albert Lee, Qiang Liu, Kevin Stevens, Yan Ni, Lisa He, and Amanda Paine all helped shape up my graduate school experience in the Department of Chemical Engineering at The University of Texas at Austin, where the emphasis on world-class research has bred success.

I am also extremely grateful of presence of some people that are outside of the research lab. I have to thank Dr. Ping-Chao Liao, Dr. Tzu-Hsuan Ai, Dr. Chun-Lin Lin, Melvin Huang, Yun-Yu Hsieh and other members of ACCCF and SACCSF for their spiritual support with their constant prayers and comforts. Yen-Han "Nunue" Yang is the cornerstone, a listener, and main source of encouragement and inspiration throughout graduate school in my personal life. Finally, I have to sincerely extend my utmost appreciation to my parents, Wen Li and Hsu Shyan Tung, my sister, Kai Fei, and my aunt Becky Windham and her family who had to bear with my temper, impatience, inconsistent time management, and almost non-existence for the past seven plus years in their respective lives. They are the most loving figures I ever know, and it is truly a blessing that I can call them my family.

Last but not least, I will give glory to the praise-worthy God who lives, reigns, saves, and loves. The Lord has been my rock and shelter when I went through the valley of the shadow of death. Jesus is the salvation and the reason for who I am today. Rejoice!

I love you, Lord, my strength. The Lord is my rock, my fortress and my deliverer; my God is my rock, in whom I take refuge, my shield and the horn of my salvation, my stronghold.

– Psalm 18:1-2 NIV

Oxygen Scavenging Styrene-Butadiene-Styrene Block Copolymer Films for Barrier Applications

Kevin Tung, Ph.D.

The University of Texas at Austin, 2013

Co-Supervisors: Donald R. Paul, Benny D. Freeman

This dissertation discusses the oxidation behavior of reactive membranes that were produced by solution casting and by melt extrusion. These films, containing styrene-butadiene-styrene (SBS) block copolymer that undergoes catalytic oxidation, are of potential use as an oxygen scavenging polymer (OSP) for barrier applications. A thin film kinetic model was developed to ascertain reaction parameters that were used to describe thick film oxidation behavior. Ultimately complex structures containing these scavengers need to be produced via melt-extrusion. Therefore, processing conditions were established to ensure that melt-processed films have the same oxidation kinetics and capacity as those prepared by solution casting. Blends containing a non-reactive styrene phase and an oxygen-scavenging SBS phase were extruded and, by uptake and permeation experiments, their oxidation behaviors were monitored. The flux behavior and time lag extension as a function of oxygen pressure, film thickness, SBS scavenger and photoinitator contents were measured and compared to the theoretical model. The permeation behavior of the reactive blend films containing SBS showed that time lags can be extended via an oxidative mechanism and barrier properties be improved compared to traditional packaging membrane of native polystyrene.

Table of Contents

List of Tables

List of Figures

Chapter 1: Introduction

1.1 BARRIER FILMS FOR PACKAGING

Polymers are favored as barrier materials because they are easily formed into typical packaging shapes and are lighter weight than alternatives like glass or metal. Often, food items require packaging materials with very low oxygen permeability; however, many packaging materials have insufficient barrier properties for food items such as those listed in Table 1.1 [1]. Nanoparticles or nanoplatelets have been embedded in polymers to introduce tortuosity, which reduces the gas permeation rate [2–5]. In addition to these steady state approaches to improve barrier properties [6–12], reactive materials can be incorporated into barrier films, such as layered PET-based films [13], to adsorb, react, or scavenge penetrant molecules. This study seeks to improve barrier properties by incorporating oxygen scavenging polymers (OSP) that form oxidized products over time.

However, oxygen barrier properties alone are often not the only element that makes barrier materials sufficient for a given application. Both high oxygen barrier and high water vapor barrier characteristics may be required in the packaging of electronic display elements. Since the two high barrier properties do not usually occur in the same materials, blend films, or systems of multi-layers, or structures of both, must be developed with materials of different desired properties. The goal then becomes finding the optimal structure to achieve the best barrier performance and, at the same time, maintaining other packaging property requirements, such as optical transparency and mechanical properties.

Table 1.1: Transport properties for conventional packaging materials, and requirement for typical foodstuffs: * Less than 20% loss of CO_2 is also required **1 year shelf life. Package dimensions: 500 cm^3, wall thickness 11 mil, ΔP_{O_2} = 20 cm Hg [1]

Food/beverage	Estimated max. tolerable O_2 gain, ppm	Required O_2 permeability, Barrer**	Polymer	O_2 Permeability (Barrer) 25ºC
Canned milk, meats, canned vegetables	1 to 5	$5.6 – 28 \times 10^{-7}$	EVOH	0.0002 (20ºC)
Beer, ale, wine	1 to 5*	$5.6 – 28 \times 10^{-7}$	PVDC	0.00061
Canned fruits, Nuts	5 to 15	$2.8 – 8.4 \times 10^{-6}$	Nitrile resin	0.0039
Fruit juice, drinks	10 to 40	$5.6 – 22 \times 10^{-6}$	PET	0.057
Dressings, oils, shortening, liquors	50 to 200	$2.8 – 11 \times 10^{-5}$	PE	2.86

In the past, a method was developed to include oxygen scavenging polymers, or OSPs, in a polymeric film or bottle wall. Specifically, MXD-6 was incorporated as a sacrificial polymer between layers of PET, as shown in Figure 1.1 [8]. Using cobalt neodecanoate as the oxidation catalyst, MXD-6 reacts with oxygen through a transient mechanism that reduces oxygen permeance. Furthermore, with increasing catalyst loading, time lags to oxygen permeance are extended and can reach hundreds of days with no detection of oxygen transmission. This work shows that incorporating a thin layer of active scavenging material with layers of PET can greatly improve barrier properties of packaging material.

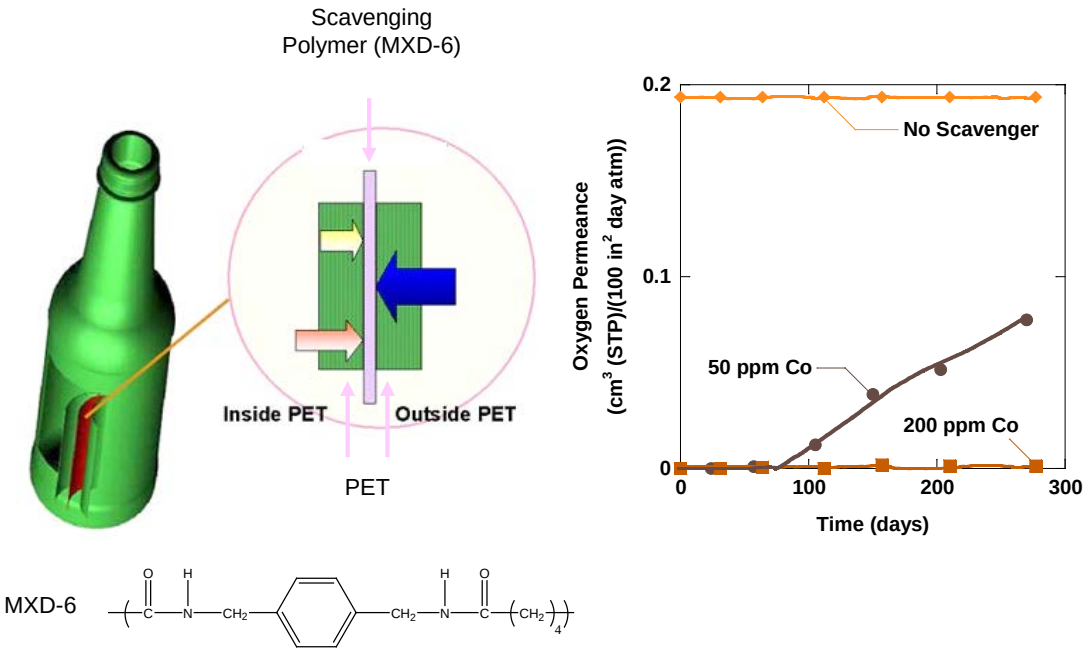

Figure 1.1: Sandwich structure of PET and 4 wt% MXD-6 formed into one-liter cylindrical bottle; Permeance = 0 indicates that no O_2 transmission was detected [8]

Baer et al. [14] at Case Western Reserve University (CWRU) developed a coextrusion process that can produce multi-layered systems (Figure 1.2). Several issues sometimes associated with polymeric barrier materials—such as opacity, function specificity, low flexibility, and high cost—can be alleviated with layered structures. This coextrusion process is the enabling technology for an NSF Science and Technology Center, the Center for Layered Polymer Systems (CLiPS), with which this work is associated.

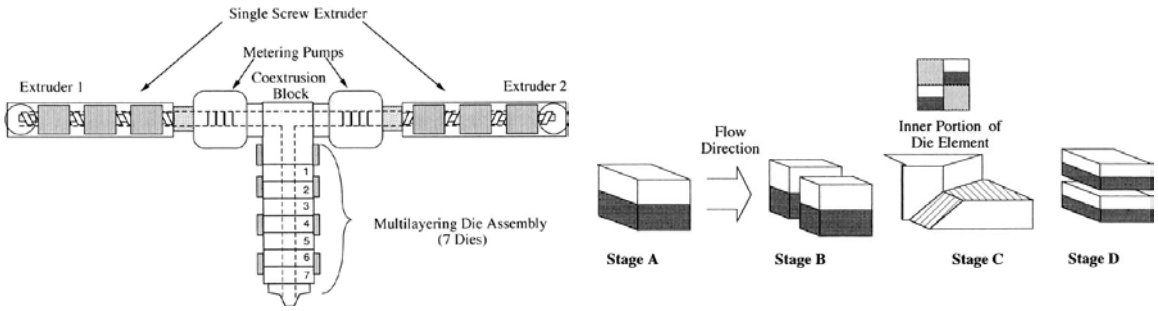

Figure 1.2: The extrusion set-up that can make nanosystems of up to 4,096 layers with each layer less than 100 nm thick [14].

Figure 1.2 shows that the coextrusion process [14] consists of multiple extruders equipped with an assembly of n multi-layering blocks. Each die element cuts each layered stream in half, and a multiple array of such die elements in series can produce a system of 2^{n+1} layers. In fact, 2-D nanotechnology-polymeric systems of up to 4,096 layers and layer thicknesses less than 100 nm have been successfully produced at CWRU, as illustrated in Figure 1.2. While most of the prior scavenging work was done on blend systems [7,9,10,12,15], our ultimate goal is to investigate the oxygen scavenging performance of multilayer systems.

While this result is encouraging and certainly practical, there is a need to understand the fundamental oxidation kinetics of these scavenging components. Our laboratories wish to contribute a fundamental investigation of oxygen scavenging polymers via a series of systematic studies. As a result, recent efforts have been made to characterize oxidation behaviors of 1,4 PB [16–19], another popular scavenging material.

1.2 OXYGEN SCAVENGING PERFORMANCE OF 1,4 POLYBUTADIENE

Catalytic oxidation of 1,4 polybutadiene has yielded two profound results. As illustrated in Figure 1.3, oxygen is immobilized at the reactive sites, and oxygen uptake increases with time until reaching equilibrium in 2-3 weeks [18]. This uptake can be several orders of magnitude higher than the intrinsic oxygen solubility of a 1,4 PB film, which is about 0.003 wt% at ambient conditions. The solubility of oxygen in 1,4-polybutadiene is 0.957 x 10^{-6} cm^3(STP)/(cm^3 Pa) [20]. Furthermore, reaction behavior was found a function of film thickness.

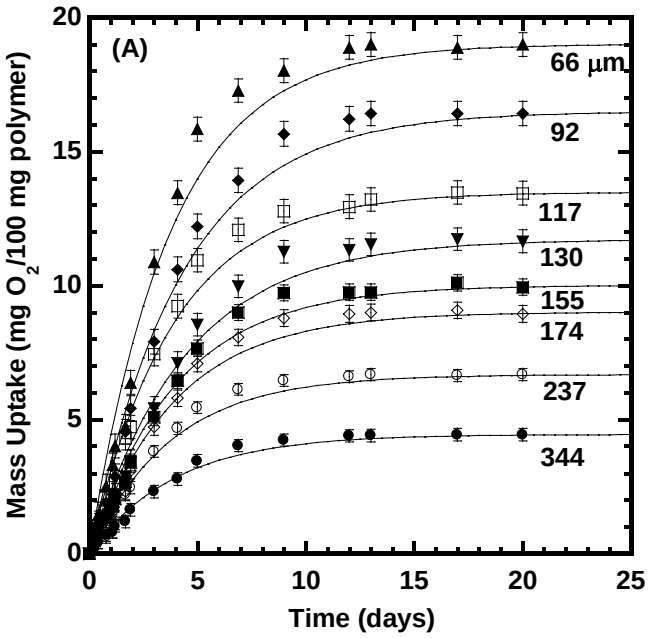

Figure 1.3: The oxidation kinetics of 1,4 polybutadiene monitored by oxygen mass uptake over time. The numbers in the Figure are the film thickness in micrometers [18].

Gas permeability values were found to be 2 to 3 orders of magnitude lower as a result of oxidation [18], as shown in Figure 1.4. Simultaneously these two phenomena of active scavenging and forming barrier structures function to improve barrier properties: As oxygen molecules are immobilized at reactive sites, the resulting oxidized films can self-retard oxygen permeance due to intrinsically low gas permeability. Both factors reduce oxygen permeance. Their combined effect in this material phenomenally improves its barrier properties.

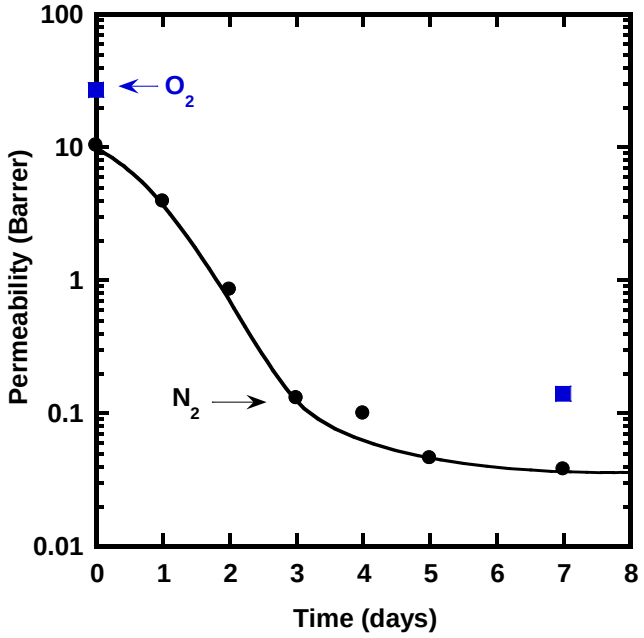

Figure 1.4: The oxidation kinetics of 1,4 polybutadiene monitored by gas permeation experiments over time [18].

1.3 MOTIVATION AND VISION

The extent of oxygen uptake in barrier experiments like these appears to plateau to an asymptotic value over times of the order of weeks or months [18]. The plateau value is essentially independent of film thickness when below a certain "critical thickness," but for thicker films the plateau value decreases with increasing thickness [21–23]. This complex process involves the physical dissolution of oxygen into the polymer, oxygen diffusing through the polymer, and reaction of the polymer with oxygen [24,25], with physical parameters being significantly affected by the chemical state of the OSP. There is ample evidence that the oxidation process is spatially heterogeneous, involving a moving front in thick films [17–19,21–23,26]. The apparent plateau in oxygen uptake for thick films does not mark a true end-point in the process but simply a greatly reduced rate of uptake limited by a much lower rate of diffusion through the oxidized layer; this reduction is attributed to changes in the intrinsic transport characteristics of the polymer due to the formation of polar structures during oxidation reactions and, of course, the growing thickness of this oxidized region.

Prior analyses of oxygen uptake by a scavenging polymer [18,27] have not adequately reduced the results to fundamental parameters that can subsequently be used to model the oxygen flux emerging from a blend or layered film during its functional lifetime, i.e., prior to the eventual breakthrough of oxygen when all the OSP has reached its scavenging capacity [26,28–31]. Implementation of this technique requires a judicious combination of experimental development of formulations, mathematical modeling, and determination of model parameters by matching models to experiments [17–19,26,28–31]. Elucidating these relationships and identifying the critical parameters is the focus of this dissertation.

1.4 DISSERTATION OUTLINE

There are seven chapters in this dissertation, including this introductory chapter. Chapter 2 discusses the fundamental theories of gas permeation, diffusion, and sorption in polymers, as well as principles of polymer degradation with a modified photo-oxidation mechanism in the presence of a metal catalyst. Previous theoretical models, important modeling parameters, and design equations are also briefly summarized. Materials and experimental techniques are presented in Chapter 3.

Chapter 4 discusses the characterization of oxygen scavenging capacity and kinetics of SBS films. A simple thin film kinetic model used to extract reaction parameters for future modeling work, as well as a semi-quantitative model describing thick film oxidation behavior at long oxidation times, are presented.

The establishment of adequate processing conditions via uptake experiment to ensure that active scavenging would still occur in spite of the demanding temperatures required for melt processing appears in Chapter 5.

Blend film oxidation behavior as characterized by permeation experiments as a function of useful parameters such as oxygen partial pressure, film thickness, and scavenger and photoinitator loadings are presented in Chapter 6, where measured time lags were also compared with the theoretically predicted values. Chapter 7 contains the conclusions and recommendations for future work.

1.5 REFERENCES

[1] R. Coles, M.J. Kirwan, Food and Beverage Packaging Technology, 2nd ed., John Wiley & Sons, Ltd, 2011.

[2] K.F. Finger, A.P. Lemberger, T. Higuchi, L.W. Busse, D.E. Wurster, Investigation and development of protective ointments IV. The influence of active fillers on the permeability of semisolids, Journal of the American Pharmaceutical Association. 49 (2006) 569–573.

[3] D.R. Paul, Effect of immobilizing adsorption on the diffusion time lag, Journal of Polymer Science Part A-2: Polymer Physics. 7 (1969) 1811–1818.

[4] D.R. Paul, D.R. Kemp, The diffusion time lag in polymer membranes containing adsorptive fillers, Journal of Polymer Science: Polymer Symposia. 41 (2007) 79–93.

[5] D.R. Paul, W.J. Koros, Effect of partially immobilizing sorption on permeability and the diffusion time lag, Journal of Polymer Science: Polymer Physics Edition. 14 (1976) 675–685.

[6] T.A. Blinka, F.B. Edwards, N.R. Miranda, D. V Speer, J.A. Thomas, Zeolite in Packaging Film, U.S. Patent US20010008662 A1, 1998.

[7] P.J. Cahill, S.Y. Chen, Oxygen scavenging condensation copolymers for bottles and packaging articles, U.S. Patent US6083585 A, 2000.

[8] M.A. Cochran, R. Folland, J.W. Nicholas, R. Robinson, Packaging, U.S. Patent 5,021,515, 1991.

[9] K. Katsumoto, T.Y. Ching, Multi-component Oxygen Scavenging Composition, U.S. Patent 5,776,361, 1998.

[10] D. V Speer, W.P. Roberts, C.R. Morgan, Methods and Compositions for Oxygen Scavenging, U.S. Patent US6449923 B1, 1993.

[11] D. V Speer, W.P. Roberts, C.R. Morgan, A.W. VanPutte, Multilayer structure for a package for scavenging oxygen, U.S. Patent US5350622 A, 1996.

[12] M. Stewart, R.N. Estep, B.B. Gamble, M.D. Clifton, D.R. Quillen, L.S. Buehrig, et al., Blends of oxygen scavenging polyamides with polyesters which contain zinc and cobalt, U.S. Patent WO2006063032 A3, 2006.

[13] S.N. Dhoot, B.D. Freeman, M. Stewart, Barrier Polymers, in: J.I. Kroschwitz (Ed.), Encyclopedia of Polymer Science and Technology, 3rd ed., Wiley-Interscience, New York, 2003: pp. 193–263.

[14] C.D. Mueller, S. Nazarenko, T. Ebeling, T.L. Schuman, A. Hiltner, E. Baer, Novel structures by microlayer coextrusion?talc-filled PP, PC/SAN, and HDPE/LLDPE, Polymer Engineering & Science. 37 (1997) 355–362.

[15] K. Katsumoto, T.Y. Ching, Goodrich, D. V Speer, Photoinitiators and oxygen scavenging composition, U.S. Patent 6,139,770, 2000.

[16] R.H. Li, Metal-catalyzed oxidation of polybutadiene in oxygen scavenging packaging application (Ph.D. Thesis), The University of Texas at Austin, 2010.

[17] H. Li, D.K. Ashcraft, B.D. Freeman, M. Stewart, M.K. Jank, T.R. Clark, Non-invasive headspace measurement for characterizing oxygen-scavenging in polymers, Polymer. 49 (2008) 4541–4545.

[18] H. Li, K.K. Tung, D.R. Paul, B.D. Freeman, Effect of film thickness on auto-oxidation in cobalt-catalyzed 1,4-polybutadiene films, Polymer. 52 (2011) 2772–2783.

[19] H. Li, K.K. Tung, D.R. Paul, B.D. Freeman, M. Stewart, J. Jenkins, Characterization of Oxygen Scavenging Films Based on 1,4-Polybutadiene, Industrial & Engineering Chemistry Research. 51 (2012) 7138–7145.

[20] G.J. Van Amerongen, Influence of structure of elastomers on their permeability to gases, Journal of Polymer Science. 5 (1950) 307–332.

[21] M. Coquillat, J. Verdu, X. Colin, L. Audouin, R. Nevière, Thermal oxidation of polybutadiene. Part 1: Effect of temperature, oxygen pressure and sample thickness on the thermal oxidation of hydroxyl-terminated polybutadiene, Polymer Degradation and Stability. 92 (2007) 1326–1333.

[22] M. Coquillat, J. Verdu, X. Colin, L. Audouin, R. Nevière, Thermal oxidation of polybutadiene. Part 2: Mechanistic and kinetic schemes for additive-free non-crosslinked polybutadiene, Polymer Degradation and Stability. 92 (2007) 1334–1342.

[23] M. Coquillat, J. Verdu, X. Colin, L. Audouin, R. Nevière, Thermal oxidation of polybutadiene. Part 3: Molar mass changes of additive-free non-crosslinked polybutadiene, Polymer Degradation and Stability. 92 (2007) 1343–1349.

[24] K.T. Gillen, R.L. Clough, Rigorous experimental confirmation of a theoretical model for diffusion-limited oxidation, Polymer. 33 (1992) 4358–4365.

[25] L.M. Rincon-Rubio, B. Fayolle, L. Audouin, J. Verdu, A general solution of the closed-loop kinetic scheme for the thermal oxidation of polypropylene, Polymer Degradation and Stability. 74 (2001) 177–188.

[26] S. Carranza, D.R. Paul, R.T. Bonnecaze, Design formulae for reactive barrier membranes, Chemical Engineering Science. 65 (2010) 1151–1158.

[27] S.W. Bigger, O. Delatycki, New approach to the measurement of polymer photooxidation, Journal of Polymer Science, Part A: Polymer Chemistry. 25 (1987) 3311–3323.

[28] M.C. Ferrari, S. Carranza, R.T. Bonnecaze, K.K. Tung, B.D. Freeman, D.R. Paul, Modeling of oxygen scavenging for improved barrier behavior: Blend films, Journal of Membrane Science. 329 (2009) 183–192.

[29] S. Carranza, D.R. Paul, R.T. Bonnecaze, Analytic formulae for the design of reactive polymer blend barrier materials, Journal of Membrane Science. 360 (2010) 1–8.

[30] S. Carranza, Modeling of Oxygen Scavenging Polymers and Composites (Ph.D. Thesis), The University of Texas at Austin, 2010.

[31] S. Carranza, D.R. Paul, R.T. Bonnecaze, Multilayer reactive barrier materials, Journal of Membrane Science. 399-400 (2012) 73–85.

Chapter 2: Background and Theories

2.1 FUNDAMENTALS OF GAS TRANSPORT IN POLYMER

Transport of small molecules through dense, non-porous polymeric membranes is described by the solution-diffusion model, first suggested by Graham in 1866 [1]. This model consists of three steps: 1) upstream penetrant molecules dissolve into the membrane, 2) the dissolved molecules diffuse through the polymer, and 3) penetrant desorbs from the membrane at its downstream surface. At steady state, the gas flux at any point inside the membrane is described by Fick's first law [2,3] :

$$N_A = -D\frac{dC}{dx} \tag{2.1}$$

where N_A is the molar flux of penetrant molecules A in the polymer, D is the diffusion coefficient of the penetrant molecules in the polymer, and C is the local concentration of the penetrant in the polymer. At steady state, integrating eq. (2.1) across the membrane thickness, l, yields the following:

$$N_A \int_0^l dx = -D \int_{C_1}^{C_2} dC \rightarrow N_A = -D\frac{C_2 - C_1}{l - 0} \tag{2.2}$$

The steady-state transport rate of penetrant through polymer films is characterized by a permeability coefficient, P , which is defined as follows [4,5],

$$P = \frac{N_A l}{p_2 - p_1} = \frac{C_2 - C_1}{p_2 - p_1} D \tag{2.3}$$

Permeability coefficients are often expressed in barrers, where 1 barrer = 1×10^{-10} $\frac{cm^3(STP)\cdot cm}{cm^2\cdot s\cdot cmHg}$. The equilibrium gas solubility coefficient is the ratio of the concentration of gas dissolved in the polymer divided by the continuous gas pressure. Assuming downstream pressure (p_1) is much less than upstream pressure (p_2), $C_1 << C_2$, permeability can then be rewritten as [3]:

$$S = C / p \rightarrow P = S \times D \tag{2.4}$$

where S is the apparent solubility coefficient at the upstream face of the film. Eq. (2.4) suggests that P depends on the product of two intrinsic properties. S is a thermodynamic term that relates to penetrant condensability and indicates the number of penetrant molecules sorbed into the polymeric film. D is a kinetic term that describes that penetrant molecules' mobility during the diffusion process in the polymeric membrane. Penetrant molecular size, polymer morphology, and affinity to the polymer matrix [3] can all influence diffusion coefficients, while solubility coefficients are sensitive to penetrant condensability [3].

Transport in systems that consist of multiple polymers, such as blend films and layered structures, can also be described. The permeability P_{blend} of a heterogeneous or immiscible blend, as in Figure 2.1, has often been described using the Maxwell model [6]

$$P_{blend} = P_c\left[1+3\phi_d\left(\left[\frac{P_d/P_c+2}{P_d/P_c-1}\right]-\phi_d\right)^{-1}\right] \tag{2.5}$$

where ϕ_d is the volume fraction of the dispersed polymer dispersed in blend films, and P_d and P_c are the gas permeability of the dispersed and continuous phase, respectively.

The Maxwell model was originally applied to permeation in systems in which the dispersed phase consisted of a low volume fraction of spherical particles. Another theoretically-based model, developed by Bruggeman, gives higher estimates of permeability than the Maxwell model when the low-permeability component is the continuous phase [7,8].

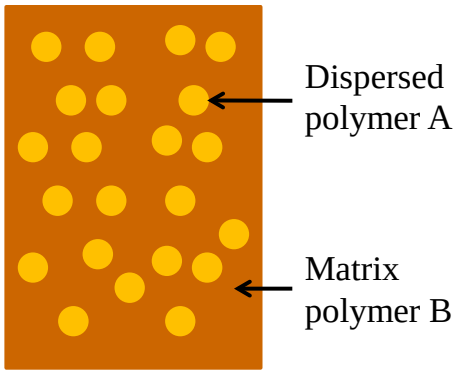

Figure 2.1: Polymer blend that consists of polymers A and B

2.2 POLYMER DEGRADATION DUE TO OXIDATION AND PHOTO-OXIDATION

The exposure of polymers to certain environmental conditions can lead to gradual polymer degradation involving chemical processes [9]. Many factors can play a role in degradation, including thermal [10–12] and radiative [13–19] processes, amongst others. Depending on the extent of degradation, the mechanical strength, elasticity, density, and other polymer physical properties and chemical structures can be altered [20]. Photo-oxidation is a type of oxidation that is facilitated by radiant energy, such as UV light. The

oxidative degradation occurs on the polymer surface in the presence of oxygen and can break up the polymer backbone, reducing the polymer's molecular weight. With time, oxidation progresses inwards, and the oxidized material typically loses its tensile strength, becoming more brittle. Other characteristics typical of photo-oxidation include discoloration and loss of surface smoothness.

2.2.1 Photo-oxidation of butadiene-containing polymers in the absence of metal catalyst

There have been multiple reports of photo-oxidation of polymers, especially on elastomeric butadiene-containing polymers [14–19]. Historically, there have been studies of photo-oxidation of polybutadiene at wavelengths > 300 nm [14]; a dedicated mechanistic study on the photo-oxidation of commercial polybutadiene [19]; and a series of photo-oxidation studies on elastomeric polybutadiene, 1,2-polybutadiene, and styrene-butadiene-styrene copolymer [15–17]. These studies have addressed polybutadiene oxidation and identified several intermediates in the auto-oxidation chain. Some also included valuable kinetic studies related to the formation of O-containing products, such as hydroxyl and carbonyl groups. Clearly the phenomenon of photo-oxidation on commercial butadiene-containing polymers is of longstanding interest.

2.2.2 Photo-oxidation of butadiene-containing polymers in the presence of metal catalyst

In Beavan’s mechanistic work [19], a plausible mechanism was introduced to describe the photo-oxidative process on polybutadiene, which is the primary butadiene in the current work on Styrene-Butadiene-Styrene (SBS) block copolymer. An additional

step to Beavan's mechanistic work is necessary to account for diradical formation by benzophenone photo-initiation prior to the actual oxidation. UV light is first absorbed by the benzophenone, which yields a diradical molecule with two unpaired electrons. The benzophenone diradical then abstracts a hydrogen atom on the alpha carbon to the double bond and forms a butadiene radical that is considered a reactive site available for oxidation. Subsequent oxidation and proton abstraction yield a hydroperoxide intermediate that is essential to forming later structures with oxygen-containing functional groups.

The concentration of oxidative sites (butadiene radicals) is a function of photoinitator content and the total amount of UV energy [19]. As benzophenone photoinitiator (PI) absorbs UV energy, radicals are released, and through oxidation hydroperoxides form on the oxidative sites [19]. In other words, the number of sites available for oxidation can be increased by greater UV exposure time (the total UV energy required to release benzophenone diradicals) and/or by higher PI content (number of available benzophenone diradicals) [19]. This part of the oxidation mechanism is shown in Figure 2.2.

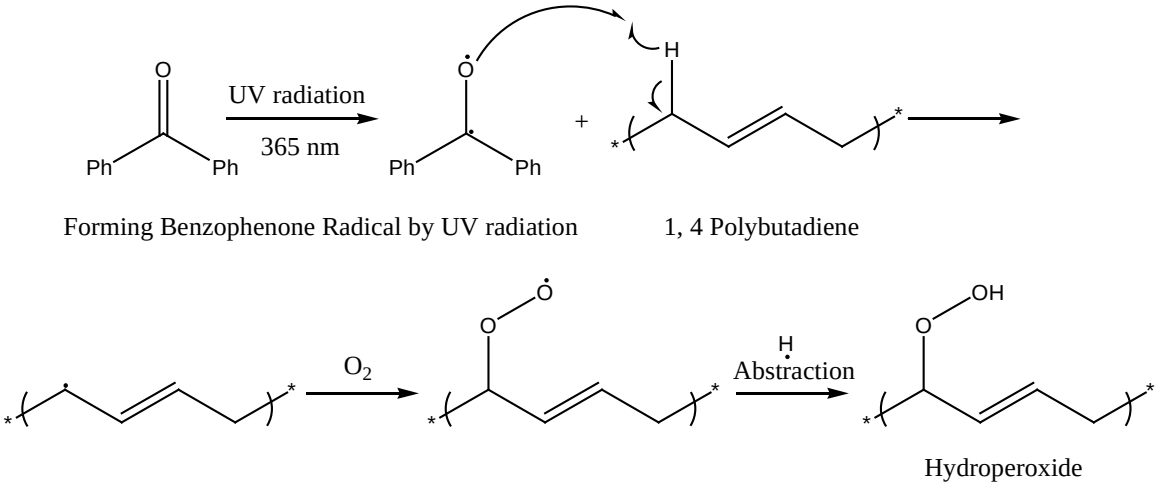

Figure 2.2: As benzophenone absorbs UV energy, radicals are released and form hydroperoxide through oxidation. Clearly the available amount of oxidative sites is a function of PI content and UV exposure [19].

It is documented that, among the heavy metals, cobalt can undergo hydroperoxide decomposition most effectively [21]; thus it was chosen as the catalytic agent to form oxidation products from the hydroperoxide intermediate. Cobalt decomposes hydroperoxide and produces carbon-oxygen radicals that can either rearrange to form carbonyls and release hydrogen radicals that form water, or abstract hydrogen to form alcohols. Catalytically decomposed hydroperoxides oxidize to form structures with oxygen-containing functional groups. Clearly, the rate of oxidation is governed largely by the catalyst concentration. In other words, the oxidation rate increases with increasing catalyst content. This part of the oxidation mechanism is shown in Figure 2.3.

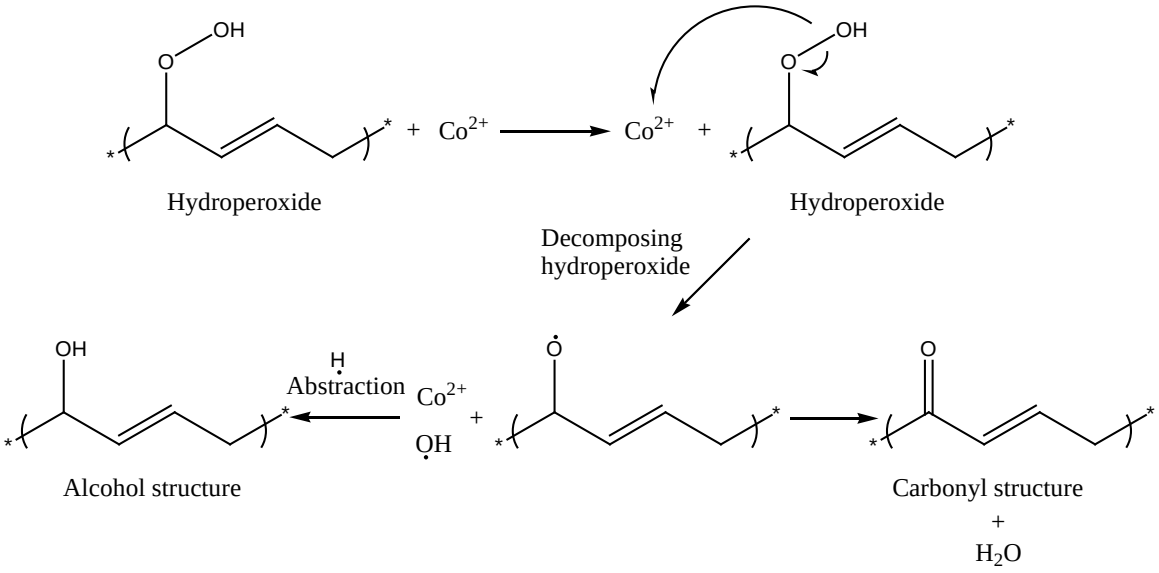

Figure 2.3: Catalyst-decomposed hydroperoxides oxidize to form structures with O-containing functional groups. As a result, rate of oxidation is directly correlated with catalyst loading [19].

2.2.3 Secondary reactions

Beavan's work also proposed a few secondary reactions [19], shown in Figure 2.4. In addition to the primary oxidation products A1 and B1, Beavan proposed other secondary reactions that would form A2, B2, and B3 via β-scission of the alkoxy radical [19]. The message here is that oxidation is a complex process involving multiple chemical steps. This adapted mechanism attempts to define the roles of additives, and the effect of which on reaction parameters such as the effective reaction rate constant k_R and effective stoichiometric oxidation coefficient $\hat{\nu}$ will be discussed in this dissertation.

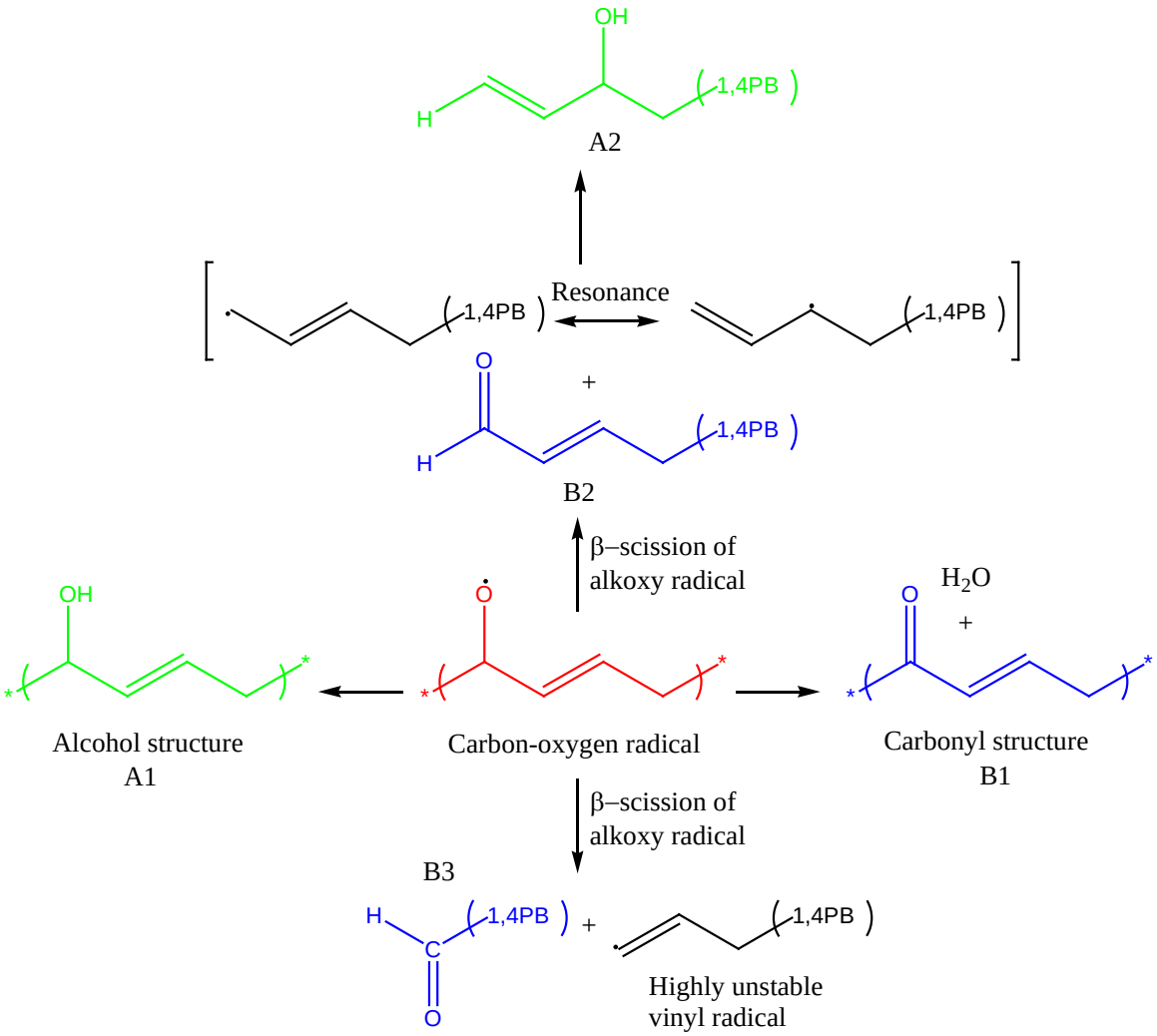

Figure 2.4: A variety of oxidation products can form due to secondary reactions. Carbon-oxygen radicals can proceed to form products that may potentially change the values of $\hat{v}$, the stoichiometric oxidation coefficient [19].

2.2.4 Summary

In summary, the photoinitiator (PI) content and length of UV exposure directly influence the number of sites initially activated for oxidation. More sites will become activated for oxidation if films are loaded with higher PI content and/or experience longer

UV exposure (higher total UV energy). The number of sites available for oxidation influences the degree of primary and secondary reactions. On the other hand, oxidation rate may be a function of catalyst loading. In other words, a scavenger film loaded with more cobalt catalyst may undergo faster oxidation. As a result, the rate of oxidation is directly related to the value of the effective reaction rate constant k_R.

2.3 METAL-CATALYZED OXIDATION

A specific type of metal-catalyzed oxidation uses the transition metal and its ability to switch between several oxidation states and to accommodate various coordination numbers to facilitate reaction of organic substrates [21]. The catalytic oxidation of polymer, similar to any other ionic or radical reaction, consists of the steps of initiation, propagation, and termination [22]. Typically an initiator is necessary to start the reaction. Some common initiators include, but are not limited to, α,α-azobisisobutyronitrile and benzophenone. In oxidation, an alkyl hydroperoxide (ROOH, where R represents the polymer structure) is commonly formed as an intermediate through oxidation. The hydroperoxide intermediate typically can be decomposed by the transition metal catalyst [21]. This is considered the most common pathway for catalysis in metal-catalyzed polymer autoxidation [21].

In metal-catalyzed oxidation, the presence of transition metal ions helps with two things: 1) production of free radicals that initiate oxidation, and 2) decomposition of intermediate hydroperoxide that proceeds the propagation steps. Clearly, the rate of oxidation is related to metal catalyst concentration until the catalyst reaches a certain concentration, above which addition of metal catalyst no longer impacts the reaction rate. This effect is observed in autoxidation catalyzed by cobalt catalyst [23].

2.3.1 Metal-catalyzed oxidation of polybutadiene in oxygen scavenging packaging application

Recently there was a series of experimental studies on the metal-catalyzed oxidation of butadiene-containing polymer, specifically 1,4 polybutadiene [24]. Li reported the scavenging and barrier properties of 1,4 polybutadiene. Li found that, when a metal catalyst was added to films of 1,4 polybutadiene, 1,4 polybutadiene underwent accelerated oxidation [14–16,19,25,26]. In addition, Li reported that 1,4 polybutadiene oxidation behavior was correlated with catalyst loading, film thickness, oxygen partial pressure, and temperature [27,28]. In oxygen uptake experiments that studied the effect of catalyst loading at constant temperature (30 °C) and pressure (ambient condition), reactive films of 1,4 polybutadiene at ~ 100 μm can sorb approximately 15 wt% oxygen over a week [29].

Analytical techniques such as FTIR and XPS analysis confirm the existence of oxidation at film surfaces, whereas the film interiors remained less oxidized. Moreover, oxygen uptake exhibited a maximum with catalyst loading [29]. As a result, it was reported that oxygen scavenging in butadiene containing polymer proceeds as a type of a heterogeneous oxidation that is a function of catalyst loading [29].

Effect of film thickness on oxidation behavior was also studied in 1,4 polybutadiene films containing 200 ppm of cobalt catalyst [30]. Thick films of different thicknesses (thickness varied from 66 μm to 344 μm) were oxidized in air, and they showed an increasing oxygen uptake with decreasing film thicknesses when normalized by polymer mass, while the area-normalized oxygen uptake remained independent of thickness. Thus there was an oxidizing front progressing from film surfaces towards the film center as a characteristic of a heterogeneous oxidation [30].

On the other hand, films that are thinner than 6 μm appear to oxidize homogeneously, as indicated by their oxygen uptake per unit mass being essentially independent of thickness [30]. The oxidation in thin films appeared to have a faster reaction rate than that in thicker films as thin films typically exhibit higher oxygen uptake value at ~ 30 wt % (thin film experiment typically reached a constant uptake value in 1 – 2 days).

Clearly, there is an outside oxidized layer that forms at film surfaces. Li used two separate techniques to estimate the thickness of these layers when left oxidized for a long times [30]. Recognizing that oxygen uptake is a function of thickness, Li plotted the uptake data against inverse thicknesses and found the critical oxidized layer thickness by using a simple model of surface oxidation [30]. Scanning electron microscopy (SEM) was used to examine the cross sections of oxidized 1,4 polybutadiene; SEM images showed a scalloped, layered structure, which implied that heterogeneous oxidation occurred in thicker films [30].

Li's work suggested that the rate of oxidation was related to two parameters: (1) the number of reactive sites in 1,4 polybutadiene, and (2) the tortuosity in the diffusional pathway of the oxygen molecules to penetrate the highly oxidized region and reach unoxidized regions in 1,4 polybutadiene film center. These factors naturally contribute to the oxidation process, which exhibited a period of acceleration and then slowed down. To test these hypotheses, both nitrogen and oxygen permeability were measured and found to be 2 orders of magnitude lower than in unoxidized samples [30].

Consequently, a two-phase model was developed to use the measured permeability data for estimating the gas permeability of 1,4 polybutadiene thick film as a result of oxidation. This simple model consisted of oxidized layers at outer film surfaces

and an unoxidized interior with a thickness corresponding to the critical thickness mentioned above. The estimated permeability coefficients in thick films agreed well with the experimental data, supporting the physical validity of the two-phase model [30]. Consequently, this thin film oxidation experiment made two valuable contributions: 1) thin layers of polybutadiene might offer more efficient use of the polymer, and 2) permeability coefficients from thin film oxidation may be used for modeling simulation in oxygen scavenging packaging applications.

In addition to investigating catalyst loading and film thickness effects on oxidation behavior, Li also reported interesting findings on uptake at various temperatures [24]. When oxidized between -20 and 45 ºC, polybutadiene exhibited different oxidation kinetics and final oxygen uptake values. Specifically, a sample oxidized at 45 ºC has a similar oxygen uptake but a faster rate of oxidation than the 30 ºC-oxidized sample. On the other hand, the sample oxidized at 5 ºC appears to oxidize much more slowly, but also more homogenously, than at higher temperatures. The lower temperature sample had higher oxygen uptake as well. In Li's oxygen partial pressure studies, oxygen uptake was higher and the rate of oxidation faster in experiments with higher oxygen partial pressure [24].

2.4 MODELING OF METAL-CATALYZED OXYGEN SCAVENGING POLYMERS

The large array of experimental variable combinations in oxygen barrier behavior makes modeling and simulation reasonable ways to proceed, especially since the significant time lag of transient permeation limits the number of experiments that can be performed within the reasonable scope of this project. Using analogous models, we hope to predict the optimal structure – blend, layered, or both – for barrier performance. The

modeling work is being done in collaboration with Dr. Susana Carranza and Prof. Roger Bonnecaze at the University of Texas at Austin.

2.4.1 Modeling of oxygen scavenging polymers and composites

Modeling studies of reactive barrier materials are based on our ongoing work with reactive homogeneous films [31] and polymer blends [32,33] of butadiene-containing block copolymers. In Carranza's work, oxidation was assumed to be dependent on both the concentrations of the mobile species and of the immobilized reactive sites [34]. Carranza and coworkers developed a set of non-linear partial differential equations, which were solved numerically to reveal three distinct regimes: early, intermediate and long times [34].

A shrinking core model, shown in Figure 2.5, simulates oxygen fluxes exiting the downstream surface of the reactive blend film, in which reactive particles are dispersed in a permeable but nonreactive matrix polymer. This model assumes the oxidation rate to be much faster than the diffusion process in the shell: that is, oxidation occurs instantaneously when oxygen reaches the surface. As a result, scavenging material is consumed, the radius of the reactive polymer core decreases with time, and the shell of the oxidized scavenging polymer thickens [32].

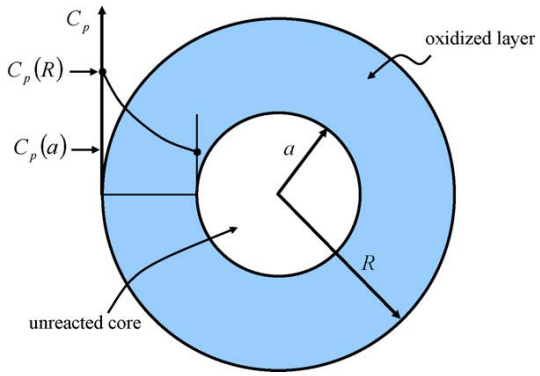

Figure 2.5: Shrinking core model for diffusion and reaction mechanisms within an oxygen scavenging particle within a blend film [32]. $C_p(R)$ and $C_p(a)$ is the oxygen concentration at outer radius R and at the radius of oxidizing core a, respectively.

One practical parameter that can be improved when in reactive membranes with better barrier properties is the time lag, θ, which is the amount of time it takes to exhaust reactive sites at long times. However, solutions and asymptotic analysis of Carranza's simulation model revealed that early and intermediate time behaviors are as important as those at long times. Moreover, equations that predict the barrier performance for all three time regimes were analytically developed, reducing the challenge of solving for coupled non-linear differential equations.

For barrier applications, it is important to know the values of time lags of typical packaging materials, such as polystyrene (PS) and polyethylene teraphthlate (PET): For a 200 μm film, $\theta_{0,PET} \sim 3.3\ hr$ and $\theta_{0,PS} \sim 0.14\ hr$. Clearly the time lag when PET is used as the matrix polymer incorporated with reactive particles can be very long. The oxygen diffusion coefficient is 5.6×10^{-9} and $1.4 \times 10^{-7}\ cm^2/sec$ for PET [35] and PS [36], respectively. These time lags ($\theta_0 = \frac{L^2}{6 \times D}$) were calculated for non-reactive systems.

Using the reactive barrier film as the primary model, another model was developed for polymer blends containing reactive particles, and the three regimes observed for homogeneous films held true for blends. This multiscale model, illustrated in Figure 2.6, uses average effective properties to model transport throughout the entire film and expands the methodology developed for homogeneous films. Analytical design equations were again developed for each regime and are, as expected, very similar to those for homogeneous films. There are a few significant differences between reactive barrier membranes and reactive blends, such as the volume fraction of the polymer blend and various reaction rate constants that describe oxidation rates in different structures. As a result, the dimensionless parameter groups used in the analysis and equations are defined differently [32,33].

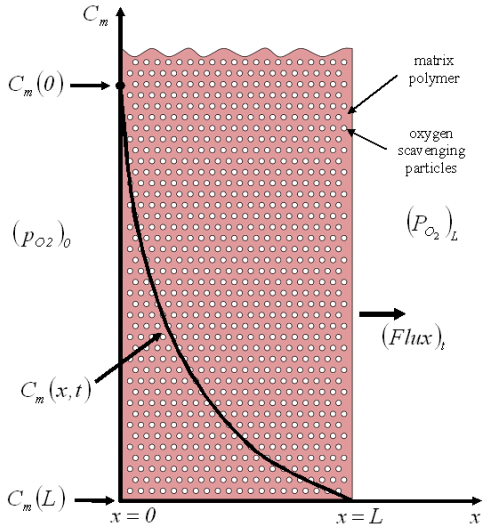

Figure 2.6: Spherical reactive particles are evenly and continuously dispersed within matrix polymer. Shrinking cores assumed reaction is fast compared to diffusion, and as the radius of the unreactive core decreases with time, oxygen concentration decreases in the film [32]. $C_m(0)$ and $C_m(L)$ is the oxygen concentration in the matrix polymer at position $x = 0$ and L, respectively. $P_{O_2}(0)$ and $P_{O_2}(L)$ is the oxygen partial pressure at the upstream and downstream side of the matrix membrane, respectively. $C_m(x,t)$ describes the oxygen concentration at any time at any position, and $(Flux)_t$ describes the quantity of oxygen penetrant exiting the downstream face in the matrix polymer.

A leakage permeation, i.e., the flux from the downstream film surface that occurs before steady state is achieved, is predicted by the current modeling work [32,33]. Figure 2.7a shows the effect of the reaction rate constant on the downstream accumulation of oxygen, Q_t, versus time. The cumulative oxygen value approaches an asymptote that extrapolates to θ on the time axis, except in the case where no scavenging occurs, i.e., k = 0. Figure 2.5b shows the leakage flux versus time profile in log scale.

Such logarithmic-scaled plots show two points of rapid increase in oxygen flux: at times of the order of θ_0, and at times of the order of θ, with a plateau region in between. The cumulative flux is lower with higher reaction rate parameters; i.e., as the scavenging reactions becomes faster (larger reaction rate constant) more oxygen is scavenged, so less oxygen can diffuse through the downstream film surface, resulting in lower leakage plateau flux.

Carranza also did initial modeling [34] to describe the transient mass uptake in a diffusion-limited reactive film by oxygen uptake experiments. Guided by experimental evidence that the diffusion coefficient is reduced as the polymer oxidizes, the model incorporates an effective diffusivity that is a function of the number of reactive sites [34]. Similarly, three regimes were observed and analytical design equations were developed to estimate oxygen uptake at early and long times, in excellent agreement with the experimental data for all data sets.

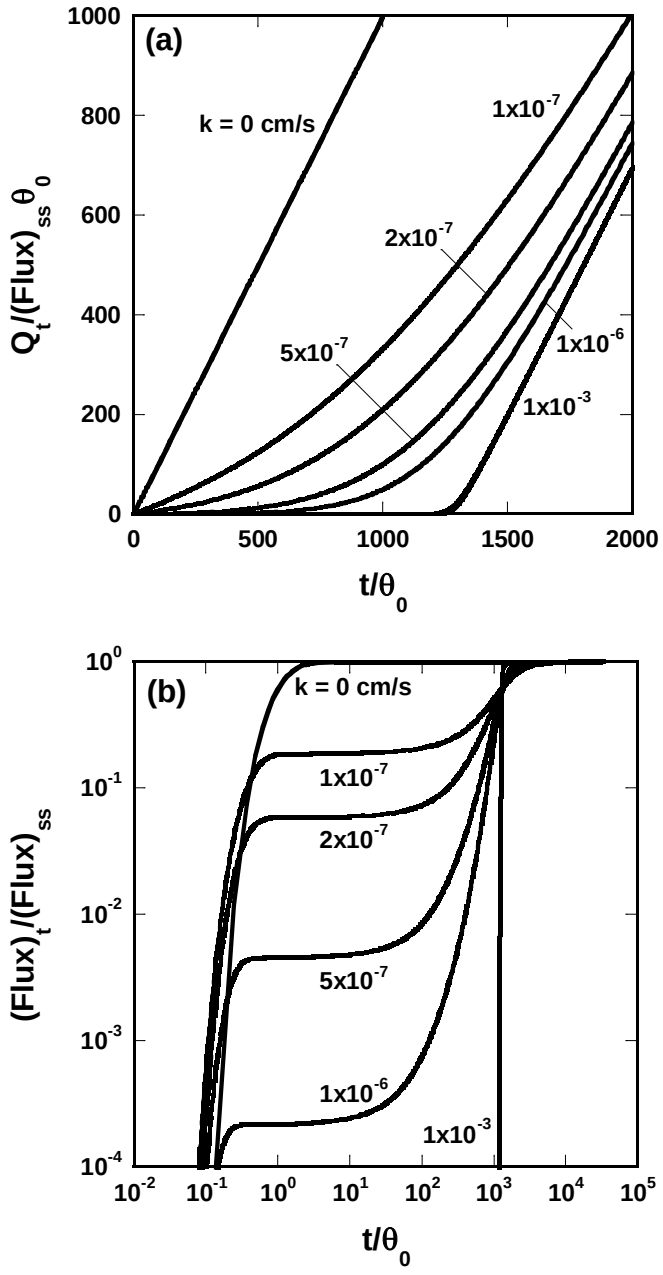

Figure 2.7: (a) Predicted transient permeation behavior for a blend film; (b) leakage flux charted using a log scale [32]. $Q_t/(Flux)_{ss}\theta_0$ is the dimensionless quantity of the cumulative amount of permeate Q_t normalized by the steady state flux, $(Flux)_{ss}$ and the time lag without scavenging θ_0. $(Flux)_t/(Flux)_{ss}$ is the dimensionless quantity of the flux at any time, $(Flux)_t$, normalized by the steady state flux.

2.4.2 Nomenclature and modeling parameters

This section summarizes parameters developed in the simulation work and their nomenclature in Table 2.1:

Table 2.1: Useful parameters and their nomenclature developed in modeling work

Parameter	Definition	Example value/ expression	Unit	Ref
$\boldsymbol{A_0}$	Initial reactive polymer particle surface area	$4\pi R^2$	cm^2	[32]
$\boldsymbol{\beta}$	reactive polymer capacity to consume O_2 when fully oxidized	$\frac{n_0}{\hat{v}}$	$\frac{mol_{O_2}}{cm^3 polymer}$	[33]
$\boldsymbol{\beta_{100}}$	β at 100 ppm Co^{2+} loading	7.9×10^{-3}	"	[33]
$\boldsymbol{\beta_{200}}$	200 ppm	7.8×10^{-3}	"	[33]
$\boldsymbol{\beta_{400}}$	400 ppm	7.3×10^{-3}	"	[33]
$\boldsymbol{\beta_{800}}$	800 ppm	6.5×10^{-3}	"	[33]
$\boldsymbol{C_{m,0}}$	O_2 concentration at membrane upstream	$S_m \cdot P_{O_{2,0}}$	$\frac{mol}{cm^3}$	[32]
$\boldsymbol{D_m}$	O_2 diffusivity of matrix polymer (Polystyrene)	P_m/S_m	$\frac{cm^2}{sec}$	[32]
$\boldsymbol{D_p}$	O_2 diffusivity of fully oxidized reactive polymer	3×10^{-8}	$\frac{cm^2}{sec}$	[32]
$\boldsymbol{Flux_{plat}}$	Plateau leakage flux	$2J_{SS}\Phi_b e^{-\Phi_b}$	$\frac{mol}{cm^2 \cdot sec}$	[33]
$\boldsymbol{H}$	Partition coefficient	S_m/S_p	ND	[32]
$\boldsymbol{J_{SS}}$	Steady state flux	$\frac{C_{m,0} \times D_m}{L}$	$\frac{mol}{cm^2 \cdot sec}$	[33]
$\boldsymbol{k = k_R}$	Reaction rate constant of reactive polymer particle		$\frac{cm^3}{mol_{PB} \cdot sec}$	[32] [33]
$\boldsymbol{k_{R,100}}$	k_R at 100 ppm Co^{2+} loading	7.9	"	[36]
$\boldsymbol{k_{R,200}}$	200 ppm	17.1	"	[36]
$\boldsymbol{k_{R,400}}$	400 ppm	25.3	"	[36]
$\boldsymbol{k_{R,800}}$	800 ppm	48.3	"	[36]

Table 2.1: Continued

k_p	Effective surface reaction rate constant in the moving front regime	$\left(D_p k_R n_0\right)^{1/2}$	$\frac{cm}{sec}$	[33]
L	Reactive blend film thickness	70	μm	[32]
m	Scavenger morphology	3: spherical 2: cylindrical	N/A	[33]
n_0	Initial butadiene concentration in polymer	0.0122	$\frac{mol_{PB}}{cm^3 polymer}$	[36]
P_p	O_2 permeability of fully oxidized reactive polymer	1.8×10^{-15}	$\frac{mol \cdot cm}{cm^2 \cdot s \cdot cm\, Hg}$	[36]
P_m	O_2 permeability of matrix polymer (Polystyrene)	1.4×10^{-14}	$\frac{mol \cdot cm}{cm^2 \cdot s \cdot cm\, Hg}$	[36]
$P_{O_2,0}$	O_2 pressure at upstream	3	atm	[32]
		228	$cm\, Hg$	[32]
R	reactive polymer radius	1	μm	[32]
S_m	O_2 solubility of matrix polymer (Polystyrene)	1.0×10^{-7}	$\frac{mol}{cm^3 \cdot cm\, Hg}$	[32]
t_{onset}	Onset of the initial plateau	$\frac{R^2 S_m}{6\phi P_p \Phi_p} \times$ $[\Phi_b \coth(\Phi_b) - 1]$	sec	[33]
t_{sf}	Steady front time (as leakage ends)	$\frac{R^2 n_0}{6\hat{v} P_{O_2} P_p \Phi_p}$	sec	[33]
V_0	Initial reactive polymer particle volume	$4\pi R^3/3$	cm^3	[33]
$\hat{v}$	Oxidation stoichiometric constant		$\frac{mol_{PB}}{mol_{O_2}}$	[36]
$\hat{v}_{100}$	$\hat{v}$ at 100 ppm Co^{2+} loading	1.54	"	[36]
$\hat{v}_{200}$	200 ppm	1.56	"	[36]
$\hat{v}_{400}$	400 ppm	1.67	"	[36]
$\hat{v}_{800}$	800 ppm	1.88	"	[36]
Φ_p	Thiele modulus of reactive polymer particle	$\left(R^2 k_R n_0 / D_p\right)^{1/2}$	ND	[33]
Φ_b	Thiele modulus of reactive blend	$\frac{L}{R}\left(\frac{3\phi P_p}{P_m}\right)^{1/2} \Phi_p^{1/2}$	ND	[33]
τ	Characteristic time	$R/3k_p$: spherical $R/2k_p$: cylindrical	sec	[33]
ϕ	Scavenger vol. fraction	0.2	ND	[32]

2.4.3 Equations used to define permeation behaviors in blend films

Practically speaking, there are four parameters that define the characteristics of a leakage flux through reactive blend films: leaking amount, start (onset) time, end (steady front) time, and time lag due to scavenging [33]. This section summarizes a few useful equations developed in the simulation on reactive blend film.

Oxygen molecules are immobilized at the reactive sites in blend films. Ideally they will all be scavenged, but it has been predicted that oxygen could permeate and avoid being captured, resulting in a "leakage" flux, as illustrated in Figure 2.6.

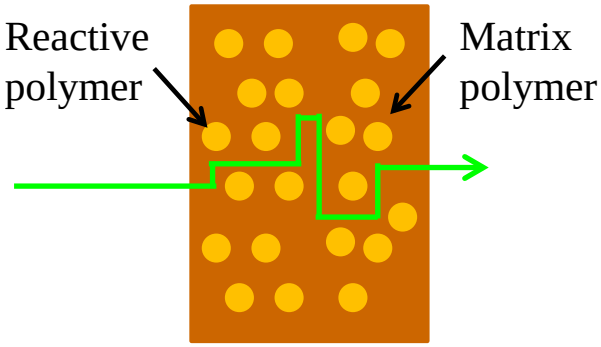

Figure 2.6: Leakage flux occurs when penetrant avoids being immobilized at reactive sites [32,33].

Leakage plateau flux, $Flux_{plat}$, is expressed as follows [33]:

$$Flux_{plat} = \frac{\Phi_b J_{ss}}{\sinh(\Phi_b)}, or\ 2J_{SS}\Phi_b e^{-\Phi_b}, in\ the\ limit\ of\ \Phi_b \gg 1 \qquad (2.7)$$

where Φ_b is the Thiele Modulus of the polymer blend film and $J_{SS} = D_m C_m(0)/L$ is the steady state flux exiting downstream when all reactive sites have been consumed.

The onset of the initial plateau, t_{onset} is defined as follows [33]:

$$t_{onset} = \tau \frac{\Phi_b \coth(\Phi_b) - 1}{2\phi/H} \tag{2.8}$$

where ϕ is the reactive polymer volume fraction in the blend film, $H = S_m/S_p$ is a partition coefficient relating the O_2 solubility of the polymer matrix, S_m, to the O_2 solubility of the oxidized polymer S_p, and $\tau = \frac{V_0}{A_0 k_p}$ is the characteristic time of polymer with various shapes (for a spherical reactive polymer particle $\frac{V_0}{A_0} = \frac{R}{3}$, and for a cylindrical reactive polymer $\frac{R}{2}$).

The steady front time, t_{sf}, is the time when the leakage flux ends and transitions to a fast rise in the downstream flux, and can be expressed as

$$t_{sf} = \tau \frac{H}{2\nu\phi} \tag{2.9}$$

where $\nu = \frac{\hat{\nu} C_m(0)}{\phi n_0}$ is the ratio between dissolved oxygen concentration and reactive polymer capacity. $C_{m,0} = S_m \cdot P_{O_2}$ is the O_2 concentration at the upstream face in the membrane, n_0 describes the polymer reactive capacity, and $\hat{\nu}$ is the stoichiometric oxidation coefficient.

The time lag due to scavenging, θ, is dependent on the oxygen solubility in the matrix polymer, as shown in the following [32]:

$$\frac{\theta}{\theta_0} = 1 + \frac{3\phi\beta}{C_m(0)} = 1 + \frac{3\phi n_0}{\hat{\nu} S_m(0) P_{O_2}} \tag{2.10}$$

where β is the reactive polymer oxidation capacity [32].

Clearly, increasing $C_m(0)/\beta$ accelerates the rate of change of the shrinking core radius, resulting in an increase in θ/θ_0. Increasing ϕ accelerates the rate of oxygen concentration within the matrix, resulting in an increase of θ/θ_0. The time lag extension is independent of the reaction rate constant k_R and the scavenging reaction kinetics.

In addition to the equations above, a couple of useful analytical equations were developed to express the total oxygen permeation through the membrane, as well as the transient flux at intermediate times after plateau flux. The total oxygen permeate through the membrane, Q_t, is obtained by integration of the downstream flux and can be expressed as [33]:

$$Q_t = \frac{2J_{ss}t_{SF}\Phi_b}{\exp(\Phi_b)}(1 + \nu(1 - \Phi_b) + b(\exp\left(\sqrt{\frac{t}{t_{SF}}}\right) - e)) \quad (2.11)$$

The intermediate flux is algebraically expressed as the following [33]:

$$Intermediate\ Flux = bJ_{ss}\frac{L/x_F}{\exp(\Phi_b(1-x_F/L))} \quad (2.12)$$

2.5 SUMMARY

Although reactive barrier materials in complex structures have been used in industry, the fundamental issues associated with incorporating a scavenging polymer with a metal catalyst are not well understood; reports on the effect of cobalt catalyst loading include only a limited number of catalyst concentrations and a fixed number of layers. There have been several kinetic and mechanistic studies of oxidation in the presence of metal catalyst and photo-oxidation. However, no attempts have been made to understand the scavenging kinetics on photo-initiated and/or metal-catalyzed oxidation. Furthermore,

there is no available methodology for predicting performance of any given formulation for optimization [37]. A mathematical scavenging model that can simulate an array of experimental variables within a short amount of time would thus be very useful [38–43]. Part of the proposed research effort involves developing such models to understand these issues as well as to predict performance using preliminary data. The model can be some combination of: (1) simulating oxygen consumption by reaction using reactive polymers and (2) treating oxygen diffusion in the matrix polymer as a one-dimensional approximation.

2.6 REFERENCES

[1] T. Graham, On the absorption and dialytic separation of gases by colloid septa, Philosophical Magazine and Journal of Science. 32 (1866) 401–420.

[2] W.J. Koros, Barrier Polymers and Structures: Overview in Barrier Polymers and Structures, American Chemical Society, Washington, D. C., 1990.

[3] Y. Yampolskii, I. Pinnau, B. Freeman, Materials Science of Membranes for Gas and Vapor Separation, John Wiley & Sons, Ltd, Chichester, UK, 2006.

[4] K. Ghosal, B.D. Freeman, Gas separation using polymer membranes: an overview, Polymers for Advanced Technologies. 5 (1994) 673–697.

[5] J.G. Wijmans, R.W. Baker, The solution-diffusion model: a review, Journal of Membrane Science. 107 (1995) 1–21.

[6] J.C. Maxwell, A Treatise on Electricity and Magnetism, Clarendon Press, 1873.

[7] J.H. Petroupoulos, Mechanisms and Theories for Sorption and Diffusion of Gases in Polymers, CRC Press, 1994.

[8] J. Crank, The Mathematics of Diffusion, 2nd ed., Oxford University Press, Oxford, 1975.

[9] M.C. Celina, R.L. Clough, G.D. Jones, Interactive Behavior in Polymer Degradation, in: M.C. Celina, R.A. Assink (Eds.), Polymer Durability and Radiation Effects, American Chemical Society, Washington, DC, 2007: pp. 37–47.

[10] M. Coquillat, J. Verdu, X. Colin, L. Audouin, R. Nevière, Thermal oxidation of polybutadiene. Part 1: Effect of temperature, oxygen pressure and sample thickness on the thermal oxidation of hydroxyl-terminated polybutadiene, Polymer Degradation and Stability. 92 (2007) 1326–1333.

[11] M. Coquillat, J. Verdu, X. Colin, L. Audouin, R. Nevière, Thermal oxidation of polybutadiene. Part 2: Mechanistic and kinetic schemes for additive-free non-crosslinked polybutadiene, Polymer Degradation and Stability. 92 (2007) 1334–1342.

[12] M. Coquillat, J. Verdu, X. Colin, L. Audouin, R. Nevière, Thermal oxidation of polybutadiene. Part 3: Molar mass changes of additive-free non-crosslinked polybutadiene, Polymer Degradation and Stability. 92 (2007) 1343–1349.

[13] S.W. Bigger, O. Delatycki, New approach to the measurement of polymer photooxidation, Journal of Polymer Science, Part A: Polymer Chemistry. 25 (1987) 3311–3323.

[14] M. Piton, A. Rivaton, Photooxidation of polybutadiene at long wavelengths ($\lambda >$ 300 nm), Polymer Degradation and Stability. 53 (1996) 343–359.

[15] C. Adam, J. Lacoste, J. Lemaire, Photo-oxidation of elastomeric materials. 1. Photooxidation of polybutadienes, Polymer Degradation and Stability. 24 (1989) 185–200.

[16] C. Adam, J. Lacoste, J. Lemaire, Photo-oxidation of elastomeric materials: Part II—Photo-oxidation of styrene-butadiene copolymer, Polymer Degradation and Stability. 26 (1989) 269–284.

[17] C. Adam, J. Lacoste, J. Lemaire, Photo-oxidation of elastomeric materials: Part IV—Photo-oxidation of 1,2-polybutadiene, Polymer Degradation and Stability. 29 (1990) 305–320.

[18] K. Katsumoto, T.Y. Ching, Goodrich, D. V Speer, Photoinitiators and oxygen scavenging composition, U.S. Patent 6,139,770, 2000.

[19] S.W. Beavan, D. Phillips, Mechanistic Studies on the Photooxidation of Commercial Polybutadiene, European Polymer Journal. 10 (1974) 593–603.

[20] L. Audouin, V. Langlois, J. Verdu, J.C.M. Bruijn, Role of oxygen diffusion in polymer ageing: kinetic and mechanical aspects, Journal of Materials Science. 29 (1994) 569–583.

[21] R.A. Sheldon, J.K. Kochi, Metal Catalysis in Peroxide Reactions, in: Metal-catalyzed Oxidation of Organic Compounds, Academic press, New York, 1981: pp. 38–48.

[22] J. Wise, K.T. Gillen, R.L. Clough, Quantitative model for the time development of diffusion-limited oxidation profiles, Polymer. 38 (1997) 1929–1944.

[23] J.N. Morris, L. Reich, S. Stivala, Elements of Polymer Degradation, McGraw-Hill Book Company, New York, 1972.

[24] R.H. Li, Metal-catalyzed oxidation of polybutadiene in oxygen scavenging packaging application (Ph.D. Thesis), The University of Texas at Austin, 2010.

[25] R.G. Bauman, S.H. Maron, Oxidation of Polybutadiene. I. Rate of Oxidation, Journal of Polymer Science. 22 (1956) 1–12.

[26] D.J. Nagle, M. Celina, L. Rintoul, P.M. Fredericks, Infrared microspectroscopic study of the thermo-oxidative degradation of hydroxy-terminated polybutadiene/isophorone diisocyanate polyurethane rubber, Polymer Degradation and Stability. 92 (2007) 1446–1454.

[27] D. V Speer, W.P. Roberts, C.R. Morgan, Methods and Compositions for Oxygen Scavenging, U.S. Patent US6449923 B1, 1993.

[28] M. Stewart, R.N. Estep, B.B. Gamble, M.D. Clifton, D.R. Quillen, L.S. Buehrig, et al., Blends of oxygen scavenging polyamides with polyesters which contain zinc and cobalt, U.S. Patent WO2006063032 A3, 2006.

[29] H. Li, K.K. Tung, D.R. Paul, B.D. Freeman, M. Stewart, J. Jenkins, Characterization of Oxygen Scavenging Films Based on 1,4-Polybutadiene, Industrial & Engineering Chemistry Research. 51 (2012) 7138–7145.

[30] H. Li, K.K. Tung, D.R. Paul, B.D. Freeman, Effect of film thickness on auto-oxidation in cobalt-catalyzed 1,4-polybutadiene films, Polymer. 52 (2011) 2772–2783.

[31] S. Carranza, D.R. Paul, R.T. Bonnecaze, Design formulae for reactive barrier membranes, Chemical Engineering Science. 65 (2010) 1151–1158.

[32] M.C. Ferrari, S. Carranza, R.T. Bonnecaze, K.K. Tung, B.D. Freeman, D.R. Paul, Modeling of oxygen scavenging for improved barrier behavior: Blend films, Journal of Membrane Science. 329 (2009) 183–192.

[33] S. Carranza, D.R. Paul, R.T. Bonnecaze, Analytic formulae for the design of reactive polymer blend barrier materials, Journal of Membrane Science. 360 (2010) 1–8.

[34] S. Carranza, Modeling of Oxygen Scavenging Polymers and Composites (Ph.D. Thesis), The University of Texas at Austin, 2010.

[35] A. Polyakova, R.Y.F. Liu, D.A. Schiraldi, A. Hiltner, E. Baer, Oxygen-barrier properties of copolymers based on ethylene terephthalate, Journal of Polymer Science Part B: Polymer Physics. 39 (2001) 1889–1899.

[36] K.K. Tung, R.T. Bonnecaze, B.D. Freeman, D.R. Paul, Characterization of the oxygen scavenging capacity and kinetics of SBS films, Polymer. 53 (2012) 4211–4221.

[37] S.N. Dhoot, B.D. Freeman, M. Stewart, Barrier Polymers, in: J.I. Kroschwitz (Ed.), Encyclopedia of Polymer Science and Technology, 3rd ed., Wiley-Interscience, New York, 2003: pp. 193–263.

[38] K.F. Finger, A.P. Lemberger, T. Higuchi, L.W. Busse, D.E. Wurster, Investigation and development of protective ointments IV. The influence of active fillers on the permeability of semisolids, Journal of the American Pharmaceutical Association. 49 (2006) 569–573.

[39] D.R. Paul, Effect of immobilizing adsorption on the diffusion time lag, Journal of Polymer Science Part A-2: Polymer Physics. 7 (1969) 1811–1818.

[40] D.R. Paul, D.R. Kemp, The diffusion time lag in polymer membranes containing adsorptive fillers, Journal of Polymer Science: Polymer Symposia. 41 (2007) 79–93.

[41] N.K. Lape, C. Yang, E.L. Cussler, Flake-filled reactive membranes, Journal of Membrane Science. 209 (2002) 271–282.

[42] E.E. Nuxoll, E.L. Cussler, The third parameter in reactive barrier films, AIChE Journal. 51 (2005) 456–463.

[43] R.A. Siegel, E.L. Cussler, Reactive barrier membranes: some theoretical observations regarding the time lag and breakthrough curves, Journal of Membrane Science. 229 (2004) 33–41.

Chapter 3: Materials and Experimental Methods

3.1 MATERIALS

3.1.1 Butadiene-containing SBS block copolymer

Styrene-butadiene-styrene (SBS) block copolymers are more convenient oxygen scavenging polymers than are the polybutadiene used in previous studies [1–3], owing to their ease of handling and processing and their potential compatibility (i.e., interfacial tension and adhesion) with the selected structural polymer. The SBS used here is a commercial product of Kraton Polymers, Inc. (Houston, Texas), D1102, containing 28 wt. % styrene and 72 wt. % butadiene, of which 92 wt. % is 1,4-polybutadiene, with an overall M_n = 100,000.

Polystyrene (PS) is a glassy polymer at room temperature and can be melt-processed when heated above its T_g (~ 100 °C) to blend with SBS in various compositions. The polystyrene phase in SBS improves rheological compatibility with polystyrene. The PS used here is a commercial, general purpose, easy flow resin from The Dow Chemical Company (Midland, Michigan), Styron 615. The structures of polybutadiene, polystyrene, and SBS block copolymer and their physical properties are shown in Figure 3.1(a) and (b) and Table 3.1.

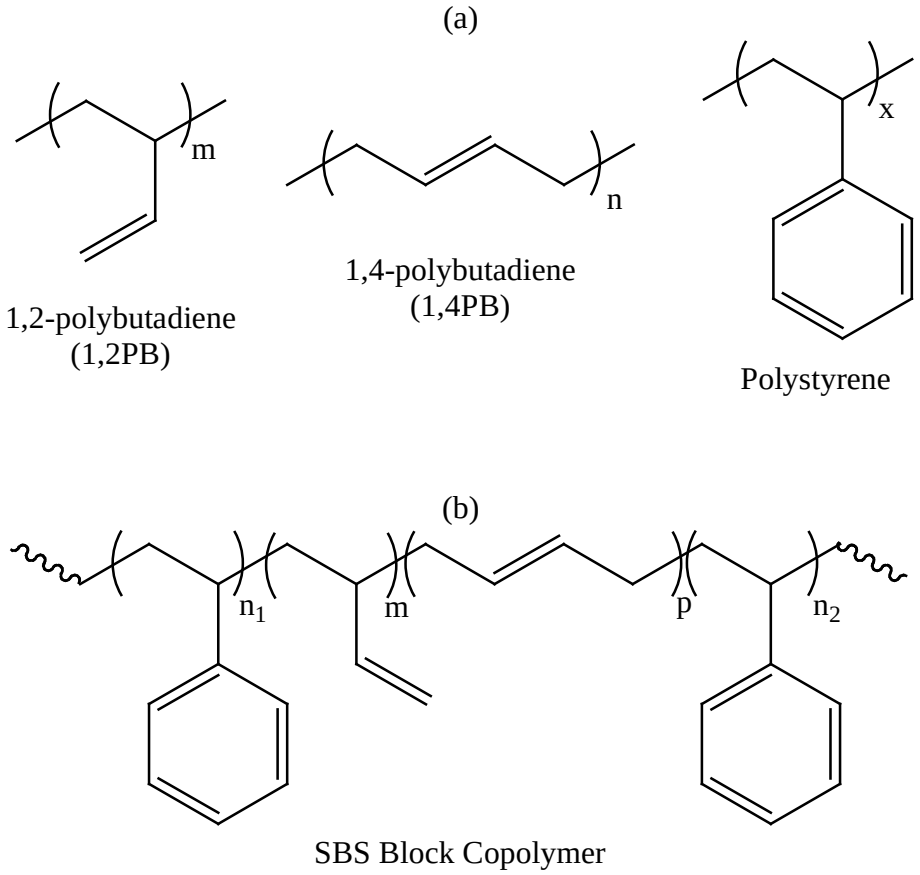

Figure 3.1: Chemical structures of scavenging system and catalyst. (a) 1,2PB, 1,4PB, polystyrene and (b) butadiene-containing SBS block copolymer [4,5].

3.1.2 Cobalt metal catalyst

The oxidation catalyst [1,6] was purchased from Shepherd Chemical Company (Cincinnati, OH) in the form of blue solid pastilles containing 20.5 wt % cobalt neodecanoate (the balance being excipient fillers). The cobalt catalyst was diluted with cyclohexane 100 times (by volume) in a volumetric flask. Cyclohexane (99.9%) was purchased from Fisher Chemical and used as received. Silicon wafers (5-in. and 2-in.

diameter) were purchased from Addison Engineering Inc. (San Jose, CA). The chemical structure of the cobalt catalyst is shown in Figure 3.2.

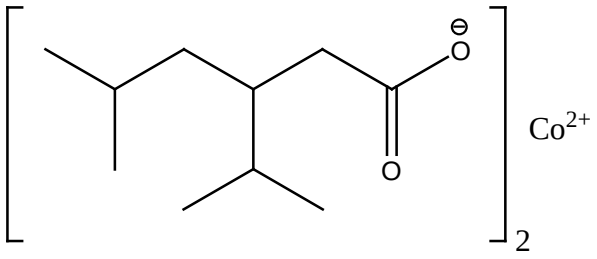

Figure 3.2: The chemical structure of cobalt neodecanoate

Table 3.1: Physical properties of SBS D1102, PS Styron 615, and 1,4-polybutadiene

	Composition	T_g **(°C)**	$\mathbf{M_n}$	$\boldsymbol{P}$ $10^{-10}\frac{cm^3(STP)\cdot cm}{cm^2\cdot s\cdot cm\,Hg}$		$\boldsymbol{\rho}$ g/cm^3
Sample/gas				N_2	O_2	
SBS D1102 [5]	72% PB; 92% 1,4-PB	-92, 100	100,000	22	56	0.94
1,4 PB [1]	36% cis, 55% trans, 9% vinyl	-92	230.000	10.3	24.3	0.89
PS	-	100	-	0.50	3.1	1.06

3.1.3 Photoinitiator and photo-initiation process

Benzophenone (>99%) is typically used as a photoinitator to produce radicals that trigger oxidation given the proper source of UV energy [7–14]. The photoinitiator, shown in Figure 3.3, was purchased from Sigma-Aldrich and used as received. The Longwave Ultraviolet Mercury Spot Lamp (Upland, CA) provides a distance-dependent UV power (W/cm^2; between the specimen and bulb) that is monitored and displayed. The time of

irradiation can be calculated easily by taking the ratio of UV power generated by the mercury lamp and the UV energy needed to trigger oxidation. A standard amount of UV, i.e., $12\,J/cm^2$ (~12 minutes of exposure), will trigger oxidation with virtually no induction period in the reactive polymer system that we show in Table 3.2. The photo-initiation set-up is shown in Figure 3.4.

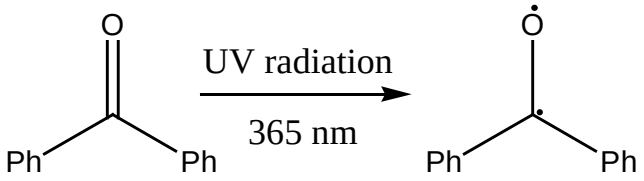

Figure 3.3: Benzophenone diradicals can be released with appropriate UV radiation

Table 3.2: Adding both cobalt catalyst and photoinitiator virtually eliminates any induction period prior to oxidation.

Benzophenone, wt%	Cobalt Catalyst, ppm	Induction Period
1	0	35 days
0	200	42 days
1	200	2 hours

In scavenger characterization, the gas of direct interest is oxygen, the permeation of which is, ideally, minimized in conventional packaging design. Nitrogen is an inert gas molecule similar in size to oxygen that can be used to determine and confirm changes in gas transport properties in samples without furthering oxidation. Nitrogen and oxygen gases were purchased from Matheson Tri-Gas, Inc. (Basking Ridge, NJ) and had a purity of 99.9% for the EXTRA DRY grade. All gases were used as received.

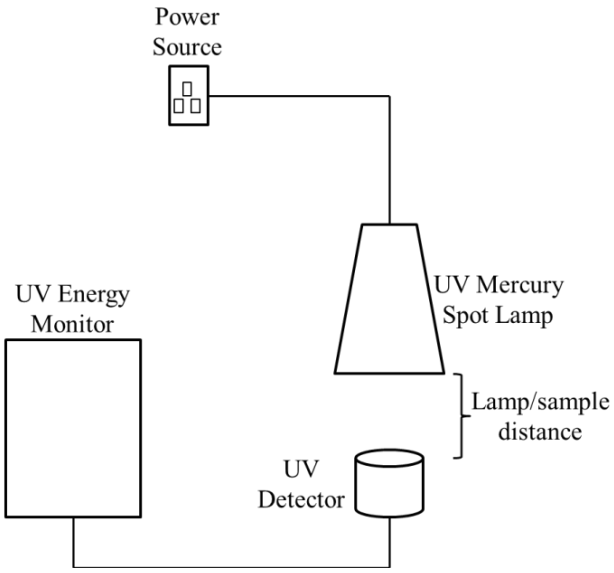

Figure 3.4: Schematic diagram of photo-initiation set-up process.

3.2 MEMBRANE CASTING AND CHARACTERIZATION

3.2.1 Solution Casting

Reactive films were made by both solution casting and spin coating techniques [3]. A normalized film making process was developed to keep all experimental data comparable. In solution casting, the polymer was dissolved in cyclohexane to make a 2 wt. % solution in an amber glass bottle. Predetermined amounts of cobalt neodecanoate solution and benzophenone were added to the stirred solution. After the additives were fully dissolved, the homogeneous solution was poured into a glass ring (5.1 cm in diameter) resting on a glass plate. The nascent film on the glass plate was held under nitrogen in a glove box covered with aluminum foil to allow the cyclohexane to slowly evaporate, as shown in Figure 3.5. The resulting films were stored in a vacuum oven at

room temperature for an additional 6 hours to fully remove the solvent. In this study, solution casting was used to form films with thicknesses ranging from 50 to 250 μm.

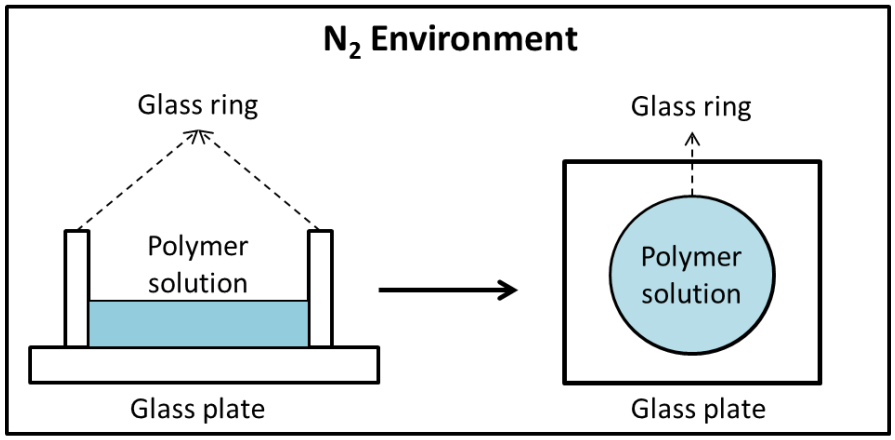

Figure 3.5: Solution casting experimental set-up.

3.2.2 Spin Coating

In spin coating, SBS solutions were filtered through a 5.0 and 0.2 μm Whatman® PURADISCTM Teflon syringe filter before use. From the filtered SBS solution, thin films were spin coated onto a clean, polished, native-oxide silicon (100) wafer using a Laurel WS-400B-8NPP/LITE model spin coater (North Wales, PA) at 1000 rpm for 60 seconds. If a thicker film was needed, one or two extra layers of polymer solution were coated onto the first polymer layer. In this study, spin coating was used to form films with thicknesses ranging from 1 to 15 μm. For oxygen mass uptake experiments, these films were left on the silicon wafers to oxidize. Since silicon wafers are impermeable to gases, the SBS films were oxidized from only one surface.

To prepare film samples for permeation experiments, 3 cm x 3 cm pieces of the thin films were cut with a razor blade and then detached from the wafer surface by

immersing the wafer-film composite in deionized water. A thin wire frame described earlier [1,15,16], shown in Figure 3.6, was used to transfer the films into a vacuum oven, where they were dried at room temperature for 1 hour before use.

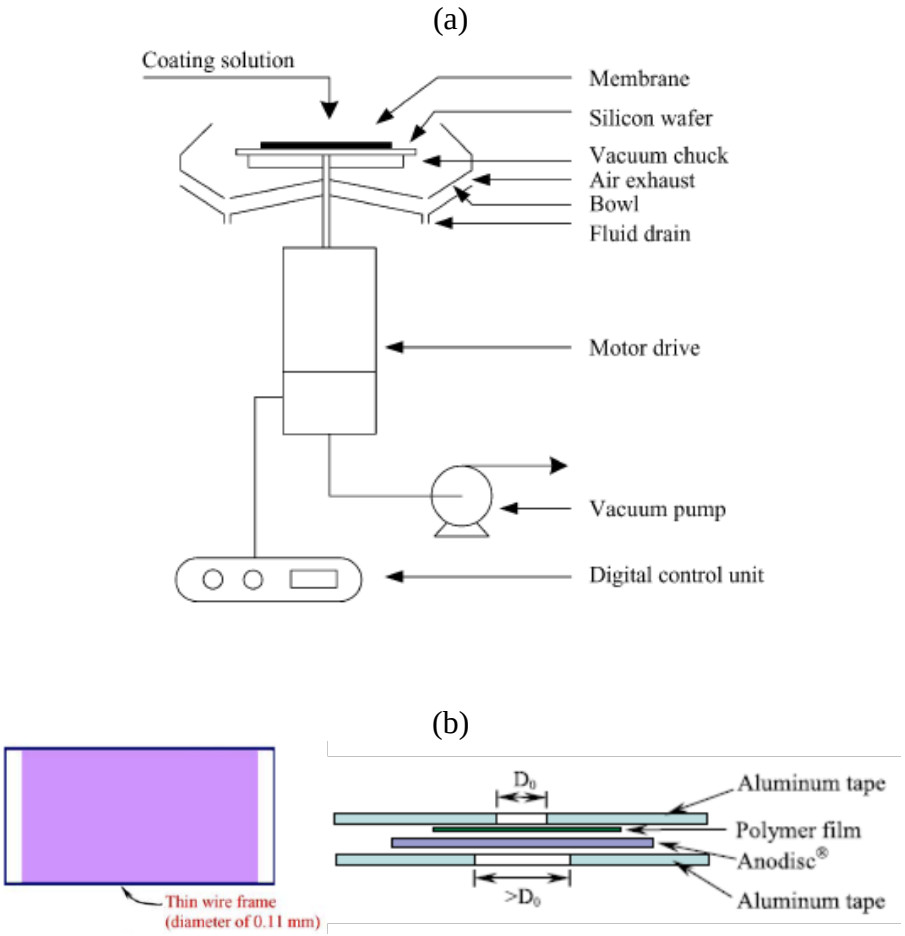

Figure 3.6: Spin coating [1,15,16] experimental set-up (a) spin coater and (b) permeation sample preparation.

3.2.3 Melt-extrusion

3.2.3.1 Identifying melt-processing conditions

The conditions at which the current blend system, polystyrene and SBS block copolymer could be successfully melt-processed were first identified. The Kraton D1102 material safety data sheet (MSDS) recommends maintaining a fire watch if the material reaches 225 °C (437 °F) during processing. Figure 3.7 shows that polystyrene and D1102 have similar melt viscosities at 180 – 190 °C, as determined by a melt flow indexer.

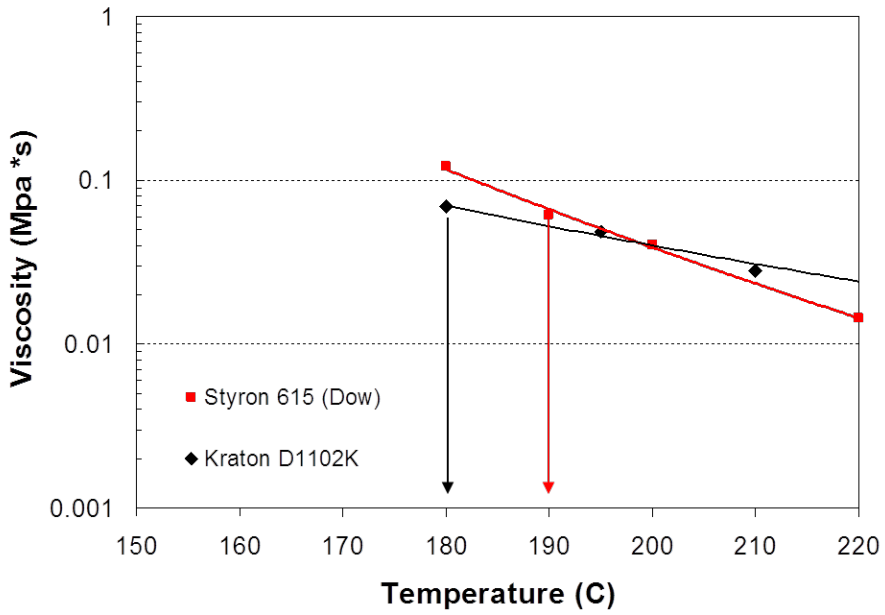

Figure 3.7: Melt flow index of Kraton D1102 and Dow Styron 615 PS materials for low temperature melt extrusion.

A series of temperature and residence time experiments was performed to discern SBS D1102 degradation via discoloration. SBS was melt-processed in a N_2-purged DSM

at different temperatures and residence times. The extrudates at temperatures greater than 190 °C and long residence time clearly show discoloration due to thermal degradation, but there is minimal degradation/no color change in samples processed at temperatures lower than 180 °C, as shown in Figure 3.8. The proper processing temperature for D1102 and PS is 180 °C, and the twin screw extruder must be fully purged during blending.

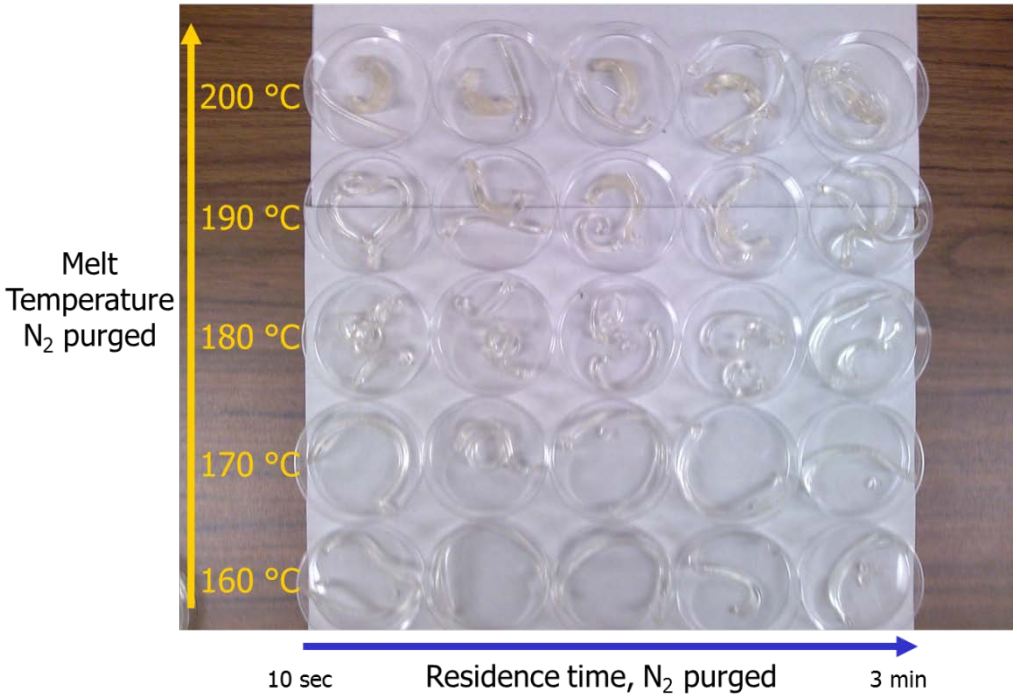

Figure 3.8: Identifying proper processing temperature and residence time for D1102. The extrudate processed at higher temperature, as well as those with higher residence time, show discoloration due to thermal degradation.

3.2.3.2 Extruding blend films

DSM Microcompounder (Xplore®, The Netherlands) is a desk-top twin screw extruder that was used to melt-process blends. We first determined the mass of each

blending component. These extrudates, each of which had a different weight composition of polystyrene and SBS, were allowed to blend for 10 minutes in a N_2-purged DSM at a processing temperature of 180 °C. Melt-processed blend films were then made using a film die, where the films are cooled with nitrogen gas and collected from an uptake roller. Figure 3.9 shows the experimental set-up to melt process blend films.

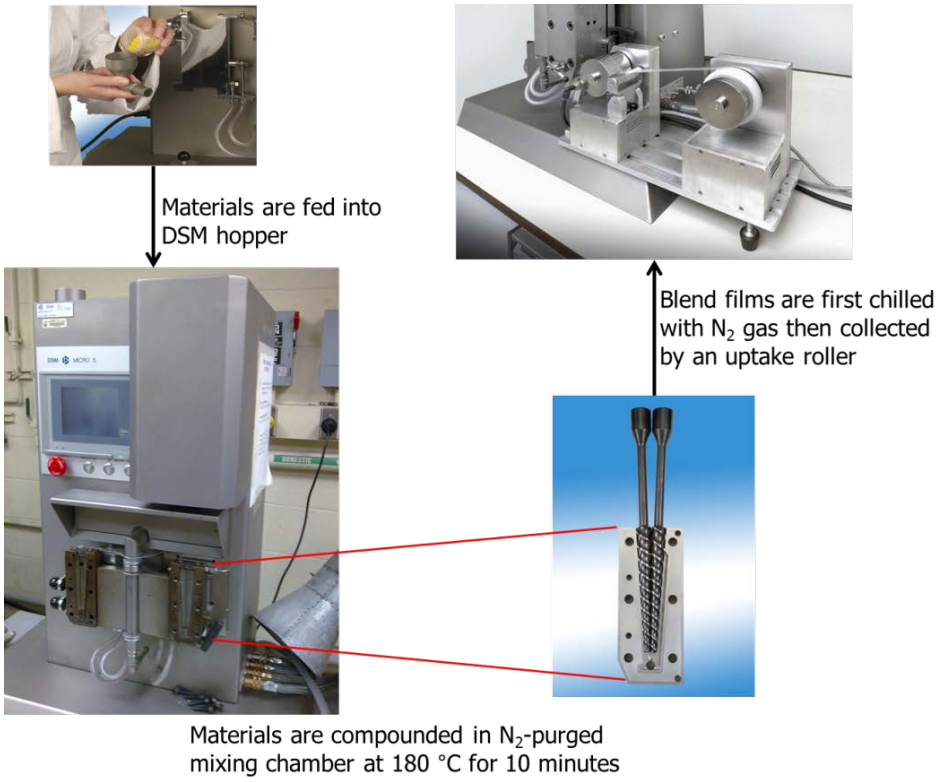

Figure 3.9: Experimental set-up for melt extruding blend films. DSM Micro-compounder photos from DSM Xplore.

3.2.4 Measuring Film Thickness

There are two experimental methods for measuring film thickness, and the chosen method depends largely on whether the films are free-standing or attached to the silicon

wafers. Thicknesses of free-standing solution cast films were determined using a Mitutoyo Litematic VL-50A instrument (Mitutoyo Corporation, Japan) designed especially to measure the thickness of soft, rubbery films like 1,4 polybutadiene and SBS block copolymer. To avoid direct contact between the measuring tip of the micrometer and the tested soft films, pieces of cover glass were placed on both sides of the film during measurement.

While the thin films were on the silicon wafer, their thicknesses were determined using a KLA-Tencor Instrument Alpha-step 200 profilometer (Mulpitas, CA). First, a small nick was made on the films with a razor blade. Physical contact of the profilometer tip with the film and the wafer gives a measure of the nick depth or the thickness of the spin-coated film. Thicknesses were also calculated based on mass, volume, and density relationships, and the calculated and experimentally measured values were in good agreement. Thin film thickness was found to be a function of polymer solution concentration by weight. Figure 3.10 shows how the Kraton D1102 weight concentration correlated with SBS thin film thickness.

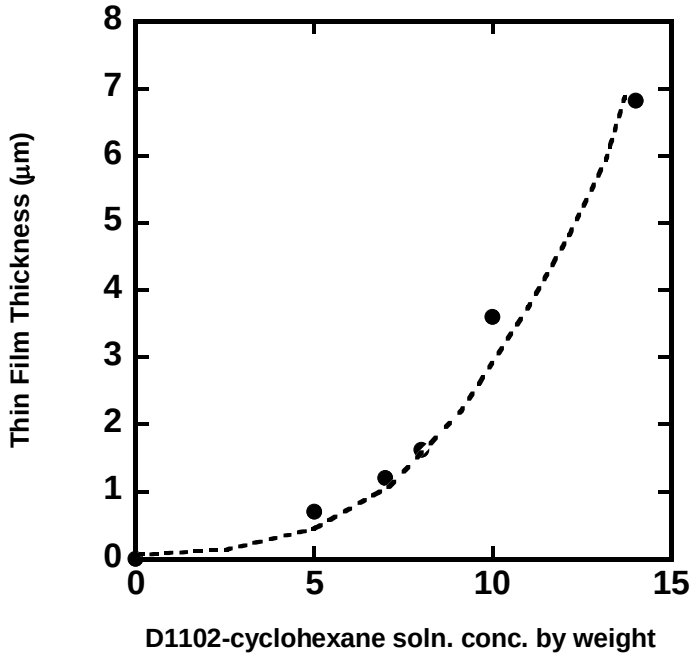

Figure 3.10: SBS thin film thickness versus the dissolved polymer concentration by weight in cyclohexane. The thin films were spin coated at 1000 rpm for 60 seconds onto a silicon wafer using the coating technique described in the previous section.

3.2.5 Measuring Film Density

Polymer density was characterized using Archimedes' principle [17], which gives

$$\rho_p = \frac{M_A}{M_A - M_L}\rho_0 \tag{2.1}$$

where ρ_p and ρ_0 are the densities of the target polymer and the auxiliary liquid used, respectively, while M_A and M_L are the film mass in air and in the auxiliary liquid, respectively. Film density was determined using a Mettler Toledo AB54-S/FACT

analytical balance (accuracy to 0.1 milligram) and a density kit. Hexane ($0.655\, g/cc$, Fisher Scientific) served as the auxiliary liquid.

3.2.6 Measuring oxygen uptake

A UV light source providing a predetermined amount of energy was used to irradiate the SBS films containing the photoinitiator benzophenone to initiate oxidation. The overall UV energy provided is a function of UV light intensity, film distance from the light source, and exposure time. To prevent premature oxidation, polymer films were kept free of oxygen by storing under an inert atmosphere (nitrogen) until the oxygen uptake experiments began. The irradiated films were kept in a temperature controlled chamber at 35 °C for the duration of the oxidation experiment. Oxygen mass uptake was tracked by monitoring weight changes of the films on a Mettler Toledo AB54-S/FACT analytical balance (accuracy to 0.1 milligram); oxygen uptake was taken as the difference between the film mass at any given time and its initial mass before the start of sorption experiments. Film samples were oxidized in ambient air, ~21% oxygen, as a function of time. In addition, uptake experiment was also characterized at higher oxygen pressures (20, 60, and 100 psi O_2) using a Rubotherm Magnetic Suspension Balance, which weighs samples without contact in an electromagnetic enforced, pressure-controlled environment (high accuracy to 1 μg) [18].

The oxidation of butadiene units under the conditions of interest here involves rather complex chemistry, which was described in the detailed modified oxidation mechanism discussion in Chapter 2, Section 2. The butadiene units can be imagined as reactive sites that consume oxygen [2,3,8]. Since SBS D1102 has a density of 0.94 g/cm^3 and contains 72 wt. % butadiene, the concentration of butadiene units is approximately

12.2 $mmol_{PB} / cm^3$. For subsequent analysis, the initial concentration of unreacted butadiene units will be designated as n_0; the stoichiometric coefficient $\hat{\nu}$, which defines the ratio of moles of butadiene units that react with each mole of O_2, will be determined experimentally. To achieve the reaction rates fast enough for practical use in barrier systems, the cobalt catalyst mentioned earlier must be added.

3.3 SCANNING ELECTRON MICROSCOPY (SEM)/ENERGY DISPERSIVE SPECTROSCOPY (EDS)

3.3.1 Scanning Electron Microscopy (SEM)

Samples of thick films oxidized for ~90 days were used for SEM analysis. A surface perpendicular to the plane of the film was exposed by cutting the film first with a glass knife and then with a diamond knife (Micro Star Technologies, Huntsville, TX) using an RMC-Boeckeler PowerTome PT-XL (Boeckeler Instruments Inc., Tucson, AZ) at cryogenic temperature (-125°C) and a cutting speed of 0.8 mm/sec. The resulting SEM samples were secured perpendicularly with carbon tape on low profile 45°/90° SEM mounts (Ted Pella Inc., Redding, CA) and then coated with a 10 nm layer of indium using an Emitech K575K sputter coater (Quorum Technologies Ltd., West Sussex, United Kingdom) operated 150 μW for 10 seconds. The samples were viewed using a Zeiss NEON 40 FE-SEM (Carl Zeiss SMT Inc., Peabody, MA) operated at 5 kV and ~ 20 mm working distance. The SEM images were made immediately to limit further oxidation of the microtomed surfaces.

The scanning electron microscope uses a focused high-energy electron beam to generate signals at selected areas of specimen surfaces to reveal information about external morphology, chemical composition, and orientation of materials making up the

sample. The end result is a 2-dimensional image that displays spatial variations in these properties.

3.3.2 Energy Dispersive Spectroscopy (EDS)

Partially oxidized films were immersed into liquid nitrogen and fractured to create a cross-sectional surface. The resulting samples were then immediately secured with carbon tape on an SEM mount with no metal coating. Afterwards, energy dispersive x-ray spectroscopy (detector = Bruker EDS Quantax 4010) was used for elemental analysis of partially oxidized films, looking for oxygen-containing functional groups throughout the film thickness.

EDS can be used to find the chemical composition of materials by mapping the elemental composition over a selected sample area [5]. Together, SEM and EDS provide fundamental compositional information about oxidized polymers by means of stoichiometric ratios and multiple elemental line scanning.

3.4 TRANSMISSION ELECTRON MICROSCOPY (TEM)

TEM uses a transmitted electron beam to determine polymer morphology. A surface perpendicular to the plane of the film was cryogenically conditioned by cutting with a glass knife; it was then microtomed with a diamond knife (Micro Star Technologies, Huntsville, TX) using an RMC-Boeckeler PowerTome PT-XL (Boeckeler Instruments Inc., Tucson, AZ) at a cutting speed of 0.8 mm/sec.

The resulting cross-polymer sections, ~ 50 nm, were floated onto 200-mesh copper grids from Ted Pella, Inc. (Redding, CA) and dried, then subsequently stained with OsO_4 for 4 hours. The transmission electron microscope used, TEM TECNAI G2

F20 X-TWIN, is an analytical system with high-resolution imaging and atomic resolution microanalysis capabilities, optimized for high spatial resolution analysis. TEM images of the stained samples show contrast differences. Osmium tetroxide is primarily used to stain unsaturated rubbers [19,20] (or, in this case, the butadiene phase) to form an osmate ester of the form shown in Figure 3.11,

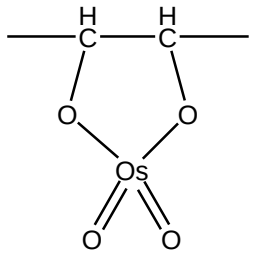

Figure 3.11: Osmate ester is formed when butadiene is oxidized by osmium tetraoxide [21].

3.5 DIFFERENTIAL SCANNING CALORIMETER (DSC)

A Q-100 DSC equipped with a liquid nitrogen cooling system (LNCS) from TA Instruments (New Castle, DE) was used to perform differential scanning calorimeter experiments. Polymer samples weighing around 5 mg were placed in aluminum DSC pans, and helium, flowing at 25 ml/min, was used as the blanketing gas in DSC analysis. First the tested sample was brought from ambient to -150ºC; it was then held isothermally for 5 minutes to equilibrate and stabilize the system, thus completing the DSC sweep. The glass transition temperature (T_g) was taken as the midpoint of the measured step change in heat capacity after the sample was scanned from -150 to 150 ºC at a heating rate of 10 ºC/min.

3.6 DETERMINING GAS TRANSPORT PROPERTIES

3.6.1 Measuring Gas Permeability

The permeability of SBS films to nitrogen and oxygen was measured using a constant volume/variable pressure apparatus [22], shown in Figure 3.12. A liquid nitrogen trap was installed between the permeation apparatus and vacuum pump to prevent any possible vacuum oil contamination of the permeation system.

Because conventional food packaging is usually designed to minimize oxygen permeance, oxygen is a gas of direct interest in characterizing these new oxygen scavenging materials. Nitrogen is an inert, non-oxidizable gas molecule similar in size to oxygen that can be used to detect and confirm changes in gas transport properties in samples without furthering oxidation.

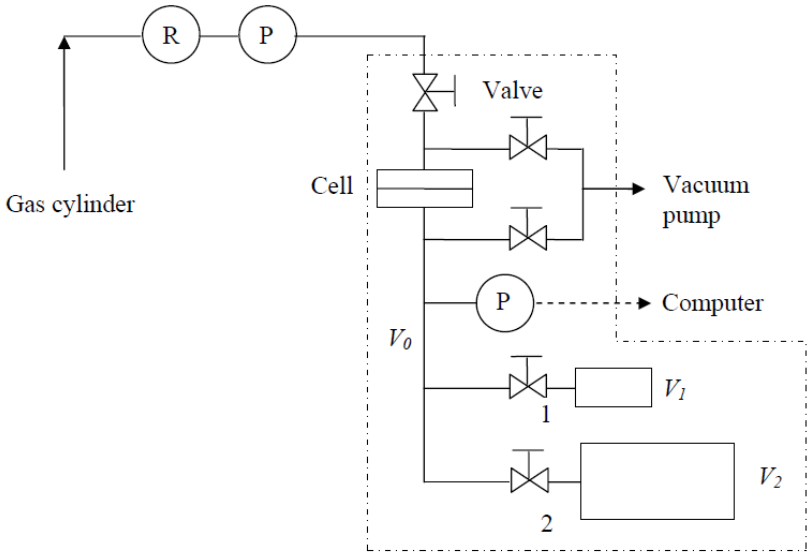

Figure 3.12: Schematic of a constant volume/variable pressure apparatus for gas permeability measurements [22].

Solution cast thick films were masked, with openings on their upstream and downstream sides, using impermeable aluminum tape. Spin-coated thin films mounted on a copper wire frame were carefully placed at the center of a Whatman Anodisc® for mechanical support [1,15,16]. Aluminum tape with center openings to permit gas permeation was then applied to both sides. The gas permeability P [23] was calculated from

$$P = \frac{V \cdot l}{p_1 \cdot A \cdot R \cdot T}\left[\left(\frac{dp_2}{dt}\right)_{ss} - \left(\frac{dp_2}{dt}\right)_{leak}\right] \tag{2.2}$$

where p_1 is the upstream absolute pressure, T is absolute temperature, A is the film area, l is the film thickness, V is the downstream volume, R is the gas constant, and $\left(\frac{dp_2}{dt}\right)_{ss}$ and $\left(\frac{dp_2}{dt}\right)_{leak}$ are the pseudo-steady state rates of pressure rise in the downstream volume at a fixed upstream pressure and under vacuum, respectively. A downstream pressure less than 10 torr was maintained during all measurements.

3.6.2 Measuring Gas Diffusivity

The nitrogen and oxygen permeability coefficients were determined from the slopes of the linear, steady-state region of increasing downstream permeate pressure versus time. Moreover, the intercept of the steady-state line on the time axis, or the time lag, θ, was used to calculate polymer gas diffusivity, as shown in Figure 3.13 [22].

$$D = L^2 / 6\theta \tag{2.3}$$

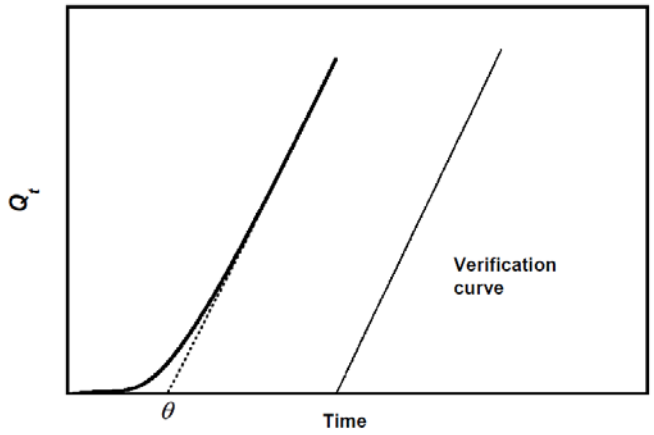

Figure 3.13: A typical time profile for the amount of accumulated permeate, Q_t, in a transient permeation experiment [22].

3.6.3 Measuring Gas Solubility

The widely used [18,19] dual-volume pressure-decay method with dual transducers and dual cells was used to determine gas solubility coefficients of the fully oxidized polymer [22]. The system consists of a sample cell containing a polymer sample and a charge cell connected to a gas cylinder. The sample cell, which contains approximately 0.5 g of fully oxidized polymer, is first evacuated, sealed with a VCR gasket, and isolated from the charge cell, which is charged with an experimental gas at a pressure of interest. For our purposes, the sorption apparatus was placed in a constant temperature water bath at 35 °C. From the pressure transducer attached to the charge volume, along with the known charge cell volume and temperature, we calculated the initial gas concentration in the charge volume. Then the valve connecting the sample and charge cells was opened and closed, releasing gas from the charge volume into the sample volume to allow pressure stabilization, which is monitored as a function of time (Figure 3.14).

The pressure in the sample cell decreases as the polymer sample sorbs gas, and a stable, final pressure value was ultimately reached when the polymer had sorbed all of the gas that it could. In other words, equilibrium was achieved. The concentration of gases remaining in the sample cell gas phase can be calculated from this final pressure in the sample cell. The concentration of gas sorbed by the sample is the difference between the initial and final gas concentrations in the gas phase of the sample cell.

Following equilibrium, more gas was admitted to pressurize the charge volume. Gas was again released into the sample volume, and the described sorption measurement was repeated at a higher pressure.

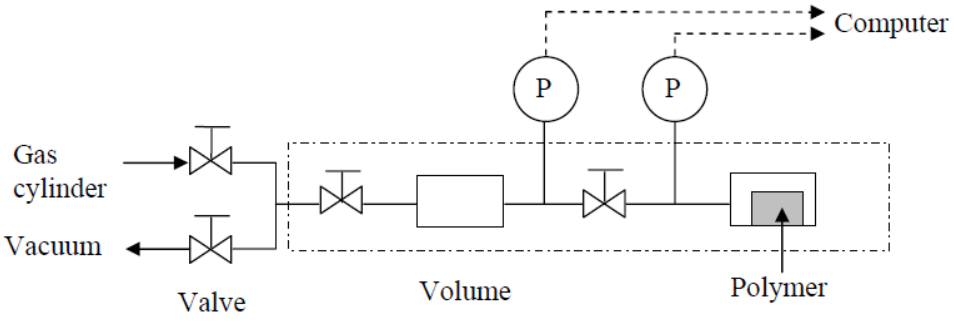

Figure 3.14: Schematic of a dual volume, dual transducer apparatus, or barometric pressure decay system, for gas sorption measurements [22].

Initial and final pressure values in the sample and charge cells were used to calculate the concentration of gas sorbed in the fully oxidized polymer at a specific pressure value. Subsequently, the N_2 and O_2 sorption isotherms were constructed by relating the concentration of sorbed gas in the sample for several pressures. The sorption coefficient was then calculated from [22]

$$S = C / p \tag{2.4}$$

The permeability is given by the product of diffusion and sorption coefficients [22],

$$P = D \times S \tag{2.5}$$

Using Equation (2.5), we estimated gas solubility coefficients of unoxidized polymer by using the known values of gas permeability and diffusion coefficients. Similarly, the ratio of gas permeability and solubility coefficient of a fully oxidized polymer gives its diffusion coefficient.

3.8 REFERENCES

[1] H. Li, K.K. Tung, D.R. Paul, B.D. Freeman, Effect of film thickness on auto-oxidation in cobalt-catalyzed 1,4-polybutadiene films, Polymer. 52 (2011) 2772–2783.

[2] H. Li, D.K. Ashcraft, B.D. Freeman, M. Stewart, M.K. Jank, T.R. Clark, Non-invasive headspace measurement for characterizing oxygen-scavenging in polymers, Polymer. 49 (2008) 4541–4545.

[3] H. Li, K.K. Tung, D.R. Paul, B.D. Freeman, M. Stewart, J. Jenkins, Characterization of Oxygen Scavenging Films Based on 1,4-Polybutadiene, Industrial & Engineering Chemistry Research. 51 (2012) 7138–7145.

[4] R.H. Li, Metal-catalyzed oxidation of polybutadiene in oxygen scavenging packaging application (Ph.D. Thesis), The University of Texas at Austin, 2010.

[5] K.K. Tung, R.T. Bonnecaze, B.D. Freeman, D.R. Paul, Characterization of the oxygen scavenging capacity and kinetics of SBS films, Polymer. 53 (2012) 4211–4221.

[6] R.A. Sheldon, J.K. Kochi, Metal Catalysis in Peroxide Reactions, in: Metal-catalyzed Oxidation of Organic Compounds, Academic press, New York, 1981: pp. 38–48.

[7] E.A. Lissi, M. V Encinas, Photoinitiators for Free Radical Polymerization , in: J.F. Rabek (Ed.), Photochemistry and Photophysics, CRC Press, Boca Raton, 1991.

[8] S.W. Beavan, D. Phillips, Mechanistic Studies on the Photooxidation of Commercial Polybutadiene, European Polymer Journal. 10 (1974) 593–603.

[9] S.W. Bigger, O. Delatycki, New approach to the measurement of polymer photooxidation, Journal of Polymer Science, Part A: Polymer Chemistry. 25 (1987) 3311–3323.

[10] M. Piton, A. Rivaton, Photooxidation of polybutadiene at long wavelengths ($\lambda >$ 300 nm), Polymer Degradation and Stability. 53 (1996) 343–359.

[11] C. Adam, J. Lacoste, J. Lemaire, Photo-oxidation of elastomeric materials. 1. Photooxidation of polybutadienes, Polymer Degradation and Stability. 24 (1989) 185–200.

[12] C. Adam, J. Lacoste, J. Lemaire, Photo-oxidation of elastomeric materials: Part II—Photo-oxidation of styrene-butadiene copolymer, Polymer Degradation and Stability. 26 (1989) 269–284.

[13] K. Katsumoto, T.Y. Ching, Goodrich, D. V Speer, Photoinitiators and oxygen scavenging composition, U.S. Patent 6,139,770, 2000.

[14] C. Adam, J. Lacoste, J. Lemaire, Photo-oxidation of elastomeric materials: Part IV—Photo-oxidation of 1,2-polybutadiene, Polymer Degradation and Stability. 29 (1990) 305–320.

[15] Y. HUANG, D.R. Paul, Experimental methods for tracking physical aging of thin glassy polymer films by gas permeation, Journal of Membrane Science. 244 (2004) 167–178.

[16] Y. Huang, D.R. Paul, Physical aging of thin glassy polymer films monitored by gas permeability, Polymer. 45 (2004) 8377–8393.

[17] D. Walsh, P. Zoller, Standard Pressure Volume Temperature Data for Polymers, CRC Press, 1995.

[18] S. Areerat, E. Funami, Y. Hayata, D. Nakagawa, M. Ohshima, Measurement and prediction of diffusion coefficients of supercritical CO2 in molten polymers, Polymer Engineering and Science. 44 (2004) 1915–1924.

[19] E.H. Andrews, Crystalline Morphology in Thin Films of Natural Rubber. II. Crystallization Under Strain, Proceedings of the Royal Society A: Mathematical, Physical and Engineering Sciences. 277 (1964) 562–570.

[20] K. Kato, The osmium tetroxide procedure for light and electron microscopy of ABS plastics, Polymer Engineering and Science. 7 (1967) 38–39.

[21] D.R. Paul, C.B. Bucknall, Polymer Blends: Formulation and Performance, Wiley-Interscience, 2000.

[22] W.J. Koros, D.R. Paul, Design considerations for measurement of gas sorption in polymers by pressure decay, Journal of Polymer Science: Polymer Physics Edition. 14 (1976) 1903–1907.

[23] D.R. Paul, Fundamentals of Transport Phenomena in Polymer Membranes, in: Enrico Drioli & Lidietta Giorno (Ed.), Comprehensive Membrane Science and Engineering, 1st ed., Elsevier B.V., 2010: pp. 75–90.

Chapter 4: Characterization of the Oxygen Scavenging Capacity and Kinetics of SBS Films

4.1 INTRODUCTION

This chapter explores the oxygen uptake by an oxygen scavenging system, viz., a styrene-butadiene-styrene, SBS, block copolymer containing varying amounts of a cobalt catalyst, for a wide range of film thicknesses. For thin enough films, the rate of oxygen uptake is not limited by diffusion, and the results can be analyzed by a simple chemical kinetic model to obtain stoichiometric and reaction rate parameters. For thicker films, oxygen diffusion becomes limiting, and the results can be understood semi-quantitatively in terms of a moving-boundary model. The "critical thickness" dividing the two regimes deduced from long term oxygen uptake data agrees well with post-mortem microscopic inspection of partially oxidized films. The parameters deduced here should be useful for future design and modeling of blend and laminate barrier films based on this SBS/cobalt catalyst system.

This chapter adapted from: K.K. Tung, R.T. Bonnecaze, B.D. Freeman, D.R. Paul, Characterization of the oxygen scavenging capacity and kinetics of SBS films, Polymer. 53 (2012) 4211–4221.
Dr. Tung is the main author who did the experiments as well as the writing of the publication. Professor Bonnecaze is a coauthor who helped with advanced modeling and theoretical insight. Professors Freeman and Paul are coauthors and principal investigators who provided the lab space/equipment, research funding, as well as their expertise in the field of oxygen scavenging.

4.2 RESULTS AND DISCUSSIONS

4.2.1 Gas sorption and permeation

The gas transport properties of un-oxidized and fully oxidized SBS films were characterized and are recorded in Table 4.1. Nitrogen and oxygen transient permeation experiments were conducted with a ~350 μm un-oxidized film at 35 °C. The nitrogen and oxygen permeability coefficients were determined from the steady-state region, while the time lag was used to calculate the nitrogen and oxygen diffusion coefficients. The solubility coefficients were calculated from the ratio of the permeability and diffusion coefficients. Gas transport properties of commercial SBS D1102 are reasonably close to those of other SBS materials reported in the literature [1–5].

Table 4.1: Gas transport properties of SBS, 1,4 PB, and PS

	P $10^{-10}\frac{cm^3(STP)\cdot cm}{cm^2\cdot s\cdot cm\,Hg}$		S $10^{-4}\frac{cc(STP)}{cm^3\cdot cm\,Hg}$		D $10^{-6}\frac{cm^2}{s}$		ρ g/cm^3
Sample/gas	N_2	O_2	N_2	O_2	N_2	O_2	
SBS D1102*	22	56	4.5	9.1	4.6	6.0	0.94
SBS D1102* (Fully oxidized)	0.18	0.41	13	16	0.01	0.03	1.2
SBS [1]	9.7	23.9	6.9	9.9	2.4	1.4	-
SBS [2]	14	40	-	-	-	-	-
SBS D1101 [5]	-	26.1	-	-	-	-	-
SBS D1107 [5]	-	19.0	-	-	-	-	-
1,4 PB [3]	10.3	24.3	-	-	-	-	-
1,4 PB [3] (Fully oxidized)	0.04	0.14	-	-	-	-	-
cis-1,4 PB [4]	6.5	19.1	5.9	13	1.1	1.5	-
PS*	0.50	3.1	8.9	23	0.06	0.14	1.06
PS [2]	0.22	1.2	-	-	-	-	-
PS [5]	0.24 – 0.30	1.8 – 2.4	-	-	-	-	-

* This work

A 3.7 μm reactive film containing 800 ppm cobalt catalyst was exposed to an upstream oxygen pressure of 7 atm for rapid oxidation over 4 – 6 hours at 35 °C in a gas permeation cell, and this sample will be referred to as “fully oxidized” since it is the sample oxidized under the most extreme conditions. The gas permeability dropped quickly with time, and the final stabilized nitrogen and oxygen permeability coefficients shown in Table 4.1 were determined. For the gas solubility coefficients, the fully oxidized sample was first placed in a sorption cell and allowed to absorb nitrogen at various pressures up to 7 bar at 35 °C. This dual-volume pressure-decay method [6] uses initial and final pressure values in the sample and charge cells to calculate the concentration of gas sorbed per unit volume of fully oxidized polymer at a specific pressure.

A nitrogen sorption isotherm at 35 °C was first measured, followed by an oxygen sorption isotherm. Afterwards a second nitrogen sorption isotherm was measured and found to be similar to the first nitrogen sorption isotherm. This exercise ensures data reproducibility and confirms the sample of interest is indeed fully oxidized or at least as highly oxidized as one might achieve at these conditions. The concentrations of nitrogen and oxygen sorbed in the fully oxidized sample were found to vary linearly with gas pressure. The values of nitrogen and oxygen solubility coefficients of fully oxidized polymer were determined and are shown in Table 4.1, which also shows values of diffusion coefficients calculated as the ratio of permeability and solubility coefficients of fully oxidized polymer.

Oxidation reduced the O_2 and N_2 permeability coefficients of the SBS films by approximately 2 orders of magnitude, which is comparable to that observed earlier for reactive films of 1,4 polybutadiene [3]. This level of change in gas permeability is due to the reduction in the gas diffusion coefficients as the butadiene segments are converted to

more polar oxygen-containing units and perhaps crosslinked [3]. In general, addition of oxygen-containing functional groups are expected to reduce the polymer free volume [4,7,8]. On the other hand, gas solubility coefficients were found to increase slightly by a factor of two to three. This result is reasonable since oxidized SBS rubber essentially becomes a glassy polymer, similar to that observed in earlier work on 1,4 polybutadiene oxidation [3]. Typically, glassy polymers sorb greater quantities of gas than do rubbery polymers [9].

4.2.2 Oxygen uptake: Critical thickness

A set of reactive SBS films, with catalyst loadings of 100, 200, 400, 800 ppm, were cast with a wide range of thicknesses from 1 to 300 μm and were allowed to oxidize for approximately 90 days at 35 °C. The oxygen uptake M_t observed at any time t was normalized by the polymer mass prior to any oxidation. Figure 4.1(a) shows an example of oxygen uptake versus time curves at 200 ppm catalyst loading for a range of thicknesses from 2.8 to 266 μm. Other catalyst loadings yield similar, but quantitatively different, responses.

The thinner films, < 14 μm, represented by the solid points in Figure 4.1(a) appear to fall on the same uptake curve that is independent of film thickness. Thus, these thinner films oxidize uniformly throughout their thickness and eventually reach a constant extent of oxidation. This constant uptake value at long oxidation times for the 200 ppm catalyst loading samples, 26.6 ± 1.0 $\frac{gram\,of\,oxygen}{100\,gram\,of\;polymer}$, can be considered as the oxygen uptake that can be achieved when given an infinite amount of time, M_∞. This value is the same for all thin films of each catalyst loading within experimental error; values of M_∞ obtained at all catalyst loadings for thin film samples are recorded in Table 4.2.

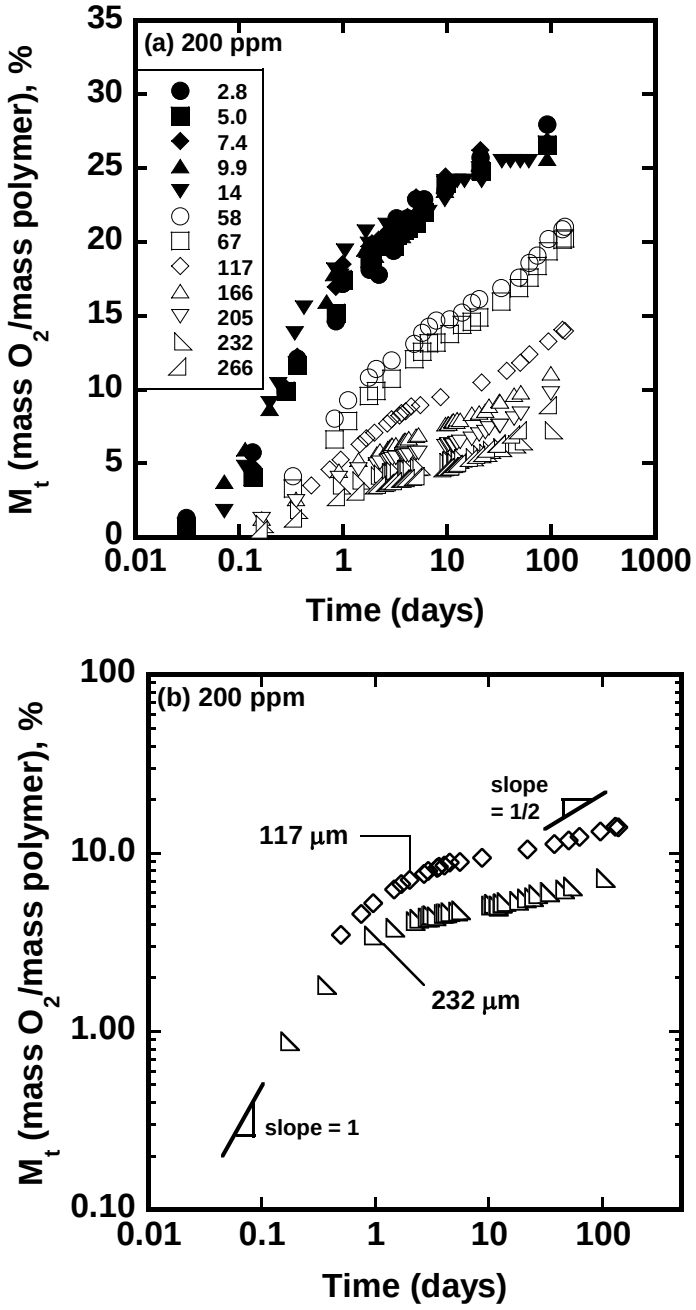

Figure 4.1: Effect of thickness (2.8 to 266 μm) on oxygen uptake for SBS films containing 200 ppm catalyst: (a) Data for thin films (solid points) collapse into a single curve that eventually reaches a constant extent of oxidation, while for thick films (open points) uptake strongly depends on thicknesses. (b) A plot using log-log coordinates suggests that early time uptake varies as t while at longer times a $\sqrt{t}$ regime is approached.

The thicker films, > 58 μm, have similar oxidation kinetics as the thinner films at early oxidation times, where the oxygen uptake increases rapidly with time. However, the oxygen uptake at long oxidation times is found to be a function of film thicknesses, i.e., the uptake, normalized by the original polymer mass, at any time decreases with increasing film thicknesses. Moreover, the rate of oxygen uptake was found to decrease with time as can be seen by comparing the respective slopes in the early and long time regimes, as illustrated in Figure 4.1(b) for 117 and 232 μm thick films using log-log coordinates. At short times, the uptake appears to increase linearly in time but this gives way at much longer times to a slower regime where M_t appears to be approaching an increase proportional to $t^{1/2}$ suggestive of a diffusion controlled regime as developed later. Oxygen uptake versus time curves at 100, 400, and 800 ppm catalyst loading for a range of thicknesses are shown in Figure 4.1(c), (d), and (e). These catalyst loadings yield similar, but quantitatively different, responses.

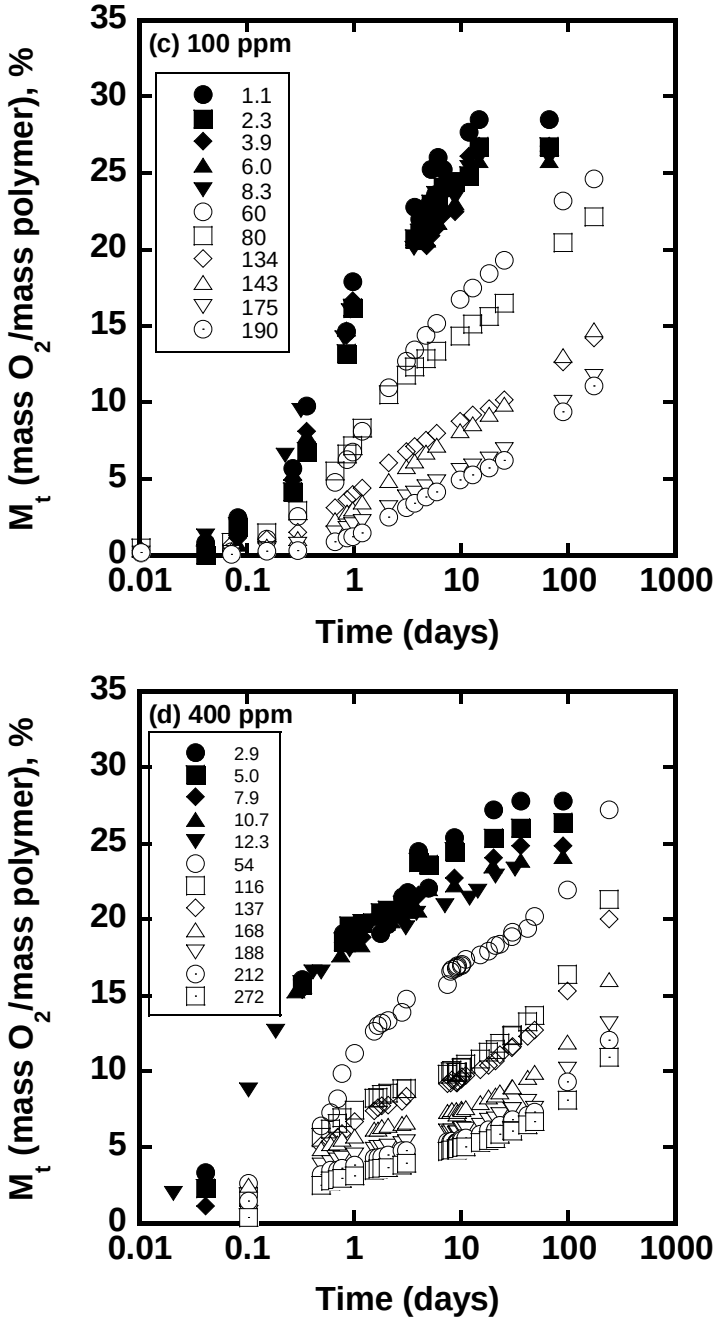

Figure 4.1 (cont): Effect of thickness on oxygen uptake for SBS films containing (c) 100 and (d) 400 ppm catalyst: Data for thin films (solid points) collapse into a single curve that eventually reaches a constant extent of oxidation, while for thick films (open points) uptake strongly depends on thicknesses.

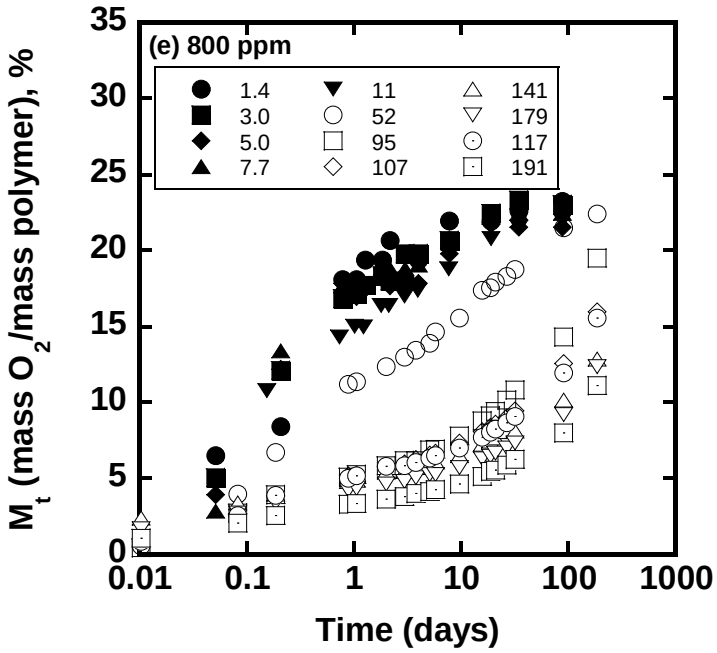

Figure 4.1 (cont): Effect of thickness on oxygen uptake for SBS films containing (e) 800 ppm catalyst: Data for thin films (solid points) collapse into a single curve that eventually reaches a constant extent of oxidation, while for thick films (open points) uptake strongly depends on thicknesses.

The implication of the M_t dependence on film thickness is that the thinner films are fully oxidized at long times on the order of 90 days whereas the thicker films are only partially so and are continuing to oxidize. There is considerable evidence that for thick films oxidation is heterogeneous with an outer oxidized layer that slowly moves inward. It has been suggested that observations like these can be interpreted in terms of a critical thickness, L_c. In other words, homogeneous oxidation is possible for film thicknesses $L \le 2L_c$ and heterogeneous oxidation when $L > 2L_c$, as illustrated in Figure 4.2.

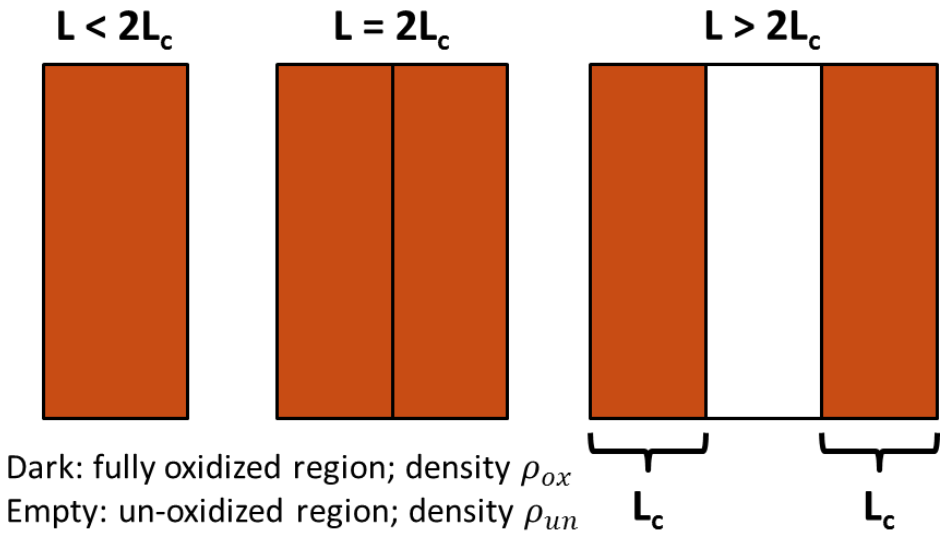

Figure 4.2: Illustration of the concept of critical thickness. Homogeneous oxidation is possible for film thicknesses $L \le 2L_c$ while heterogeneous oxidation occurs when $L > 2L_c$.

Figure 4.3 shows oxygen uptake at ~90 days for reactive films containing 100, 200, 400, and 800 ppm catalyst loadings plotted against inverse film thicknesses, as suggested previously [3,10]. In the homogeneous oxidation region where $L \le 2L_c$ oxygen uptake forms a horizontal line independent of thickness at an average value we designate as M_∞. In the heterogeneous oxidation region where $L > 2L_c$ oxygen uptake M_t increases, $t \cong$ 90 days, with decreasing film thicknesses and takes the form of $M_t \propto 1/L$. The intersection of these two lines yields a thickness $L = 2L_c$ which divides the homogeneous and heterogeneous regimes of oxidation. The values of L_c for the various catalyst loadings at ~90 days of oxidation estimated by this analysis are recorded in Table 4.2.

Based on the ideas outlined above, we expect the ultimate uptake of oxygen M_∞ to be approximately the same for all films regardless of thickness. For thin enough films, this limit is reached within the time scale of these oxidation observations; whereas, for very thick films, it is presumed that reaching this limit would require longer times than for these observations, i.e., 90 days.

The quantity M_∞ can be expressed in terms of the molar density of butadiene repeating units available for oxidation $n_0 = 12.2\, mmol_{PB} / cm^3$ for the current SBS copolymer, the stoichiometric oxidation coefficient $\hat{\nu}$ that describes how many moles of butadiene repeating units oxidized per mole of oxygen molecules, and the density of un-oxidized polymer, ρ_{un} as follows:

$$M_\infty = 32 n_0 / \rho_{un} \hat{\nu} \tag{4.1}$$

Table 4.2 shows values of $\hat{\nu}$ calculated from the M_∞ for thin films, i.e., $L \le 2L_c$, that were fully oxidized at 90 days, see Figure 4.3. These $\hat{\nu}$ values indicate that each butadiene unit takes up 1.1 – 1.3 oxygen atoms on average over the range of catalyst loadings used here.

With the view that ultimately the oxygen uptake of all reactive films would approach M_∞ at long enough time, it is then reasonable in the kinetic analyses discussed later to express oxygen uptake data as normalized values, i.e., M_t / M_∞.

Table 4.2: Kinetics parameters from thin film analysis; critical thicknesses ~ 90 days

Parameter	**Units**	**Catalyst Loading, ppm**			
		100	200	400	800
$\boldsymbol{M_\infty}$	$\frac{g\,of\,O_2}{100\,g\,of\ polymer}$	26.7 ± 1.1	26.6 ± 1.0	24.9 ± 1.7	21.9 ± 1.0
$\hat{\boldsymbol{v}}$	$\frac{mol_{PB}}{mol_{O_2}}$	1.54 ± 0.06	1.56 ± 0.06	1.67 ± 0.11	1.88 ± 0.12
$1/\hat{\boldsymbol{v}}$	$\frac{mol_{O_2}}{mol_{PB}}$	0.65 ± 0.03	0.64 ± 0.03	0.60 ± 0.04	0.53 ± 0.03
$\boldsymbol{k_R}$	$\frac{cm^3}{mol_{PB}\cdot sec}$	7.9 ± 0.5	17.1 ± 2.4	25.3 ± 4.2	48.3 ± 6.0
$\boldsymbol{L_c}$ $(1/\boldsymbol{L})$	μm	31.1 ± 0.1	33.8 ± 0.1	40.8 ± 0.4	35.1 ± 0.2
$\boldsymbol{L_c}$ $(\boldsymbol{SEM})$	μm	30.0 ± 2.0	32.0 ± 2.0	38.0 ± 2.0	35.0 ± 2.0

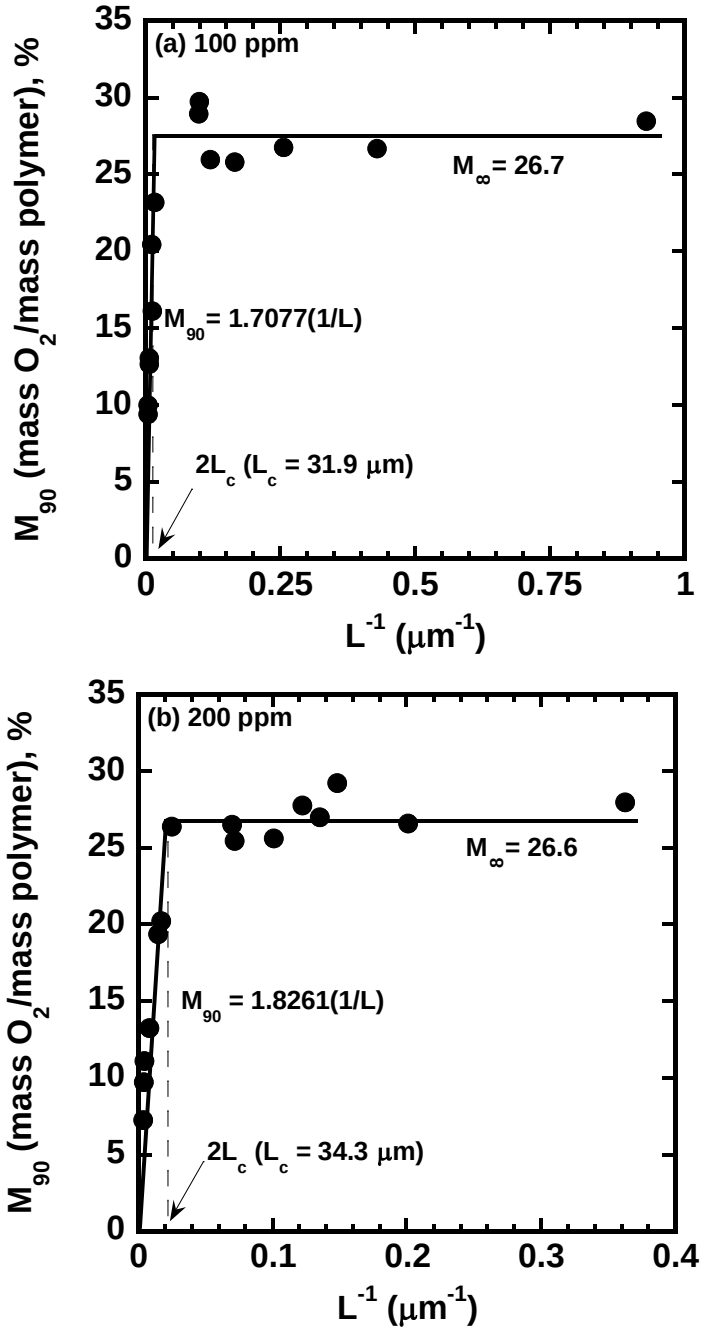

Figure 4.3: Oxygen uptake at ~90 days for reactive films containing (a) 100 and (b) 200 ppm cobalt catalyst loadings plotted against inverse film thicknesses. For $L \le 2L_c$, $M_{90} \sim M_\infty$, while for $L > 2L_c$, M_{90} varies as $1/L$.

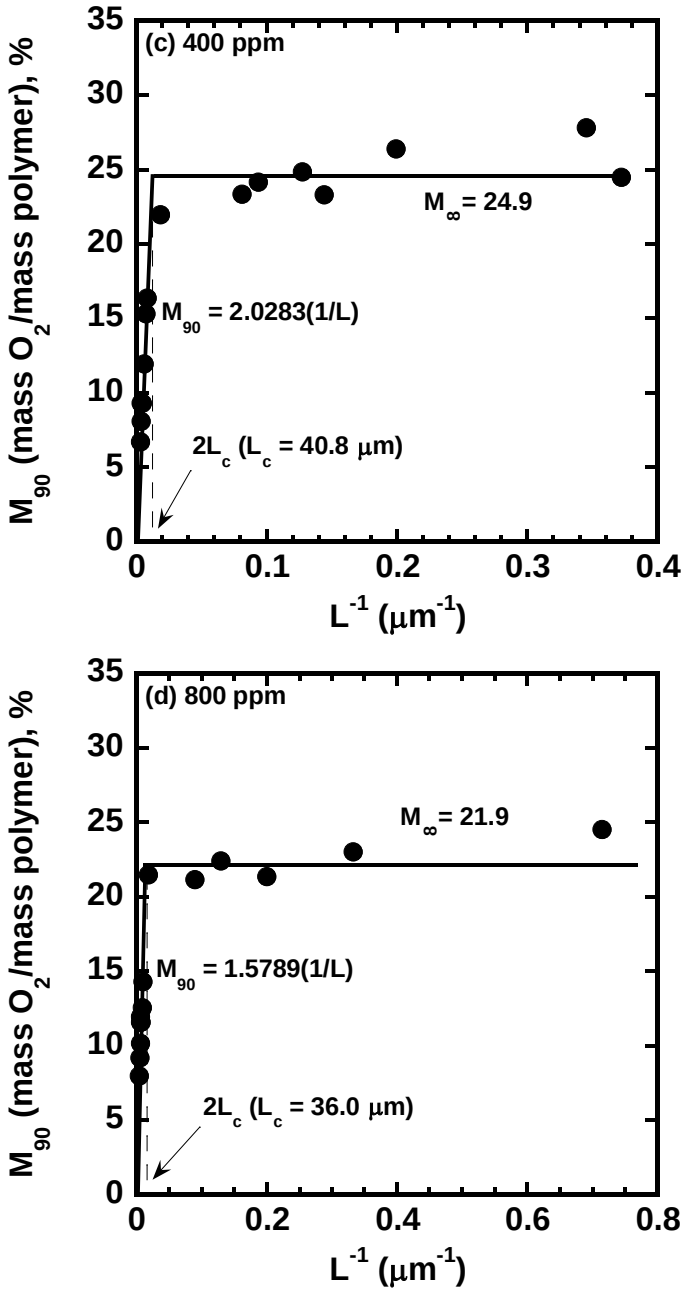

Figure 4.3 (cont):Oxygen uptake at ~90 days for reactive films containing (c) 400 and (d) 800 ppm cobalt catalyst loadings plotted against inverse film thicknesses. For $L \le 2L_c$, $M_{90} \sim M_\infty$, while for $L > 2L_c$, M_{90} varies as $1/L$.

4.2.3 SEM/EDS observations

It has been shown in earlier work that an un-oxidized film of 1,4 polybutadiene reveals a flat and smooth surface when microtomed [3]. In the current work, the SEM images were collected for SBS films oxidized for 90 days based on catalyst loadings of 100, 200, 400, and 800 ppm at 35 °C in air. Figure 4.4(a) shows an SEM image of a microtomed cross-sectional surface of a partially oxidized film containing 200 ppm of catalyst. Here, the outer region is brittle and forms a scalloped fracture pattern when cut by microtoming. This can be attributed to oxidation forming a brittle, glassy polymer region. On the other hand, the inner region remains similar to that seen in the un-oxidized SBS and 1,4 polybutadiene [3] samples.

An EDS analysis, as shown in Figure 4.4(b), clearly shows a high concentration of oxygen-containing functional groups in the outer surface layer in a cross-section of a film of SBS (200 ppm of catalyst), fractured by liquid nitrogen, that was oxidized for 5 days. This supportive illustration confirms that the brittleness found in the outer region of an oxidized film cross-section is primarily due to an oxidation front that progressively moves inward with time. Evidently a surface layer concentrated with oxidation by-products separates the inner regions that remain largely un-oxidized in a butadiene-containing reactive film [3,11,12]. The formation of such oxidized layers is the result of heterogeneous oxidation, i.e., a diffusion-controlled reaction, as in previous work on 1,4 polybutadiene reactive films [3]. The SEM image of a 200 ppm sample cross-section suggests a critical thickness, when oxidized for 90 days, observed at 32 ± 2 μm, which, along with values of samples of other catalyst loadings, are recorded in Table 4.2. These SEM-observed critical thicknesses and those determined by the inverse thickness analysis at 90 days agree very well, within experimental error, as illustrated in Figure 4.5.

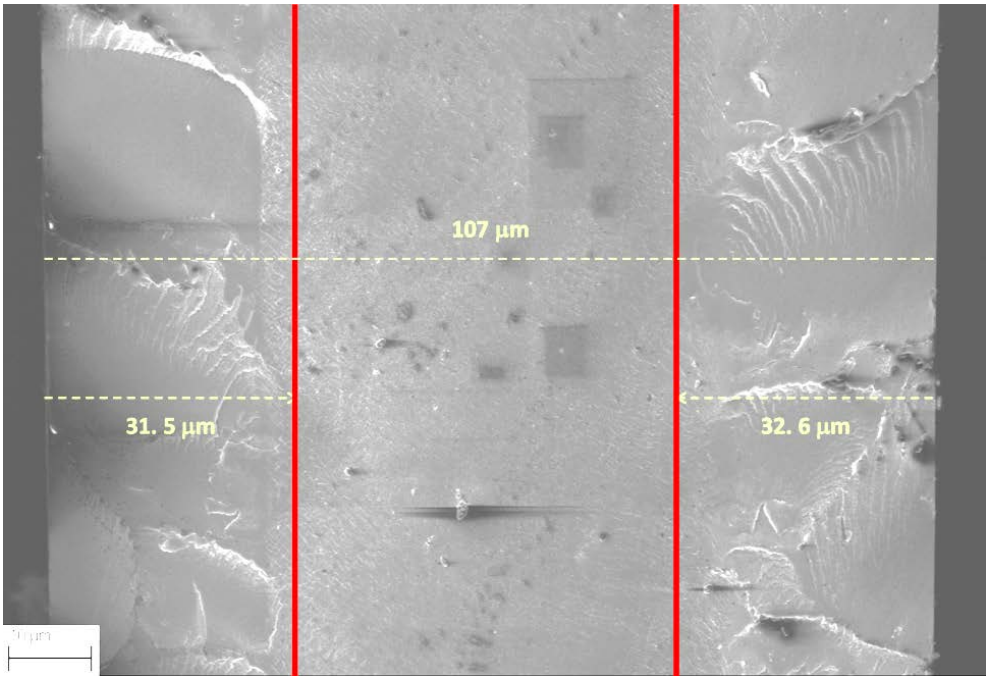

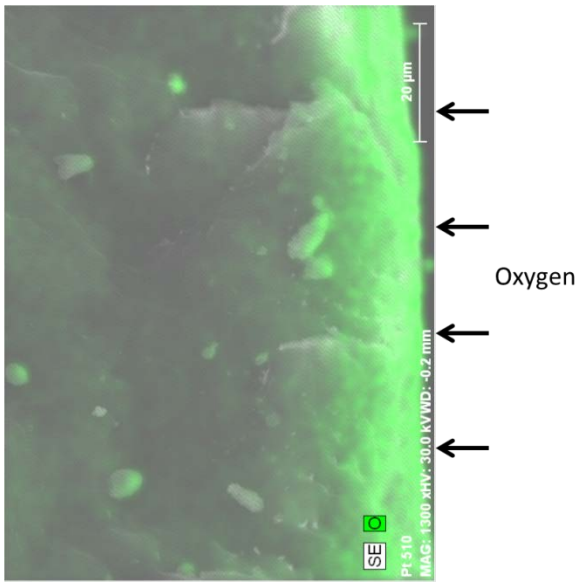

Figure 4.4: (a) An SEM image of a microtomed cross-sectional surface from an oxidized SBS film containing 200 ppm cobalt catalyst reveals outer oxidized layers with a thickness approximately 32 ± 2 µm at ~ 90 days. (b) EDS image analysis clearly shows an accumulation of oxygen-containing functional groups at the outer surfaces of an SBS film (200 ppm of catalyst) that was oxidized for 5 days.

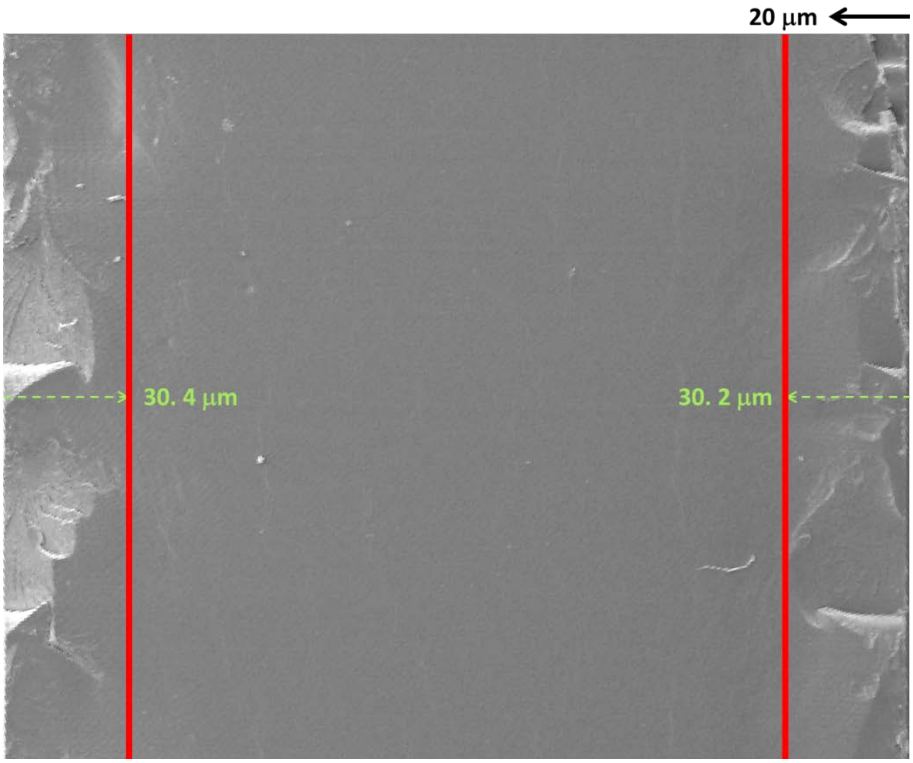

Figure 4.4 (cont): An SEM image of a microtomed cross-sectional surface from an oxidized SBS film containing 100 ppm cobalt catalyst reveals outer oxidized layers with a thickness approximately 30 ± 2 μm at ~ 90 days.

Figure 4.4 (cont): An SEM image of a microtomed cross-sectional surface from an oxidized SBS film containing 400 ppm cobalt catalyst reveals outer oxidized layers with a thickness approximately 38 ± 2 µm at ~ 90 days.

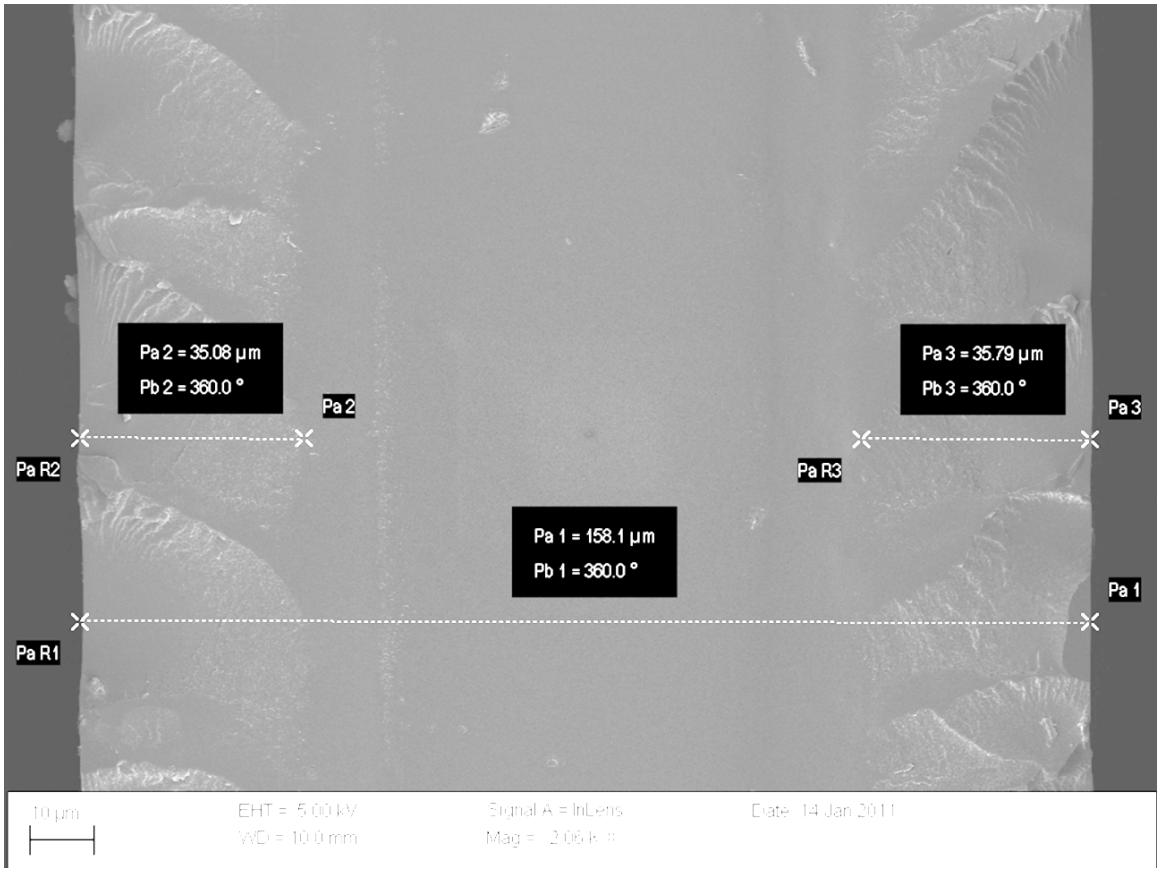

Figure 4.4 (cont): An SEM image of a microtomed cross-sectional surface from an oxidized SBS film containing 800 ppm cobalt catalyst reveals outer oxidized layers with a thickness approximately 35 ± 2 µm at ~ 90 days.

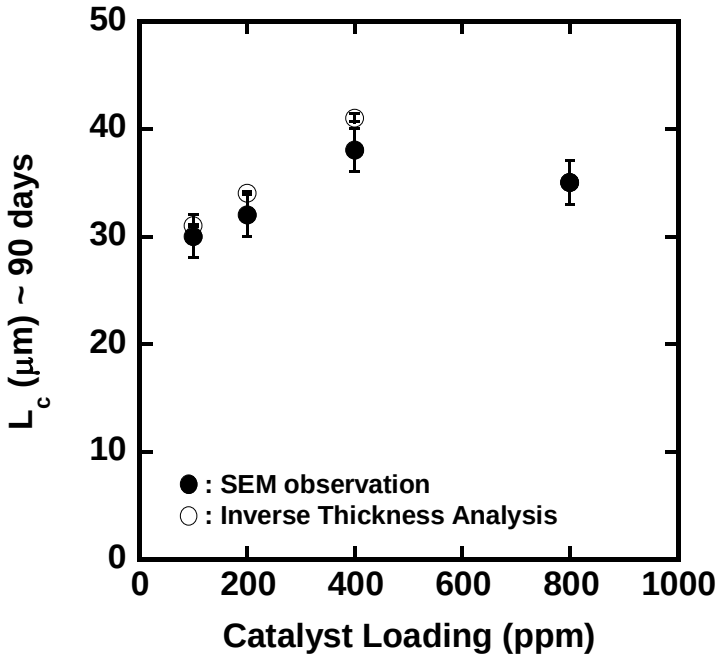

Figure 4.5: The critical thicknesses at ~90 days evaluated by two separate analyses, SEM and oxygen uptake experiment, agree with each other within experimental error.

4.2.4 Kinetic analysis of thin films

Based on the discussion above it is reasonable to expect for thin enough OSP films (certainly less than L_c) that diffusion of oxygen is much faster than the reaction kinetics. In this limit of rapid oxygen diffusion, the concentration of dissolved oxygen in the film C is uniform throughout the thickness and would not vary with time; this oxygen concentration designated here as C_0 can be determined from the solubility of oxygen in the un-oxidized film at least in the early stages of the uptake experiment. On the other hand, the number of un-oxidized butadiene units, n, would be a function of time, starting from n_0 at $t = 0$, but would not be a function of position in the film. This scenario is schematically illustrated in Figure 4.6.

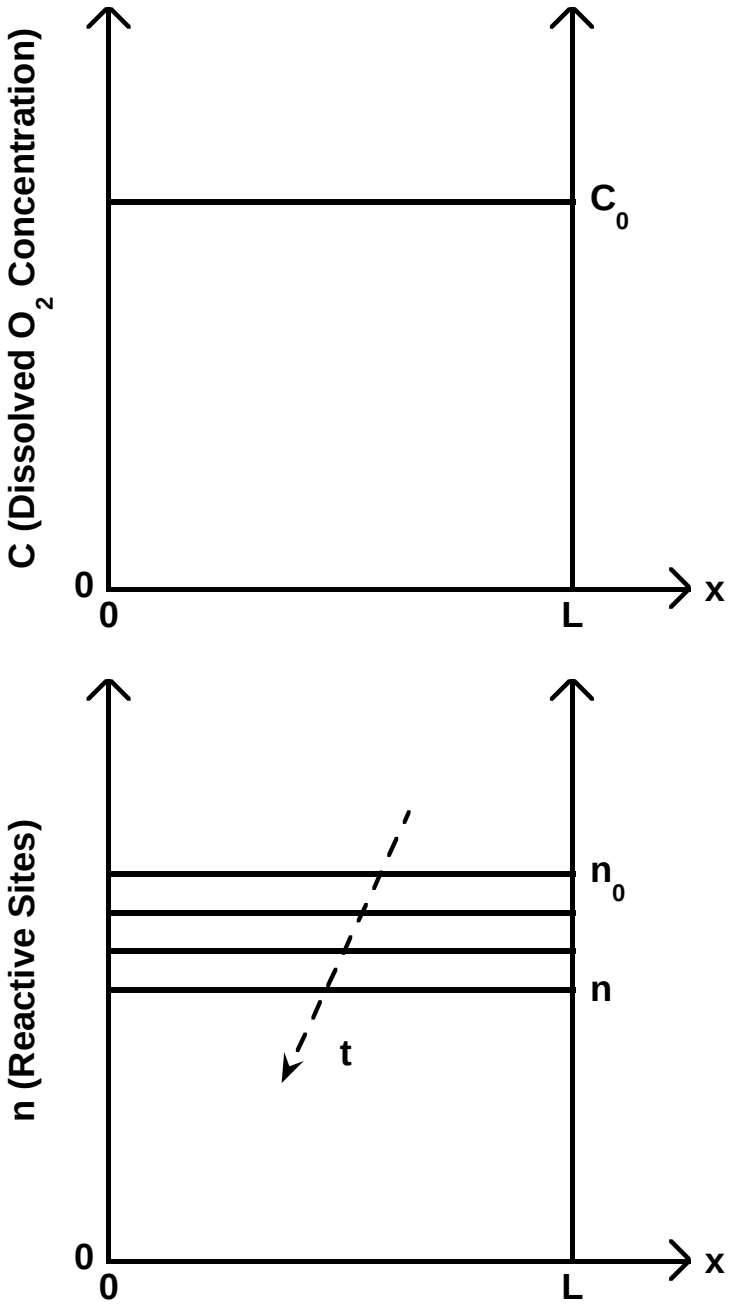

Figure 4.6: Situation when oxidation is controlled by reaction kinetics because oxygen diffusion is relatively more rapid.

The following simple kinetic model should describe the uptake processes assuming the reaction can be approximated as first order

$$\frac{\partial n(t)}{\partial t} = -\hat{\nu} k_R C n(t) = -\hat{\nu} k_R C_0 n(t) \tag{4.2}$$

where k_R is the first order reaction rate parameter. Using the initial conditions that $n = n_0$ at $t = 0$, the model solution becomes

$$n = n_0 e^{-\hat{\nu} k_R C_0 t} \tag{4.3}$$

The mass of oxygen uptake, based on original polymer mass, is thus given by

$$M_t = \frac{32}{\rho_{un} \hat{\nu}} (n_0 - n) \tag{4.4}$$

using Equation (4.1) for M_∞, the desired result becomes

$$\frac{M_t}{M_\infty} = \frac{n_0 - n}{n} = 1 - e^{-\hat{\nu} k_R C_0 t} = 1 - e^{-t/t_{ox}} \tag{4.5}$$

when $t_{ox} = \hat{\nu} k_R C_0$ defines a time scale for the oxidation process. For short enough times, a simple series expansion of the exponential term leads to

$$\frac{M_t}{M_\infty} = \hat{\nu} k_R C_0 t \tag{4.6}$$

From the oxygen solubility coefficient for the un-oxidized SBS given in Table 4.1 and the partial pressure of oxygen in air, we obtain $C_0 = 6.71 \cdot 10^{-7} moles O_2 / cm^3$.

Figure 4.7 shows the oxygen uptake data, normalized by the individual M_∞ for each film (not the average M_∞), plotted on log-log coordinates versus time for thin reactive films containing various catalyst loadings. The fractional oxygen uptake increases linearly with time and eventually reaches unity at times long enough for full oxidation. The rapid oxidation at early times can be modeled by Equation (4.6). Knowing $\hat{\nu}$ and C_0, the reaction rate constant k_R for each film can be extracted from the data; the results are recorded in Table 4.2. These reaction rate constants increase monotonically with catalyst loading, within experimental error, as shown in Figure 4.8.

The dotted lines in Figure 4.7 represents the model prediction, Equation (4.6), of M_t / M_∞ calculated from the average k_R at each catalyst loading, see Table 4.2. The model results agree very well with the experimental M_t / M_∞ data over most of the oxidation process, as shown in Figure 4.7; however, at long oxidation times, typically more than 1 day into oxidation, the model begins to over-predict the experimental M_t / M_∞ values. This probably reflects some level of diffusion control and a breakdown of the assumptions of the model.

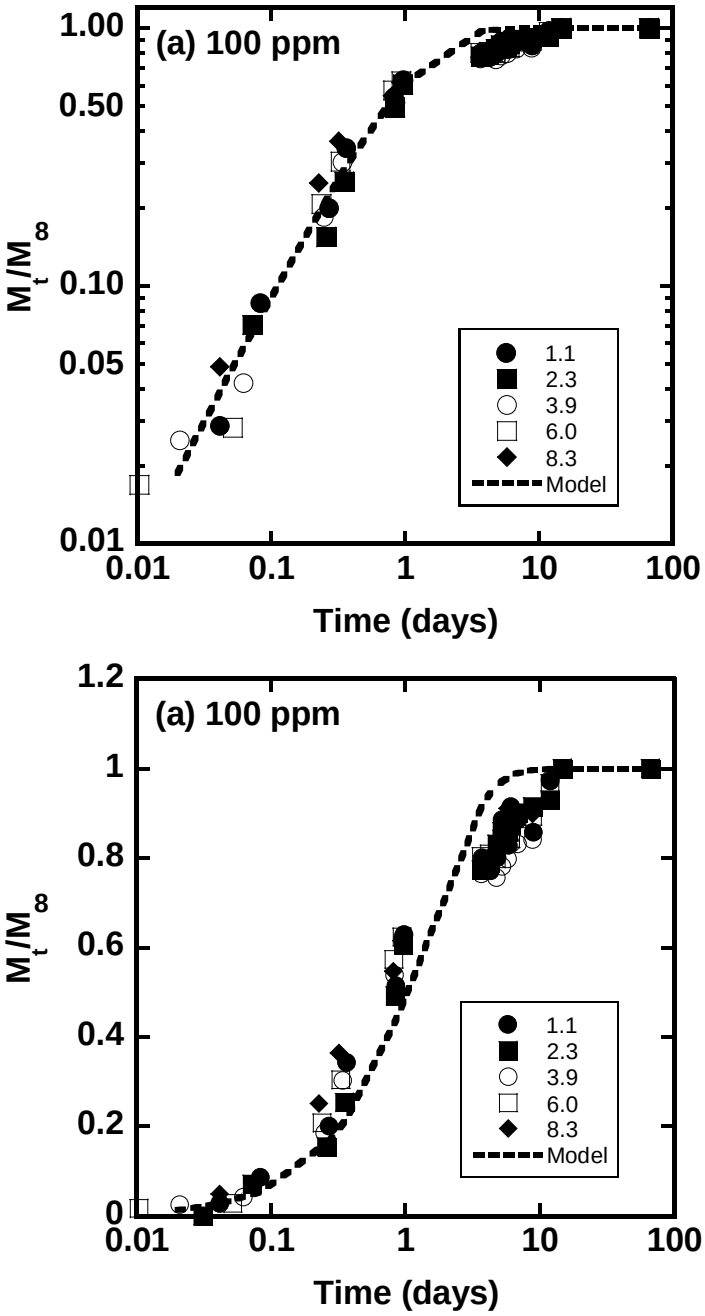

Figure 4.7: Plots of thin film oxygen uptake data versus time using logarithmic and linear coordinates for SBS films containing (a) 100 ppm of cobalt catalyst normalized by M_∞. The dashed lines show kinetic model predictions using the average values of k_R and $\hat{\nu}$ for each catalyst loading.

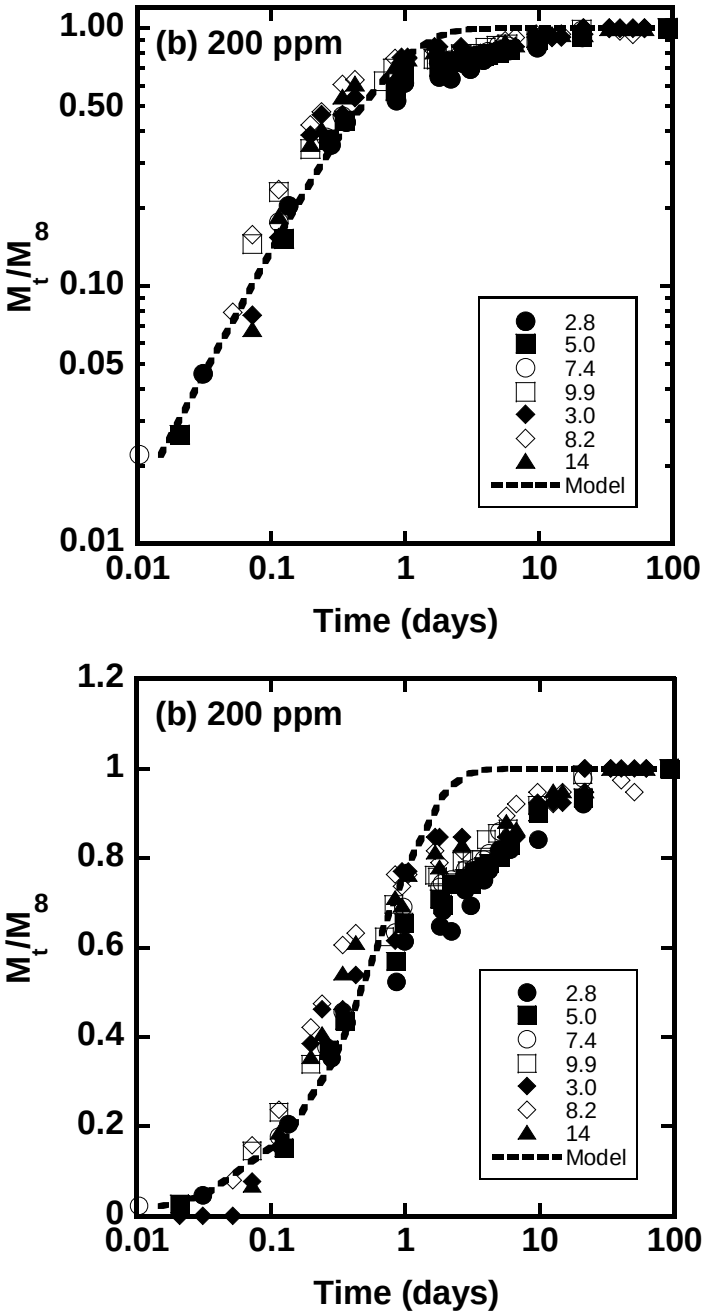

Figure 4.7 (cont): Plots of thin film oxygen uptake data versus time using logarithmic and linear coordinates for SBS films containing (b) 200 ppm of cobalt catalyst normalized by M_∞. The dashed lines show kinetic model predictions using the average values of k_R and $\hat{\nu}$ for each catalyst loading.

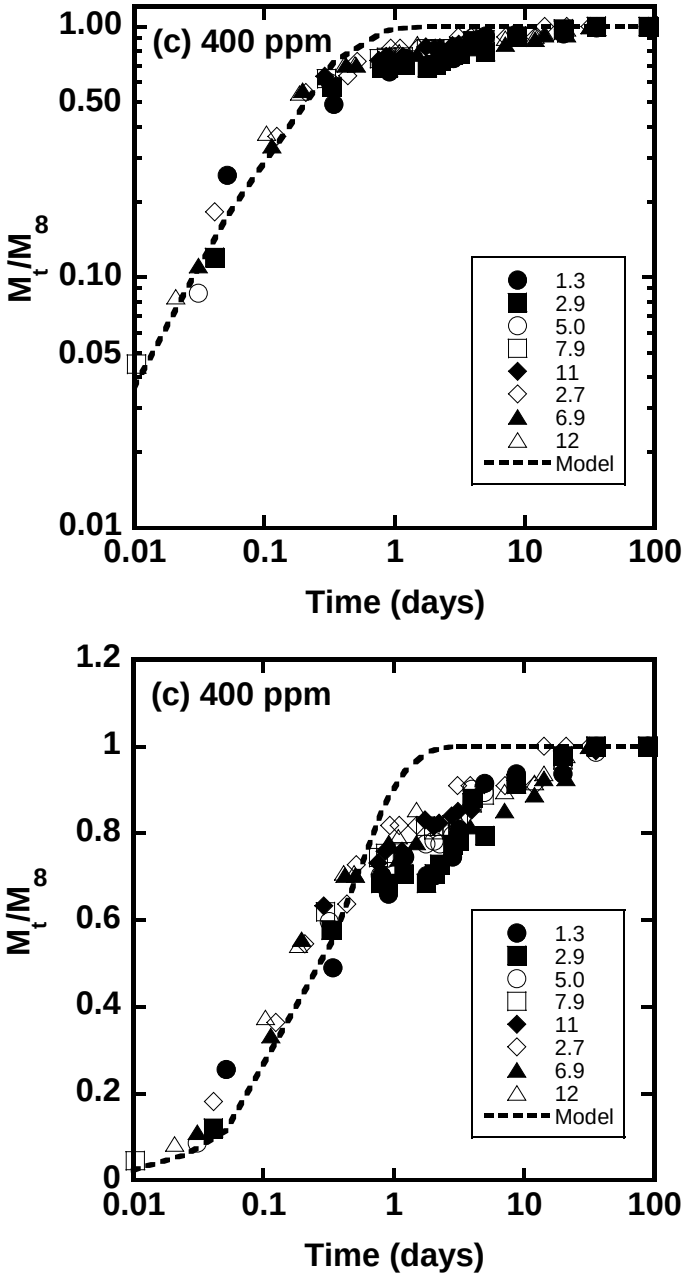

Figure 4.7 (cont): Plots of thin film oxygen uptake data versus time using logarithmic and linear coordinates for SBS films containing (c) 400 ppm of cobalt catalyst normalized by M_∞. The dashed lines show kinetic model predictions using the average values of k_R and $\hat{\nu}$ for each catalyst loading.

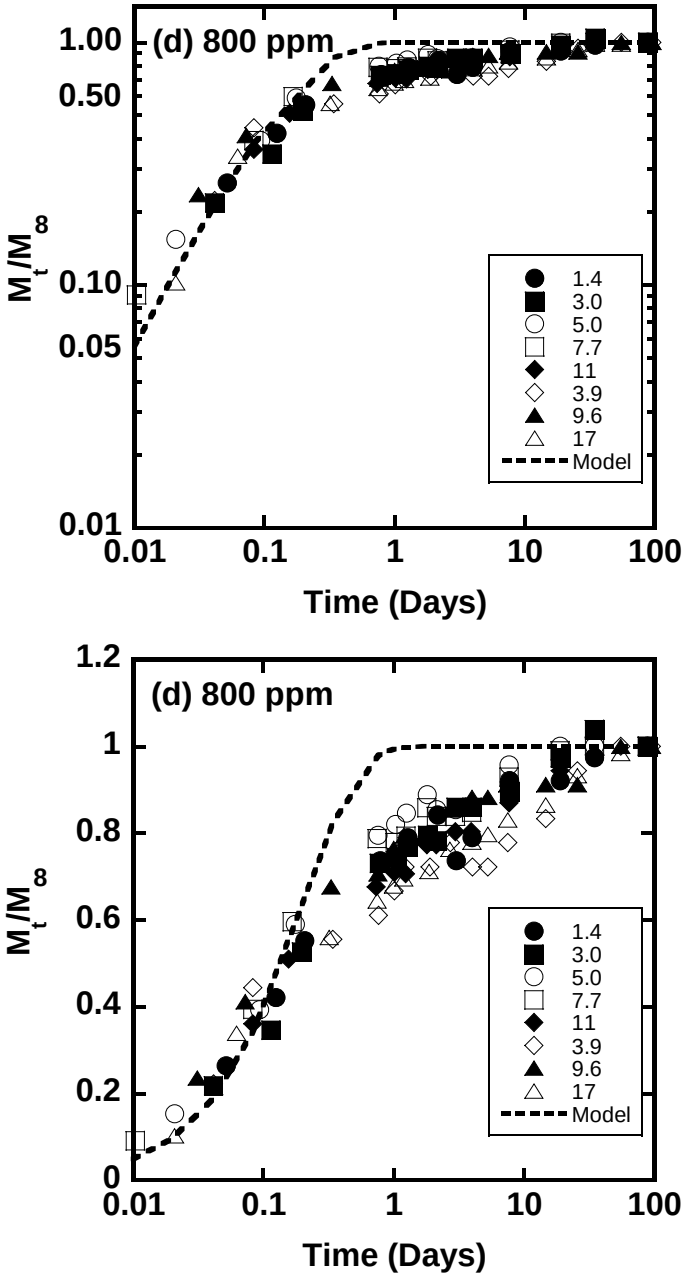

Figure 4.7 (cont): Plots of thin film oxygen uptake data versus time using logarithmic and linear coordinates for SBS films containing (d) 800 ppm of cobalt catalyst normalized by M_∞. The dashed lines show kinetic model predictions using the average values of k_R and $\hat{\nu}$ for each catalyst loading.

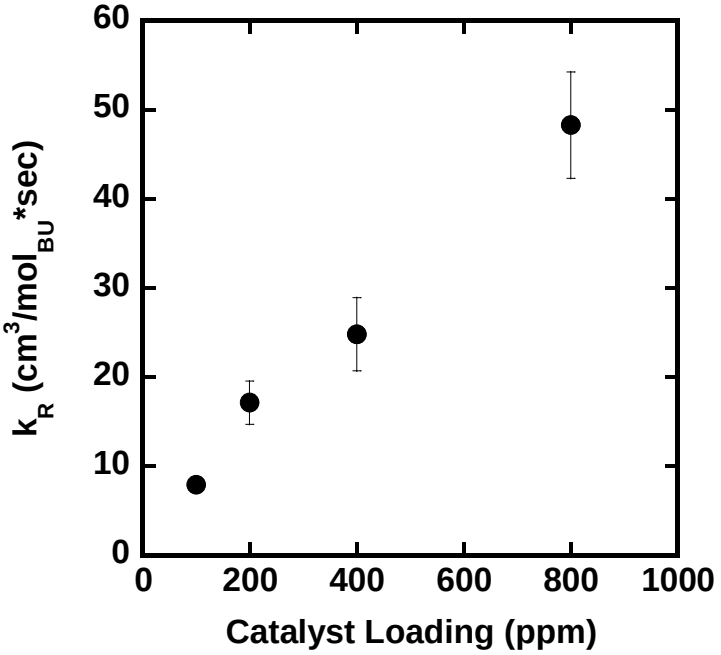

Figure 4.8: Reaction rates constant k_R versus cobalt catalyst loading in SBS films.

4.2.5 An approximate model for thick films

In the very earliest stages of oxygen uptake in thick films, $L > 2L_c$, a regime like that described above should exist where diffusion is not limiting, as suggested in Figure 4.3. However, as time progresses, diffusion should become more and more important until diffusion is the rate controlling process. Models that describe this progression, at least conceptually, have been proposed [13–17]. However, here we develop a simpler approach to illustrate the final stages of this uptake process.

Figure 4.9 illustrates the physical basis of the proposed model. It envisions sharp oxidation fronts at x_f and $L - x_f$ moving inward from the two faces of the film. In the two outer layers of thickness x_f, all the butadiene units have been completely reacted up so $n = 0$ whereas in the core none of the butadiene units have yet reacted so $n = n_0$. The

core shrinks in time as oxygen diffuses through the already oxidized outer layers at a pseudo-steady rate (for both faces of the film) given by

$$Molar\ O_2\ Flux = \frac{D_{ox} C_0}{x_f} \tag{4.7}$$

where D_{ox} is diffusion coefficient of oxygen in the oxidized polymer and C_0 is the dissolved oxygen concentration at the external surface of the oxidized polymer film. In the following calculations of M_t and M_∞, the contribution of any dissolved oxygen is considered negligible.

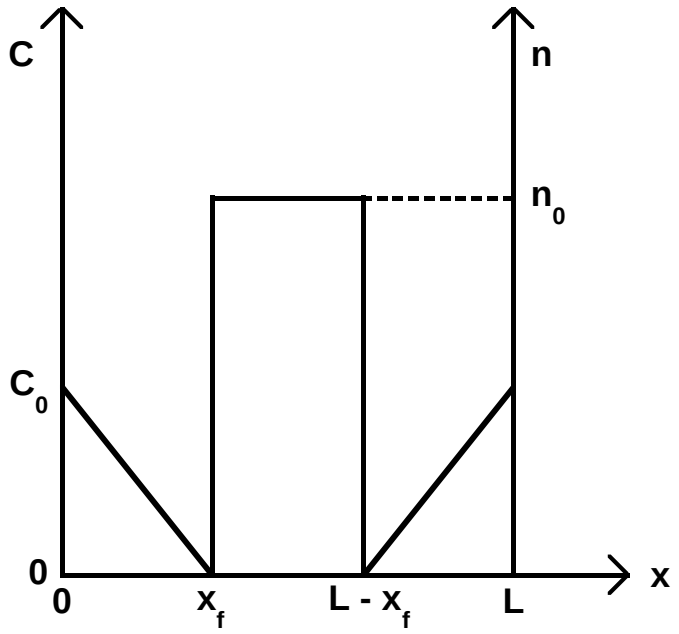

Figure 4.9: Physical picture for the approximate moving-boundary model for thick film oxidation behavior at long oxidation times.

The rate of uptake can be approximated as

$$\frac{\partial M_t}{\partial t} = \frac{2M_\infty}{L}\frac{dx_f}{dt} = \frac{32n_0}{\rho_{un}\hat{v}}\frac{2}{L}\frac{dx_f}{dt} \tag{4.8}$$

A corresponding relationship can be obtained from the molar flux from Fick's law given in Equation (4.7), i.e.,

$$\frac{\partial M_t}{\partial t} = \frac{2\times 32}{\rho_{un}L}\left(molar\ O_2\ \ flux\right) = \frac{64}{\rho_{un}L}\frac{D_{ox}C_0}{x_f} \tag{4.9}$$

Equation (4.8) and (4.9) can be equated and subsequently integrated to obtain

$$\int_{x_{f0}}^{x_f} x_f dx_f = \int_{t_0}^{t} \frac{D_{ox}\hat{v}C_0}{n_0} dt \tag{4.10}$$

Solving for x_f gives

$$x_f = \left[x_{f_0}^2 + \frac{2D_{ox}\hat{v}c_0}{n_0}\left(t - t_0\right)\right]^{1/2} \tag{4.11}$$

The normalized oxygen uptake is then

$$\frac{M_t}{M_\infty} = \frac{2}{L}\left[x_{f_0}^2 + \frac{2D_{ox}\hat{v}c_0}{n_0}\left(t - t_0\right)\right]^{1/2} \tag{4.12}$$

Since the model envisioned in Figure 4.9 would not apply until longer times, the beginning limits of integration are not well defined. However, we might expect that

$$x_{f_0} = L_c \tag{4.13}$$

and that t_0 would be proportional to t_{ox}, as defined earlier, thus

$$t_0 \sim \frac{\alpha}{\hat{v} k_R C_0} \tag{4.14}$$

where α is a proportionality factor. The model can be written in the following general form

$$\frac{M_t}{M_\infty} = \left(a + bt\right)^{1/2} \tag{4.15}$$

where the values of a and b predicted by the model are as follows

$$a \sim 4\left[\left(\frac{L_c}{L}\right)^2 - \frac{2\alpha D_{ox}}{k_R n_0 L^2}\right] \tag{4.16}$$

and

$$b \sim \frac{8 D_{ox} \hat{v} C_0}{n_0 L^2} \tag{4.17}$$

Equation (4.15) can be re-expressed in the form

$$\left(\frac{M_t}{M_\infty}\right)^2 = a + bt \qquad (4.18)$$

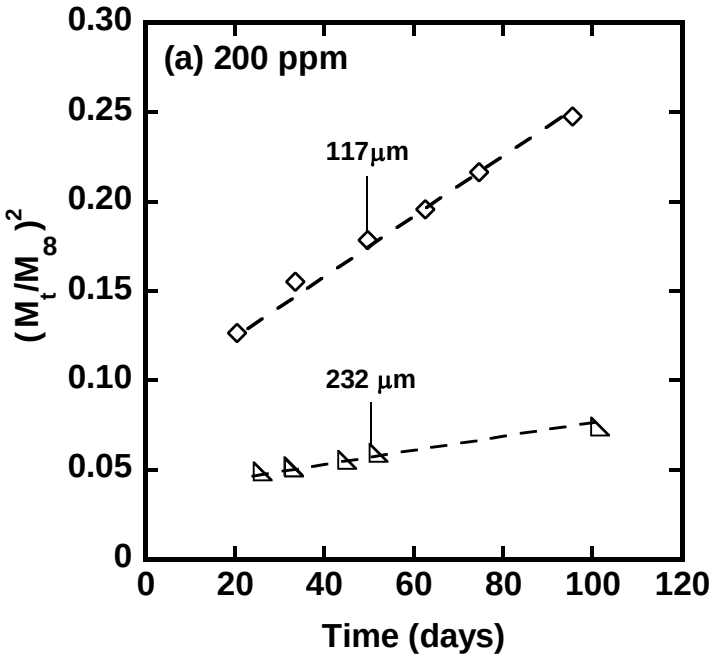

Figure 4.10: (a) Representative plots of thick film oxygen uptake versus time at long oxidation times to obtain values of slopes b and intercepts a in Equation (21), see Table 4.3.

Figure 4.10(a) shows an example of $\left(M_t / M_\infty\right)^2$ plotted versus oxidation times, excluding the early time data where this model is not expected to apply, for two thick films containing 200 ppm of catalyst. The experimental data of $\left(M_t / M_\infty\right)^2$ data increase linearly with time, as expected from the model for thick films. Quite similar plots were obtained for all thick films at each catalyst loading shown in Figure 4.10(b) – (e). From these linear plots the slopes b and intercepts a were extracted for all thick films and recorded in Table 4.3. In fact, plotting M_t / M_∞ versus $\left(a + bt\right)^{1/2}$ for all thick films,

using values of a and b from plots like Figure 4.10, makes a universal straight line with slope of unity, as shown in Figure 4.11. This plot validates the form of the model and the method of extracting slopes b and intercepts a from the data. Note that Figure 4.11 neglects data from the early time regime, when diffusion is fast and oxidation is kinetically controlled. As expected the short time data do not collapse into a single curve, since the current model considers an oxidation that is controlled by diffusion for films with thicknesses $L > 2L_c$.

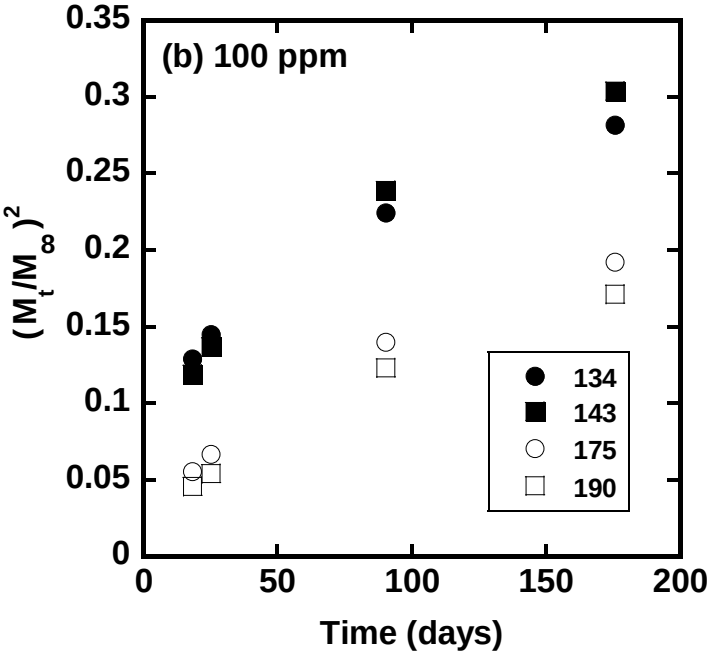

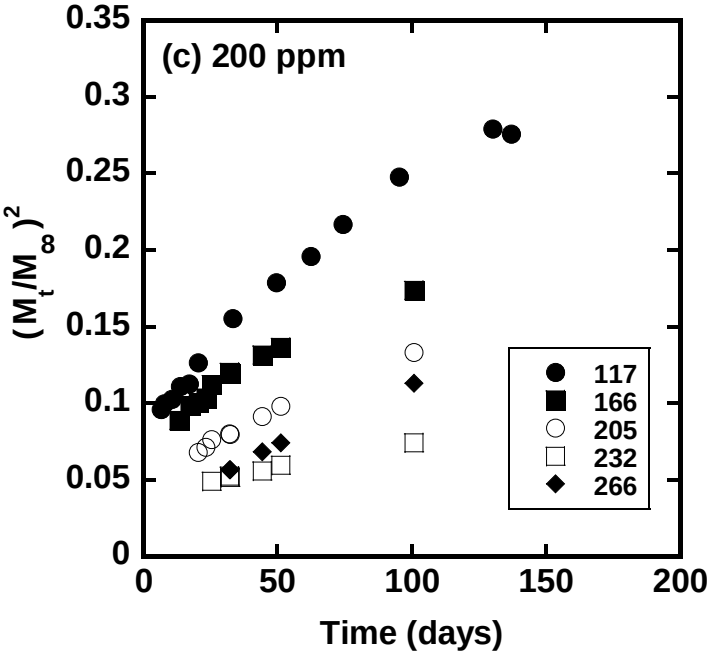

Figure 4.10 (cont): Oxygen uptake versus time plots of thick films at a range of film thickness (~100 – 300 μm) containing (b) 100 and (c) 200 ppm catalyst loadings at long oxidation times to obtain values of slopes b and intercepts a in Equation (21), see Table 4.3.

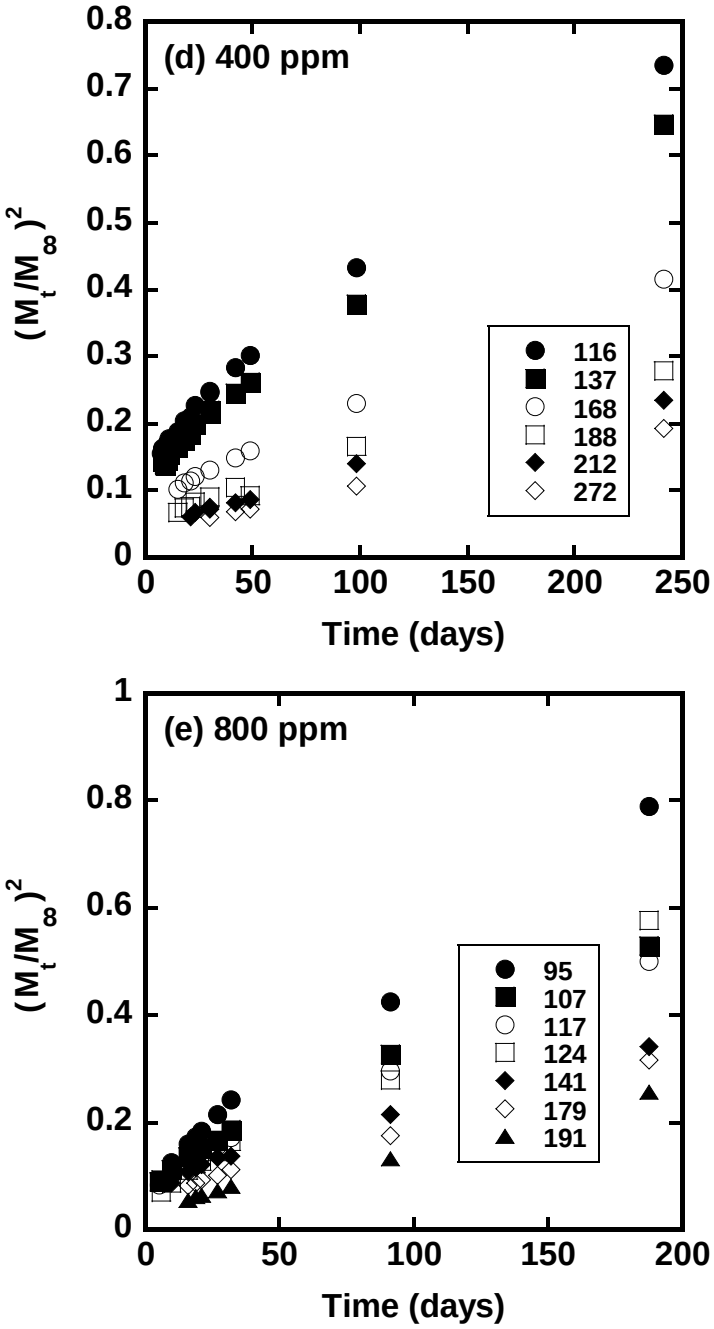

Figure 4.10 (cont): Oxygen uptake versus time plots of thick films at a range of film thickness (~100 – 300 μm) containing (d) 400 and (e) 800 ppm catalyst loadings at long oxidation times to obtain values of slopes b and intercepts a in Equation (21), see Table 4.3.

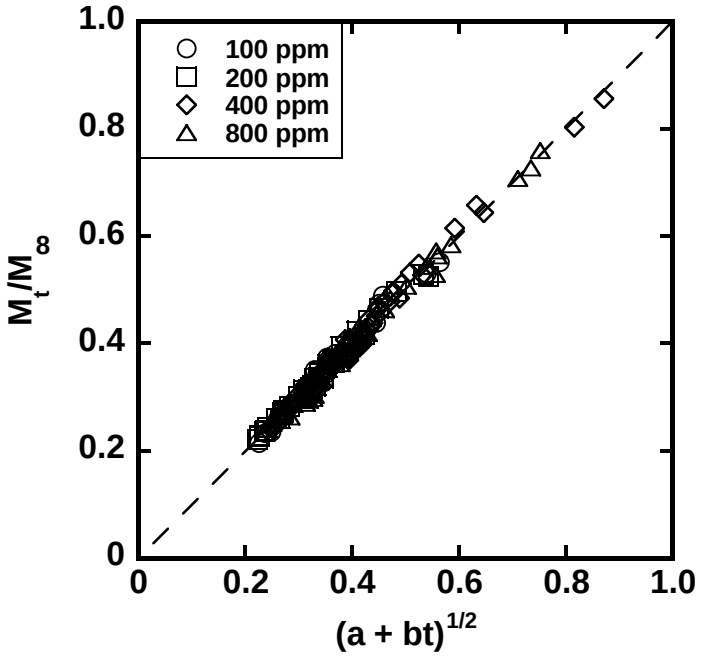

Figure 4.11: Universal plot of M_t / M_∞ versus $(a+bt)^{1/2}$ for all thick films at long oxidation times. Data points for the early time regime are not included.

Equations (4.16) and (4.17) predict that a and b should scale as the inverse square of film thickness. The solid points in Figure 4.12 show the values of a and b determined by statistically fitting the long time data for thick films to Equations (4.16) and (4.17) plotted versus L on log-log coordinates. The solid lines in Figure 4.12 are the predictions by Equations (4.16) and (4.17) using average values of L_c and $\hat{\nu}$ and assuming $\alpha \sim 0$. The data points generally lie parallel to the predicted lines, verifying the L^{-2} dependence expected, but the model over predicts both a and b. Assigning finite values to α would bring the theoretical intercepts into better agreement with the experimental values; however, the slopes would remain over predicted. Thus, the model

does not quantitatively reproduce the oxygen uptake data for thick films when the measured parameters are inserted into Equations (4.16) and (4.17). At least part of this failure might have to do with the fact that the model for the early stages of oxidation in thick films where reaction kinetics controls has not been rigorously merged with the late stage where diffusion controls. Certainly there is an intermediate stage where both kinetics and diffusion must be considered. In any case, this model does appear to capture, at least qualitatively, the behavior for thick films.

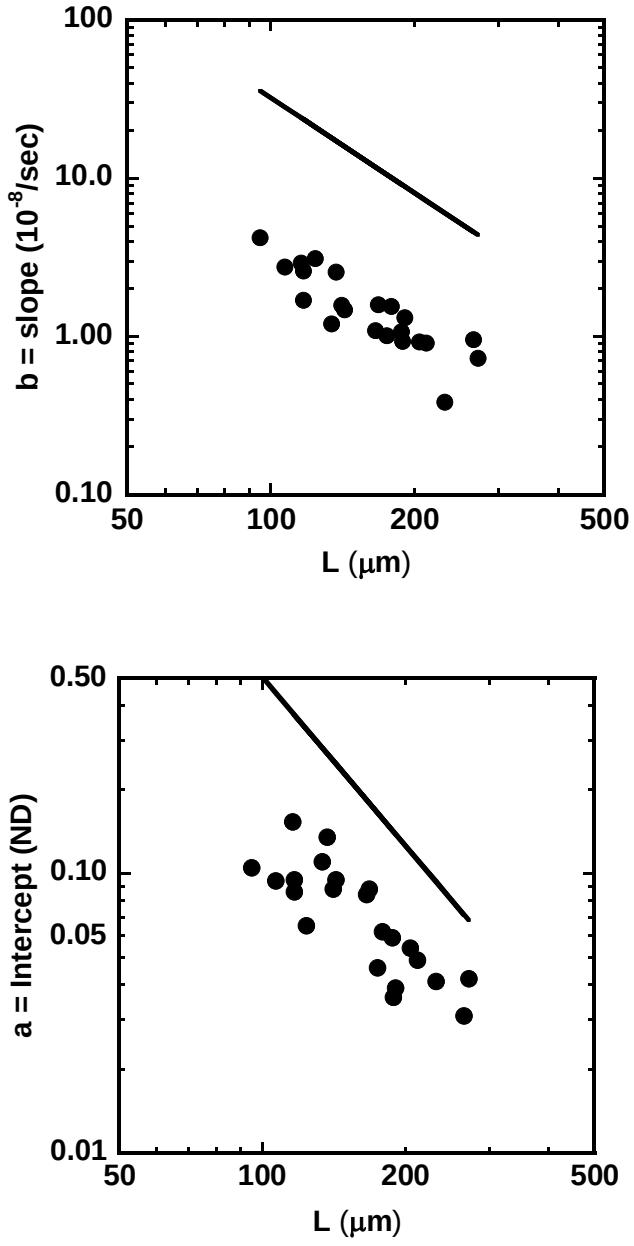

Figure 4.12: Slopes *b* and intercepts *a* calculated from the data via fitting to Equation (21) plotted versus thickness *L* plotted on logarithmic coordinates. The data are consistent with L^{-2} dependence of both a and b as predicted by the model, i.e., the solid lines were constructed using average vales of critical thickness ($L_c = 35.5\,\mu m$) and stoichiometric coefficients ($\hat{\nu} = 1.68\, mol_{PB} / mol_{O_2}$) for all catalyst loadings. The absolute values of a and b are lower than the theoretical predictions.

Table 4.3: Values of slopes b and intercepts a theoretically extracted from all thick film oxygen uptake data at long oxidations

$\boldsymbol{Catalyst\ ppm}$	$\boldsymbol{L\ \mu m}$	$\boldsymbol{b = Slope\ 10^{-8}/sec}$	$\boldsymbol{a = Intercept\ ND}$
100	134	1.20	0.110
	143	1.47	0.095
	175	1.01	0.046
	189	0.93	0.036
200	117	1.69	0.095
	166	1.08	0.084
	205	0.92	0.054
	232	0.83	0.041
	266	0.95	0.031
400	116	2.90	0.153
	137	2.54	0.135
	168	1.58	0.088
	188	1.07	0.059
	212	0.91	0.049
	272	0.72	0.042
800	95	4.20	0.105
	107	2.74	0.094
	117	2.58	0.086
	124	3.09	0.065
	141	1.57	0.088
	179	1.54	0.062
	191	1.31	0.039

4.3 SUMMARY

A styrene-butadiene-styrene block copolymer with varying amounts of a cobalt catalyst was evaluated as an oxygen scavenging component for barrier systems. The oxygen uptake of SBS films containing four catalyst loadings and having a wide range of thicknesses was experimentally measured and analyzed by simple theories. For thin enough films, the rate of oxygen uptake is controlled by the reaction of the butadiene

units with oxygen and is not affected by oxygen diffusion. A simple thin film model allowed extraction of reaction rate and stoichiometric parameters from the experimental data for the oxidation conditions considered in the current study.

At long times for thicker films, the oxygen uptake process is limited by the rate of oxygen diffusion, and a simplified moving boundary model describes this region semi-quantitatively. The division between the two regimes can be understood in terms of the concept of a "critical thickness L_c" introduced in earlier papers. For films with thickness $L \leq 2L_c$, chemical kinetics is largely the rate controlling process and such films became fully oxidized over the time scale of the current observation, ~ 90 days. For thicker films with thicknesses $L > 2L_c$ full oxidation was not achieved within 90 days. Values for L_c were deduced by a simple two regime analysis of the data. These values agree well with observations of cross-sectional surfaces of partially oxidized films made by SEM analysis. The outer region becomes hard and brittle while the interior retains more of the appearance of the native SBS copolymer.

The fully oxidized polymer has an oxygen permeability that is two orders of magnitude lower than that of the un-oxidized SBS material. This fact contributes to the trend towards diffusion control of oxygen uptake in thick films at long times. This fact may be quite beneficial when a scavenging component is incorporated into barrier films as layers by co-extrusion [17]. However, the oxidized form of SBS is still 2 to 3 times more permeable to oxygen than the conventional barrier material poly(ethylene terephthalate) [18].

Future design and modeling of blend and laminate barrier films based on the SBS/cobalt catalyst system should benefit from the fundamental understanding of reaction kinetics and parameters deduced by the current study. A remaining need is for a theoretical model to predict the critical thickness from basic principles rather than using

the extensive experimental protocols discussed here. This would be helpful in designing experiments (i.e., how thin should the films be?) for extraction of kinetic and stoichiometric data quickly and efficiently.

4.4 REFERENCES

[1] J. Kim, P. Kim, H. Lee, Syntheses and gas-transport properties of alkylsilane-modified SBS membranes, Journal of Applied Polymer Science. 66 (1997) 1117–1122.

[2] K.W. Song, K.R. Ka, C.K. Kim, Changes in Gas-Transport Properties with the Phase Structure of Blends Containing Styrene−Butadiene−Styrene Triblock Copolymer and Poly(2,6-dimethyl-1,4-phenylene oxide), Industrial & Engineering Chemistry Research. 49 (2010) 6587–6592.

[3] H. Li, K.K. Tung, D.R. Paul, B.D. Freeman, Effect of film thickness on auto-oxidation in cobalt-catalyzed 1,4-polybutadiene films, Polymer. 52 (2011) 2772–2783.

[4] G.J. Van Amerongen, Influence of structure of elastomers on their permeability to gases, Journal of Polymer Science. 5 (1950) 307–332.

[5] Liesl K. Massey, Permeability Properties of Plastics and Elastomers - A Guide to Packaging and Barrier Materials, 2nd ed., William Andrew Publishing/Plastics Design Library, 2003.

[6] W.J. Koros, D.R. Paul, Design considerations for measurement of gas sorption in polymers by pressure decay, Journal of Polymer Science: Polymer Physics Edition. 14 (1976) 1903–1907.

[7] T.K. Kwei, Introduction to physical polymer science, second edition, by L. H. Sperling, Wiley, New York, 1992, 594 pp., Journal of Polymer Science Part A: Polymer Chemistry. 31 (1993) 1097–1097.

[8] W.M. Lee, Selection of barrier materials from molecular structure, Polymer Engineering and Science. 20 (1980) 65–69.

[9] D.R. Paul, Fundamentals of Transport Phenomena in Polymer Membranes, in: Enrico Drioli & Lidietta Giorno (Ed.), Comprehensive Membrane Science and Engineering, 1st ed., Elsevier B.V., 2010: pp. 75–90.

[10] M. Coquillat, J. Verdu, X. Colin, L. Audouin, R. Nevière, Thermal oxidation of polybutadiene. Part 1: Effect of temperature, oxygen pressure and sample thickness on the thermal oxidation of hydroxyl-terminated polybutadiene, Polymer Degradation and Stability. 92 (2007) 1326–1333.

[11] H. Li, D.K. Ashcraft, B.D. Freeman, M. Stewart, M.K. Jank, T.R. Clark, Non-invasive headspace measurement for characterizing oxygen-scavenging in polymers, Polymer. 49 (2008) 4541–4545.

[12] H. Li, K.K. Tung, D.R. Paul, B.D. Freeman, M. Stewart, J. Jenkins, Characterization of Oxygen Scavenging Films Based on 1,4-Polybutadiene, Industrial & Engineering Chemistry Research. 51 (2012) 7138–7145.

[13] M.C. Ferrari, S. Carranza, R.T. Bonnecaze, K.K. Tung, B.D. Freeman, D.R. Paul, Modeling of oxygen scavenging for improved barrier behavior: Blend films, Journal of Membrane Science. 329 (2009) 183–192.

[14] S. Carranza, D.R. Paul, R.T. Bonnecaze, Analytic formulae for the design of reactive polymer blend barrier materials, Journal of Membrane Science. 360 (2010) 1–8.

[15] S. Carranza, D.R. Paul, R.T. Bonnecaze, Design formulae for reactive barrier membranes, Chemical Engineering Science. 65 (2010) 1151–1158.

[16] S. Carranza, Modeling of Oxygen Scavenging Polymers and Composites (Ph.D. Thesis), The University of Texas at Austin, 2010.

[17] S. Carranza, D.R. Paul, R.T. Bonnecaze, Multilayer reactive barrier materials, Journal of Membrane Science. 399-400 (2012) 73–85.

[18] G.S. Andrade, D.M. Collard, D.A. Schiraldi, Y. Hu, E. Baer, A. Hiltner, Oxygen barrier properties of PET copolymers containing bis(2-hydroxyethyl)hydroquinones, Journal of Applied Polymer Science. 89 (2003) 934–942.

Chapter 5: Establishing processing condition by characterizing oxidation behavior of melt-processed SBS and polystyrene blends

5.1 INTRODUCTION

The previous chapter discusses the oxygen uptake behavior of solution cast films for formulations that contain a catalyst and a photoinitiator. This was a rapid and convenient way to develop potentially useful formulations of scavenging materials. However, the ultimate implementation of this concept will require melt extrusion (or coextrusion) of films at the temperatures required for processing the base polymers. Thus, it is necessary to validate that the previously described formulations can be melt-processed and still retain the appropriate scavenging behavior. Potential reasons for differences between solution-cast and melt-processed formulations include oxidation [1–8] or degradation [6,9] of the SBS and loss of activity of the catalyst or photoinitator [8,10].

This chapter examines the oxygen uptake behaviors of melt-processed Kraton SBS and their blends with polystyrene as a function of SBS composition. By using semi-quantitative modeling, we compared the uptake activity of melt-processed Kraton SBS to that of blend films prepared by solution casting. This chapter will show that, with the appropriate set of processing conditions, melt-extruded films are capable of scavenging oxygen at the same rate and with the same uptake capacity as analogous films prepared without melt-processing.

5.2 COMPARING OXIDATION BEHAVIOR OF MELT-PROCESSED AND SOLUTION CAST KRATON SBS

5.2.1 Phase morphology and oxidation behavior of melt-processed SBS block copolymers

Kraton SBS formulations were melt-processed into films that were then subjected to oxygen uptake experiments at the same experimental conditions as those of solution cast films. This protocol was followed to ensure that the previously identified processing conditions (180 °C processing temperature and 10 min residence time, shown in Chapter 3, section 2.3.1) can produce melt-processed SBS reactive films that scavenge at similar rates when compared to the solution cast formulation.

Figures 5.1 and 5.2 show the morphology of solution cast and melt-processed Kraton SBS, respectively. The cylindrical morphology of the PS phase, visible as lighter areas in TEM images from the Kraton SBS, was also observed in other studies [11,12]. The Kraton SBS films prepared by melt-processing appear to have their microdomains in a fixed direction along the line of extrusion, while the solution cast films do not show aligned phases.

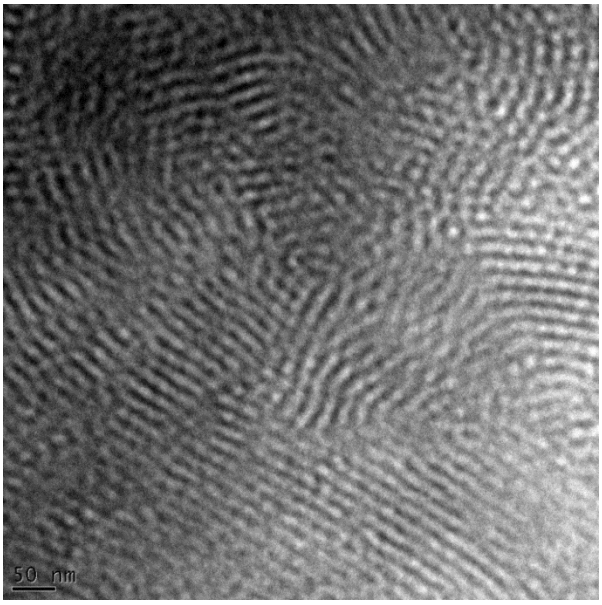

Figure 5.1: Cylindrical morphology of the polystyrene phase does not orient in a fixed direction within the butadiene phase in solution cast Kraton SBS films.

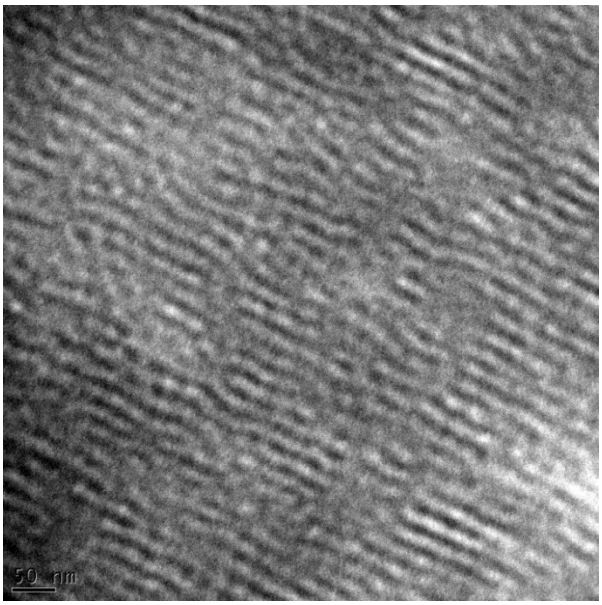

Figure 5.2: Cylindrical morphology of the butadiene phase is aligned with the polystyrene phase in melt-processed Kraton SBS films and is oriented in the extrusion machine direction.

Reactive films of SBS block copolymer were prepared with 1 wt% of photoinitiator and catalyst loading at 400 and 800 ppm. The solution cast SBS films were pelletized and then extruded by the DSM at 180 °C after 10 minutes residence time. The resulting thermally treated reactive film was allowed to oxidize after being exposed to a fixed level of UV energy for 12 minutes (~ 12 J/cm^2), the same as the solution cast films. The film weight increase due to oxidation was monitored for approximately 90 days, and curves representing the mass uptake kinetics of the films were generated for different film thicknesses and catalyst loadings. The M_t uptake results for melt-processed Kraton SBS films at thicknesses from 100 to 200 μm, loaded with 400 ppm and 800 ppm catalyst, are shown in Figures 5.3 and 5.4, respectively.

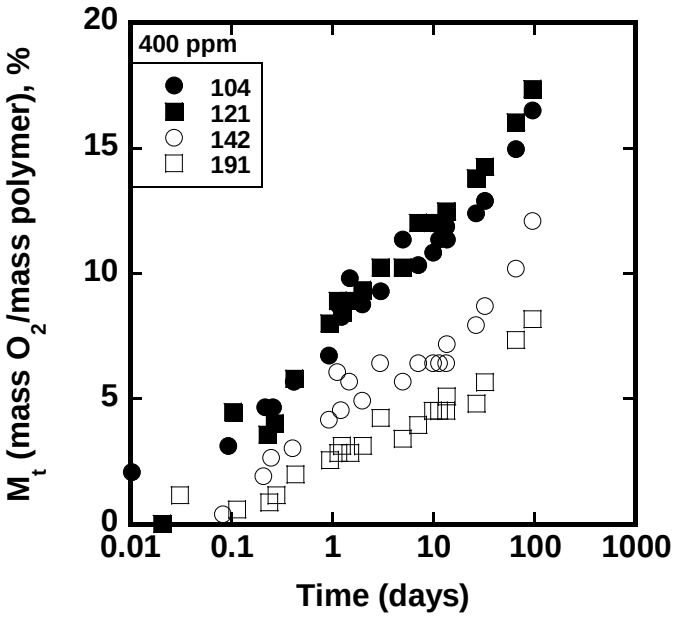

Figure 5.3: Mass uptake kinetics of 400 ppm Kraton SBS (~ 100 to 200 μm in legend) films that have been extruded at 180 °C for 10 minutes.

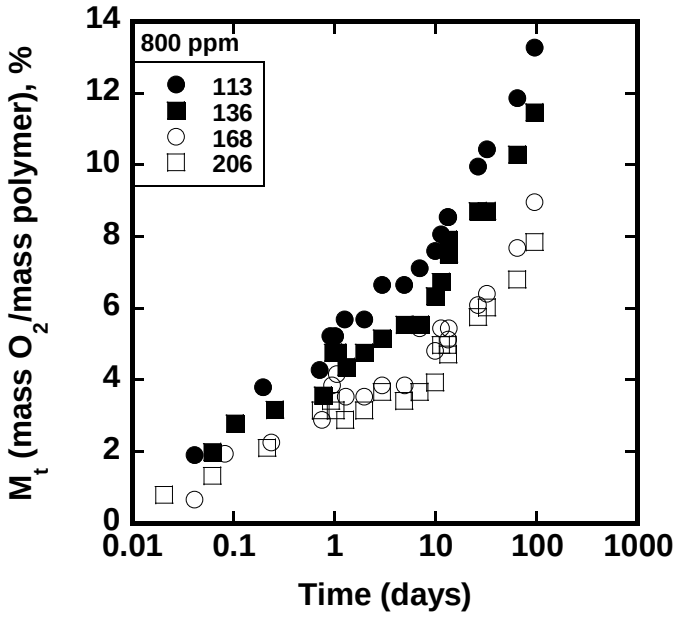

Figure 5.4: Mass uptake kinetics of 800 ppm Kraton SBS films (~ 100 to 200 μm in legend) that have been extruded at 180 °C for 10 minutes.

There is some level of scavenging activity in these reactive films even after thermal treatment. Initially oxygen uptake increases rapidly with time, and there appears to be a thickness effect on the kinetics. These M_t versus time results were recast to display the quantity $\left(\frac{M_t}{M_\infty}\right)^2$ versus time to allow a further analysis using the uptake theories (Equation 4.22). Mass uptake activity at long oxidation times with catalyst loadings of 400 and 800 ppm are shown in Figures 5.5 and 5.6, respectively.

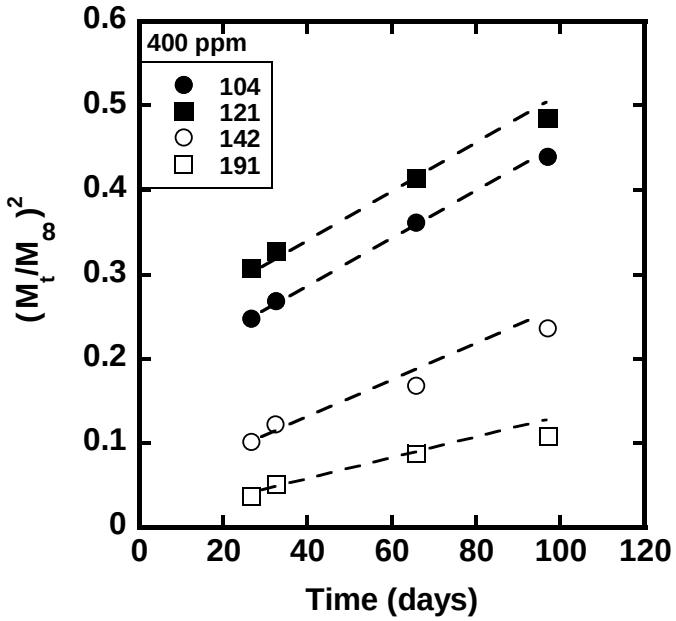

Figure 5.5: Oxygen uptake at long oxidation times for melt-processed Kraton SBS films (~ 100 to 200 μm in legend) with 400 ppm catalyst loading.

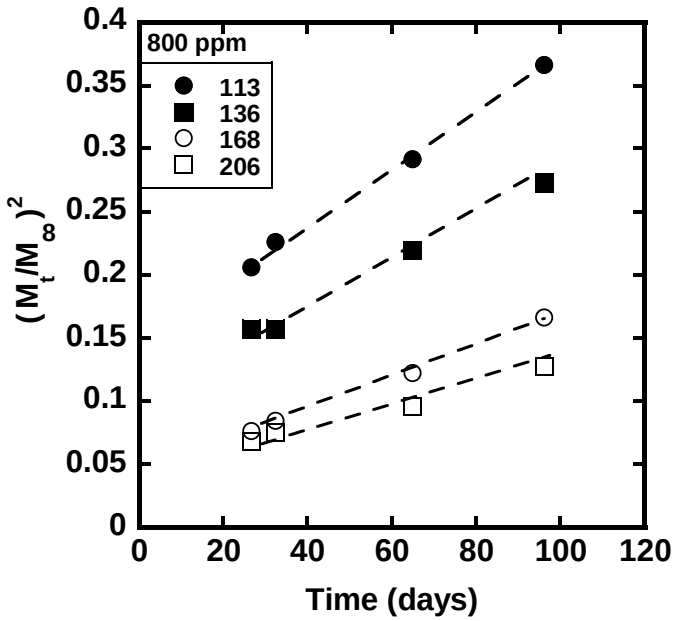

Figure 5.6: Oxygen uptake at long oxidation times for melt-processed Kraton SBS films (~ 100 to 200 μm in legend) with 800 ppm catalyst loading.

5.2.2 Comparing parameter values at long oxidation times parameters between melt-processed and solution cast Kraton SBS block copolymers

The values of slope and intercept from these oxygen uptakes at long oxidation times can be obtained by regression fitting, as shown in Figure 4.10 [13]. Both the slope and the intercept (Equations 4.16 and 4.17) are fitted parameters that define the oxidation kinetics at long oxidation times. When all other variables are held constant, these equations suggest an *inverse* relationship between the intercept and the reaction rate constant k_R, and a *direct linear* relationship between slope and the stoichiometric oxidation coefficient.

The slope and intercept values of melt-processed and solution cast films with 400 and 800 ppm catalyst loading at various thicknesses are shown in Table 5.1. Figures 5.7 and 5.8 show the effect of processing on the uptake activities of 400 and 800 ppm reactive films, respectively. While the uptake data for solution cast films with 400 and 800 ppm catalyst loading at various thicknesses can be found in section 2.5 in Chapter 4, selected data are presented in the following section for convenient comparison.

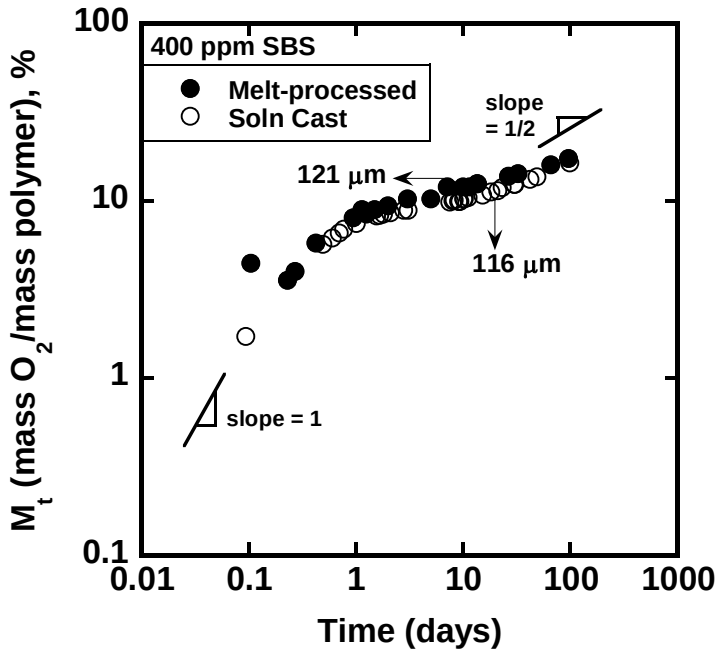

Figure 5.7: The uptake activity of a melt-processed film (121 μm) with 400 ppm catalyst loading is comparable to that of a solution cast film (116 μm) at similar thickness. A plot using log-log coordinates suggests that early time uptake varies with t while at longer times a $\sqrt{t}$ regime is approached.

The oxidation behavior of melt-processed Kraton SBS films are comparable to that of films prepared by solution casting at a similar thickness. Specifically, on plots using log-log coordinates, the rate of oxygen uptake was found to decrease with time, and approaches to square root of time suggestive of a diffusion controlled mechanism. This is true for both melt-processed and solution-cast films; a similar observation was reported in the past [13].

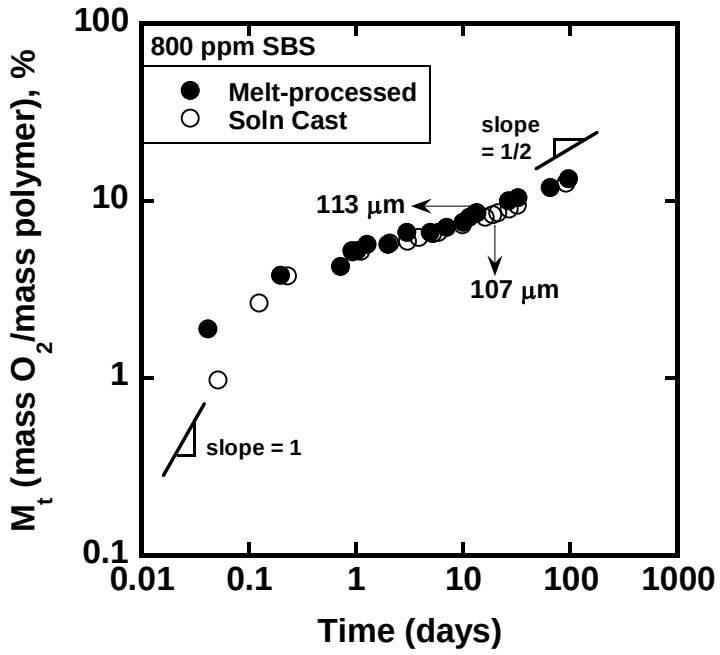

Figure 5.8: The uptake activity of a melt-processed film (113 μm) with 800 ppm catalyst loading is comparable to that of a solution cast film (107 μm) at similar thickness. A plot using log-log coordinates suggests that early time uptake varies with t while at longer times a $\sqrt{t}$ regime is approached.

The values of oxygen uptake per unit time, as well as the slope and intercept at long oxidation times, are comparable in all reactive films of similar thickness, independent of the preparation techniques. Thus, films prepared by solution casting and melt-processing will have similar oxidation kinetics and behavior. The slope and intercept values extracted from long time oxidation uptake data plotted against thickness are shown in Figures 5.9 and Figure 5.10, respectively.

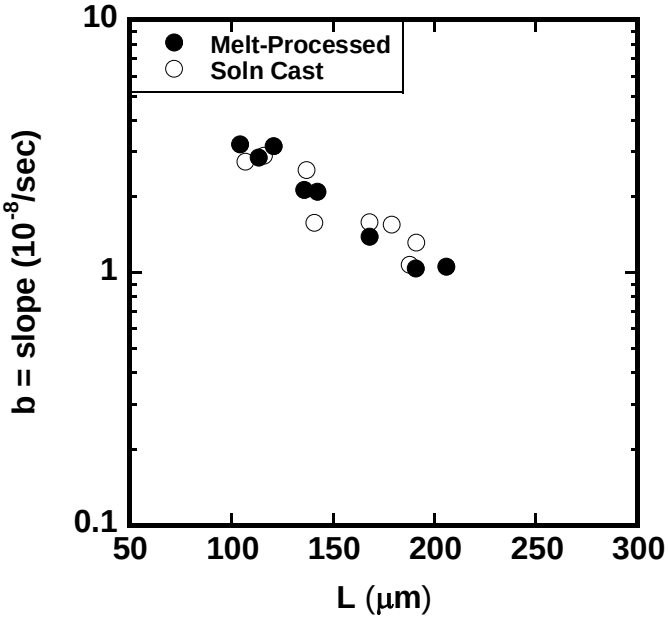

Figure 5.9: The slope values extracted from long time oxidation uptakes of melt-processed films are comparable to those of solution cast films.

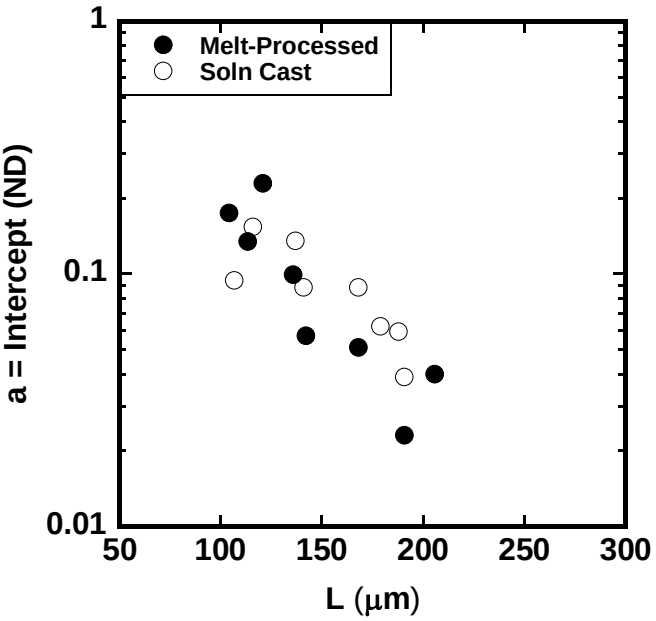

Figure 5.10: The intercept values extracted from long time oxidation uptakes of melt-processed films are comparable to those of solution cast films.

The effect of film thickness can be observed by comparing slope and intercept values from uptake data of Kraton SBS films prepared by melt-processing and solution casting techniques. Their slope and intercept values continue to show the expected L^{-2} dependence, as predicted by the semi-quantitative model [13]. Thus, melt-processed Kraton SBS films have oxidation kinetics similar to those of films prepared by solution-casting.

Table 5.1: The values for slope and intercept of solution-cast and melt-processed film at similar catalyst loading and thicknesses

	Solution Cast			**Melt-Processed**		
Catalyst ppm	L μm	$b = Slope$ $10^{-8}/sec$	$a = Intercept$ ND	L μm	$b = Slope$ $10^{-8}/sec$	$a = Intercept$ ND
400	116	2.90	0.153	104	3.21	0.174
	116	2.90	0.153	121	3.15	0.228
	168	1.58	0.088	142	2.08	0.057
	188	1.07	0.059	191	1.03	0.023
800	107	2.74	0.094	113	2.84	0.134
	141	1.57	0.088	136	2.11	0.099
	179	1.54	0.062	168	1.38	0.051
	191	1.31	0.039	206	1.05	0.040

5.3 CHARACTERIZING OXIDATION BEHAVIOR OF POLYSTYRENE FILMS BLENDED WITH REACTIVE KRATON SBS BLOCK COPOLYMERS VIA UPTAKE EXPERIMENTS

5.3.1 Film preparation

Polystyrene films blended with SBS were produced following the procedures outlined in section 2.3.2 in Chapter 3. The reactive film was solution cast in cyclohexane with 400 and 800 ppm catalyst loading and 1 wt% photoinitiator. Blend films with varying amounts (from 0 to 100%) of pelletized reactive SBS film and polystyrene matrix polymer were melt-extruded in the DSM.

5.3.2 Effect of oxidation on glass transition temperature

When blends with increasing SBS content were tested, the T_g of the butadiene phase in SBS block copolymers becomes more evident with SBS content, as shown in Figure 5.11. For these unoxidized blends, the T_g of the styrene segments in the pure block copolymer was below what would be expected for pure polystyrene, approximately 100 °C. This well-known phenomenon [12] was attributed to the relatively low molecular weight of PS in the copolymer (28,000; 28% of Kraton D1102 SBS block copolymer comprises the polystyrene block), the diffuse interphase between component domains, and surface energy [12]. The polystyrene phase in the copolymer can interdiffuse with the polystyrene matrix due to favorable polymer-polymer interactions. This effect has been reported previously and typically contributes to the observed merging of glass transition temperatures [14].

Given sufficient oxidation time (in this case 1 year), the DSC transition corresponding to the butadiene phase completely disappears. This indicates that the reactive sites in the butadiene phase have been fully oxidized, leaving in these oxidized

blends at most an extremely small amount of butadiene, which cannot be detected by DSC, as shown in Figure 5.12.

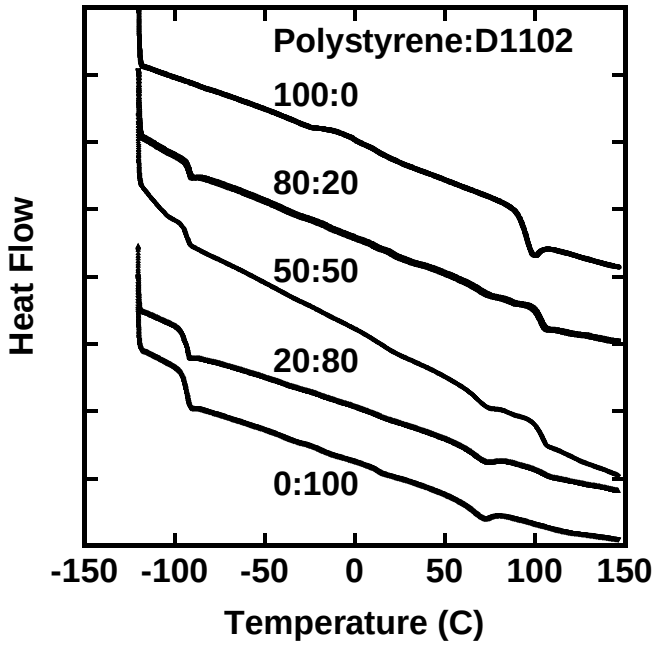

Figure 5.11: The DSC thermograms of unoxidized blends. While the T_g of butadiene phase (~ 80 °C) in SBS becomes more clear with increasing SBS content, the peak that suggests the T_g of PS (~100 °C) grows larger in size when SBS concentration decreases.

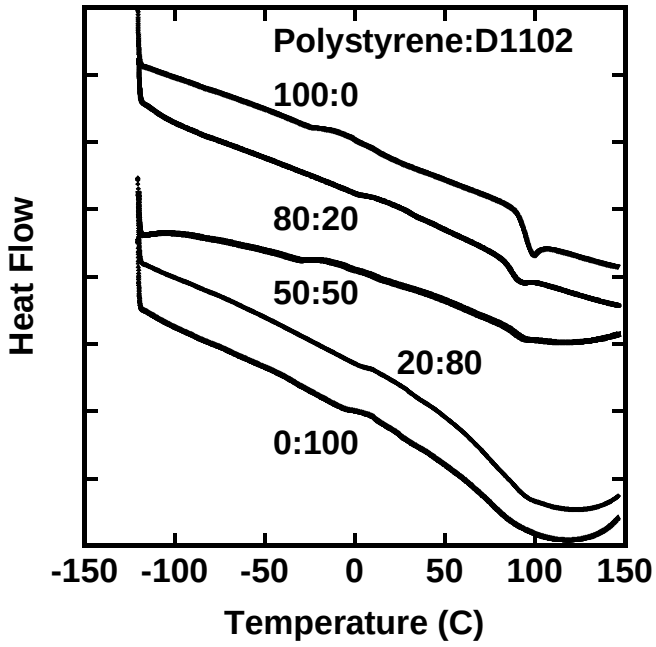

Figure 5.12: DSC thermograms of oxidized blends. The T_g of the butadiene phase disappeared in all samples, suggesting these films have been fully oxidized.

5.3.3 Effect of oxidation on film density

The density values of PS/SBS blend films allowed to oxidize in 35 °C air for more than a year, as well as those of unoxidized blends, are shown in Figure 5.13. The densities of unoxidized and fully oxidized SBS block copolymers were 0.94 and 1.2 g/cm^3, respectively. The densities of unoxidized and oxidized blends scale linearly with increasing mass percentage of SBS block copolymer in blends due to the higher density of oxidized SBS. The density of the fully oxidized melt-processed Kraton SBS, 1.2 g/cm^3, agrees with the value separately measured for fully oxidized solution-cast material [13]. These reactive blends are, therefore presumably, fully oxidized. An increase in density due to addition of polar groups (such as oxygen-containing functional groups due

to oxidation) should yield a decrease in fractional free volume (FFV) that may in turn, reduce diffusivity and, consequently, permeability [15,16].

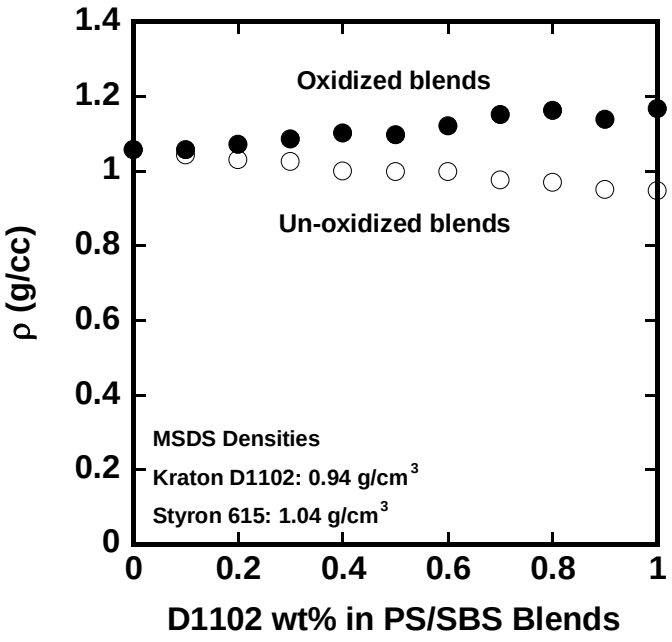

Figure 5.13: The density values for reactive blends at various compositions after oxidation.

5.3.4 Effect of oxidation on O_2 and N_2 permeabilities of PS blend films with SBS scavenger

Oxygen and nitrogen permeability were characterized for unoxidized blends, and the results are shown in Figure 5.14. In general, gas permeability of unoxidized polymer blends increases with increasing content of SBS, which has higher gas permeability than polystyrene when unoxidized. On the other hand, in blends with higher SBS loading, polystyrene is the dispersed phase within a continuous matrix of SBS. A phase inversion takes place, resulting in an abrupt increase in gas permeability near SBS contents of 40 –

50 % in these unoxidized blends. In other work, a phase inversion was found near 40 - 50% SBS content for blends containing SBS triblock copolymer and PPO [12].

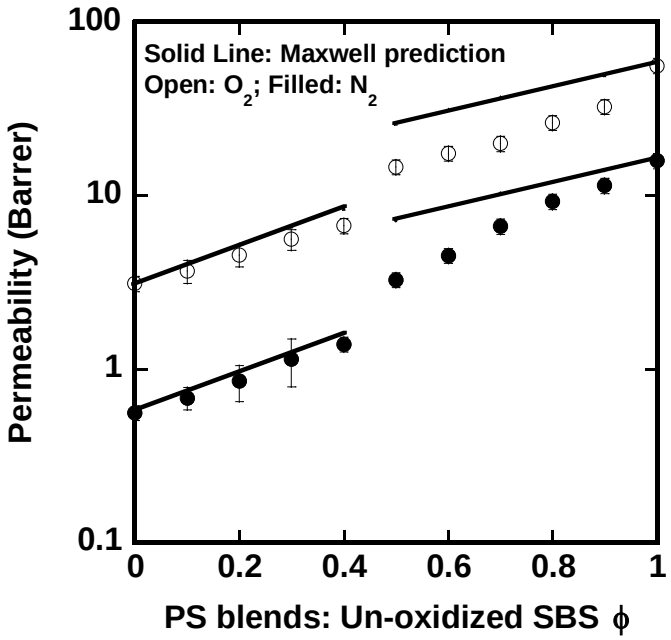

Figure 5.14: The gas permeability of unoxidized blends scales with SBS content, which has a higher permeability than its polystyrene matrix. A phase inversion was found near SBS content of 40 – 50%, which is incorporated in calculating Maxwell prediction as solid lines.

A polymer at low loading typically displays a spherical morphology within a different polymer matrix [17]. Figure 5.15 shows that the morphology of the butadiene phase of a polystyrene film blended with 20 wt% SBS scavenger is not entirely spherical, possibly due to stretching of the material during melt-extrusion. Previous simulation work has suggested that permeation behavior in blend films is related to phase morphology. Specifically, cylindrical dispersed phases have surface area to volume ratios

that are 2/3 those of phases with spherical morphologies [18]. This TEM image was made along the extrusion direction from the front side of the film sample.

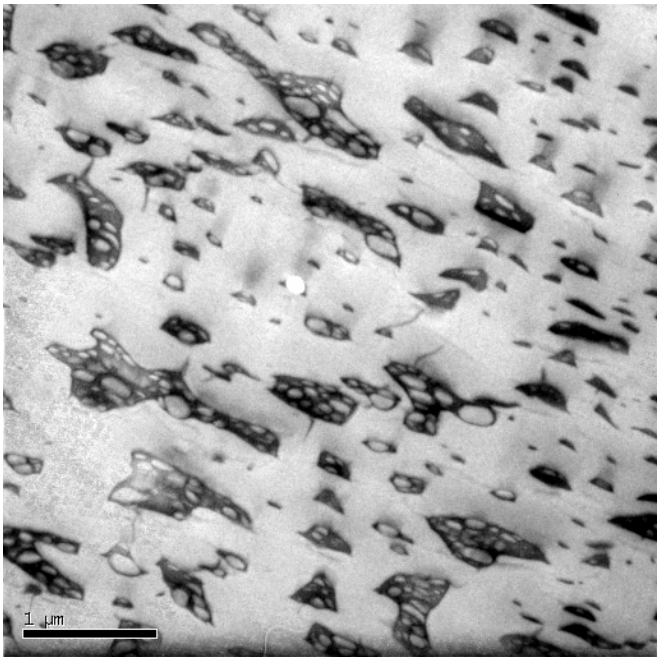

Figure 5.15: The dark, butadiene phase in a polystyrene film blended with 20 wt% SBS appears to have a morphology that is not entirely spherical. This may be due to extensive stretching in extrusion. The lighter phase is the polystyrene domain.

Gas permeability was also characterized for oxidized blends, which decrease in permeability with increasing SBS content [13], as shown Figure 5.16. As observed in work on oxidized solution cast films [13], addition of polar, oxygen-containing functional groups is expected to reduce the polymer free volume, which may lead to reduced values of diffusivity and permeability [15,19,20].

A phase inversion in these oxidized blends was also found at an SBS content of 40 – 50 %, where gas permeability shows a sharp decrease, similar to what was observed in the permeation behavior of unoxidized blends. The trend of permeability reduction agrees with what was reported in previous work on the effect of oxidation on metal-catalyzed, solution-cast 1,4 PB and SBS, where gas permeability was reduced by 2 orders of magnitude as a result of oxidation [13,21].

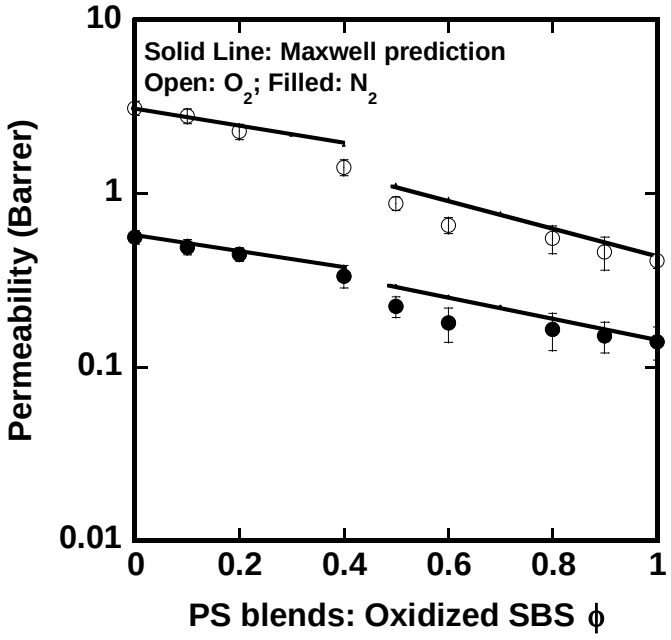

Figure 5.16: The gas permeability of oxidized blends decreases with SBS content, as the fully oxidized SBS has lower permeability than the matrix polystyrene. Similarly, a phase inversion was found near oxidized SBS content of 40 – 50% and is incorporated in calculating Maxwell prediction as solid lines.

The Maxwell equation (Equation 2.5) was used to estimate the gas permeability of SBS/PS blends incorporating 10 and 20% SBS as a function of oxidation, as shown in Table 5.2. Maxwell's equation is commonly employed to estimate the permeability

relationship in blends that involve spheres of one component dispersed in a matrix of another polymer [22,23]. The oxygen and nitrogen permeabilities of fully oxidized SBS of 0.14 and 0.41 Barrer, respectively [13], were here in calculating the Maxwell-predicted values of unoxidized and oxidized blends. These model calculations are shown as solid lines in Figures 5.15 and 5.16, respectively.

Table 5.2: Gas permeability values and prediction of reactive blend films and its components

Sample/ Permeability (Barrer)	**Measured O_2**	**Maxwell O_2**	**Measured N_2**	**Maxwell N_2**	**Measured α**	**Maxwell α**
Polystyrene [13]	~3.1	---	~0.50	---	6.2	---
Un-oxidized scavenger [13]	~56	---	~22	---	2.5	---
Oxidized scavenger [13]	~0.41	---	~0.14	---	2.9	---
20% SBS in PS – Un-oxidized	4.5 ± 0.7	5.2 ± 0.5	0.9 ± 0.20	0.9 ± 0.09	5.2	5.8
20% SBS in PS – Oxidized	2.3 ± 0.3	2.5 ± 0.3	0.5 ± 0.04	0.5 ± 0.50	5.1	5.6
10% SBS in PS – Un-oxidized	3.7 ± 0.6	4.1 ± 0.4	0.7 ± 0.10	0.7 ± 0.07	5.9	5.5
10% SBS in PS – Oxidized	2.8 ± 0.3	2.8 ± 0.3	0.5 ± 0.05	0.5 ± 0.50	5.8	5.8

Values of gas permeability and selectivity of PS blends with 10% and 20 % SBS loading estimated by the Maxwell equation agree closely with measured values within the uncertainty of the measurement. However, at higher SBS loading, the deviation from the Maxwell prediction of the experimental measurement can be attributed to the breakdown

of the assumption that the dispersed phase is spherical in the Maxwell model in both unoxidized and oxidized blends. Increasing content of the dispersed phase in the blends usually yields less spherical and more cylindrical morphology [17,23].

5.3.5 Characterizing oxidation behavior of blend films of polystyrene and SBS block copolymer

Reactive blends ~ 55 – 75 μm containing 400 and 800 ppm catalyst loading were melt-processed and allowed to oxidize at 35 °C in air, and their uptake data are shown in Figures 5.17 and 5.18, respectively. Note that a melt-processed Kraton SBS film was not available in this thickness range, so the uptake data is for a Kraton SBS film at a similar thickness prepared by solution casting. This is reasonable, as shown in previous sections, because processing has little effect on the oxidation behavior of melt-processed Kraton films.

Oxygen uptake activity increases with scavenger loading. The blends that contain higher SBS loading have higher uptakes than those that contain less SBS. In addition, blend films with lower SBS loading seem to reach their maximum oxidation capacity more quickly than those that contain more, while those with higher SBS loading continue to uptake oxygen over longer periods of time.

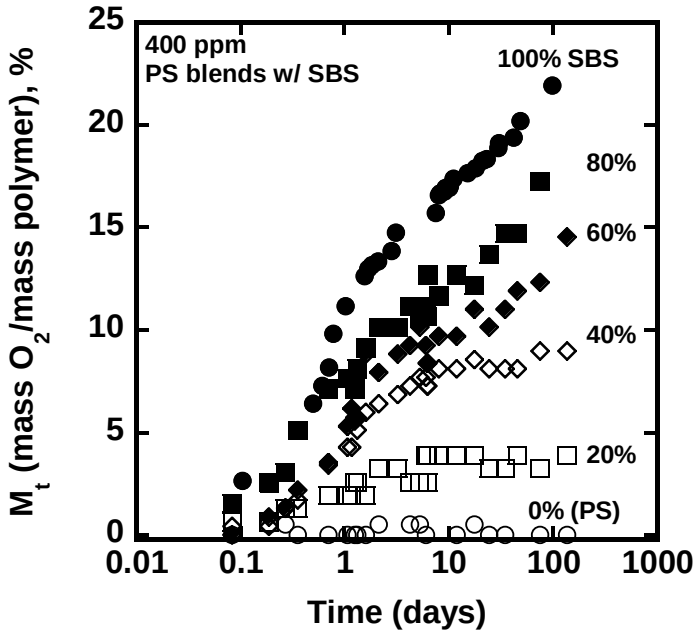

Figure 5.17: Mass uptake of reactive blends ~ 60 – 75 μm with 400 ppm catalyst loading.

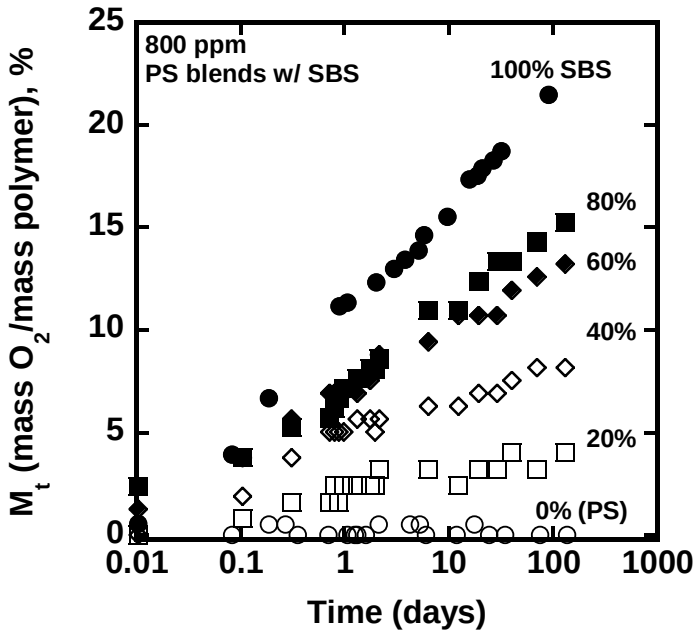

Figure 5.18: Mass uptake of reactive blends ~ 55 – 70 μm with 800 ppm catalyst loading.

When the uptake data of reactive blends with 400 and 800 ppm catalyst are normalized by the SBS mass, as shown in Figures 5.19 and 5.20, the SBS mass-normalized uptake data approximately collapsed onto a master curve. The uptake data for melt-processed reactive Kraton SBS is included in these figures. Differences in uptake among samples may arise from thickness differences. Although permeation behavior in oxidizing blends of varying composition is related to phase morphology [18], the reaction time scale ratio of 2/3, caused by morphology differences, and the surface area to volume ratios [18] will likely have little effect on the reaction time scale in uptake experiments.

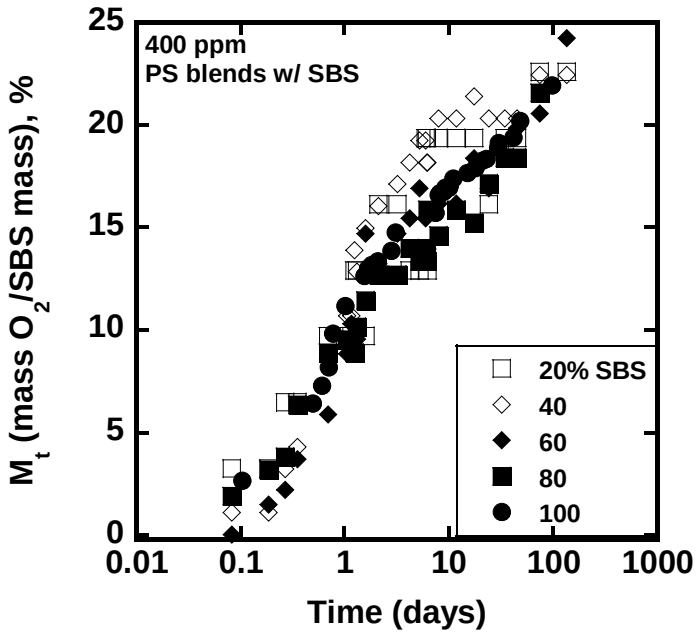

Figure 5.19: SBS mass-normalized uptake data of blends ~ 60 – 75 μm with 400 ppm catalyst loading

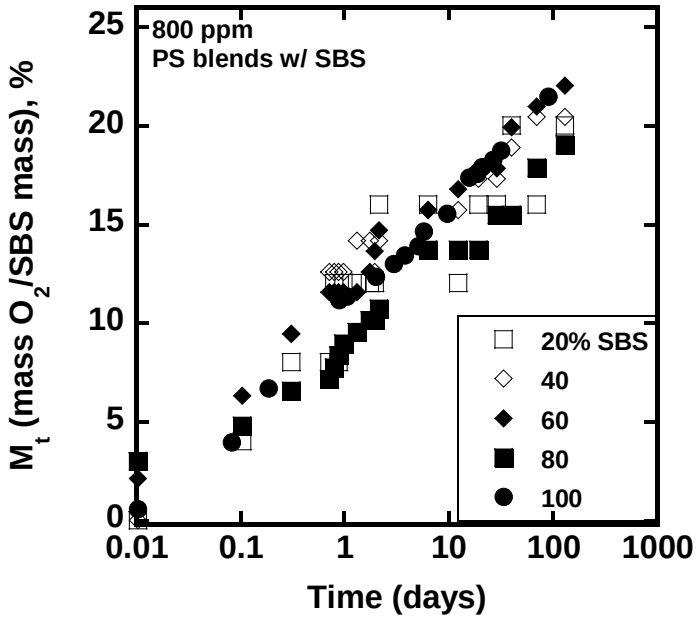

Figure 5.20: SBS mass-normalized uptake data of blends ~ 55 – 70 μm with 400 ppm catalyst loading

Subsequent analysis of the effects of SBS composition on blend film kinetics followed the framework of earlier studies. Uptake data were re-cast to extract values of slope and intercept and to consider the effects of blending that were revealed after plotting against SBS composition. However, this model was developed to describe kinetics of SBS homopolymer films, and its theoretical basis certainly was not intended for blends.

Plots of $\left(\frac{M_t}{M_\infty}\right)^2$ were constructed versus time to analyze normalized long time uptake behavior to values of M_∞ that were previously measured in thin film kinetic experiments for both 400 and 800 ppm catalyst loadings [13]. The results for films with 400 and 800 ppm catalyst loading are shown in Figures 5.21 and 5.22, respectively.

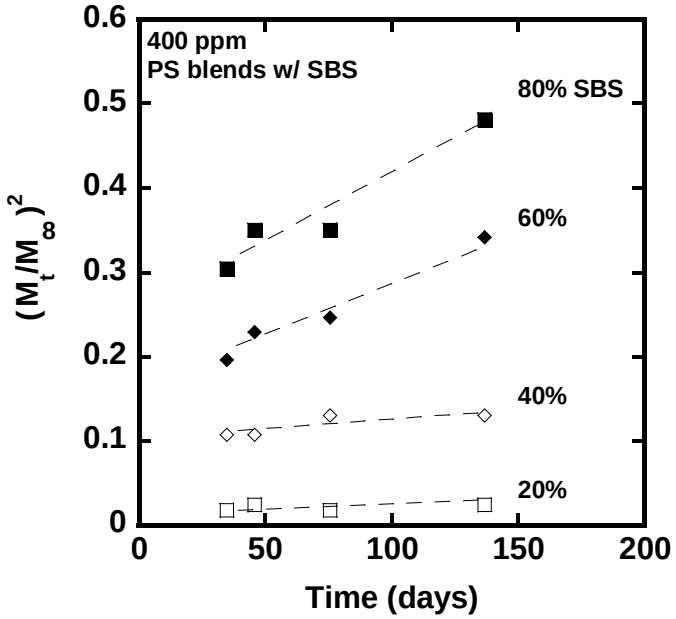

Figure 5.21: Oxygen uptake in PS blend films ~ 60 – 75 μm normalized by total mass at long oxidation times with 400 ppm catalyst loading at various SBS loading.

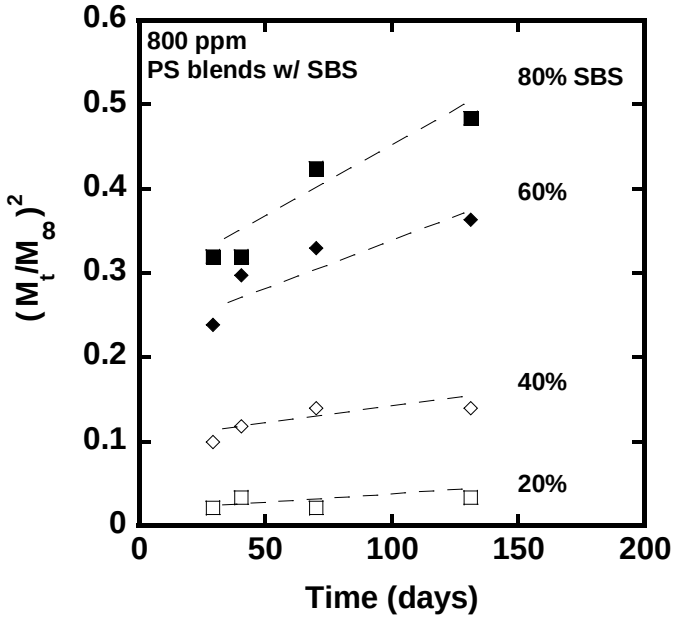

Figure 5.22: Oxygen uptake in PS blend films ~ 55 – 70 μm normalized by total mass at long oxidation times with 800 ppm catalyst loading at various SBS loading.

The polystyrene films blended with reactive SBS continued to oxidize for over 100 days when the SBS content was at least 40%. Moreover, the slope and intercept values appear higher in films that have higher loading of reactive SBS. The slope and intercept values extracted from long-time oxidation uptake data are plotted versus SBS mass fraction and shown in Figures 5.23 and Figure 5.24, respectively, as well as in Table 5.3. These results suggest that reactive blend films with higher SBS content would show faster oxidation kinetics and higher uptake capacity, with a maximum in these values achieved in pure melt processed Kraton SBS films.

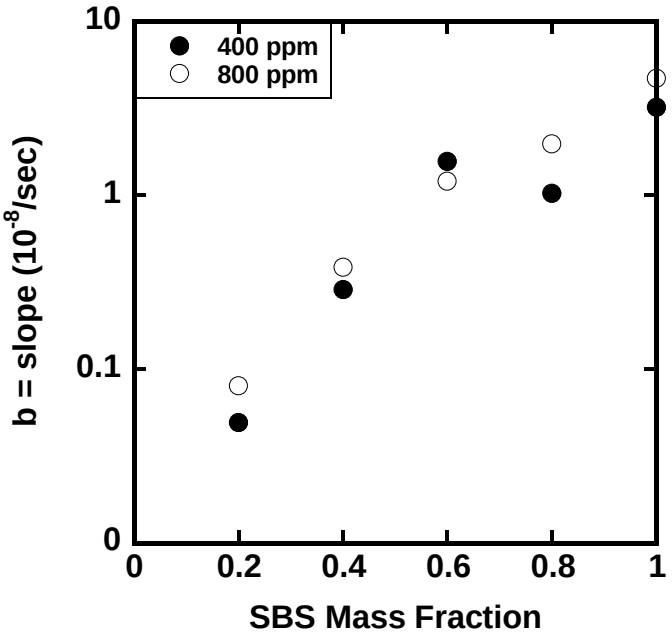

Figure 5.23: The slope values extracted from uptake data of reactive blend films ~ 60 – 75 μm at long oxidation times scale with SBS loading.

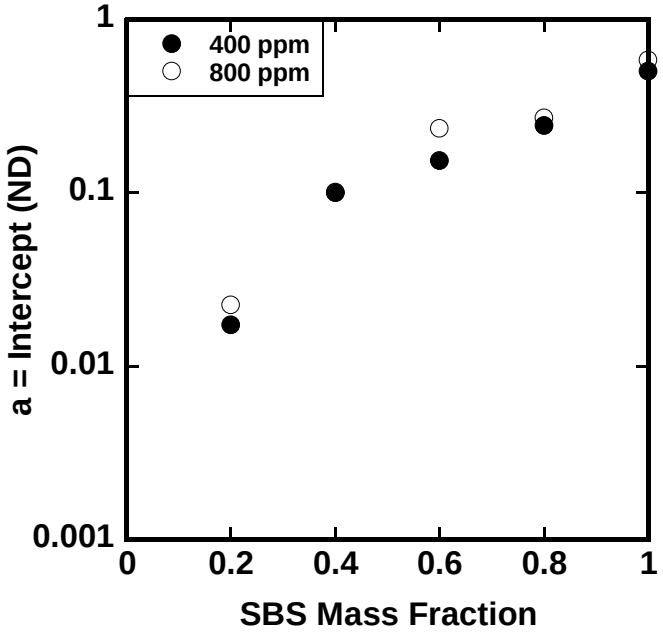

Figure 5.24: The intercept values extracted from uptake data of reactive blend films ~ 55 – 70 μm at long oxidation times scale with SBS loading.

Plots of $\frac{M_t}{M_\infty}$ versus time were constructed to analyze normalized uptake behavior to values of M_∞ that were previously measured in thin film kinetic experiments for 400 and 800 ppm catalyst loadings [13]. The uptake data of polystyrene blends that contain 20, 40, 60, 80, and 100% SBS were respectively normalized to the 20, 40, 60, 80, and 100% absolute value of M_∞. The results for films with 400 and 800 ppm catalyst loading are shown in Figures 5.25 and 5.26, respectively.

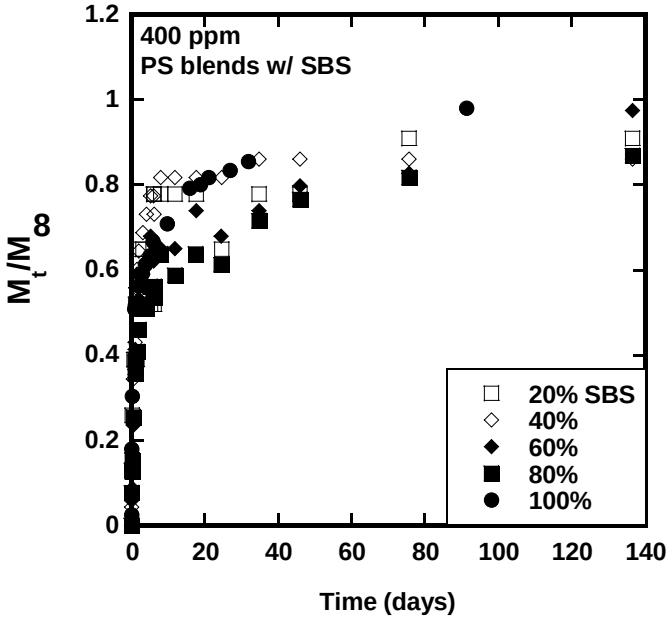

Figure 5.25: Oxygen uptake in SBS/PS blend films ~ 60 – 75 μm with 400 ppm catalyst loading normalized by M_∞ at various compositions.

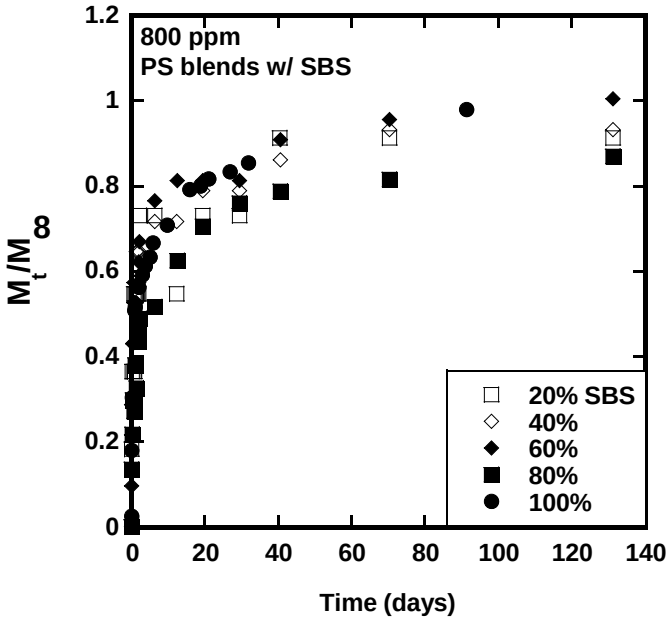

Figure 5.26: Oxygen uptake in SBS/PS blend films ~ 55 – 70 μm with 800 ppm catalyst loading normalized by M_∞ at various compositions.

The polystyrene films blended with reactive SBS continued to oxidize, and all values of $\frac{M_t}{M_\infty}$ were at least 85% of full oxidation for over 100 days. Moreover, the uptake data of blends of 20, 40, 60, 80, and 100% SBS loading seem to collapse into a master curve when proportionally normalized by the M_∞. Thus, blend films have oxidation kinetics and capacity comparable to those of reactive films of 100% Kraton SBS.

Table 5.3: Values of slope and intercept of reactive blends at various compositions

$\boldsymbol{Catalyst\ ppm}$	$\boldsymbol{SBS\ Mass\ fraction}$	$\boldsymbol{L\ \mu m}$	$\boldsymbol{\frac{M_\infty\ g\ O_2}{g\ polymer}}$	$\boldsymbol{b = Slope\ 10^{-8}/sec}$	$\boldsymbol{a = Intercept\ ND}$
400	1.0	60 ± 5	24.9	3.20	0.51
	0.8	70 ± 5	19.9	1.02	0.25
	0.6	75 ± 5	14.9	1.56	0.15
	0.4	75 ± 5	10.0	0.29	0.10
	0.2	60 ± 5	5.0	0.05	0.02
	0	100 ± 5	0.00	0.00	0.00
800	1.0	60 ± 5	21.9	4.70	0.59
	0.8	70 ± 5	17.6	1.97	0.27
	0.6	60 ± 5	13.2	1.20	0.24
	0.4	60 ± 5	8.8	0.39	0.10
	0.2	55 ± 5	4.4	0.08	0.02
	0	100	0.00	0.00	0.00

5.4 SUMMARY

Reactive films were melt-processed and their oxidation kinetics were monitored and compared with those prepared by the solution casting. By comparing the values of slope and intercept from the uptake data at long oxidation times, we identified comparable oxidation behavior for reactive films produced by either technique. This

suggests that processed films can scavenge oxygen at a similar rate and capacity as those prepared by solution casting.

Polystyrene films were blended with reactive Kraton SBS at the same processing conditions, and their oxygen uptake activities were recorded. The values of slope and intercept from uptake data of PS blends normalized by M_∞ increase with SBS loading and approach values for melt-processed Kraton SBS. Furthermore, the blend film uptake data collapsed into a master curve when proportionally normalized to the values of M_∞. Any discrepancies in slope and intercept values may be attributed to slight differences in film thickness. This result shows that, using the current processing conditions, blend films have adequate oxidation kinetics and capacity and confirms that reactive blend films can scavenge oxygen at a rate comparable to that of melt-processed films.

5.5 REFERENCES

[1] M. Coquillat, J. Verdu, X. Colin, L. Audouin, R. Nevière, Thermal oxidation of polybutadiene. Part 2: Mechanistic and kinetic schemes for additive-free non-crosslinked polybutadiene, Polymer Degradation and Stability. 92 (2007) 1334–1342.

[2] M. Coquillat, J. Verdu, X. Colin, L. Audouin, R. Nevière, Thermal oxidation of polybutadiene. Part 1: Effect of temperature, oxygen pressure and sample thickness on the thermal oxidation of hydroxyl-terminated polybutadiene, Polymer Degradation and Stability. 92 (2007) 1326–1333.

[3] R.L. Clough, K.T. Gillen, Oxygen diffusion effects in thermally aged elastomers, Polymer Degradation and Stability. 38 (1992) 47–56.

[4] L.M. Rincon-Rubio, B. Fayolle, L. Audouin, J. Verdu, A general solution of the closed-loop kinetic scheme for the thermal oxidation of polypropylene, Polymer Degradation and Stability. 74 (2001) 177–188.

[5] M. Coquillat, J. Verdu, X. Colin, L. Audouin, R. Nevière, Thermal oxidation of polybutadiene. Part 3: Molar mass changes of additive-free non-crosslinked polybutadiene, Polymer Degradation and Stability. 92 (2007) 1343–1349.

[6] M.A. Villetti, J.S. Crespo, M.S. Soldi, A.T.N. Pires, R. Borsali, V. Soldi, Thermal Degradation of Natural Polymers, Journal of Thermal Analysis and Calorimetry. 67 (2002) 295–303.

[7] R.G. Bauman, S.H. Maron, Oxidation of Polybutadiene. I. Rate of Oxidation, Journal of Polymer Science. 22 (1956) 1–12.

[8] J.J. Carberry, Chemical and Catalytic Reaction Engineering, Dover Publication, 2001.

[9] W.M. Haynes, ed., CRC Handbook of Chemistry and Physics, 93rd Edition, 93rd ed., CRC Press, 2012.

[10] E.J. Erekson, E.L. Sughrue, C.H. Bartholomew, Catalyst degradation in high temperature methanation, Fuel Processing Technology. 5 (1981) 91–101.

[11] T. Lee, N. Yao, I.A. Aksay, Nanoscale Patterning of Barium Titanate on Block Copolymers, Langmuir. 13 (1997) 3866–3870.

[12] K.W. Song, K.R. Ka, C.K. Kim, Changes in Gas-Transport Properties with the Phase Structure of Blends Containing Styrene−Butadiene−Styrene Triblock Copolymer and Poly(2,6-dimethyl-1,4-phenylene oxide), Industrial & Engineering Chemistry Research. 49 (2010) 6587–6592.

[13] K.K. Tung, R.T. Bonnecaze, B.D. Freeman, D.R. Paul, Characterization of the oxygen scavenging capacity and kinetics of SBS films, Polymer. 53 (2012) 4211–4221.

[14] G. Riess, G. Hurtrez, P. Bahadur, Block Copolymers, in: H.F. Mark, N.M. Bikales, O. C.G., G. Menges (Eds.), Encyclopedia of Polymer Science and Technology, Vol. 2, John Wiley & Sons, Ltd, New York, 1985: p. 324.

[15] W.M. Lee, Selection of barrier materials from molecular structure, Polymer Engineering and Science. 20 (1980) 65–69.

[16] D.W. Van Krevelen, Properties of Polymers, 3rd Edition Their Correlation with chemical Structure; their Numerical Estimation and Prediction from Additive Group Contributions, Elsevier Science, Amsterdam, 2003.

[17] D.R. Paul, C.B. Bucknall, Polymer Blends: Formulation and Performance, Wiley-Interscience, 2000.

[18] S. Carranza, D.R. Paul, R.T. Bonnecaze, Analytic formulae for the design of reactive polymer blend barrier materials, Journal of Membrane Science. 360 (2010) 1–8.

[19] G.J. Van Amerongen, Influence of structure of elastomers on their permeability to gases, Journal of Polymer Science. 5 (1950) 307–332.

[20] T.K. Kwei, Introduction to physical polymer science, second edition, by L. H. Sperling, Wiley, New York, 1992, 594 pp., Journal of Polymer Science Part A: Polymer Chemistry. 31 (1993) 1097–1097.

[21] H. Li, K.K. Tung, D.R. Paul, B.D. Freeman, Effect of film thickness on auto-oxidation in cobalt-catalyzed 1,4-polybutadiene films, Polymer. 52 (2011) 2772–2783.

[22] C.N.M. Lloyd M. Robeson, Allen Noshay, Markus Matzner, Physical property characteristics of polysulfone/poly-(dimethylsiloxane) block copolymers, Die Angewandte Makromolekulare Chemie. 29 (1973) 47–62.

[23] L.M. Robeson, Polymer Blends in Membrane Transport Processes, Industrial & Engineering Chemistry Research. 49 (2010) 11859–11865.

Chapter 6: Evaluating the oxidation behavior of melt-processed SBS and PS-SBS blend films via permeation experiments

6.1 INTRODUCTION

In prior chapters, the oxidation kinetics of styrene-butadiene-styrene (SBS) block copolymer were studied either as freestanding films [1–5] or as the dispersed phase within a polymer matrix. A kinetic model was developed and reaction parameters were extracted via uptake and permeation analysis of SBS thin films. Processing conditions were established and verified to ensure that active scavenging would still occur in spite of the demanding temperatures required for melt processing.

This chapter presents results of permeation studies designed to investigate the effects of parameters such as oxygen partial pressure, film thickness, and scavenger and photoinitiator (PI) loading on oxidation behavior of polystyrene blend films containing an oxygen scavenger. The cumulative amount of permeate and oxygen fluxes were monitored. Experimental time lags were measured and compared with the theoretical predictions from previous work [6]. The effect of oxidation on permeation behavior and time lag extension are discussed.

6.2 EFFECTS OF CATALYST LOADING, UV EXPOSURE, AND PHOTOINITIATOR (PI) CONTENT ON OXIDATION BEHAVIOR OF SBS CONTAINING POLYMERS

6.2.1 Characterizing catalytic effect on SBS oxidation behavior via permeation and thin film uptake experiments

Some of the parameters that can influence the rate of oxidation of butadiene-containing polymers include the catalyst loading, the UV exposure time, and the photoinitiator content [7]. Since there are few literature studies available, it is important to investigate the effects of these parameters on scavenging activity of butadiene-containing polymers and then to identify an optimum set of scavenging conditions for barrier films to consume oxygen via a reactive situation.

To investigate the effect of catalyst loading on oxygen transport through SBS, films of pure SBS at two catalyst loadings – 800 and 2,666 ppm – and 1% PI were melt-processed. These films of approximately 200 μm in thickness were subsequently exposed to UV for 12 minutes prior to permeation tests with an upstream oxygen pressure of 100 psi. Figure 6.1 shows that over time, the oxygen flux of melt-processed films at both loadings decreased by orders of magnitude from the initial flux ($\sim 1.5 \times 10^{-4} \frac{cc}{cm^2\ sec}$) of unoxidized films (oxygen permeability of approximately 56 barrer [5]). The sample with 2,666 ppm catalyst loading began to exhibit much more rapid suppression of oxygen flux than the sample at 800 ppm loading after only two hours of testing.

Oxidation of the butadiene phase in the SBS block copolymer results in the formation of oxygen-containing polar groups, and the oxidized phase has substantially lower permeability than the native butadiene. The oxidation occurs initially near the SBS film surface, resulting in a superficial crust layer that serves as a barrier to oxygen transport and has been previously identified [5]. Importantly, at approximately the tenth hour there was virtually no detectable increase in the cumulative amount of permeate due to instrumental limitations.

The reduction in oxygen flux occurs more rapidly in the film with a higher catalyst loading. The change in chemical structure associated with oxidation is believed to be the primary contributor to the flux reduction. A similar combined effect was reported for oxidation studies on 1,4-polybutadiene [2], where a reduction of 2 to 3 orders of magnitude in gas permeability was ascribed to the formation of a dense crust layer on the surface of the polymer matrix – a direct result of active scavenging and oxidation of the polymer.

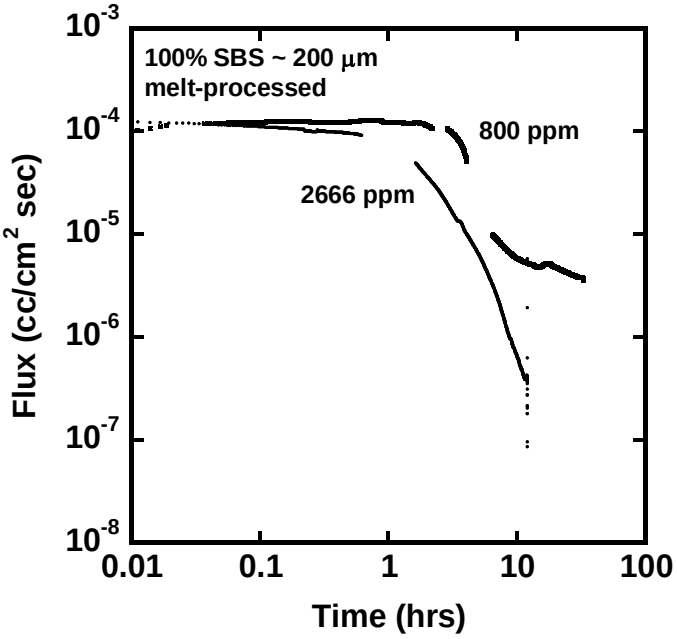

Figure 6.1: Scavenging alters the chemical structure of the polymer membrane, thus reducing flux behaviors of melt-processed pure SBS films ~ 200 μm as a function of catalyst.

Previous work showed that both reaction rate constant, k_R ($\frac{cm^3}{mol_{PB}*sec}$), and $\hat{v}$ (mol_{PB}/mol_{O_2}), scale monotonically with catalyst loading up to 800 ppm (Figure 4.8)

[5]. To determine the rate constant that would correspond to a catalyst loading at 2,666 ppm, SBS thin films of approximately 3 – 5 μm were prepared using 1% photoinitiator concentration and allowed to oxidize by UV exposure for 12 minutes. Values of k_R and $\hat{v}$ were extracted following the previously developed thin film kinetic analysis [5], and the results are shown in Figure 6.2, where both k_R and $\hat{v}$ seem to plateau to constant value at catalyst loadings above 800 ppm, within experimental error.

The observed trend for both parameters is similar to what has been reported in past studies of metal-catalyzed autoxidation [8–10], where the oxidation rate initially increases but later slows with increasing catalyst loading [11,12] due to limited extent of oxidation. Because the reaction rates do not increase when the catalyst loading is increased from 800 to 2,666 ppm, the precipitous decrease in oxygen flux shown in Figure 6.1 could be due to any number of factors; these include a catalyst solubility limit. Of course, the formation of a rather impermeable crust layer also impedes the transport of oxygen through the film.

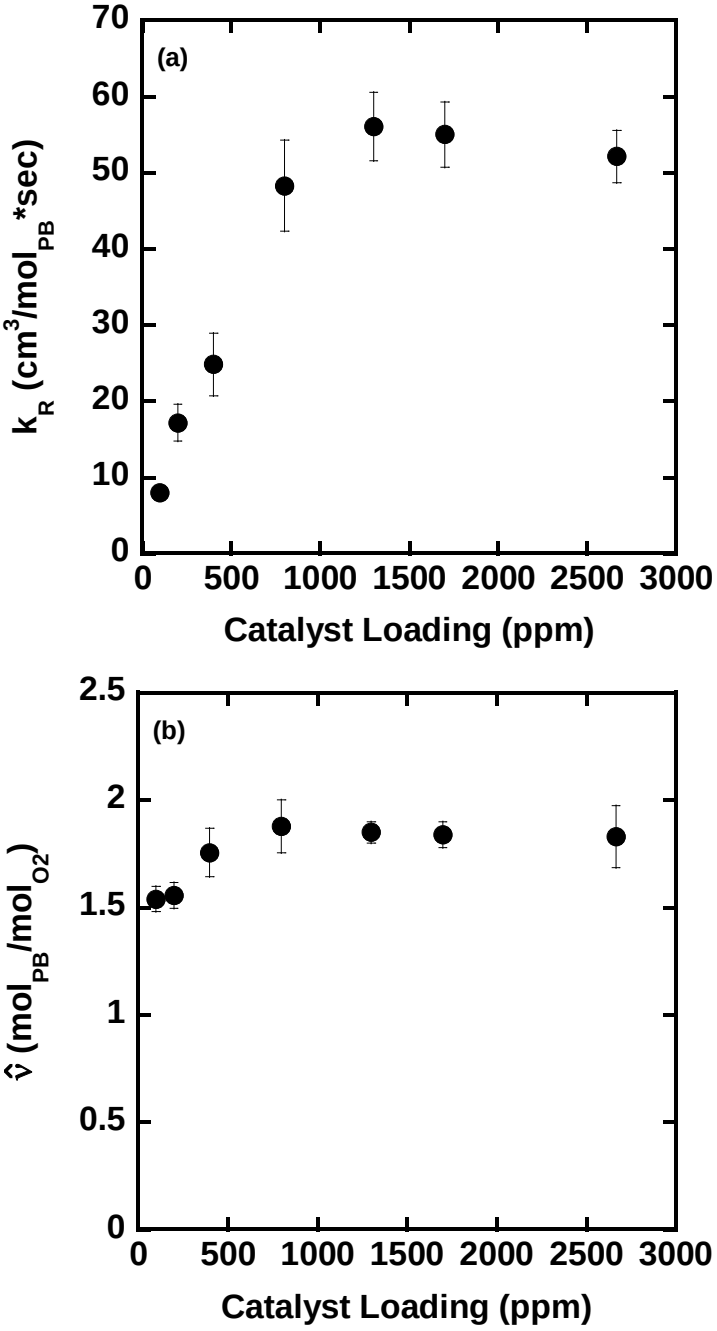

Figure 6.2: (a) The rate constants were extracted by the thin film kinetic model and reach a plateau at higher catalyst loading. (b) The stoichiometric oxidation coefficient, $\hat{\nu}$, presented as a function of catalyst loading in SBS thin films.

6.2.2 Characterizing the effect of UV exposure on SBS oxidation behavior via uptake experiments

To investigate the effect of UV exposure on scavenging kinetics, pure SBS films of about 120 μm thickness were prepared with 200 ppm catalyst loading and 1% photoinitiator content. These films were exposed under UV at varying length of time, and their oxygen mass uptake, as shown in Figure 6.3, was found to be a strong function of UV exposure time. Films that had been exposed for longer initiating times showed more rapid oxygen uptake, which suggests faster oxidation kinetics.

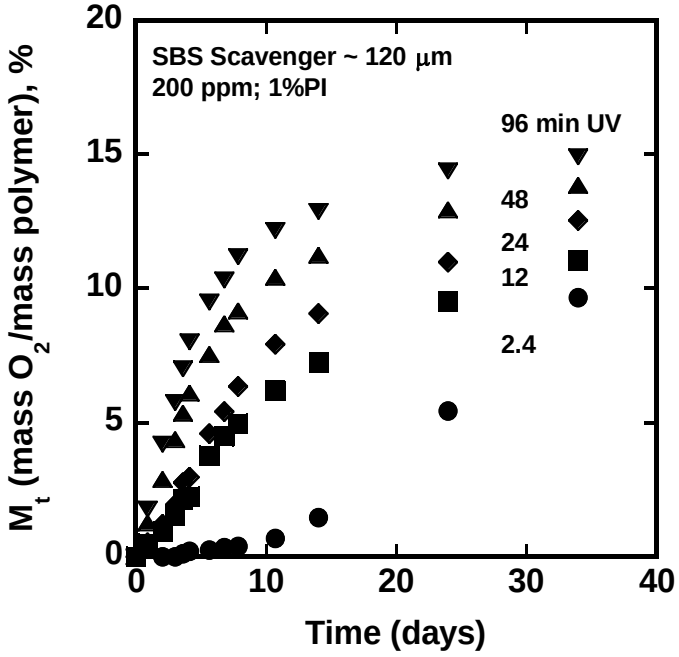

Figure 6.3: Mass uptake as a function of time at various film UV exposure times.

This result is reasonable since the concentration of benzophenone diradicals that initiate oxidation is a function of UV exposure time [7,13,14]. In films with higher levels of UV exposure, more benzophenone and butadiene radicals become available for

oxidation. Higher radical concentration results in higher oxygen uptake rates than that in films with lower UV exposure.

6.2.3 Effect of photoinitiator content on oxidation behavior of PS blends with SBS via permeation experiment

It has been shown that the rate of oxidation can be accelerated at high catalyst loading (2,666 ppm) and by a longer UV exposure period (i.e., 48 – 96 minutes). The oxidized structure formed is an effective barrier material that can limit that rate of oxygen permeation. The effect of PI content on oxidation behavior can be important, as its purpose is to release, upon UV absorption, radicals that trigger oxidation [7].

Therefore, polystyrene blends with 10% SBS and 2,666 ppm catalyst loading were melt-extruded at a thickness of approximately 200 μm at a variety of photoinitiator contents. These blends were exposed to UV for 96 minutes before oxygen permeation tests at an upstream pressure of 20 psi at 35 °C. Figure 6.4 shows that the cumulative amount of permeate, Q_t, gradually increased with time. While there is no clear trend, the sample with 3% PI loading was found to have the lowest cumulative amount of permeation.

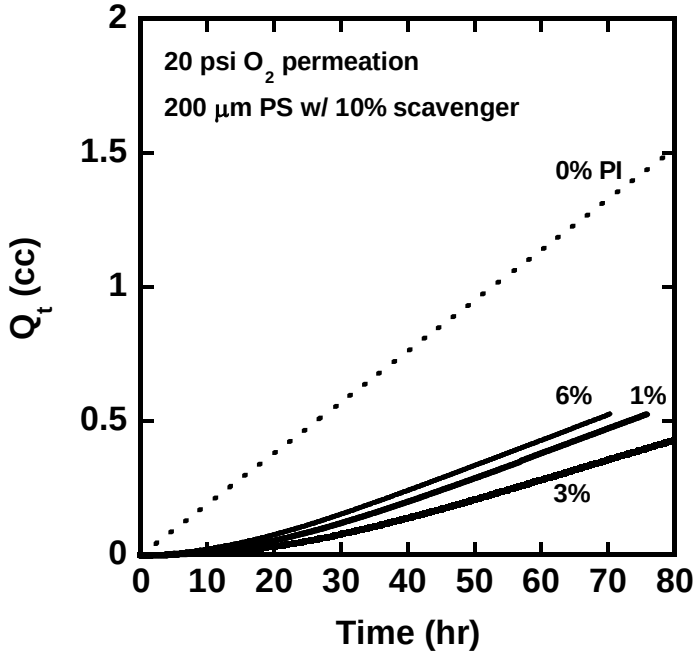

Figure 6.4: Effect of PI% on cumulative permeate Q_t of reactive blend films loaded with 10% SBS at 2,666 ppm that was exposed to UV for 96 minutes.

Figure 6.5 recasts the data of Figure 6.4 in terms of flux. Initially, fluxes were low due to active scavenging and gradually increased in value due to diminishing oxidation activity before reaching steady state, which suggests that all reactive sites had been exhausted. The sample with 3% PI loading was found to exhibit the greatest scavenging activity, suppressing oxygen flux at early times relative to other PI loadings. Because no benefit of increasing PI loading to 6% was realized, it is possible that there is a solubility limit between 3 and 6% PI loading. Above that limit, additional PI loading would not improve scavenging behavior.

Note that the photoinitiator was first solution cast with the SBS, which was subsequently melt-processed with polystyrene to form reactive blends. It is possible that, due to melt-processing at an elevated temperature, the photoinitiator could migrate or

leach into the polystyrene phase. Moreover, the fact that benzophenone (the photoinitiator) has a chemical structure that is similar to polystyrene favors this partitioning possibility. Also, at higher PI loading, benzophenone diradicals may be reduced by a self-termination step, which is a typical neutralizing step in radical chemistry [11]. Nonetheless, this activity identified a PI% for which reactive blend films show a scavenging activity that seems to suppress the oxygen flux, which is a characteristic of a reactive barrier material.

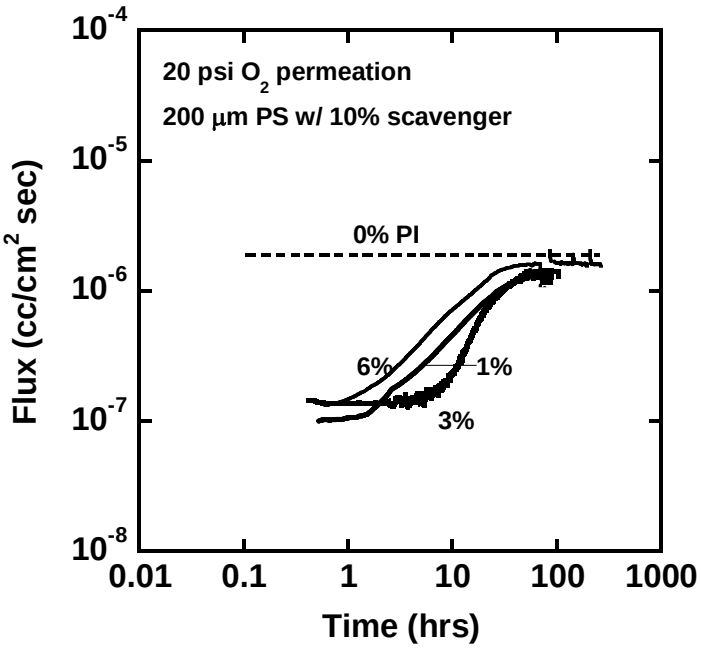

Figure 6.5: Effect of PI% on flux of reactive blend films loaded with 10% SBS at 2,666 ppm that has been UV exposed for 96 minutes.

6.2.4 Identifying the level of UV absorption as a function of photoinitiator content

To identify whether it is possible for photoinitiator to leach from SBS into polystyrene, a simple test can be done to relate the photoinitator concentration and the UV intensity absorbed by the tested polystyrene films. The intensity of the UV irradiation produced by the UV lamp is UV_0; however, the intensity of UV irradiation that emerges from a polymer film placed in front of the UV lamp has a lower UV intensity, UV_{exp}. The absorbed UV intensity is, therefore, the difference between UV_0 and UV_{exp}, which may be normalized by

$$(UV_0 - UV_{exp})/UV_0 \quad (6.1)$$

Four polystyrene films were melt-processed with 0, 1, 3, and 6% PI at 180 °C for 10 minutes. In addition, a fifth polystyrene film containing 0% photoinitiator was pressed against an SBS film loaded with 6% PI at 180 °C for 10 minutes. This set of temperatures and times was the condition under which all blend films were processed, as shown in Chapter 5. All polystyrene films, which were about 125 μm thick, were placed at a fixed distance between a UV lamp and a radiometer where the UV intensity was measured. The normalized UV energy absorbed by each film piece is shown in Figure 6.6.

The normalized UV energy absorbed by the polystyrene films showed a linear increase with increasing PI content. Neat polystyrene does not absorb UV energy at 365 nm. However, after a neat polystyrene film was pressed against a reactive membrane loaded with 6% PI, the neat polystyrene apparently absorbed UV energy. Specifically, the UV energy absorbed by this film was similar to the absorption level shown by the polystyrene film loaded with 3% PI. This result suggests that some amount of

photoinitiator may have migrated from the SBS into the polystyrene film through direct contact by being pressed at an elevated temperature for an extended period of time.

If any of the PI leaches from the reactive polymer to the matrix polymer, the leached PI will continue to absorb UV energy and form diradicals. However, those diradicals will be in the matrix polymer and cannot perform hydrogen abstraction from the butadiene reactive sites [7], as discussed previously in Section 2, Chapter 2. Therefore, the number of diradicals that can initiate oxidation in reactive blends of polystyrene and reactive polymers can be effectively reduced due to a reduced amount of PI in the reactive polymer dispersed phase. Samples with 3% PI loading seem to optimize oxidation performance in the current blend system.

In this chapter, all permeation tests and simulation were performed on PS/SBS blends containing 2,666 ppm catalyst and 3% PI. These samples were UV irradiated for 48 minutes to allow for higher oxygen uptake quickly. Following the analysis in Chapter 4, the thin film kinetic model [5] was used to extract the values of the reaction rate constant, k_R, and the stoichiometric oxidation coefficient, $\hat{v}$, to be 55 $\frac{cm^3}{mol_{PB}*sec}$ and 2.1 mol_{PB}/mol_{O_2}, respectively. In addition, it was also verified that melt-processed films with this scavenging condition have similar oxidation kinetics and capacity by the analysis presented in Chapter 5.

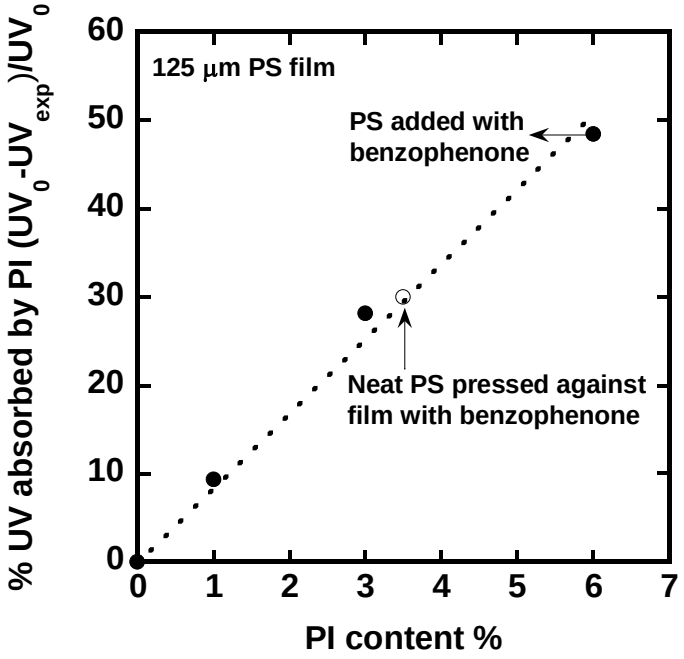

Figure 6.6: The effect of photoinitiator content on absorbed UV energy. The amount of UV energy absorbed scales linearly with PI content, shown as filled circles. The empty circle is the amount of UV energy absorbed by the neat polystyrene film after being pressed against the reactive polymer.

6.3 DEFINING TIME LAGS DUE TO SCAVENGING AND SIMULATING PRESSURE EFFECT ON FLUX BEHAVIOR OF REACTIVE BLEND FILMS

6.3.1 Time lags due to scavenging

The time lag without any scavenging, $\theta_0 = \frac{L^2}{6D_{PS}}$, was determined based on the experimental film thickness and the oxygen diffusion coefficient in polystyrene ($D_{PS} = 1.4 \times 10^{-7} cm^2/sec$ [5]). The cumulative amount of permeate is typically plotted as a function of time from a permeation test result, as illustrated in Figure 6.7.

In a dense film, the permeation behavior, which is described by the solution-diffusion mechanism, is as follows. The total amount of permeate, Q_t, typically experiences an initial lag before it rises to approach steady-state. A linear extrapolation

from this region to the time axis can be used to determine permeability and time lags [15,16]. In a permeation test on the same film with a capability to react with the permeant, time lags may become greater. Experiments [17–25] and theoretical models [6,26–29] have both demonstrated that the time lag, θ, associated with gas transport through a film can be greatly extended by incorporation of a reactive species into the polymeric matrix. In this case, the steady-state region would also suggest that all reactive sites have been exhausted, or that permeation is occurring so rapidly that the scavenging is not detectable. The permeability determined from the steady-state region can be readily estimated by Maxwell equation [30,31].

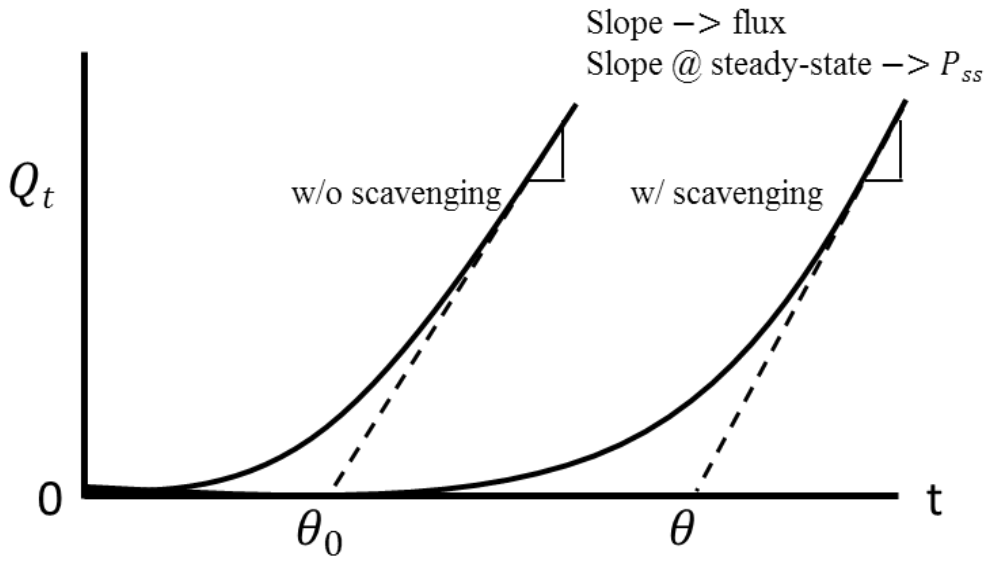

Figure 6.7: A schematic illustration of the method of determining time lags. Time lags were determined as the intercepts with the time axis with the linear extrapolation from steady state region of the Q_t versus time curve. Time lag is greater by scavenging due to oxidation where oxygen is immobilized, thus delaying the breakthrough time. The flux and permeability are proportional to the slopes of the Q_t curve.

The measured time lags were compared with those including scavenging, as predicted by equation (2.10) [6]:

$$\frac{\theta}{\theta_0} = 1 + \frac{3\phi\beta}{C_m(0)} \tag{2.10}$$

Equation 2.10 can be recast into the following

$$\frac{\theta}{\theta_0} = 1 + \frac{3\phi n_0}{\hat{\nu} S_m(0) P_{O_2}} \rightarrow \theta = \frac{L^2}{6D_{PS}} \times \left(1 + \frac{3\phi n_0}{\hat{\nu} S_m(0) P_{O_2}}\right) \tag{6.2}$$

by recognizing the relationships [28]

$$\beta = \frac{n_0}{\hat{\nu}} \tag{6.3}$$

and

$$C_m(0) = S_m(0) \times P_{O_2} \tag{6.4}$$

Equation 6.2 implies that time lag due to scavenging is a function of reaction parameters such as film thickness, L, scavenger content, ϕ, and oxygen pressure, P_{O_2}. Values of oxygen diffusivity in the matrix polymer [5], D_{PS}, solubility of oxygen in the matrix polymer [5], S_m, the reactive site molar density, n_0, and the stoichiometric oxidation coefficient, $\hat{\nu}$, were kept constant when calculating theoretical time lags. The values of these modeling parameters are shown in Section 4.2 in Chapter 2.

In this dissertation, the slopes of Q_t versus time curves were determined from the ratio of the forward running average of cumulative permeate amount and the experimental time. The slope values were subsequently used to determine the transient flux and permeability over time. The steady-state permeability of all reactive blend films studied in this dissertation was in excellent agreement with those measured separately on fully oxidized blend films. The steady state permeability values were determined and agree with values predicted by the Maxwell Equation, as shown in Chapter 5. The experimental parameters, mathematical details, and assumptions made in calculating transient fluxes are described in the Appendix. The experimentally measured and predicted time lags, steady state fluxes, permeability, and other permeation parameters of all tests are shown in Table 6.1.

6.3.2 Pressure effect simulation on flux behavior of PS reactive blend films containing SBS scavenger

Recently much effort has gone into developing theories to predict permeation [6,28,32,33] and uptake [5] behavior of films containing SBS block copolymer via permeation and uptake experiments. One of the benefits of developing such models is to provide guidance on experimental design with reasonable physical assumptions based on select data. Sets of analytical equations have been developed to describe the flux behavior of reactive blend films containing SBS scavengers [28]. Simulation of the effect of oxygen pressure on permeation behavior of reactive blends is shown in Figure 6.8. These simulated polystyrene films were 100 μm and contained 10% scavenger. The simulation was done using the modeling parameters and equations (Equation 2.7 – 2.12) disclosed in Sections 4.2 and 4.3 in Chapter 2, respectively.

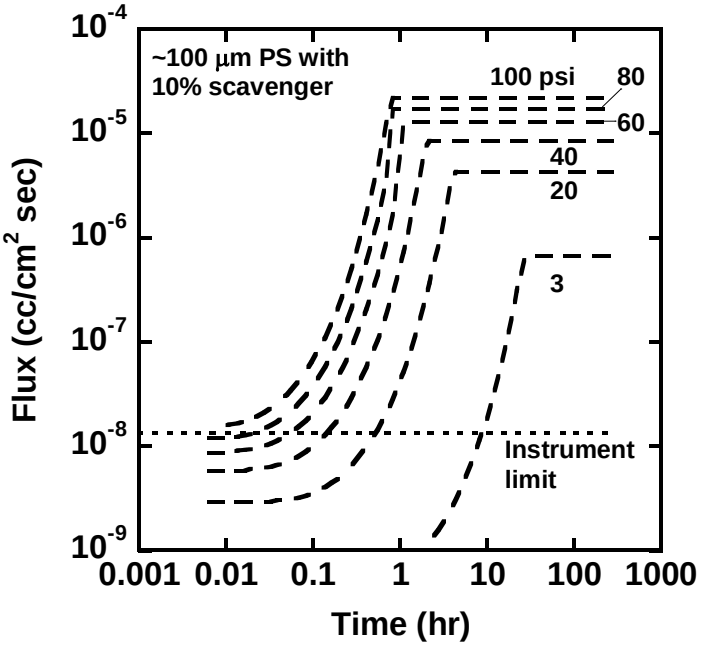

Figure 6.8: The modeled pressure effect on flux of reactive polystyrene blends of 100 μm with 10% scavenger. The simulation at 100 psi may be measured by the current instrument under current experimental configuration.

The flux behavior is simulated to be a function of oxidation time. Initially fluxes begin lower at a plateau where oxidation is occurring and rise to steady state due to diminishing and eventual exhaustion of the reactive sites. The simulated flux is pieced together by prediction, using three analytical equations [28]: plateau flux (Equation 2.7), intermediate flux (Equation 2.12), and steady state flux ($J_{SS} = D_m C_m(0)/L$). This would explain the sudden change of flux leading up to the steady-state in simulation. The permeation simulation at 100 psi shows the highest predicted flux, and it is always greater than the measurement limit of current instruments (shown as a horizontal dashed line in Figure 6.8). Moreover, as pressure changes while the simulated flux value increases, the trend seems to stay roughly the same shape. This simulation suggests that a

permeation test with samples of approximately 100 μm thickness with an upstream oxygen pressure of 100 psi can produce measurable fluxes.

6.4 CHARACTERIZING OXIDATION BEHAVIOR OF REACTIVE BLEND FILMS VIA PERMEATION EXPERIMENTS

6.4.1 Effect of scavenger loading on permeation behavior of PS reactive blend films containing SBS scavenger

Following the simulation guidance, reactive PS films of 100 μm in thickness blended with 5, 10, and 20% SBS scavenger were melt-extruded and exposed to UV irradiation before they were subjected to permeation tests with an upstream oxygen pressure of 100 psi. Figure 6.9(a) shows that the cumulative amount of permeate, Q_t, increased shortly after an early time lag. Furthermore, the cumulative amounts of permeate as a function of SBS content were normalized by their steady state fluxes and time lags without any scavenger, as shown in Figure 6.9(b).

The time lag was greater in samples with greater loading, and thus greater capacity, of oxygen scavenger, which was qualitatively predicted in previous dimensionless analysis and simulation by Ferrari [6]. The difference between theoretically predicted and measured time lags, as shown in Table 6.1, could be due to the butadiene phase morphology appearing to be not entirely spherical, possibly due to extensive stretching. This may affect the number density, $\rho = \frac{3\phi}{4\pi R^3}$, of spherical particles as assumed in past theories [6], and thus influence the theoretical basis that predicts the time lag extension.

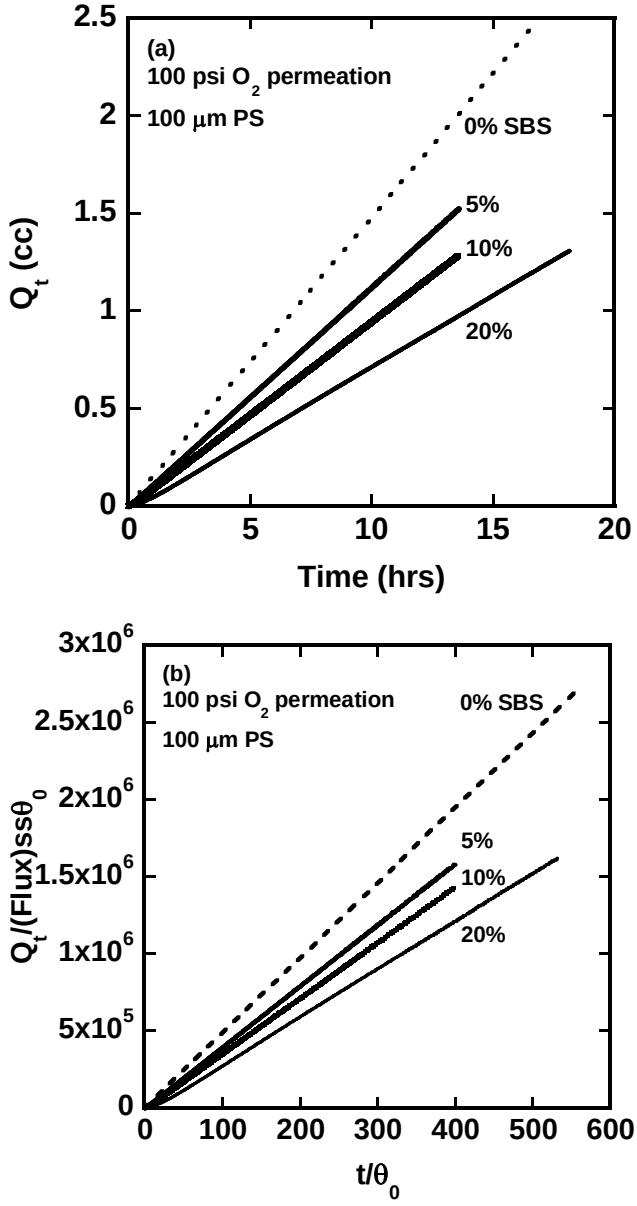

Figure 6.9: (a) The cumulative amount of permeate of reactive PS blends ~ 100 μm increased with decreasing scavenger loading. (b) Normalized cumulative amounts of permeate time plots reveal the scavenging effect as a function of scavenger content.

The oxygen fluxes of all blends as a function of time are shown in Figure 6.10(a). Due to active scavenging, initial fluxes were low and then increased nonlinearly due to diminishing oxidation activity before reaching steady state, suggesting complete exhaustion of reactive sites. Furthermore, blends with higher SBS content had lower steady state fluxes, due to the lower permeability of fully oxidized SBS [5].

Overall, the fluxes are lower for samples with higher scavenger loading as they have a higher capacity to scavenge oxygen, and thus decrease the fluxes more effectively. Blend films that were loaded with greater amounts of scavenger had more reactive sites and, therefore, an increased capacity to scavenge oxygen. Interestingly, the flux behavior of the reactive blend with 10% scavenger is quite different from, and orders of magnitude higher than, its simulated counterpart shown earlier in Figure 6.8. The simulation shows an oxygen flux that is more suppressed than that shown by the experiment. Thus, the simulation assumes faster oxidation kinetics than that in the experiments and thus over-predicts the oxidation performance.

Figure 6.10(b) shows the normalized fluxes as a function of normalized time for several scavenger contents. Here the sample with greatest scavenger content had the longest time lag due to active scavenging before the flux increased and approached steady state. The number of reactive sites available for oxygen scavenging is proportional to the SBS content. Samples with lesser loading appear to become fully oxidized more quickly. Fluxes before time lags were no more than an order of magnitude lower than the steady state values; the difference between the steady state value and the transient value before time lags depends on the scavenging capacity. The scavenger content effect is that the overall number of available reactive sites controls the level of time lag extension, which was also found in the past theories [6].

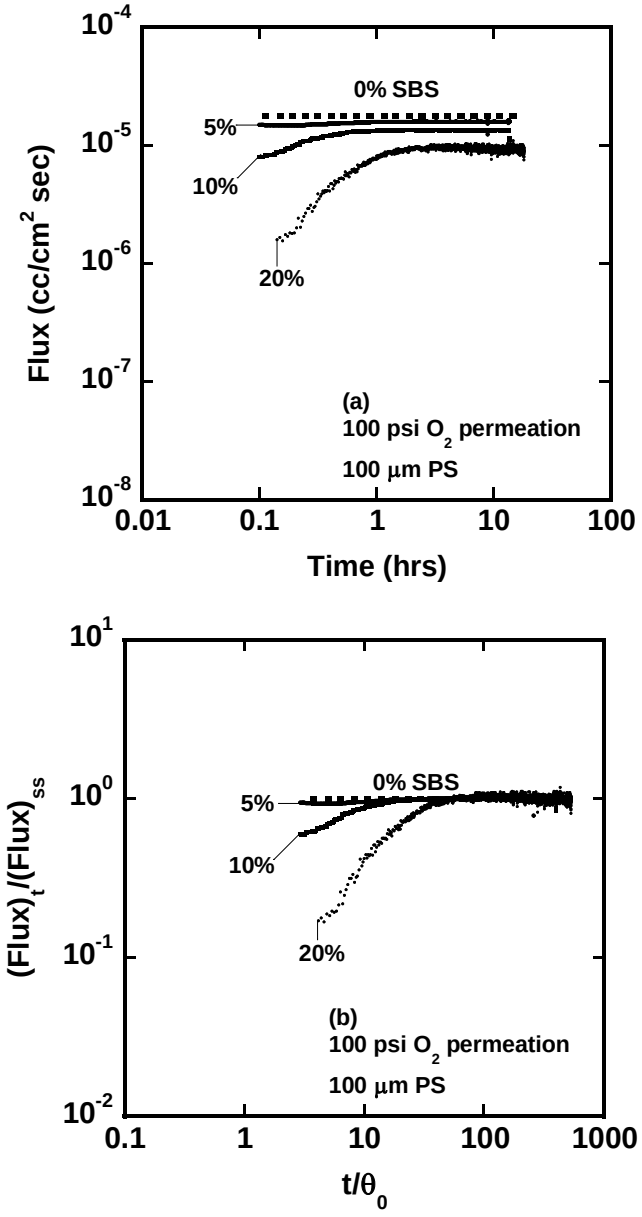

Figure 6.10: (a) Effect of scavenger loading on flux behaviors of reactive blend films. Samples with greater scavenger loading show lower fluxes due to the intrinsically lower permeability of SBS when oxidized. (b) Normalized flux plots as a function of scavenger loading. The blend film with greater scavenger loading showed the longest lag before approaching steady state.

6.4.2 Effect of film thickness on permeation behavior of PS reactive blend films containing SBS scavenger

In Figure 6.10, fluxes are shown orders of magnitude higher than the lowest values that can be measured by the instrument, and their values increase rather rapidly due to fast oxidation at high pressure. A lower upstream pressure may be used to slow the oxidation process. As a result, the following set of permeation experiments was performed with lower upstream pressure to measure the thickness effect on flux behavior.

Polystyrene films were melt-extruded with 10% SBS scavenger to produce blend films of approximately 100, 200, and 275 μm in thickness. These blends were subsequently subjected to permeation tests with upstream pressurized at 20 psi. Figure 6.11(a) shows that permeate volume, Q_t, gradually increased with time after an early time lag, shown in Table 6.1. These data can also be normalized by their steady state fluxes and time lags without any scavenger to reveal the effect of film thickness on scavenging, as shown in Figure 6.11(b). While the permeate volume increased, the time lag was found to scale with film thickness. This relationship between film thickness and time lag has previously been predicted by theoretical modeling [6].

It has been reported that time lag is independent of the kinetics of the scavenging reactions and the parameters that affect the rate of reaction [6]. Therefore, time lag extension is a function of only the capacity to absorb oxygen, ϕ, n_0, and $\hat{v}$, as well as the solubility of oxygen in the matrix polymer, S_m, and the oxygen partial pressure, P_{O_2}. Time lag extension is also a function of film thickness, which affects the native time lag without any scavenging. Similarly, the difference in experimentally measured and predicted time lags may be due to the imperfect spherical morphology of the butadiene phase in reactive blend films. This would affect the theoretical development of the time lag extension.

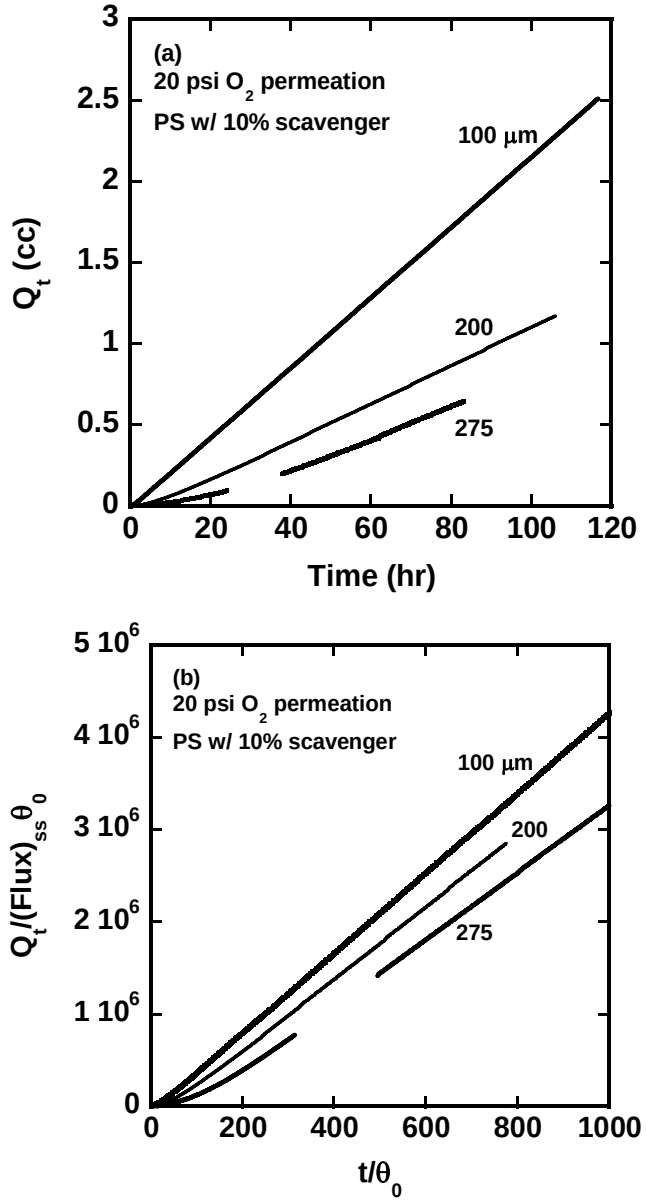

Figure 6.11: (a) The cumulative amount of permeate of reactive PS blends ~ 100, 200, and 275 μm with 10% SBS increased with decreasing film thickness. The thicker samples also have greater time lags. (b) Normalized Q_t plot reveal the scavenging effect as a function of film thickness. The gap seen in 275 μm data was due to pressure reading being over the limit of the instrument.

Figure 6.12(a) shows the oxygen fluxes of blends as a function of time for several film thicknesses. Fluxes, initially low due to active scavenging, gradually increased due to diminishing oxidation activity over time. The normalized fluxes for films of various thicknesses, as shown in Figure 6.12(b), indicate that the thicker samples have greater time lags during active scavenging before the fluxes increase and eventually reach steady state.

In general, blend films that are thicker have lower fluxes and show a slower response to oxidation and therefore approach steady state more slowly, as predicted in previous simulation work [6]. This may be due to the combined effects of a film being thicker (flux ~ L^{-1}) and a higher scavenger volume that would consume more oxygen and thus extend the time lag longer. Since the time scale for diffusion is proportional to the square of film thickness, L^2, but the time scale of reaction is proportional to film thickness, L, there should be less time for scavenging before the breakthrough of oxygen flux in thinner films. Consequently, diffusion is more rapid than the reaction. As a result, time lags scale with film thickness, agreeing with the prediction made by past theories [6].

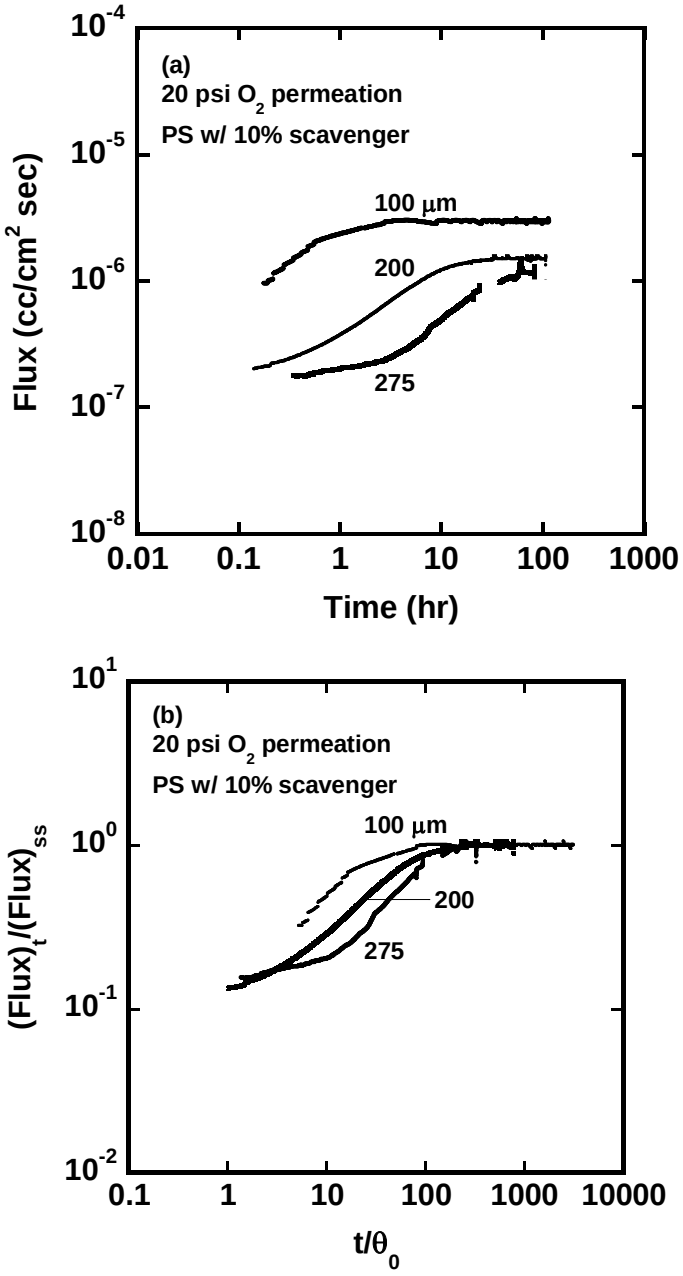

Figure 6.12: (a) Effect of film thickness on flux behaviors of reactive blend films. Thicker samples have lower fluxes and greater time lags. (b) Normalized flux plots as a function of film thickness. The thickest sample showed the longest lag before approaching steady state. The gap seen in 275 μm data was due to pressure reading being over the limit of the instrument.

6.4.3 Effect of oxygen pressure on permeation behavior of PS reactive blend films containing SBS scavenger

Flux behavior had been experimentally captured to demonstrate the concept of improving barrier properties of blends by adding scavengers to extend time lags. Because the oxygen partial pressure inside a food package may vary over the lifetime of the product, it is important to investigate the effect of oxygen partial pressure on oxygen flux through reactive polymer blends. To this end, polystyrene was blended with 10% SBS scavenger to form melt-extruded films of approximately 200 μm in thickness. These reactive blends were subjected to permeation tests at various differential pressures of 3, 20, 40, 60, 80, and 100 psi.

Figure 6.13(a) shows that the cumulative amount of permeate, Q_t, increased with time after early time lags. In addition, the sample that was subjected to lower differential pressures shows lower Q_t overall, and the total permeate was found to increase with oxygen pressures. The cumulative amounts of permeate can be normalized by their steady state fluxes and time lags without any scavenger, resulting in non-dimensional quantities, as shown in Figure 6.13(b). Also shown in Figure 6.13, time lags can be extended 10 to more than 300 times due to oxygen scavenging compared to time lags of native polystyrene films with no scavenger added. The experimentally measured and predicted time lag values can be found in Table 6.1. This relationship has been predicted by previous theoretical modeling in reactive blend films as a function of pressure [6].

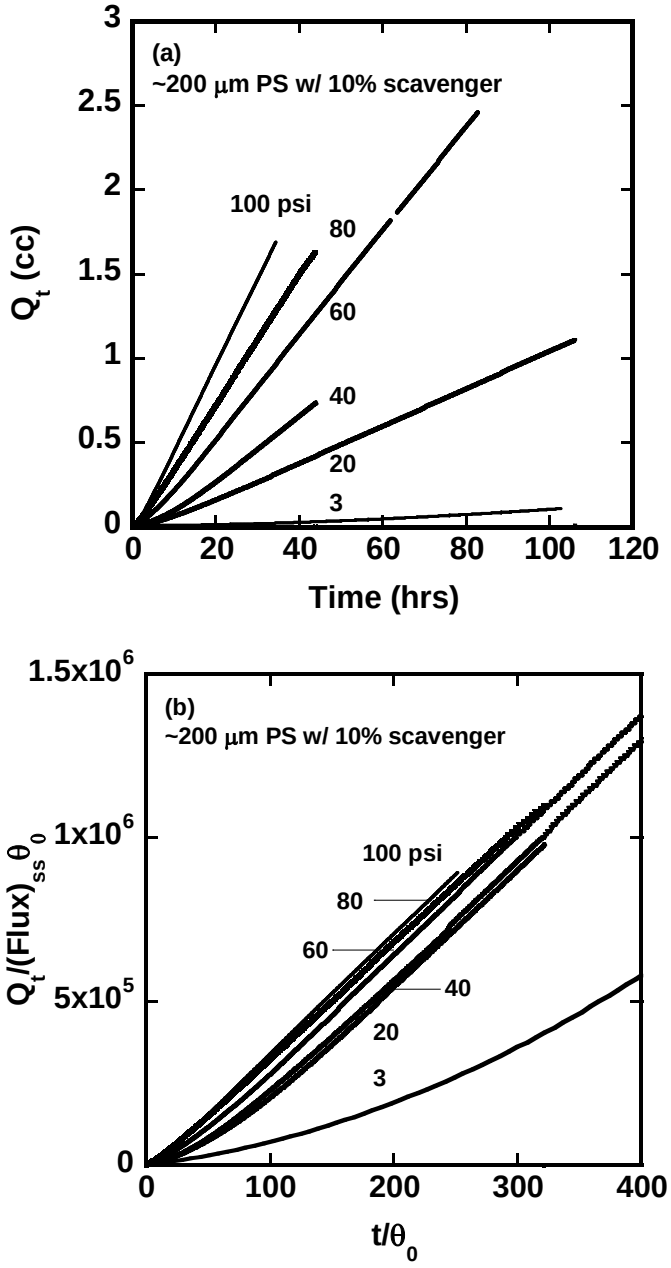

Figure 6.13: (a) The cumulative amount of permeate of reactive PS blends with SBS increased with upstream pressure. (b) Normalized cumulative amounts of permeate time plots reveal the scavenging effect as a function of pressure that can extend time lags by orders of magnitude.

Figure 6.14(a) shows the measured flux of all blends as a function of time for several different upstream pressures. Initially, fluxes were low due to active scavenging but increased in value due to diminishing oxidation activity before reaching steady state, where reactive sites have been completely exhausted. Blends that were exposed to higher pressure have higher transient fluxes and approach higher steady state fluxes more quickly than those exposed to lower pressure. The fluxes can be normalized by their steady state flux and are shown in Figure 6.14(b) as a function of normalized time at different pressures. The blend sample that was exposed to 3 psi O_2 (~ 0.21 atm O_2) showed the greatest time lag during active scavenging before the flux rose to steady state (see Appendix). A similar observation of plateau flux has been previously reported [6].

Interestingly, the shape of the normalized flux/normalized time curve changed as the oxygen pressure (and thus oxygen concentration) was increased. Specifically, the sample with the highest external oxygen pressure had the fastest rise in flux and approached steady state more rapidly than the other samples. These results suggest that the kinetics vary with oxygen pressure, and the kinetics order in the current system may be different from what was assumed in previous work [5,6,28].

The qualitative shape of flux as a function of time does not resemble the simulation of pressure effect on flux behavior shown in Figure 6.15. While the time lag extension is not related to the kinetics and only to the capacity to scavenge oxygen, the deviation in the flux trend could be due to a deviation from the first order kinetics that have been assumed in the current theoretical basis and simulation models [6,28].

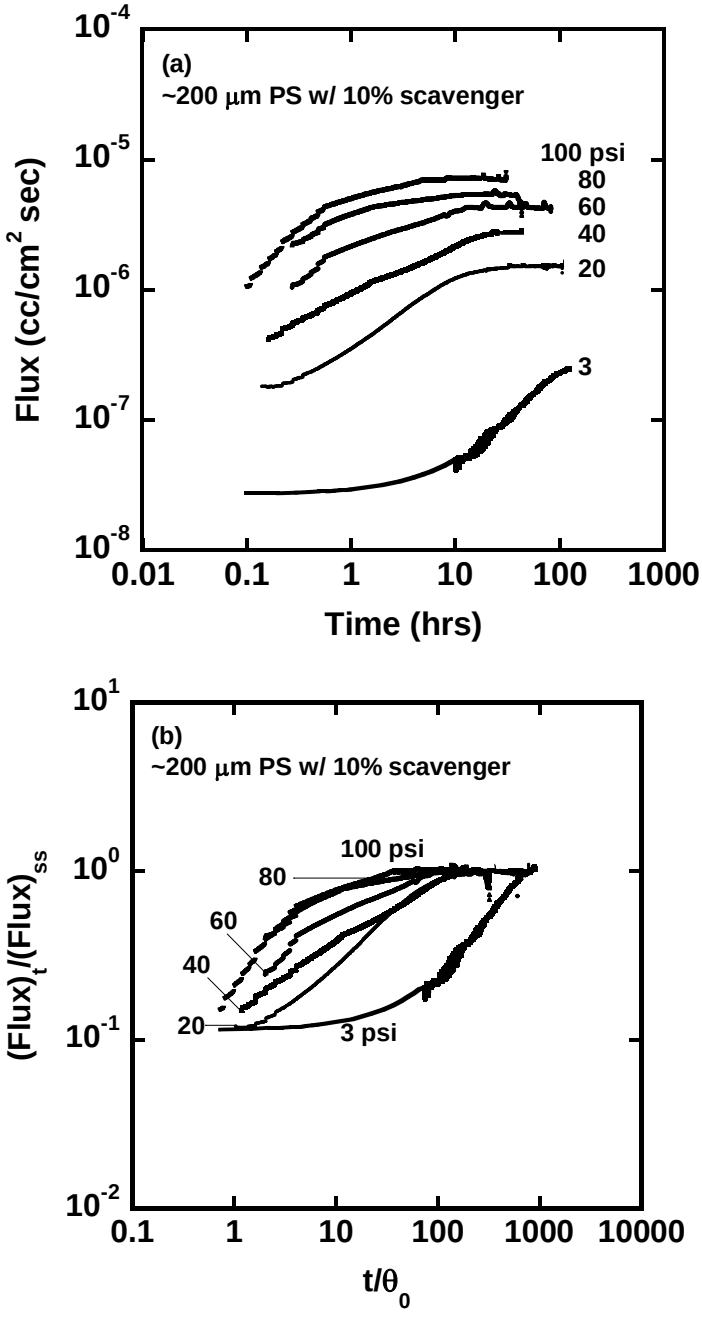

Figure 6.14: (a) Oxygen flux in blend films as a function of time at various oxygen differential pressures. (b) Normalized flux plots as a function of pressure. The blend film sample that was exposed to 3 psi O_2 showed the longest plateau before it rises to the steady state value.

Table 6.1: Experimental parameters and time lags in reactive blends as a function of SBS content, film thickness, oxygen pressure, and photoinitator (PI) content

Test	Pressure psi	Thickness μm	SBS content %	$(Flux)_{ss} \times 10^{-6} \frac{cc}{cm^2\ sec}$	P_{O_2} Barrer	θ_0 hr	θ hr	θ_{theo}	Theo/ exp
SBS %	100	100	**0**	1.8	3.1	0.034	0.034	0.034	1
	100	100	**5**	1.7	2.9	0.034	0.4	0.6	1.5
	100	100	**10**	1.3	2.6	0.034	0.8	1.2	1.4
	100	100	**20**	9.3	2.3	0.034	1.2	2.3	1.9
Thickness	20	**100**	10	3.0	2.8	0.034	1.4	5.6	4.0
	20	**200**	10	1.5	2.9	0.14	6.5	22.6	3.5
	20	**275**	10	1.1	2.9	0.26	19.0	42.6	2.2
Pressure	**3**	200	10	0.27	2.8	0.14	45	149.6	3.3
	20	200	10	1.5	2.9	0.14	6.5	22.6	3.5
	40	200	10	2.8	2.7	0.14	5.5	11.3	2.1
	60	200	10	4.3	2.8	0.14	2.5	7.6	3.0
	80	200	10	5.2	2.7	0.14	1.5	5.7	3.8
	100	200	10	7.2	2.8	0.14	1.2	4.6	3.9
PI %	**20 (1% PI)**	200	10	1.3	2.8	0.14	18	---	---
	20 (3% PI)	200	10	1.4	2.8	0.14	25	---	---
	20 (6% PI)	200	10	1.6	2.9	0.14	13	---	---

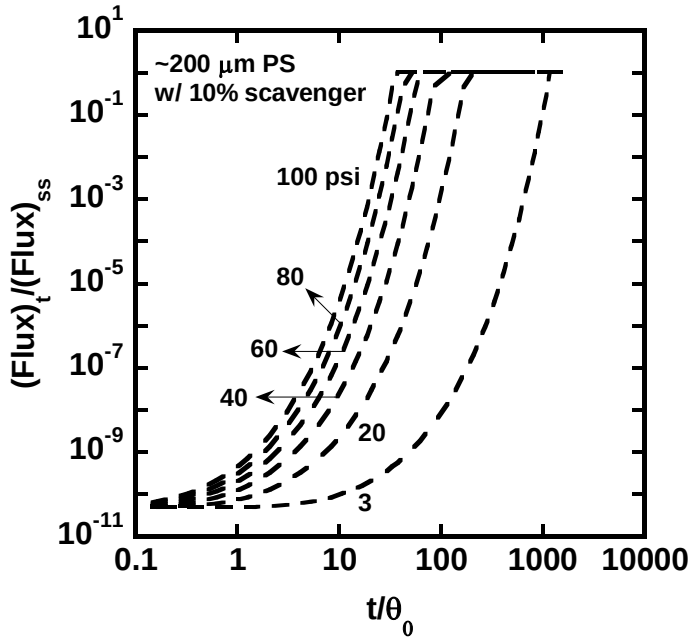

Figure 6.15: The shape of modeled pressure effect on normalized flux of reactive polystyrene blends of 200 μm with 10% scavenger does not resemble the flux behavior as an effect of pressure. The discrepancy may be due to the first order kinetics assumption in the current simulation models.

6.4 DETERMINING THE ORDER OF SBS OXIDATION KINETICS VIA UPTAKE EXPERIMENTS AT VARIOUS PRESSURES

To determine the reaction order, the effect of changing oxygen partial pressure on the oxidation rate must first be determined. Results from uptake experiments where the pressure is varied can be used to determine the kinetics order. Therefore reactive films of pure SBS films of approximately 100 μm were solution cast and allowed to oxidize at 35 °C at four different pressures – 3, 20, 60, and 100 psi O_2. While the oxygen uptake of the sample exposed to 3 psi O_2 was tracked by weight changes in air, the samples that were exposed to 20, 60, and 100 psi O_2 had their mass uptake monitored by a magnetic

suspension balance, following the procedure previously described in section 2.6, Chapter 3. Figure 6.16 shows the oxidation kinetics of SBS films determined from uptake experiments where pressure was varied.

In general, all samples demonstrated similar oxygen uptake trends with time. The initial mass uptake increases rapidly and begins to slow at later times. The decrease in rate of mass uptake at long oxidation time suggests that oxidation may become limited by the diffusion. This is well documented and has been shown previously [5,34–36]. Furthermore, oxygen uptake was found to scale with the oxygen pressure; the sample that was exposed to the highest oxygen pressure at 100 psi was found to have the greatest oxygen uptake of all samples.

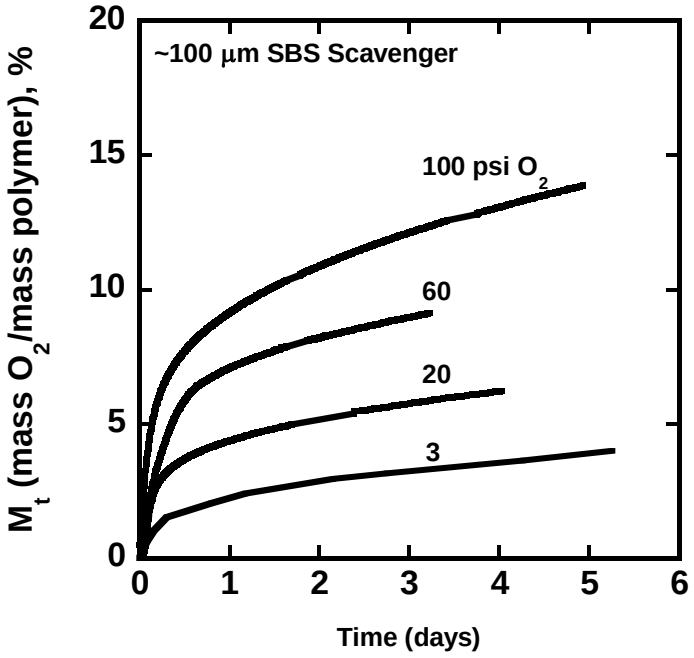

Figure 6.16: Oxygen uptake of SBS films was monitored with time at different pressures. The sample exposed to the highest pressure has the greatest oxygen uptake than other samples.

For an oxidative reaction, the reaction rate r at time t is experimentally found to be related to the oxygen concentration, C, present at that time and may be expressed by

$$r = kC^n \tag{6.2}$$

where the proportionality constant k is the rate constant and n is the order of the reaction with respect to the oxygen concentration present.

The rate of oxidation, r, can be approximated from the slopes in the early time region. The approximation was done using data points within the first 5 hours, where mass uptake occurs quickly and oxidation is controlled by kinetics. The reaction order can be determined by taking the ratio of the rates of oxidation obtained in uptake experiments where pressure is varied. Consequently, the reaction order n can be determined by solving for a rearranged, logarithmic relationship:

$$\frac{r_2}{r_1} = \left(\frac{P_2}{P_1}\right)^n \rightarrow n = \frac{\log(\frac{r_2}{r_1})}{\log(\frac{P_2}{P_1})} \tag{6.3}$$

where r_1 and r_2 is the rate of oxidation of two different experiments where pressure is varied to p_1 and p_2, respectively. The approximated rates of oxidation and the reaction order n are shown in Table 6.2.

Table 6.2: The rate of oxidation at early times at various pressures can be used to determine the order of reaction

Oxygen pressure **psi**	**Rate of oxidation** r $\frac{gram\ of\ oxygen}{100\ gram\ of\ polymer \times day}$	**Reaction order** n **N/A**
3	6.4	---
20	14.7	0.65
60	22.1	0.42
100	32.8	0.45

The rates of oxidation increase with increasing oxygen pressure; however, the ratio in rates of oxidation, r_2/r_1, is less than the ratio of oxygen pressures, P_2/P_1. These results from the uptake experiment performed at various pressures confirmed that the reaction may indeed be of a kinetics order that is less than unity, which is different from the linear, first order reaction assumption made in previous work [5,6,28]. A reaction can have different orders, and kinetics experiments are needed to determine the rate and its reaction order. The reaction order can be integers or half-integers (1/2, 3/2…) [37]. A reaction with lower kinetics order has slower response to oxygen concentration change, and when concentration is doubled, the rate of reaction is not quite doubled [37]. The fact that the oxidation may not follow first order kinetics suggests that experimental data may not be comparable with the current theoretical prediction, which assumes the kinetics to be first order. A kinetics order that is being assumed higher than the actual kinetics order found in the experiment may explain the over-prediction of oxidation performance by the current theoretical model.

6.5 CONCLUSIONS

A number of reactive blends were melt-processed and subjected to permeation tests to systematically evaluate the effects of pressure, film thickness, and scavenger and photoinitiator contents on their oxidation behavior. These reactive blends used the scavenging conditions that had been verified to give optimum flux behavior. The permeation results were shown, and the time lag extension was experimentally measured and compared with theoretical prediction.

The permeation behavior was related to scavenger loading and film thickness. The flux behavior of samples with greater SBS content, as well as greater in thickness, exhibited a longer time lag before reaching steady state. The fact that time lag extension scales with scavenger loading and film thickness is in agreement with theoretical predictions that the time lag extension should depend only on the capacity to absorb oxygen, and not the kinetics and other parameters that may affect the rate of reaction.

The upstream pressure appears to have a profound effect on flux behavior, which shows that the flux trend changes non-linearly with pressure. The sample that was subjected to very low pressure has the longest lag before rising and approaching steady state value. The time lags increase with decreasing pressure, which had been predicted qualitatively. The difference between the measured and predicted values may be due to the reactive phase morphology not appearing to be entirely spherical, which is part of the theoretical assumption.

The flux trends that increase nonlinearly as a function of pressure may be due to the actual order of kinetics, which deviates from the unity that is assumed in current theories. Moreover, uptake experiments where pressure is varied have verified that the kinetics order may be less than unity and thus nonlinear. This would explain the fact that

the flux trend does not respond linearly as a function of pressure, as well as the theoretical over-predictions of the flux behavior of reactive blend films.

This work has tested and verified the concept of improving barrier properties and extending time lags by blending active oxygen scavenger to a traditional packaging material. Time lag can be extended by orders of magnitude before reaching steady state. The experimental time lag extension was shown to depend only on the capacity to absorb oxygen. Moreover, the effect of several useful parameters on time lags followed the trend predicted by current theories, despite slight differences in values due to imperfect spherical morphology of the butadiene phase in the blends. This work validates the fundamental principles of incorporating oxygen scavengers into a polymer matrix to extend time lags and thus improve barrier properties of traditional packaging materials.

6.6 REFERENCES

[1] H. Li, D.K. Ashcraft, B.D. Freeman, M. Stewart, M.K. Jank, T.R. Clark, Non-invasive headspace measurement for characterizing oxygen-scavenging in polymers, Polymer. 49 (2008) 4541–4545.

[2] H. Li, K.K. Tung, D.R. Paul, B.D. Freeman, Effect of film thickness on auto-oxidation in cobalt-catalyzed 1,4-polybutadiene films, Polymer. 52 (2011) 2772–2783.

[3] H. Li, K.K. Tung, D.R. Paul, B.D. Freeman, M. Stewart, J. Jenkins, Characterization of Oxygen Scavenging Films Based on 1,4-Polybutadiene, Industrial & Engineering Chemistry Research. 51 (2012) 7138–7145.

[4] R.H. Li, Metal-catalyzed oxidation of polybutadiene in oxygen scavenging packaging application (Ph.D. Thesis), The University of Texas at Austin, 2010.

[5] K.K. Tung, R.T. Bonnecaze, B.D. Freeman, D.R. Paul, Characterization of the oxygen scavenging capacity and kinetics of SBS films, Polymer. 53 (2012) 4211–4221.

[6] M.C. Ferrari, S. Carranza, R.T. Bonnecaze, K.K. Tung, B.D. Freeman, D.R. Paul, Modeling of oxygen scavenging for improved barrier behavior: Blend films, Journal of Membrane Science. 329 (2009) 183–192.

[7] S.W. Beavan, D. Phillips, Mechanistic Studies on the Photooxidation of Commercial Polybutadiene, European Polymer Journal. 10 (1974) 593–603.

[8] A.T. Betts, N. Uri, Catalyst-Inhibitor Conversion in Autoxidation Reactions, in: F.R. Mayo (Ed.), Oxidation of Organic Compounds, AMERICAN CHEMICAL SOCIETY, WASHINGTON, D.C., 1968: pp. 160–181.

[9] A.T. Betts, N. Uri, The conversion of metal catalysts into inhibitors of autoxidation, Die Makromolekulare Chemie. 95 (1966) 22–39.

[10] Y. Kamiya, K.U. Ingold, THE METAL-CATALYZED AUTOXIDATION OF TETRALIN: III. CATALYSIS BY MANGANESE, COPPER, NICKEL, AND IRON, Canadian Journal of Chemistry. 42 (1964) 1027–1043.

[11] J.N. Morris, L. Reich, S. Stivala, Elements of Polymer Degradation, McGraw-Hill Book Company, New York, 1972.

[12] Y. Kamiya, E. Niki, Oxidative Degradation, in: Aspects of Degradation and Stabilization of Polymers, Vol. 3, Elsevier Scientific Publishing Company, Amsterdam, 1978: pp. 79–148.

[13] M. Piton, A. Rivaton, Photooxidation of polybutadiene at long wavelengths ($\lambda >$ 300 nm), Polymer Degradation and Stability. 53 (1996) 343–359.

[14] M. Piton, A. Rivaton, Photo-oxidation of ABS at long wavelengths ($\lambda > 300$ nm), Polymer Degradation and Stability. 55 (1997) 147–157.

[15] H.A. Daynes, The Permeability of Rubber and Methods of Testing It, Transactions, Institution of the Rubber Industry. 3 (1928) 428–453.

[16] D.R. Paul, Fundamentals of Transport Phenomena in Polymer Membranes, in: Enrico Drioli & Lidietta Giorno (Ed.), Comprehensive Membrane Science and Engineering, 1st ed., Elsevier B.V., 2010: pp. 75–90.

[17] K.F. Finger, A.P. Lemberger, T. Higuchi, L.W. Busse, D.E. Wurster, Investigation and development of protective ointments IV. The influence of active fillers on the permeability of semisolids, Journal of the American Pharmaceutical Association. 49 (2006) 569–573.

[18] D.R. Paul, Effect of immobilizing adsorption on the diffusion time lag, Journal of Polymer Science Part A-2: Polymer Physics. 7 (1969) 1811–1818.

[19] D.R. Paul, D.R. Kemp, The diffusion time lag in polymer membranes containing adsorptive fillers, Journal of Polymer Science: Polymer Symposia. 41 (2007) 79–93.

[20] D.R. Paul, W.J. Koros, Effect of partially immobilizing sorption on permeability and the diffusion time lag, Journal of Polymer Science: Polymer Physics Edition. 14 (1976) 675–685.

[21] C. Yang, E.L. Cussler, Oxygen barriers that use free radical chemistry, AIChE Journal. 47 (2001) 2725–2732.

[22] C. Yang, E.E. Nuxoll, E.L. Cussler, Reactive barrier films, AIChE Journal. 47 (2001) 295–302.

[23] N.K. Lape, C. Yang, E.L. Cussler, Flake-filled reactive membranes, Journal of Membrane Science. 209 (2002) 271–282.

[24] E.E. Nuxoll, R.A. Siegel, E.L. Cussler, Layered reactive barrier films, Journal of Membrane Science. 252 (2005) 29–36.

[25] T. Shimotori, E.L. Cussler, W.A. Arnold, Diffusion of mobile products in reactive barrier membranes, Journal of Membrane Science. 291 (2007) 111–119.

[26] R.A. Siegel, E.L. Cussler, Reactive barrier membranes: some theoretical observations regarding the time lag and breakthrough curves, Journal of Membrane Science. 229 (2004) 33–41.

[27] E.E. Nuxoll, E.L. Cussler, The third parameter in reactive barrier films, AIChE Journal. 51 (2005) 456–463.

[28] S. Carranza, D.R. Paul, R.T. Bonnecaze, Analytic formulae for the design of reactive polymer blend barrier materials, Journal of Membrane Science. 360 (2010) 1–8.

[29] S. Carranza, Modeling of Oxygen Scavenging Polymers and Composites (Ph.D. Thesis), The University of Texas at Austin, 2010.

[30] J.C. Maxwell, A Treatise on Electricity and Magnetism, Clarendon Press, 1873.

[31] L.M. Robeson, Polymer Blends in Membrane Transport Processes, Industrial & Engineering Chemistry Research. 49 (2010) 11859–11865.

[32] S. Carranza, D.R. Paul, R.T. Bonnecaze, Design formulae for reactive barrier membranes, Chemical Engineering Science. 65 (2010) 1151–1158.

[33] S. Carranza, D.R. Paul, R.T. Bonnecaze, Multilayer reactive barrier materials, Journal of Membrane Science. 399-400 (2012) 73–85.

[34] M. Coquillat, J. Verdu, X. Colin, L. Audouin, R. Nevière, Thermal oxidation of polybutadiene. Part 1: Effect of temperature, oxygen pressure and sample thickness on the thermal oxidation of hydroxyl-terminated polybutadiene, Polymer Degradation and Stability. 92 (2007) 1326–1333.

[35] M. Coquillat, J. Verdu, X. Colin, L. Audouin, R. Nevière, Thermal oxidation of polybutadiene. Part 2: Mechanistic and kinetic schemes for additive-free non-crosslinked polybutadiene, Polymer Degradation and Stability. 92 (2007) 1334–1342.

[36] M. Coquillat, J. Verdu, X. Colin, L. Audouin, R. Nevière, Thermal oxidation of polybutadiene. Part 3: Molar mass changes of additive-free non-crosslinked polybutadiene, Polymer Degradation and Stability. 92 (2007) 1343–1349.

[37] I.N. Levine, Integration of Rate Laws, in: Physical Chemistry, 5th ed., McGraw-Hill Higher Education, New York, 2001: pp. 533–539.

Chapter 7: Conclusions and Recommendations

7.1 CONCLUSIONS

This dissertation explored the oxidation behavior of reactive membranes containing styrene-butadiene-styrene (SBS) block copolymer in a polystyrene matrix. Similar to 1,4 polybutadiene (PB) [1–4], SBS is a type of butadiene-containing polymer that is of potential use as an oxygen scavenging polymer (OSP) for barrier applications [5]. The fundamental effects of parameters in these applications, such as reaction rate constants, stoichiometric oxidation coefficients, and time lag extension due to scavenging, were discussed and compared to theoretical models [6,7]. SBS block copolymer was readily and irreversibly oxidized when catalyzed by a transition metal, and the oxidation performance was monitored by uptake and permeation experiments. The results from this work show that the scavenging behavior of films containing SBS is a function of catalyst concentration, film thickness, oxygen pressure, SBS scavenger content, and photoinitiator (PI) content.

To evaluate their use in such applications, oxygen uptake was measured for solution-cast films made of Kraton D1102 SBS with four cobalt catalyst loadings over a wide range of thicknesses. Oxygen mass uptake was monitored as a function of oxidation time to understand the oxidation kinetics and the oxygen uptake capacities of reactive films, and these results were shown in Chapter 4. Oxygen uptake of thin films collapsed into a single curve that approached a constant extent of oxidation, while thicker films exhibited uptake that strongly depended on thicknesses. Moreover, a plot on log-log coordinates suggested that oxygen uptake approached a $\sqrt{t}$ regime that is different from the linear relationship with time exhibited by the early time uptake data. This was

explained by the fact that the oxygen uptake was kinetically limited for thin films, while diffusion controls the uptake at long times for thick films.

A thin film kinetic model was developed to extract the reaction rate parameters and stoichiometric oxidation coefficients that describe oxygen uptake in the absence of diffusion limitation. Both reaction parameters were found to scale with catalyst loading. An approximate moving-boundary model was developed to describe thick film oxidation behavior at long times and was found to be in semi-quantitative agreement with the measured uptake. Reaction kinetics of polymer films made of SBS block copolymer were understood via a combination of experimental and theoretical efforts.

Oxidation leads to the formation of a growing crust layer at the film's outer surfaces. Energy dispersive spectroscopy (EDS) elemental analysis shows an accumulation of oxygen–containing functional groups at film surfaces. The thickness of the oxidized region at long oxidation times was called the critical thickness L_c and had different values in experiments where catalyst loadings were varied. Thin films (i.e., $L \leq 2L_c$) oxidize fully and homogeneously, whereas heterogeneous oxidation typically occurs in thicker films (i.e., $L > 2L_c$).

Uptake data from thin and thick reactive films at long oxidation times were plotted against inverse film thickness and used to estimate the value of critical thickness. The value of critical thickness was measured on the scanning electron microscopic (SEM) image of an oxidized SBS film cross section and pointed to values similar to those determined via mass uptake experiments. This is a well-documented phenomenon and characteristic of a diffusion-controlled mechanism.

Gas permeabilities of fully oxidized thin films were two orders of magnitude lower than those of unoxidized polymers. While the solubility of oxygen in the fully

oxidized polymer was higher than in the unoxidized polymer by a factor of two, the oxygen diffusivity of the fully oxidized polymer was 2 – 3 orders of magnitude lower than that of the unoxidized polymer. The film density was found to increase as a result of oxidation, and the increase in film density may contribute to the decrease in free volume that reduces diffusivity. These findings are similar to those previously reported for oxidation kinetics studies on 1,4-polybutadiene.

Ultimately, these active scavenging components must be combined with rheologically compatible, conventional packaging material, such as polystyrene, via melt-processing. Films of SBS block copolymer were melt-processed using a set of previously identified processing conditions. The oxidation kinetics of these melt-processed SBS films were monitored by uptake experiments and were found to depend on film thickness. The slope and intercept values of the oxygen uptake data at long oxidation times were compared with those prepared by solution casting. These values were comparable, suggesting that the processed films have the same level of oxygen scavenging capability as those films prepared by solution casting.

Reactive polystyrene blend films containing SBS were prepared and allowed to oxidize. Transmission electron microscopic (TEM) images of a blend film containing 20% SBS suggested that the butadiene phase had a morphology that was not entirely spherical. DSC thermograms showed the T_g disappearance of the butadiene phase signaling the exhaustion of the reactive sites due to oxidation. The oxidized blend film density scaled with the SBS content and approached the density of fully oxidized SBS. The steady-state permeabilities of unoxidized and oxidized blend films were characterized and found to be in qualitative agreement with those estimated by the Maxwell Equation.

The transient scavenging kinetics of reactive blend films were monitored in a way similar to those of the pure SBS films. The formation of the master kinetics curve prepared by normalizing the uptake data of reactive blend films with the infinite oxygen uptake proportional to the SBS composition validates the blending technique. It was shown that the slopes and intercepts of the uptake data at long oxidation times scale with the SBS loading and approach those of pure Kraton SBS prepared by either solution casting or melt processing. The fact that the long time kinetics of processed SBS are the same as those of solution cast SBS confirms that appropriate melt-processing conditions had indeed been identified to allow retention of desirable oxidation kinetics and oxygen uptake capacity of the oxygen scavenging blend films containing SBS block copolymers. The conditions for producing melt-processed reactive films that have the same oxidation kinetics as the solution cast counterparts were discussed in Chapter 5.

The oxidation behavior of reactive polystyrene films blended with the SBS scavenger was also characterized via permeation experiments. The cumulative amount of permeate and permeate fluxes were monitored and analyzed in experiments that investigated the effects of film thickness, scavenger content, and oxygen pressure on oxidation kinetics. Time lags were determined from the time intercepts by linear extrapolation from the steady state region of the cumulative permeate. Time lags were generally found, in both experimental measurement and theoretical prediction, to be extended by 1 to 2 orders of magnitude due to scavenging. The differences between theoretically predicted and experimentally measured time lags could be due to a number of assumptions in the model that do not precisely match the experimental situation; e.g., the SBS phase morphology in the blend may not be perfectly spherical.

The fluxes were found to depend on the tested variables. The flux of the thickest sample had a time lag that was longer than that of other thinner samples. The flux of the blend with highest SBS loading was shown to have the longest lag due to its greater oxygen scavenging capacity. Similarly, the sample that was charged with the lowest upstream pressure showed a long flux plateau before its flux increased due to diminishing oxidation activity, with the flux eventually approaching steady state. The shape of the flux/time relationship where pressure is varied appeared to be different from the theoretical simulation. This effect was explained by the existence of a non-linear order of kinetics. The results from uptake experiments where pressure is varied suggest and confirm that kinetics order may not be first order. Overall, a fundamental understanding of the relationship between useful permeation parameters of reactive blend films and time lag extension was discussed, and the concept of improving barrier properties by incorporating oxygen scavenging polymers to extend the time lag was verified in Chapter 6.

7.2 RECOMMENDATIONS FOR FUTURE WORK

Polystyrene films blended with a particular type of oxygen scavenger have shown a capacity to improve barrier properties by extending oxygen permeation time lag due to oxidative reaction. The oxygen scavenging system, which includes styrene-butadiene-styrene block copolymer, metal catalyst, and photoinitator, was melt-extruded to produce reactive blends that could oxidize after UV initiation. By means of oxidation, these reactive films can have oxygen uptakes several orders of magnitude higher than the solubility of oxygen in the native polymers.

It would be worthwhile to investigate the effect of stoichiometric oxidation coefficient $\hat{v}$ on time lag extension, since it is a parameter that is previously predicted to have an inverse effect on time lag extension, as shown in equation 6.2 in Chapter 6 [6]. Currently, $\hat{v}$ seems to only differ by 10 – 20 % which suggests that the stoichiometric oxidation coefficient may be an intrinsic property that is specific to the reactive phase in the polymer. As a result, a different polymer may need to be identified to investigate the $\hat{v}$ effect on time lag, while keeping constant the values of other parameters relating with oxidation.

The scavenging performance was found to depend on the UV exposure time. Since the effect of UV exposure is largely on the formation of the photoinitator diradical that initiates oxidation, the level of UV exposure time may be related to the stoichiometric oxidation coefficient $\hat{v}$. A systematic study on UV exposure at greater intensity and/or longer time would be beneficial to explore the relationship between UV, $\hat{v}$, and oxidation behavior.

When working with SBS oxygen scavenger in future efforts, one may need to first determine the actual order of the kinetics of the scavenging reaction. The uptake experiment where oxygen pressure was varied was performed on thick films where oxidation would become diffusion limited at long times. It would be worthwhile to perform uptake tests in which pressure is varied on thin films, where oxidation is kinetically controlled throughout the entire course of the experiment. The results of these thin film uptake experiments would identify the actual kinetics order of oxidation. Furthermore, these reaction parameters extracted by the thin film kinetic model at varying pressures would be better suited to describing the oxidation behavior in permeation experiments where oxygen pressure is varied.

The existing theories that describe the permeation and uptake behavior of reactive films of SBS block copolymer would need to be modified based on the identified order of the kinetics to more accurately describe the oxidation performance of scavengers in various complex structures – homogeneous, blend, and multi-layered systems. Although changing the reaction term in the current theoretical basis may require a non-linear kinetic solution that can complicate modeling, it may bring better and closer theoretical agreement to experimental measurement.

While most scavenging work has been done on blend systems [5–12], incorporating SBS oxygen scavengers in layered films through coextrusion [13], as shown in Figure 7.1, may greatly improve transient oxygen barrier properties while retaining the flexibility of packaging materials like polystyrene or PET. Recently an enabling technology has been made available at Case Western Reserve University, where a coextrusion process consisting of multiple extruders and multi-layering blocks is available to produce a system of up to 4,096 layers with each layer thickness less than 100 nm.

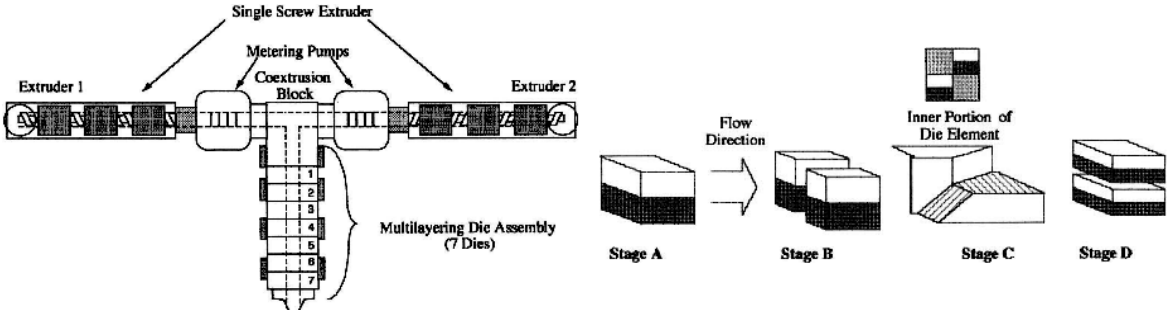

Figure 7.1: Reproduction of Figure 1.2. A coextruder with an assembly of layering dies can produce polymeric systems with multiple nano-scale layers [13].

Previously, it was demonstrated theoretically that multilayer films will outperform blends if the diffusion coefficient of the reactive polymer is smaller than that of the polymer matrix [14,15]. Therefore, it may be important to continue to use the same polystyrene matrix to standardize the film composition while producing a system of multilayers, in order to allow direct comparison of their oxidation performance with the reactive blends.

On the other hand, the polystyrene matrix used in these experiments is more permeable than Polyethylene terephthalate (PET), which is used in many packaging applications. Since the less-permeable PET is often the preferred packaging material when exceptional barrier properties are needed, it would be interesting to examine the oxidation performance of reactive blends having a PET matrix. Previously an effective Damköhler expression was developed to relate the time scales of diffusion and reaction for the reactive blend ($Da_b = \phi L^2/D_m \tau H$) [7]. For the case where scavenger loading, ϕ, film thickness, L, solubility partition coefficient H, and characteristic reaction time, τ, are fixed, the Damköhler number is greater when the matrix polymer has a lower oxygen diffusivity, D_m. Thus, the probability becomes greater for oxygen to react with the oxidative sites in the blend. As a result, reactive blends in a PET matrix would give a greater Da_b than those in a PS matrix by approximately a factor of 25; $D_m = 5.6 \times 10^{-9}\, cm^2/sec$ for PET [16] versus $1.4 \times 10^{-7}\, cm^2/sec$ for PS [5]. Thus, reactive PET blends would give greater time lag extension and possibly better early time scavenging than PS blends [6].

A different polymer – the oxidation capability of which is actively used in industry – can be considered for oxygen scavenging in future research. For instance, MXD-6 was incorporated as a sacrificial polymer between layers of PET [17] via the

aforementioned coextrusion process. Using cobalt as an oxidation catalyst, MXD-6 reacts with oxygen through a reactive mechanism and extends time lags that can reach hundreds of days with no detection of oxygen transmission. This activity indicates that MXD-6 can improve barrier properties of packaging material by extending time lags via an oxidative mechanism, similar to what has been demonstrated by the SBS block copolymer in this work.

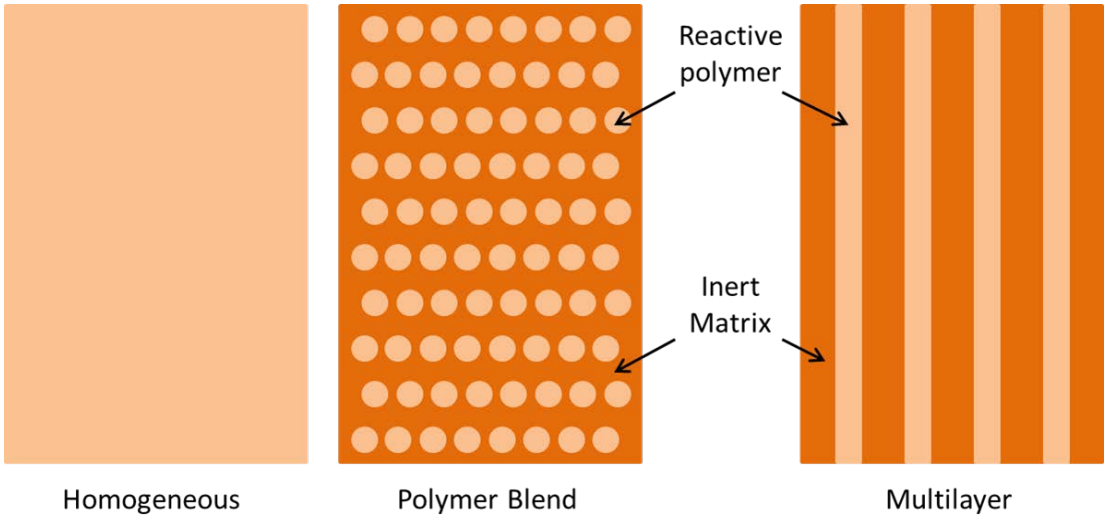

Figure 7.2: Ultimately, the oxygen scavenging performance of each system – homogeneous scavenger, reactive blends, and systems of multi-layers – should be compared and investigated.

The reactive phase morphology depends on the structures of the polymer system and has been shown to influence the oxidation performance of the blends. The reactive phase in the blends could have a spherical morphology, whereas the reactive phase in the layered system may have a morphology that closely resembles a cylindrical or lamellar phase, as illustrated in Figure 7.2. Therefore, it would be worthwhile to examine the

morphology effect of these structures, as well as of a multi-layered system where the reactive layer itself consists of the blends introduced in this work. In this structure, the reactive phase may appear to be spherical in a system of multiple layers of cylinders. Ultimately, their oxidation performance ought to be characterized via uptake and permeation experiments and compared with that of the blend film explored in this dissertation.

7.3 REFERENCES

[1] H. Li, D.K. Ashcraft, B.D. Freeman, M. Stewart, M.K. Jank, T.R. Clark, Non-invasive headspace measurement for characterizing oxygen-scavenging in polymers, Polymer. 49 (2008) 4541–4545.

[2] H. Li, K.K. Tung, D.R. Paul, B.D. Freeman, Effect of film thickness on auto-oxidation in cobalt-catalyzed 1,4-polybutadiene films, Polymer. 52 (2011) 2772–2783.

[3] H. Li, K.K. Tung, D.R. Paul, B.D. Freeman, M. Stewart, J. Jenkins, Characterization of Oxygen Scavenging Films Based on 1,4-Polybutadiene, Industrial & Engineering Chemistry Research. 51 (2012) 7138–7145.

[4] R.H. Li, Metal-catalyzed oxidation of polybutadiene in oxygen scavenging packaging application (Ph.D. Thesis), The University of Texas at Austin, 2010.

[5] K.K. Tung, R.T. Bonnecaze, B.D. Freeman, D.R. Paul, Characterization of the oxygen scavenging capacity and kinetics of SBS films, Polymer. 53 (2012) 4211–4221.

[6] M.C. Ferrari, S. Carranza, R.T. Bonnecaze, K.K. Tung, B.D. Freeman, D.R. Paul, Modeling of oxygen scavenging for improved barrier behavior: Blend films, Journal of Membrane Science. 329 (2009) 183–192.

[7] S. Carranza, D.R. Paul, R.T. Bonnecaze, Analytic formulae for the design of reactive polymer blend barrier materials, Journal of Membrane Science. 360 (2010) 1–8.

[8] P.J. Cahill, S.Y. Chen, Oxygen scavenging condensation copolymers for bottles and packaging articles, U.S. Patent US6083585 A, 2000.

[9] K. Katsumoto, T.Y. Ching, Multi-component Oxygen Scavenging Composition, U.S. Patent 5,776,361, 1998.

[10] D. V Speer, W.P. Roberts, C.R. Morgan, Methods and Compositions for Oxygen Scavenging, U.S. Patent US6449923 B1, 1993.

[11] M. Stewart, R.N. Estep, B.B. Gamble, M.D. Clifton, D.R. Quillen, L.S. Buehrig, et al., Blends of oxygen scavenging polyamides with polyesters which contain zinc and cobalt, U.S. Patent WO2006063032 A3, 2006.

[12] K. Katsumoto, T.Y. Ching, Goodrich, D. V Speer, Photoinitiators and oxygen scavenging composition, U.S. Patent 6,139,770, 2000.

[13] C.D. Mueller, S. Nazarenko, T. Ebeling, T.L. Schuman, A. Hiltner, E. Baer, Novel structures by microlayer coextrusion?talc-filled PP, PC/SAN, and HDPE/LLDPE, Polymer Engineering & Science. 37 (1997) 355–362.

[14] S. Carranza, D.R. Paul, R.T. Bonnecaze, Multilayer reactive barrier materials, Journal of Membrane Science. 399-400 (2012) 73–85.

[15] S. Carranza, Modeling of Oxygen Scavenging Polymers and Composites (Ph.D. Thesis), The University of Texas at Austin, 2010.

[16] A. Polyakova, R.Y.F. Liu, D.A. Schiraldi, A. Hiltner, E. Baer, Oxygen-barrier properties of copolymers based on ethylene terephthalate, Journal of Polymer Science Part B: Polymer Physics. 39 (2001) 1889–1899.

[17] M.A. Cochran, R. Folland, J.W. Nicholas, M. Edward, R. Robinson, Packaging, U.S. Patent 5,639,815, 1997.

Appendix: Error analysis on flux

A.1 UNPHYSICAL EARLY TIME FLUX BEHAVIOR

Transient flux can be determined by normalizing the slopes obtained from a permeation test, dQ_t/dt, from the Q_t plot versus time, as illustrated in Figure 6.7 (Chapter 6). Due to initial instrumental calibration and uncertainties that may cause data error, an error analysis is necessary to determine the portion of the data that can represent the actual physics. This is especially important when evaluating transient flux behavior of reactive blends described in this dissertation.

The following error analysis was performed on an example blend which was loaded with 6% PI in the PI content experiment. The pressure data that were used to determine Q_t and flux (Figure 6.4 and 6.5 in chapter 6) of this sample are shown here in Figure A.1.

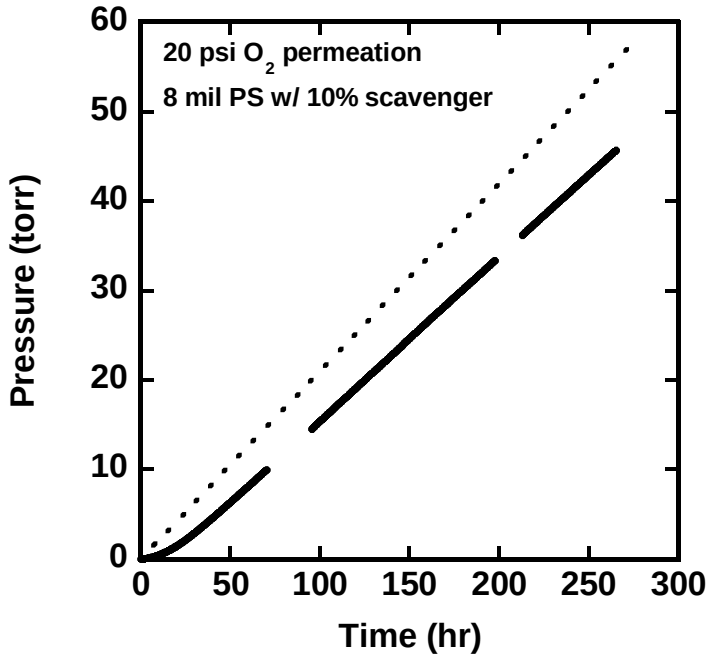

Figure A.1: The raw data of the sample loaded with 6% are used to calculate Q_t and flux.

The pressure time slope is determined as the ratio of the running forward average of pressure and time at a step size assigned to each data point. Table A.1 discloses the step size for each data point used in calculating slopes. For example, the pressure time slope at 10, 100, and 1000 seconds is determined by taking the ratio of the running forward average of pressure and time data in the following 40, 150, and 2000 seconds, respectively. An initial small step size can ensure higher accuracy in determining slopes at early times, where pressure data can be sensitive to instrumental instability and initial noise. If a greater step size was employed, then the calculation might not fully represent the actual slope value at early times.

Table A.1: The step size of pressure and time that is used in the running forward average to calculate slopes from the pressure time data.

Sec	hour	Step size (sec)		Sec	Hour	Step size (sec)	
0	0.0000	1 to 10	10	140	0.0389	140 to 350	210
1	0.0003	1 to 15	15	160	0.0444	160 to 400	240
2	0.0006	2 to 20	18	180	0.0500	180 to 500	320
4	0.0011	4 to 25	21	200	0.0556	200 to 600	400
6	0.0017	6 to 30	24	250	0.0694	250 to 700	450
8	0.0022	8 to 40	32	300	0.0833	300 to 800	500
10	0.0028	10 to 50	40	350	0.0972	350 to 1000	650
15	0.0042	15 to 60	45	400	0.1111	400 to 1250	850
20	0.0056	20 to 80	60	500	0.1389	500 to 1500	1000
25	0.0069	25 to 100	75	600	0.1667	600 to 1750	1150
30	0.0083	30 to 120	90	700	0.1944	700 to 2000	1300
40	0.0111	40 to 140	100	800	0.2222	800 to 2500	1700
50	0.0139	50 to 160	110	1000	0.2778	1000 to 3000	2000
60	0.0167	60 to 180	120	1250	0.3472	1250 to 3500	2250
80	0.0222	80 to 200	120	1500	0.4167	1500 to 4000	2500
100	0.0278	100 to 250	150	1750	0.4861	1750 to 5000	3250
120	0.0333	120 to 300	180	2000	0.5556	2000 to 6000	4000

The pressure time slope is determined from pressure data by the outlined method and shown in Figure A.2; this slope is simply proportional to the flux shown in Figure 6.5 in Chapter 6. A non-physical “hump” was found at early times prior to approximately 0.1 hour (6 minutes). This unexpected finding may be explained by the following analysis.

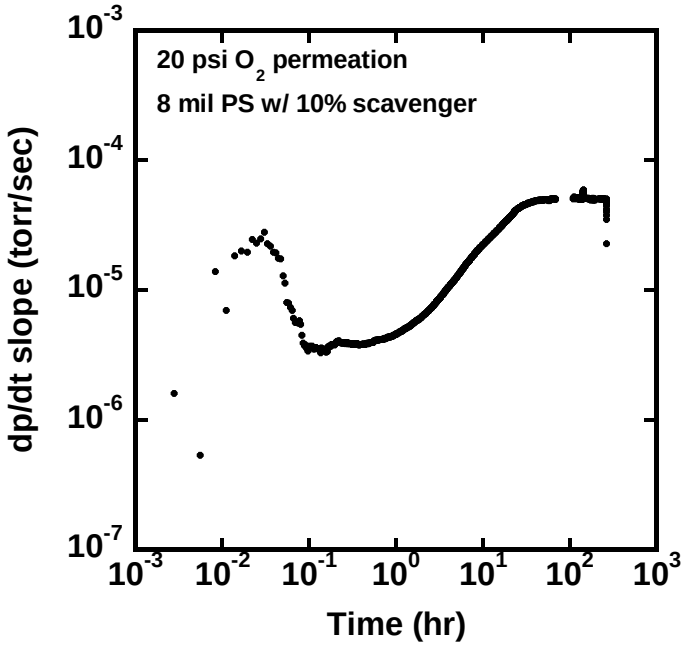

Figure A.2: The pressure time slope of the sample loaded with 6% is used to calculate Q_t and flux.

The pressure error, σ_p, of the MKS Monometer (627A11TBC) used in all permeation tests was assigned by the manufacturer as 0.15% of each measured pressure value, p

$$\sigma_p = 0.0015 * p \tag{A.1}$$

The time error, σ_t, by the instrument is assumed to be zero as the material (quartz) used to clock the permeation time, t, is used extensively and reliably. Figure A.3 illustrates that slope m of the first data point (p_1) is determined as the ratio of the running

average pressure difference p_2 and p_1 and the running average time difference $t_2$and t_1 at the step size Δt previously specified. Mathematically it means

$$m = \frac{\Delta p}{\Delta t} = \frac{p_2 - p_1}{t_2 - t_1} = \frac{p_2 - p_1}{\Delta t} = \frac{p_2}{\Delta t} - \frac{p_1}{\Delta t} \tag{A.2}$$

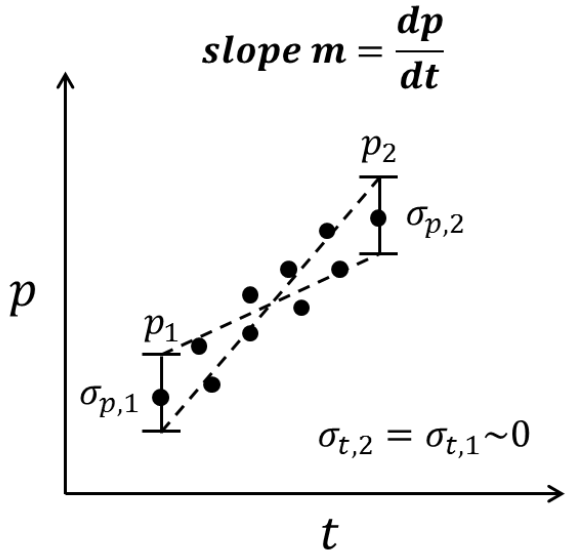

Figure A.3: Schematic illustration of determining the slope by taking the ratio of the running forward average of pressure and time data. The error associated with pressure and time is used to calculate the error in slope.

The slope of the line drawn through the data points can vary according to the error of the pressure and time data. A propagation analysis of error based on Equation A.2 is used to approximate the slope error, σ_m

$$\sigma_m = \sqrt{\frac{\sigma_{p_2}^2}{\Delta t^2} + \frac{\sigma_{p_1}^1}{\Delta t^2}} = \sqrt{2 * \frac{\sigma_p^2}{\Delta t^2}} \tag{A.3}$$

Since the pressure error specified by the manufacturer is 0.15% of each measured pressure value (Equation A.1), the slope error is simply

$$\sigma_m = \sqrt{2 * \frac{0.0015^2}{\Delta t^2}} = \frac{0.00212}{\Delta t} \quad \text{(A.4)}$$

As a result, the slope error is 0.212% of the inverse of the time size. For example, the error of a slope determined for a data point at 100th second is $1.41 \times 10^{-5} \frac{torr}{sec}$ with a step size $\Delta t = 150$. This procedure was used to determine the errors associated with all calculated slopes, which are shown in Figure A.4(a). In order to see how the error relates to the actual values, percent error was determined by taking the ratio of error and slope values. These values for percent error were plotted as a function of time and shown in Figure A.4(b).

In Figure A.4, error is quite large for early time data. A 20% line was drawn to separate those data with error higher than 20%, and those high-error data were neglected. Only pressure time slopes with less than 20% error were used to calculate the pressure time slope and flux, which are shown in Figure A.5. Thus the early time flux behavior was non-physical and was associated with error simply due to instrumental instability at early times.

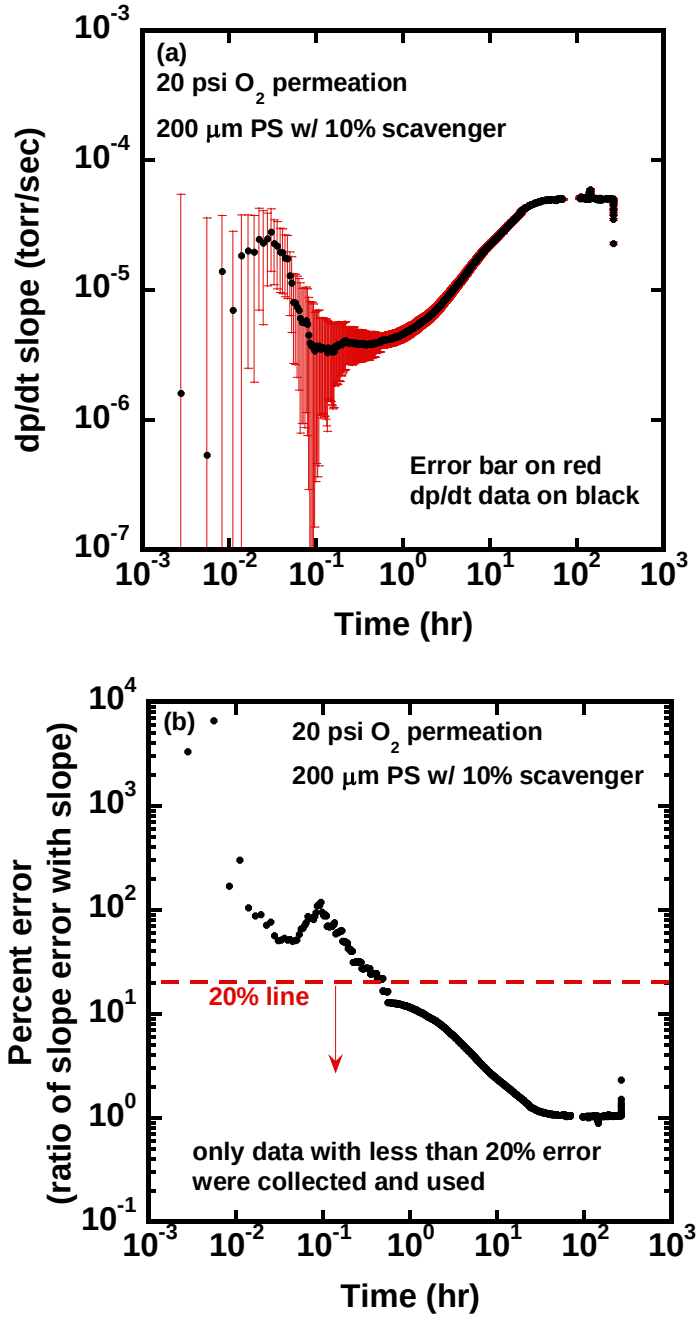

Figure A.4: (a) Slope errors were determined by propagation analysis for all slopes calculated and shown in red. The pressure time slope data are shown in black. (b) A line of "20% error" was drawn to separate the data with error greater than 20%.

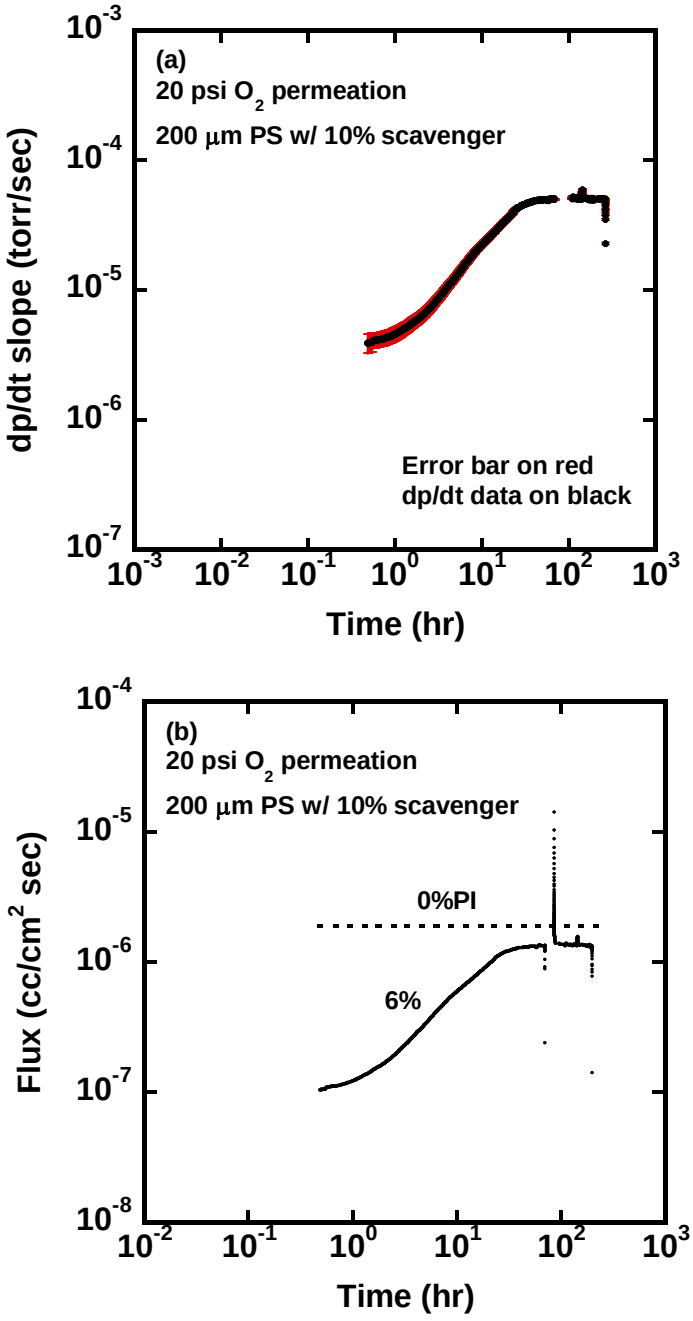

Figure A.5: (a) The pressure time slope with less than 20% error. (b) Flux calculated based on only the pressure time slopes with less than 20% error.

A.2 THE OSCILLATORY BEHAVIOR IN LOW PRESSURE PERMEATION EXPERIMENT

The procedure to calculate the transient flux of a low pressure permeation test at 3 psi as shown in Figure 6.14 in Chapter 6 requires a special note. The pressure data that was used to calculate the transient flux is shown in the following Figure A.6

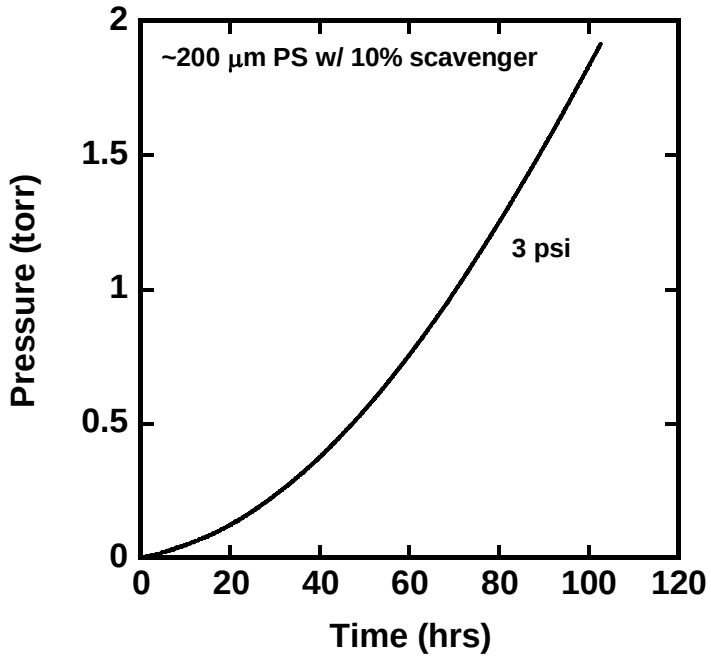

Figure A.6: The pressure data of a low permeation test at 3 psi is used to calculate Q_t and flux.

Following the outline method to calculate the pressure time slopes, the transient flux may be determined and an oscillation appeared but was not found in all other permeation tests, shown in Figure A.7. The oscillatory effect may be due to the very low pressure increase due to the low pressure nature of the experiment. All other experiments were done at pressure at least 20 psi and had shown no such oscillatory behavior at early time.

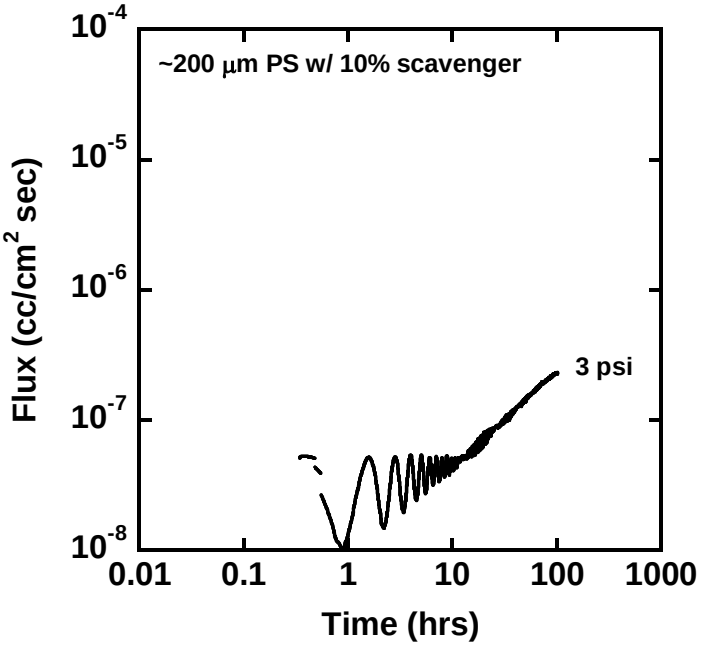

Figure A.7: Flux calculated from the pressure time slopes using procedure outlined earlier.

This non-physical behavior seems to begin to diminish at about 10 – 20 hours into the permeation. This prompted an examination of the raw pressure time data for the first 10 and 20 hours, which are shown in Figures A.8(a) and A.8(b), respectively.

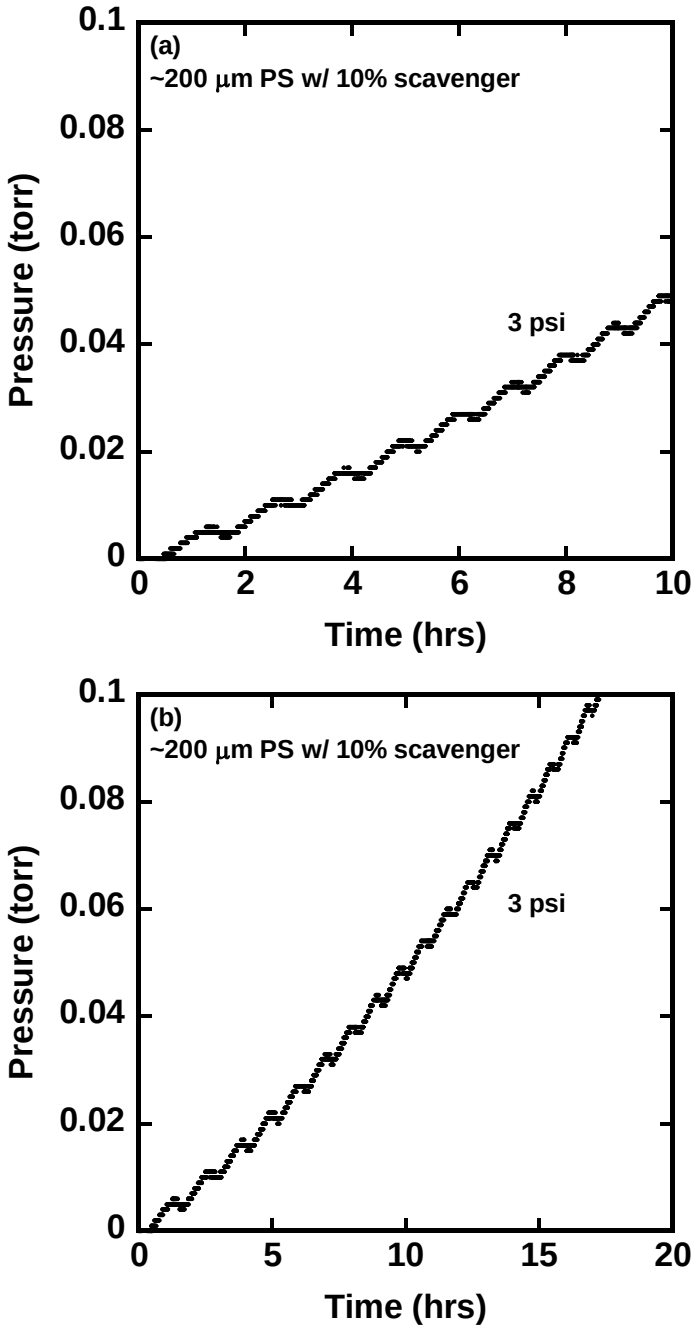

Figure A.8: The early pressure time data up to (a) 10 hours and (b) 20 hours.

The step function type of increase found in early time pressure measurement is simply due to a very low permeate that can barely be detected by the pressure transducer used in the laboratory. Due to the low pressure nature of the experiment, the low level of pressure rise is physical, but the lack of a pressure transducer with a resolution high enough cannot resolve the physical shape of low increase in pressure at early time. This will not be an issue if a steady state flux or permeability is the parameter of interest, as the experiment can simply be allowed to run longer to collect a large enough quantity of data for averaging at steady state. However, in current work where transient slope and flux are of interest, even the small pressure increase at early time is important and necessary to explain the flux behavior due to oxidation.

Since the low level of permeate increase is physical but the oscillatory effect continues to 20 hours or more, a simple second order polynomial regression fitting on the cumulate amount of permeate, Q_t, is done and shown in Figure A.9. The transient flux calculated based on the second order polynomial regression fit is shown in Figure A.10. The second order polynomial regression fitting through the center of the oscillatory region, suggestive of an excellent regression which can be used to represent the actual physical behavior.

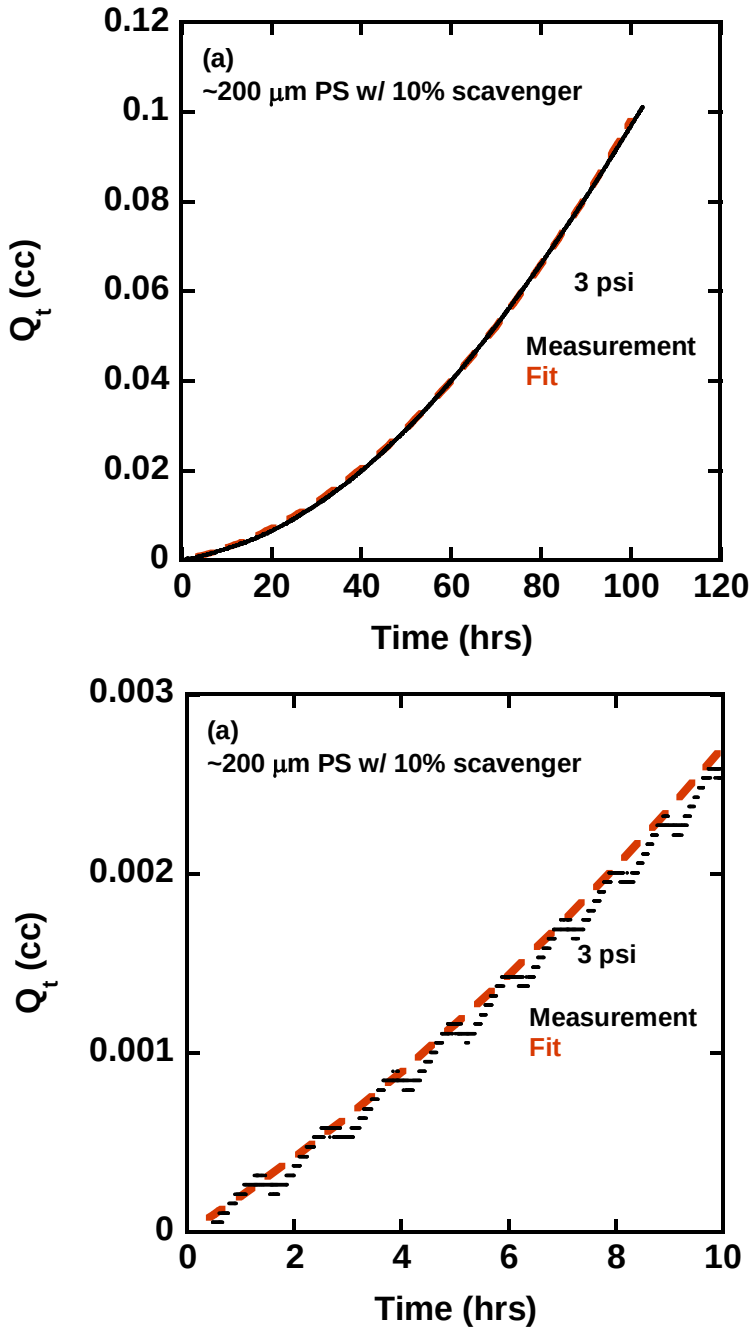

Figure A.9: A second order polynomial regression fitting was done to fit the step size increase in (a) the full measurement and (b) first 10 hour of measurement.

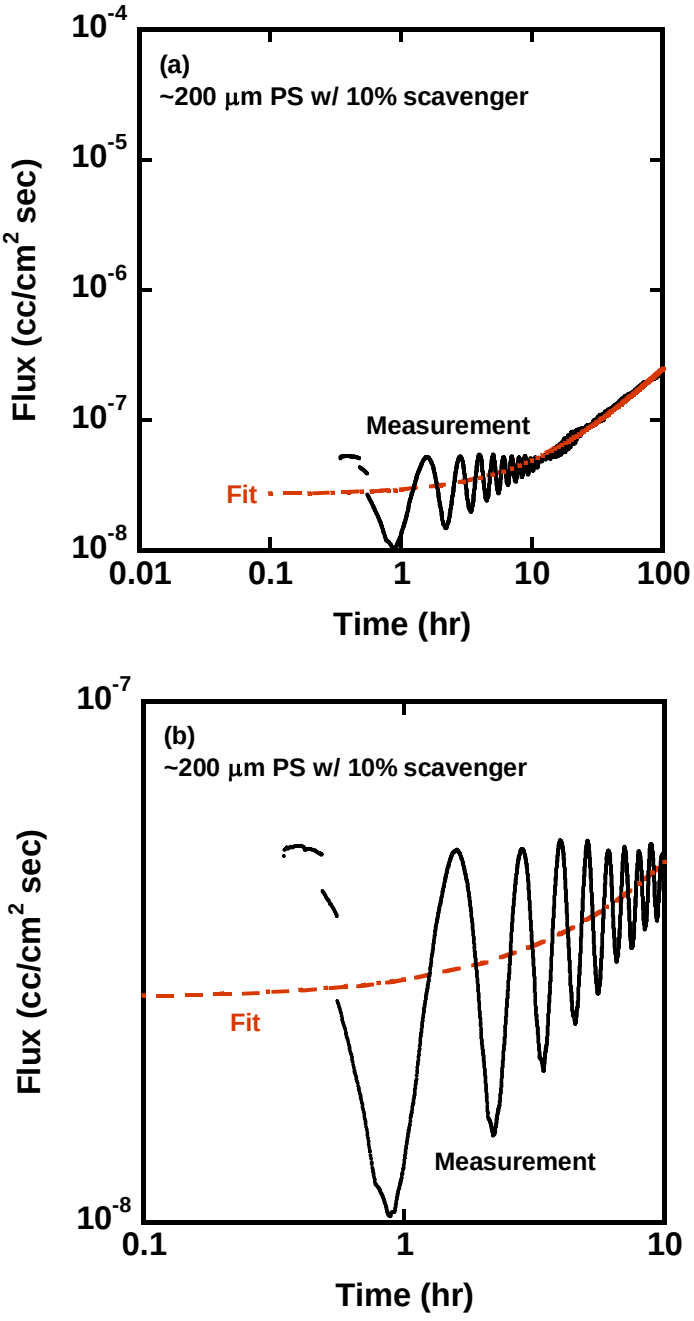

Figure A.10: The transient flux behavior calculated based on the second order polynomial fit shown earlier for (a) the entire measurement and (b) the first 10 hours of measurement.

As a result, the transient flux of this low pressure permeation test at 3 psi is approximated by a second order polynomial fitting, shown in Figure 6.14 in Chapter 6. Figure 6.14(b) that shows the dimensionless flux is reproduced for viewing convenience. On the other hand, the cumulate amount of permeate, shown in Figure 6.13(b), is plotted using the actual experimental data.

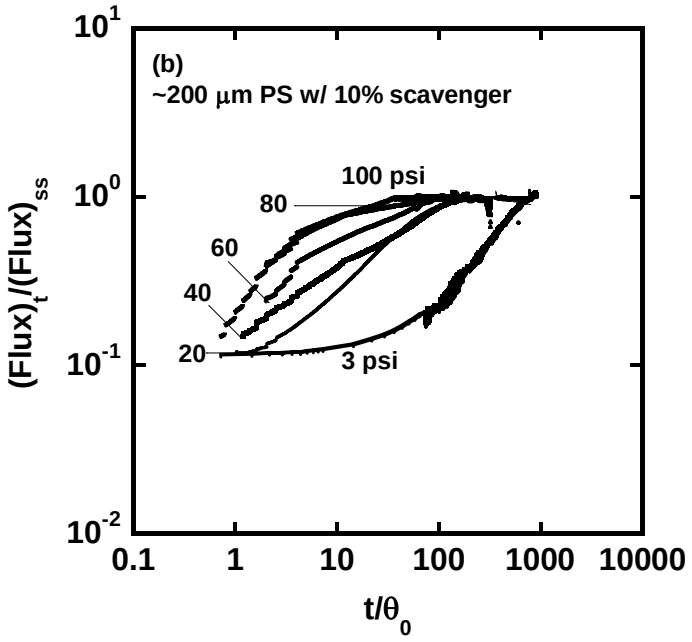

Figure A.11: Reproduction of Figure 6.14 (b). Normalized flux plots as a function of pressure. The blend film sample that was exposed to 3 psi O_2 showed the longest plateau before it rose to the steady state value

A.3 EFFECT OF SCAVENGER LOADING ON PERMEATION BEHAVIORS OF REACTIVE BLEND FILMS AT LOW PRESSURE

Another polystyrene film with 20% SBS scavenger was melt-extruded to form a reactive blend of approximately 200 μm in thickness. This particular film was subjected

to a permeation test at 3 psi. The data of pressure and cumulative amount of permeate, Q_t, of polystyrene blends with 0, 10, and 20% SBS scavengers are shown in Figure A.12. Note that Q_t and pressure data of reactive blend with 10% SBS scavenger is shown in this Chapter 6 and Appendix, respectively.

In these tests, pressure and Q_t data of all samples increase with time while the blend with the highest SBS scavenger at 20% has the lowest pressure and $Q_t$values more than 10 days of permeation test. Moreover, the pressure and Q_t data of the blend at 20% were found to be approximately 5 times smaller than those of the polystyrene blend with 10% scavenger. The pressure time slope of the blend with 20% scavenger is determined to be approximately $7 - 9 \times 10^{-7}\ torr/sec$, which is very close to the system leak rate. This suggests that, by the detection limit of the permeation instrument, almost all the oxygen that seeks to permeate through the membrane is immobilized at the reactive sites via a reactive mechanism. The flux that is being measured is the flux due to the system leak rate.

Expectedly, time lag is beyond measurement up to this permeation period. The pressure and Q_t values of this test at some point will increase when the reactive sites are consumed and eventually reach steady state flux and permeability values of fully oxidized blends of 20% SBS scavenger. Ultimately, the polystyrene blend with 20% scavenger has shown an outstanding reactive barrier property at atmospheric pressure even at times longer than 10 days of being subjected to permeation application.

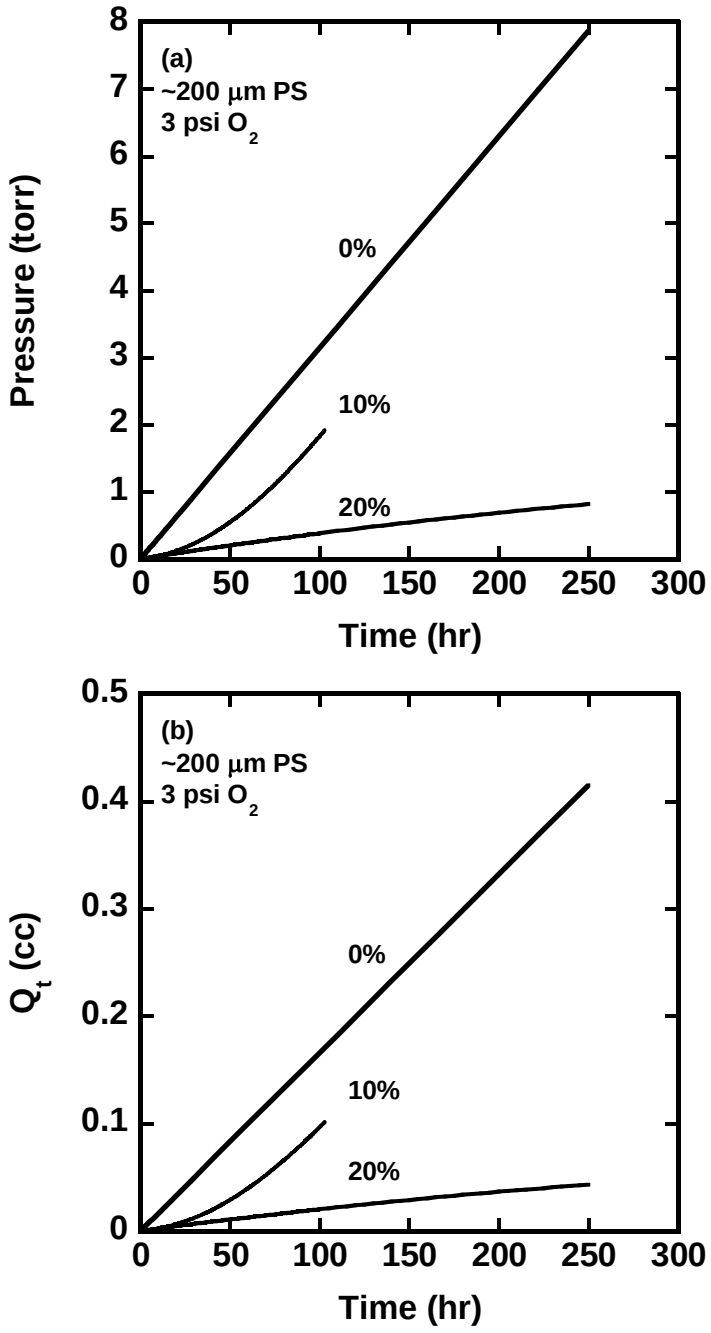

Figure A.12: The (a) pressure and (b) Q_t values of reactive PS blends ~ 200 μm increase with time but decrease with scavenger loading. These permeation tests were done at a low pressure of 3 psi.

A.4 SUMMARIES

This exercise takes the accuracy of the manometer, i.e., 0.15%, as specified by the manufacturer (MKS), and determines the slope error from the pressure time data throughout a permeation test. This provides a conservative estimate in slope error. The slope is taken as the ratio of the forward running averages of pressure time data at a specified step size for each data point. The error propagation analysis shows that the slope error is inversely related with the time step size. This analysis was applied to identify error of all calculated slopes.

A standard “20% error line” was drawn on the percent error plot to exclude slope values with errors greater than 20%, and only those slopes with less than 20% error were used to calculate the transient flux. The large error may be due to the instrumental instability at early times. In this dissertation, this method was applied to calculate fluxes of reactive blends, which begins low then increases due to diminishing oxidation activity, and approaches steady state suggesting an exhaustion of the reactive sites.

In a special case of a low pressure experiment at 3 psi an oscillation was found in the first 10 – 20 hours of the test. This was because of the incremental pressure increase at early times that was detected by the pressure transducer as a small step-function increase, which forms the oscillatory behavior seen. While the small pressure increase is physical due to the low pressure nature of the experiment, the oscillation is not and was resolved by fitting a second order polynomial regression. The polynomial regression fits through the center of the oscillatory flux and is believed to represent the actual physics. Moreover, another reactive PS blend with 20% SBS scavenger was subjected to a low pressure permeation experiment at 3 psi. The fact that the pressure time slope was found

to be close to the system leak rate suggests that almost all oxygen is consumed at the reactive sites and no flux is measured by the detection limit. Consequently, the time lag is beyond measurement, and this particular blend with 20% scavenge has an outstanding reactive barrier property measured by permeation experiment.

In this dissertation, this method was applied to calculate fluxes of reactive blend. Any non-physical behavior was examined. All fluxes shown in this dissertation were calculated from pressure time slopes with less than 20% error, except for the low pressure permeation test at 3 psi, where an oscillation was found but resolved by fitting a second order polynomial regression.

Bibliography

Adam, C, Lacoste, J., & Lemaire, J. (1989). Photo-oxidation of elastomeric materials. 1. Photooxidation of polybutadienes. *Polymer Degradation and Stability*, *24*, 185–200. doi:10.1016/0141-3910(89)90091-8

Adam, Claudie, Lacoste, J., & Lemaire, J. (1989). Photo-oxidation of elastomeric materials: Part II—Photo-oxidation of styrene-butadiene copolymer. *Polymer Degradation and Stability*, *26*(3), 269–284. doi:10.1016/0141-3910(89)90079-7

Adam, Claudie, Lacoste, J., & Lemaire, J. (1990). Photo-oxidation of elastomeric materials: Part IV—Photo-oxidation of 1,2-polybutadiene. *Polymer Degradation and Stability*, *29*(3), 305–320. doi:10.1016/0141-3910(90)90042-6

Andrade, G. S., Collard, D. M., Schiraldi, D. A., Hu, Y., Baer, E., & Hiltner, A. (2003). Oxygen barrier properties of PET copolymers containing bis(2-hydroxyethyl)hydroquinones. *Journal of Applied Polymer Science*, *89*(4), 934–942. doi:10.1002/app.12144

Andrews, E. H. (1964). Crystalline Morphology in Thin Films of Natural Rubber. II. Crystallization Under Strain. *Proceedings of the Royal Society A: Mathematical, Physical and Engineering Sciences*, *277*(1371), 562–570. doi:10.1098/rspa.1964.0040

Areerat, S., Funami, E., Hayata, Y., Nakagawa, D., & Ohshima, M. (2004). Measurement and prediction of diffusion coefficients of supercritical CO2 in molten polymers. *Polymer Engineering and Science*, *44*(10), 1915–1924. doi:10.1002/pen.20194

Audouin, L., Langlois, V., Verdu, J., & Bruijn, J. C. M. (1994). Role of oxygen diffusion in polymer ageing: kinetic and mechanical aspects. *Journal of Materials Science*, *29*(3), 569–583. doi:10.1007/BF00445968

Bauman, R. G., & Maron, S. H. (1956). Oxidation of Polybutadiene. I. Rate of Oxidation. *Journal of Polymer Science*, *22*, 1–12.

Beavan, S. W., & Phillips, D. (1974). Mechanistic Studies on the Photooxidation of Commercial Polybutadiene. *European Polymer Journal*, *10*(7), 593–603.

Betts, A. T., & Uri, N. (1966). The conversion of metal catalysts into inhibitors of autoxidation. *Die Makromolekulare Chemie*, *95*(1), 22–39.

Betts, A. T., & Uri, N. (1968). Catalyst-Inhibitor Conversion in Autoxidation Reactions. In F. R. Mayo (Ed.), *Oxidation of Organic Compounds* (Vol. 76, pp. 160–181). WASHINGTON, D.C.: AMERICAN CHEMICAL SOCIETY. doi:10.1021/ba-1968-0076

Bigger, S. W., & Delatycki, O. (1987). New approach to the measurement of polymer photooxidation. *Journal of Polymer Science, Part A: Polymer Chemistry*, *25*(12), 3311–3323.

Blinka, T. A., Edwards, F. B., Miranda, N. R., Speer, D. V, & Thomas, J. A. (1998). Zeolite in Packaging Film. United States: W. R. Grace and Company.

Cahill, P. J., & Chen, S. Y. (2000). Oxygen scavenging condensation copolymers for bottles and packaging articles. United States: BP Amoco Corporation.

Carberry, J. J. (2001). *Chemical and Catalytic Reaction Engineering* (p. 672). Dover Publication.

Carranza, S. (2010). *Modeling of Oxygen Scavenging Polymers and Composites (Ph.D. Thesis)*. The University of Texas at Austin.

Carranza, S., Paul, D. R., & Bonnecaze, R. T. (2010a). Design formulae for reactive barrier membranes. *Chemical Engineering Science*, *65*(3), 1151–1158. doi:10.1016/j.ces.2009.09.070

Carranza, S., Paul, D. R., & Bonnecaze, R. T. (2010b). Analytic formulae for the design of reactive polymer blend barrier materials. *Journal of Membrane Science*, *360*(1-2), 1–8. doi:10.1016/j.memsci.2010.04.029

Carranza, S., Paul, D. R., & Bonnecaze, R. T. (2012). Multilayer reactive barrier materials. *Journal of Membrane Science*, *399-400*, 73–85. doi:10.1016/j.memsci.2012.01.030

Celina, M. C., Clough, R. L., & Jones, G. D. (2007). Interactive Behavior in Polymer Degradation. In M. C. Celina & R. A. Assink (Eds.), *Polymer Durability and Radiation Effects* (Vol. 978, pp. 37–47). Washington, DC: American Chemical Society. doi:10.1021/bk-2007-0978.ch004

Clough, R. L., & Gillen, K. T. (1992). Oxygen diffusion effects in thermally aged elastomers. *Polymer Degradation and Stability*, *38*(1), 47–56. doi:10.1016/0141-3910(92)90022-W

Cochran, M. A., Folland, R., Nicholas, J. W., Edward, M., & Robinson, R. (1997). Packaging, U.S. Patent 5,639,815. *United States Patent*. United States: CarnaudMetalbox plc.

Cochran, M. A., Folland, R., Nicholas, J. W., & Robinson, R. (1991). Packaging, U.S. Patent 5,021,515. *United States Patent*. United States: CarnaudMetalbox plc.

Coles, R., & Kirwan, M. J. (2011). *Food and Beverage Packaging Technology* (2nd ed., p. 344). John Wiley & Sons, Ltd.

Coquillat, M., Verdu, J., Colin, X., Audouin, L., & Nevière, R. (2007a). Thermal oxidation of polybutadiene. Part 1: Effect of temperature, oxygen pressure and sample thickness on the thermal oxidation of hydroxyl-terminated polybutadiene. *Polymer Degradation and Stability*, *92*(7), 1326–1333. doi:10.1016/j.polymdegradstab.2007.03.020

Coquillat, M., Verdu, J., Colin, X., Audouin, L., & Nevière, R. (2007b). Thermal oxidation of polybutadiene. Part 2: Mechanistic and kinetic schemes for additive-free non-crosslinked polybutadiene. *Polymer Degradation and Stability*, *92*(7), 1334–1342. doi:10.1016/j.polymdegradstab.2007.03.019

Coquillat, M., Verdu, J., Colin, X., Audouin, L., & Nevière, R. (2007c). Thermal oxidation of polybutadiene. Part 3: Molar mass changes of additive-free non-crosslinked polybutadiene. *Polymer Degradation and Stability*, *92*(7), 1343–1349. doi:10.1016/j.polymdegradstab.2007.03.018

Crank, J. (1975). *The Mathematics of Diffusion* (2nd ed.). Oxford: Oxford University Press.

Daynes, H. A. (1928). The Permeability of Rubber and Methods of Testing It. *Transactions, Institution of the Rubber Industry*, *3*, 428–453.

Dhoot, S. N., Freeman, B. D., & Stewart, M. (2003). Barrier Polymers. In J. I. Kroschwitz (Ed.), *Encyclopedia of Polymer Science and Technology* (3rd ed., Vol. 5, pp. 193–263). New York: Wiley-Interscience.

Erekson, E. J., Sughrue, E. L., & Bartholomew, C. H. (1981). Catalyst degradation in high temperature methanation. *Fuel Processing Technology*, *5*(1-2), 91–101. doi:10.1016/0378-3820(81)90023-0

Ferrari, M. C., Carranza, S., Bonnecaze, R. T., Tung, K. K., Freeman, B. D., & Paul, D. R. (2009). Modeling of oxygen scavenging for improved barrier behavior: Blend

films. *Journal of Membrane Science*, *329*(1-2), 183–192. doi:10.1016/j.memsci.2008.12.030

Finger, K. F., Lemberger, A. P., Higuchi, T., Busse, L. W., & Wurster, D. E. (2006). Investigation and development of protective ointments IV. The influence of active fillers on the permeability of semisolids. *Journal of the American Pharmaceutical Association*, *49*(9), 569–573. doi:10.1002/jps.3030490903

Ghosal, K., & Freeman, B. D. (1994). Gas separation using polymer membranes: an overview. *Polymers for Advanced Technologies*, *5*(11), 673–697. doi:10.1002/pat.1994.220051102

Gillen, K. T., & Clough, R. L. (1992). Rigorous experimental confirmation of a theoretical model for diffusion-limited oxidation. *Polymer*, *33*(20), 4358–4365. doi:10.1016/0032-3861(92)90280-A

Graham, T. (1866). On the absorption and dialytic separation of gases by colloid septa. *Philosophical Magazine and Journal of Science*, *32*, 401–420.

Haynes, W. M. (Ed.). (2012). *CRC Handbook of Chemistry and Physics, 93rd Edition* (93rd ed., p. 2664). CRC Press.

HUANG, Y., & Paul, D. R. (2004). Experimental methods for tracking physical aging of thin glassy polymer films by gas permeation. *Journal of Membrane Science*, *244*(1-2), 167–178. doi:10.1016/j.memsci.2004.06.058

Huang, Y., & Paul, D. R. (2004). Physical aging of thin glassy polymer films monitored by gas permeability. *Polymer*, *45*(25), 8377–8393. doi:10.1016/j.polymer.2004.10.019

Kamiya, Y., & Ingold, K. U. (1964). THE METAL-CATALYZED AUTOXIDATION OF TETRALIN: III. CATALYSIS BY MANGANESE, COPPER, NICKEL, AND IRON. *Canadian Journal of Chemistry*, *42*(5), 1027–1043. doi:10.1139/v64-159

Kamiya, Y., & Niki, E. (1978). Oxidative Degradation. In *Aspects of Degradation and Stabilization of Polymers, Vol. 3* (pp. 79–148). Amsterdam: Elsevier Scientific Publishing Company.

Kato, K. (1967). The osmium tetroxide procedure for light and electron microscopy of ABS plastics. *Polymer Engineering and Science*, *7*(1), 38–39. doi:10.1002/pen.760070110

Katsumoto, K., & Ching, T. Y. (1998). Multi-component Oxygen Scavenging Composition, U.S. Patent 5,776,361. United States: Chevron Chemical Company.

Katsumoto, K., Ching, T. Y., Goodrich, & Speer, D. V. (2000). Photoinitiators and oxygen scavenging composition, U.S. Patent 6,139,770. United States: Chevron Chemical Company.

Kim, J., Kim, P., & Lee, H. (1997). Syntheses and gas-transport properties of alkylsilane-modified SBS membranes. *Journal of Applied Polymer Science*, *66*(6), 1117–1122. doi:10.1002/(SICI)1097-4628(19971107)66:6<1117::AID-APP12>3.0.CO;2-Z

Koros, W J. (1990). *Barrier Polymers and Structures: Overview in Barrier Polymers and Structures*. (W J Koros, Ed.)*ACS Symposium Series* (Vol. 423, pp. 1–21). Washington, D. C.: American Chemical Society.

Koros, W. J., & Paul, D. R. (1976). Design considerations for measurement of gas sorption in polymers by pressure decay. *Journal of Polymer Science: Polymer Physics Edition*, *14*(10), 1903–1907. doi:10.1002/pol.1976.180141014

Kwei, T. K. (1993). Introduction to physical polymer science, second edition, by L. H. Sperling, Wiley, New York, 1992, 594 pp. *Journal of Polymer Science Part A: Polymer Chemistry*, *31*(4), 1097–1097. doi:10.1002/pola.1993.080310435

Lape, N. K., Yang, C., & Cussler, E. L. (2002). Flake-filled reactive membranes. *Journal of Membrane Science*, *209*(1), 271–282. doi:10.1016/S0376-7388(02)00354-X

Lee, T., Yao, N., & Aksay, I. A. (1997). Nanoscale Patterning of Barium Titanate on Block Copolymers. *Langmuir*, *13*(14), 3866–3870. doi:10.1021/la960774m

Lee, W. M. (1980). Selection of barrier materials from molecular structure. *Polymer Engineering and Science*, *20*(1), 65–69. doi:10.1002/pen.760200111

Levine, I. N. (2001). Integration of Rate Laws. In *Physical Chemistry* (5th ed., pp. 533–539). New York: McGraw-Hill Higher Education.

Li, H., Ashcraft, D. K., Freeman, B. D., Stewart, M., Jank, M. K., & Clark, T. R. (2008). Non-invasive headspace measurement for characterizing oxygen-scavenging in polymers. *Polymer*, *49*(21), 4541–4545. doi:10.1016/j.polymer.2008.07.061

Li, H., Tung, K. K., Paul, D. R., & Freeman, B. D. (2011). Effect of film thickness on auto-oxidation in cobalt-catalyzed 1,4-polybutadiene films. *Polymer*, *52*(13), 2772–2783. doi:10.1016/j.polymer.2011.04.019

Li, H., Tung, K. K., Paul, D. R., Freeman, B. D., Stewart, M., & Jenkins, J. (2012). Characterization of Oxygen Scavenging Films Based on 1,4-Polybutadiene. *Industrial & Engineering Chemistry Research*, *51*(21), 7138–7145. doi:10.1021/ie201905j

Li, R. H. (2010). *Metal-catalyzed oxidation of polybutadiene in oxygen scavenging packaging application (Ph.D. Thesis)*. The University of Texas at Austin.

Liesl K. Massey. (2003). *Permeability Properties of Plastics and Elastomers - A Guide to Packaging and Barrier Materials*. (Liesl K. Massey, Ed.) (2nd ed., pp. 308, 444). William Andrew Publishing/Plastics Design Library.

Lissi, E. A., & Encinas, M. V. (1991). Photoinitiators for Free Radical Polymerization . In J. F. Rabek (Ed.), *Photochemistry and Photophysics* (Vol. 4). Boca Raton: CRC Press.

Lloyd M. Robeson, Allen Noshay, Markus Matzner, C. N. M. (1973). Physical property characteristics of polysulfone/poly-(dimethylsiloxane) block copolymers. *Die Angewandte Makromolekulare Chemie*, *29*(1), 47–62. doi:10.1002/apmc.1973.050290103

Maxwell, J. C. (1873). *A Treatise on Electricity and Magnetism* (p. 424). Clarendon Press.

Morris, J. N., Reich, L., & Stivala, S. (1972). *Elements of Polymer Degradation*. *AIChE Journal* (Vol. 18, pp. 462–463). New York: McGraw-Hill Book Company. doi:10.1002/aic.690180242

Mueller, C. D., Nazarenko, S., Ebeling, T., Schuman, T. L., Hiltner, A., & Baer, E. (1997). Novel structures by microlayer coextrusion?talc-filled PP, PC/SAN, and HDPE/LLDPE. *Polymer Engineering & Science*, *37*(2), 355–362. doi:10.1002/pen.11678

Nagle, D. J., Celina, M., Rintoul, L., & Fredericks, P. M. (2007). Infrared microspectroscopic study of the thermo-oxidative degradation of hydroxy-terminated polybutadiene/isophorone diisocyanate polyurethane rubber. *Polymer Degradation and Stability*, *92*(8), 1446–1454. doi:10.1016/j.polymdegradstab.2007.05.010

Nuxoll, E. E., & Cussler, E. L. (2005). The third parameter in reactive barrier films. *AIChE Journal*, *51*(2), 456–463. doi:10.1002/aic.10316

Nuxoll, E. E., Siegel, R. A., & Cussler, E. L. (2005). Layered reactive barrier films. *Journal of Membrane Science*, *252*(1-2), 29–36. doi:10.1016/j.memsci.2004.06.063

Paul, D. R., & Bucknall, C. B. (2000). *Polymer Blends: Formulation and Performance*. Wiley-Interscience.

Paul, D.R. (1969). Effect of immobilizing adsorption on the diffusion time lag. *Journal of Polymer Science Part A-2: Polymer Physics*, *7*(10), 1811–1818. doi:10.1002/pol.1969.160071015

Paul, D.R., & Kemp, D. R. (2007). The diffusion time lag in polymer membranes containing adsorptive fillers. *Journal of Polymer Science: Polymer Symposia*, *41*(1), 79–93. doi:10.1002/polc.5070410109

Paul, D.R., & Koros, W. J. (1976). Effect of partially immobilizing sorption on permeability and the diffusion time lag. *Journal of Polymer Science: Polymer Physics Edition*, *14*(4), 675–685. doi:10.1002/pol.1976.180140409

Paul, Donald R. (2010). Fundamentals of Transport Phenomena in Polymer Membranes. In Enrico Drioli & Lidietta Giorno (Ed.), *Comprehensive Membrane Science and Engineering* (1st ed., pp. 75–90). Elsevier B.V.

Petroupoulos, J. H. (1994). *Mechanisms and Theories for Sorption and Diffusion of Gases in Polymers*. (D R Paul & Y. P. Yampol'skii, Eds.)*Polymeric Gas Separation Membranes*. CRC Press.

Piton, M., & Rivaton, A. (1996). Photooxidation of polybutadiene at long wavelengths (λ > 300 nm). *Polymer Degradation and Stability*, *53*(3), 343–359. doi:10.1016/0141-3910(96)00093-6

Piton, M., & Rivaton, A. (1997). Photo-oxidation of ABS at long wavelengths (λ > 300 nm). *Polymer Degradation and Stability*, *55*(2), 147–157. doi:10.1016/S0141-3910(96)00116-4

Polyakova, A., Liu, R. Y. F., Schiraldi, D. A., Hiltner, A., & Baer, E. (2001). Oxygen-barrier properties of copolymers based on ethylene terephthalate. *Journal of Polymer Science Part B: Polymer Physics*, *39*(16), 1889–1899. doi:10.1002/polb.1163

Riess, G., Hurtrez, G., & Bahadur, P. (1985). Block Copolymers. In H. F. Mark, N. M. Bikales, O. C.G., & G. Menges (Eds.), *Encyclopedia of Polymer Science and Technology, Vol. 2* (p. 324). New York: John Wiley & Sons, Ltd.

Rincon-Rubio, L. M., Fayolle, B., Audouin, L., & Verdu, J. (2001). A general solution of the closed-loop kinetic scheme for the thermal oxidation of polypropylene. *Polymer Degradation and Stability*, *74*(1), 177–188. doi:10.1016/S0141-3910(01)00154-9

Robeson, L. M. (2010). Polymer Blends in Membrane Transport Processes. *Industrial & Engineering Chemistry Research*, *49*(23), 11859–11865. doi:10.1021/ie100153q

Sheldon, R. A., & Kochi, J. K. (1981). Metal Catalysis in Peroxide Reactions. In *Metal-catalyzed oxidation of organic compounds* (pp. 38–48). New York: Academic press.

Shimotori, T., Cussler, E. L., & Arnold, W. A. (2007). Diffusion of mobile products in reactive barrier membranes. *Journal of Membrane Science*, *291*(1-2), 111–119. doi:10.1016/j.memsci.2006.12.043

Siegel, R. A., & Cussler, E. L. (2004). Reactive barrier membranes: some theoretical observations regarding the time lag and breakthrough curves. *Journal of Membrane Science*, *229*(1-2), 33–41. doi:10.1016/j.memsci.2003.10.013

Song, K. W., Ka, K. R., & Kim, C. K. (2010). Changes in Gas-Transport Properties with the Phase Structure of Blends Containing Styrene−Butadiene−Styrene Triblock Copolymer and Poly(2,6-dimethyl-1,4-phenylene oxide). *Industrial & Engineering Chemistry Research*, *49*(14), 6587–6592. doi:10.1021/ie100565q

Speer, D. V, Roberts, W. P., & Morgan, C. R. (1993). Methods and Compositions for Oxygen Scavenging. United States: W.R. Grace and Company.

Speer, D. V, Roberts, W. P., Morgan, C. R., & VanPutte, A. W. (1996). Multilayer structure for a package for scavenging oxygen. United States: W.R. Grace and Company.

Stewart, M., Estep, R. N., Gamble, B. B., Clifton, M. D., Quillen, D. R., Buehrig, L. S., … Dauzvardis, M. J. (2006). Blends of oxygen scavenging polyamides with polyesters which contain zinc and cobalt. United States: Constar International Inc., Eastman Chemical Company.

Tung, K. K., Bonnecaze, R. T., Freeman, B. D., & Paul, D. R. (2012). Characterization of the oxygen scavenging capacity and kinetics of SBS films. *Polymer*, *53*(19), 4211–4221. doi:10.1016/j.polymer.2012.07.028

Van Amerongen, G. J. (1950). Influence of structure of elastomers on their permeability to gases. *Journal of Polymer Science*, *5*(3), 307–332. doi:10.1002/pol.1950.120050304

Van Krevelen, D. W. (2003). *Properties of Polymers, 3rd Edition Their Correlation with chemical Structure; their Numerical Estimation and Prediction from Additive Group Contributions*. Amsterdam: Elsevier Science.

Villetti, M. A., Crespo, J. S., Soldi, M. S., Pires, A. T. N., Borsali, R., & Soldi, V. (2002). Thermal Degradation of Natural Polymers. *Journal of Thermal Analysis and Calorimetry*, *67*(2), 295–303.

Walsh, D., & Zoller, P. (1995). *Standard Pressure Volume Temperature Data for Polymers*. (1st, Ed.) (p. 412). CRC Press.

Wijmans, J. G., & Baker, R. W. (1995). The solution-diffusion model: a review. *Journal of Membrane Science*, *107*(1-2), 1–21. doi:10.1016/0376-7388(95)00102-I

Wise, J., Gillen, K. T., & Clough, R. L. (1997). Quantitative model for the time development of diffusion-limited oxidation profiles. *Polymer*, *38*(8), 1929–1944. doi:10.1016/S0032-3861(96)00716-1

Yampolskii, Y., Pinnau, I., & Freeman, B. (2006). *Materials Science of Membranes for Gas and Vapor Separation*. (Y. Yampolskii, I. Pinnau, & B. Freeman, Eds.). Chichester, UK: John Wiley & Sons, Ltd. doi:10.1002/047002903X

Yang, C., & Cussler, E. L. (2001). Oxygen barriers that use free radical chemistry. *AIChE Journal*, *47*(12), 2725–2732. doi:10.1002/aic.690471212

Yang, C., Nuxoll, E. E., & Cussler, E. L. (2001). Reactive barrier films. *AIChE Journal*, *47*(2), 295–302. doi:10.1002/aic.690470208

Vita

Kevin “Kai Hao” Tung was born in Kaohsiung, Taiwan in 1983. He spent his childhood playing basketball before immigrating to Minnesota in 1998, where he graduated from Roseville Area High School in 2001. Afterwards, Kevin attended University of Minnesota – Twin Cities, where he finished in 2006 with the degrees of Bachelor of Science in Chemistry and Bachelor of Chemical Engineering (*cum laude*). As a Goldwater Scholar and a Pfizer Summer Research Fellow, Kevin participated in the Undergraduate Research Opportunity Program multiple times under the guidance of Profs. Richard P. Hsung and Wei-Shou Hu. Throughout his undergraduate studies, Kevin also worked as a science and engineering tutor for the Institute of Technology, as a technical aide at 3M Company in 2002, and as a graduate intern at General Mills in the summer of 2006. Upon the completion of his undergraduate studies, Kevin entered The University of Texas at Austin to begin doctoral studies in Chemical Engineering under the direction of Profs. Donald R. Paul and Benny D. Freeman. After countless days and evenings of oxygen scavenging that often seemed never-ending, Kevin graduated from The University of Texas at Austin with a Doctor of Philosophy in Chemical Engineering in August 2013. Outside of the laboratories, Kevin continues to practice shooting three pointers and passing the rock, and relentlessly works on fulfilling the Great Commandment. Kevin is excited to begin a new chapter in his professional development at Intel Corporation in Portland, Oregon.

Permanent email: kevintung7@utexas.edu

This dissertation was typed by Kevin Tung.